COMPUTATIONAL STUDIES OF SELECTED GAS HYDRATES AND HYDRATE MELTS

Ph.D. THESIS

by

SURINDER PAL KAUR

DEPARTMENT OF CHEMISTRY
INDIAN INSTITUTE OF TECHNOLOGY ROORKEE
ROORKEE – 247667, INDIA
FEBRUARY, 2018

COMPUTATIONAL STUDIES OF SELECTED GAS HYDRATES AND HYDRATE MELTS

A THESIS

Submitted in partial fulfilment of the
requirements for the award of the degree

of

DOCTOR OF PHILOSOPHY

in

CHEMISTRY

by

SURINDER PAL KAUR

DEPARTMENT OF CHEMISTRY
INDIAN INSTITUTE OF TECHNOLOGY ROORKEE
ROORKEE – 247667, INDIA
FEBRUARY, 2018

INDIAN INSTITUTE OF TECHNOLOGY ROORKEE
ROORKEE

CANDIADATE'S DECLARATION

I hereby certify that the work which is being presented in the thesis entitled, **"COMPUTATIONAL STUDIES OF SELECTED GAS HYDRATES AND HYDRATE MELTS"** in partial fulfilment of the requirements for the award of the Degree of Doctor of Philosophy and submitted in the Department of Chemistry of the Indian Institute of Technology Roorkee, Roorkee is an authentic record of my own work carried out during a period from July, 2013 to February, 2018 under the supervision of Dr. Ramachandran C. N., Assistant Professor, Department of Chemistry, Indian Institute of Technology Roorkee, Roorkee.

The matter presented in this thesis has not been submitted by me for the award of any other degree of this or any other institution.

(SURINDER PAL KAUR)

This is to certify that the above statement made by the candidate is correct to the best of my knowledge.

(Ramachandran C. N.)
Supervisor

Dated:-

Abstract

Gas hydrates are non-stoichiometric crystalline compounds formed when water and small gas molecules are brought together at low temperature and high pressure. Under these conditions, gas molecules are trapped inside the cages formed by water molecules. Gas hydrates are stabilized by the hydrogen bonding interactions between water molecules as well as by the van der Waals interaction between the guest molecules and the host cages. Depending on the size and shape of the guest molecules, gas hydrates occur in different structural forms.

The amount of hydrocarbons that can be obtained from natural gas hydrates is reported to be twice the amount that is available from conventional fossil fuels. The natural gas hydrates contain mainly methane and hence they are known as methane hydrates. There are reports that the amount of hydrocarbons that can be obtained from natural gas hydrates is twice the amount that is available from conventional fossil fuels. Gas hydrates can also be used as transportation and storage materials for various gases. However, a prior knowledge on host-guest and guest-guest interactions in gas hydrates is important for their efficient use, as it provides valuable information about stability of the hydrates under various conditions. Most of the studies in this direction are limited to the host-guest interaction in single cages. Thus, in the present thesis, an attempt has been made to give a detailed picture of such interactions by incorporating more such cages and guest species.

The thesis is divided into seven chapters. Different types of natural gas hydrates, and their applications are briefly discussed in the first chapter. The discussion on gas hydrates is followed by a literature review on gas hydrates of different molecules, their stability and various spectroscopic properties.

The second chapter focuses on the computational methodology used in the present work. Various quantum mechanical methods such as Hartree-Fock, post Hartree-Fock and density functional methods are briefly discussed in this chapter. It also covers the details on basis sets and their classifications. A description on classical molecular dynamics methods along with various types of interaction potentials and force fields commonly used in simulations is presented. The strategies adopted for modeling water cages of different size and shape are also explained. The above strategies based on the concept of strong-weak-effective-bond (SWEB) model is extended for generating initial

geometries of fused water cages with maximum number of strong t*1d* hydrogen bonds. The optimized geometries of these cages are further used for encapsulating various gas molecules.

Taking noble gas atoms as prototypes, the effect of size of guest species on the stability of their hydrates is investigated in chapter 3. For this purpose, different noble gas atoms are encapsulated in the cavities of dodecahedral, fused dodecahedral and triple-fused dodecahedral water cages and are studied by using dispersion corrected density functional method B97D in conjunction with cc-pVTZ basis set. The results showed that the size of guest species plays an important role in the host-guest interaction. Among the guest species He, Ne, Ar and Kr, interaction energy varied in the order: He@DD < Ne@DD < Ar@DD < Kr@DD and is in agreement with the earlier reports. The study on the interactions of a noble gas atom with the neighboring cavity as well as its interactions with the guest species residing in the neighboring cage indicated that such interactions are not significant for small guest species. The values of interaction energy obtained for the mixed noble gas hydrates indicated that the presence of a guest in one of the cavities favors a guest atom of larger size in the neighboring cavity. It is also revealed that the changes in enthalpy and Gibbs free energy associated with the encapsulation of noble gas atoms are independent of the presence of a neighboring cage or the guest atoms present in that.

In the fourth chapter, the encapsulations of diatomic (H_2), triatomic (CO_2) and polyatomic (CH_4) molecules which differ in both size and shape are investigated at B97D/cc-pVTZ level of theory. A variety of fused cages formed by the combinations of dodecahedral and irregular dodecahedral water cages is used for this purpose. The host-guest interactions are studied and the results are analyzed in terms of interaction energy and interaction energy per guest molecule. A comparison of the interaction energy obtained for a molecule trapped in a single cage with that obtained for various fused cages suggested that the interaction of small guest species does not extend beyond a cage. However, the interaction of large guest species is not limited to the cage where it is located; rather it extends to the neighboring cage thereby interacting with the guest species in those cages. The vibrational Raman stretching frequencies of the guest molecules confined in various types of cages are computed and analyzed. The results showed that the stretching frequencies are increased inside the cages due to confinement. However, such shifts decreased with an increase in the size of the cavity. The studies also revealed that neither an adjacent cage nor the guest species in that cage influences the stretching frequencies of a molecule encapsulated.

The nuclear magnetic resonance (NMR) chemical shifts for ^{1}H and ^{13}C nuclei of the guest molecules in their free and encapsulated states are also computed using multi reference standard method. The results indicated that both ^{1}H and ^{13}C nuclei of the guest species undergo deshielding on their encapsulation. The analysis also revealed that such deshielding is decreased with an increase in the size of the cavity. The study did not show any significant change in the NMR characteristics of an encapsulated molecule in presence of an adjacent cage or a guest molecule inside.

Considering the potential of gas hydrates as hydrogen storage materials, the structure, stability and properties of mixed hydrates of hydrogen and tetrahydrofuran are investigated in chapter 5 using B97D/cc-pVTZ level of theory. Multiple encapsulations of hydrogen molecules in two different types of water cages are studied to find out the optimum occupancy of the cages with and without the presence of tetrahydrofuran. The change in host-guest interaction energy due to the successive addition of H_2 molecules in dodecahedral and hexakaidecahedral water cages is investigated. The results suggested that H_2 molecules can be encapsulated along with tetrahydrofuran in hexakaidecahedral cage of SII hydrates, thereby increasing the hydrogen storage capacity. The thermo-chemical parameters obtained are also found to be in agreement with the above findings.

The ^{1}H and ^{13}C chemical shifts values of H_2 and THF molecules are computed to infer about the host cages in which the guest species are confined. The effect of neighboring water cages on the above parameters is also discussed. It is observed that NMR chemical shift values of H_2 are deshielded on encapsulation and the presence of THF in a neighboring cage has little influence on the chemical shift.

Considering the potential of gas hydrates as energy resource, several methods have been proposed and explored in the past to extract natural gas from hydrate sediments. Among these methods, the replacement of CH_4 by CO_2 has received wide attention due to its potential to sequestrate CO_2 along with the extraction of CH_4. However, the yield of methane recovery by this method has been reported to be 60-64%. It has been proposed that a mixture of N_2 and CO_2 can significantly improve the percentage of methane recovery from its hydrates. During the replacement of CH_4 by a mixture of CO_2 and N_2, the intermediate liquid phase formed contains CH_4, N_2 and CO_2 dissolved in it. The evolution of dissolved gas molecules in this liquid is expected to significantly influence the subsequent steps of extraction process. Thus, in the sixth chapter, the evolution of dissolved gas molecules from a mixture of CH_4, CO_2, N_2 and H_2O is studied by applying classical molecular dynamics simulations.

The study revealed that an increase in the concentration of CO_2 assists the formation of nanobubbles in a CH_4-N_2-CO_2-H_2O mixture. The composition of the bubbles formed was analyzed and it revealed that the bubbles are made of CH_4, N_2 and CO_2 molecules. To understand the role of CO_2 in assisting the formation of nanobubbles in the mixture, the distribution of gas molecules in the bubble was examined. It was found that CO_2 molecules accumulate near the surface of nanobubbles and become more prominent with an increase in the concentration of CO_2 in the mixture. The CO_2 molecules at the surface of the bubble reduced the excess pressure inside the bubble as well the surface tension at the bubble-water interface thereby assisting the bubble nucleation. To understand the effect of nanobubbles on hydrate nucleation in the mixture, the structural ordering of water molecules around the bubble is investigated. The number of rings formed by water molecules around the bubble in the CH_4-N_2-CO_2-H_2O mixture is analyzed. It is observed that water rings are formed preferentially near the surface of the bubble. The number of water rings formed per unit volume near the bubble-water interface is correlated to the dynamic nature of the bubbles. The nanobubbles which are more dynamic have a larger number of water rings formed per unit volume near its surface compared to the less dynamic ones suggesting the possibility of gas hydrate nucleation near the bubbles.

The summary and conclusions are provided in the seventh chapter.

Acknowledgements

It is my great pleasure to take this opportunity to express my sincere gratitude and respect to my supervisor **Dr. Ramachandran C. N.** for his guidance, constant encouragement, unselfish inspiration and amicable cooperation during the course of my work. I owe special gratitude to him for introducing me to the field of computational chemistry. It is my privilege to be a part of his enthusiastic research group. I express my deepest respect to him not only for his guidance throughout my Ph. D. career, but also for his motivation and inspiration towards my future endeavors. I am also grateful to **Dr. P. Smitha** for her constant love and affection.

I would also like to thank my research committee members, **Dr. P. Jeevanandam** (Chairman), **Dr. Pallavi Debnath** (Internal Expert) and **Dr. Lalita Sharma** (External Expert) for carrying out regular SRC meetings and providing valuable suggestions from time to time to accomplish my research work smoothly.

I am highly grateful to **Prof. M. R. Maurya**, Head of the Department of Chemistry, Indian Institute of Technology Roorkee, for providing me the essential infrastructural facilities to carry out research investigations. I am also thankful to **Mr. S. P. Singh**, **Mr. Ankur Sharma**, **Mr. Madan Pal**, **Mr. K.C. Tiwari** and other staff members of the Department of Chemistry for being me in every occasion.

I gratefully acknowledge my lab-mates **V. Shilpi**, **Sujith, K. S.**, **Vinit, Ankita Joshi**, **Mohan Tiwari**, **Sakshi Ganotra**, **Bhawna Singh Tomar**, **Manisha Singh, Rajdeep and Laukesh Sharma** for their constant support and maintaining excellent working atmosphere in the lab. I will always be grateful to **V. Shilpi** for always been there with me as my well-wisher. I really have no words to thank **Vinit** and **Mohan Tiwari** for all the interesting as well as funny conversations we had. They were always been there with me during good and bad times. Their company helped me to keep my childish behavior alive.

I am really thankful to my M. Sc. friends **Nisha Kaundal**, **Amritpal Singh** and **Dr. Amanpreet Singh Hundal** with whom I shared the best time of my life.

Life at IITR could not be imagined without friends. I extend my warm thanks to my friends **Sunil**, **Sapna Bondwal**, **Amandeep Kaur**, **Iram Parveen, Tawseef Dar** and **Ankita Saini**. We all enjoyed a wonderful time in bhawan as well as in campus. Special thanks to **Iram Parveen** for serving us with delicious food on Sundays.

No words are available to express thanks to M.Sc. students and my friends **Chanpreet Singh**, **Gagandeep Ahluwalia** and **Mandeep Khan** who were always available for me during the hour of need. Their company and the funny conversations keep me younger during my P.hD.

Special thanks and huge appreciation goes to **Dr. Varun Kundi**, **Dr. Abhishek Baheti**, **Dr. Mandeep Kaur Chahal**, **Dr. Nishant Verma**, **Rekha Verma, Benazir Fatma** and **Richa Khurana** for their guidance, support and encouragement. I am really thankful to them for sharing a wonderful time with me in IIT Roorkee. I am grateful to them for giving me homely environment in IITR.

I am thankful to Indian Institute of Technology Roorkee **(IITR)** and Ministry of Human Resource Development (**MHRD)**, Government of India for providing me the fellowship. I am grateful to **IITR** for providing infrastructure for my research work.

Words fail to express my gratefulness to my dearest grandmother and parents for their love, affection, constant inspiration and support in all phases of my life. I put on record my sincere love and gratitude to my beloved father and mother for their unflagging love and unconditional support throughout my life. I am grateful to them for being there when I needed them most. My special gratitude is due to my younger sister **Surjit Kaur** and brother **Akashdeep Singh** for their loving support and encouragement and being a pillar of strength for me and for all the sweet memories. They are the most important people in my world and I dedicated this thesis to them.

Finally, I bow down to **ALMIGHTY GOD** for giving me health and energy to complete this work successfully.

Surinder Pal Kaur
IIT Roorkee
February, 2018

Table of Contents

LIST OF TABLES

LIST OF FIGURES

List of Publications

Publications from the thesis

1. **Kaur, S. P.;** Ramachandran, C. N. Effect of multiple and adjacent cage occupancies on host-guest interaction and NMR chemical shifts in gas hydrates. *Comp. Theor. Chem*. **2016**, 1092, 57-67.
2. **Kaur, S. P.;** Ramachandran, C. N. Host-Guest and Guest-Guest Interactions in Noble Gas Hydrates. *Mol. Phys*. **2018**, 1, 54-63.
3. **Kaur, S. P.;** Sujith, K. S.; Ramachandran, C. N. Formation of nanobubble and its effect on the structural ordering of water in CH_4-N_2-CO_2-H_2O mixture. *Phys. Chem. Chem. Phys*. **2018** (Accepted, DOI: 10.1039/C7CP07934F)
4. **Kaur, S. P.;** Ramachandran, C. N. Hydrogen-Tetrahydrofuran mixed hydrates: A computational study. *Int. J. Hydrogen Energy*. **(under review)**

Other Publications

1. Shilpi, V.; **Kaur, S. P.;** Ramachandran, C.N. Revisiting the structural pattern and stability of $(H_2O)_{20}$ clusters using the dispersion corrected density functional method. *Chem. Phys. Lett*. 2015, 626, 39-42.
2. Shilpi, V.; **Kaur, S.P**.; Ramachandran, C.N. Density functional studies of fused dodecahedral and irregular-dodecahedral water cages. *RSC Adv.* 2015, 5, 74270-74273.

List of Conferences/Workshops

1. Attended an **ACS on Campus** workshop which was held at Indian Institute of Technology Roorkee in February, 2018.
2. Presented a poster entitled "Effect of cage occupancy on host-guest interaction and spectral properties of guest molecules in fused water cages" at 15th Indian Theoretical Chemistry Symposium (**TCS**) held at **Hyderabad** in December, 2017.
3. Presented a poster entitled "Effect of cage occupancy on spectral properties of guest molecules in fused cages" at Chemical Research Society of India (**CRSI**) symposium held at **Panjab University Chandigarh** in February, 2016.
4. Attended an **USPEX 8th workshop** which was held at **SHIV NADAR University** Noida in January, 2015.
5. Attended **Chemistry with computers** symposium which was held at **IIIT Hyderabad** in February, 2014.

Chapter-1
Introduction

1.1 Gas hydrates

Gas hydrates are solid, non-stoichiometric crystalline, ice like compounds formed when water and gas molecules are brought together under high pressure and low temperature [1, 2]. They are also known as clathrate compounds. The cavities formed by the cross-linking of water molecules act as host for small guests such as H_2, CO_2, CH_4, etc. Gas hydrates are stabilized by the intermolecular hydrogen bonding interactions between water molecules of the host cages as well as by the non-bonding interactions between the guests and the host cavities.

Gas hydrates were noted for the first time with the discovery of chlorine hydrate by Sir Humphrey Davy in 1811. Gas hydrates attained attention from economic perspective after they were reported blocking the pipelines in the oil and natural gas industries [3]. The formation of gas hydrates in pipelines disrupts the flow of oil and results in the rupturing of pipelines. Later, the importance of gas hydrates as alternate energy resources was well accepted. There are reports that the amount of hydrocarbons that can be obtained from natural gas hydrates is twice the amount available from conventional fossil fuels [2]. The naturally occurring gas hydrates contain mainly methane and hence, are generally known as methane hydrates.

It is known that ~70% of reservoirs of oil and natural gases are far from the domestic places and hence, different methods have been used for their transportation to the distinct markets. The transportation of natural gas in the form of gas hydrates is a more convenient method compared to that of liquefied natural gas (LNG) through pipelines [4, 5]. Thus, gas hydrates are considered not only as energy resources, but are also looked as means of energy storage and transportation materials. However, dissociation of gas hydrates releases methane in to the environment which is a potential greenhouse gas leading to further global warming and climate changes. It is well known that CO_2 is a greenhouse gas [6, 7]. There are reports that a given volume of methane causes 15-20 times more global warming effect than CO_2, which in turn results in the destabilization of more gas hydrates [1, 2].

Gas hydrates can be used in the separation processes. For example, in 2000, Kang and Lee used hydrate based separation technique for separating CO_2 from flue gases [8]. Englezos and his

coworkers used the above method for separating carbon dioxide and propane from paper mill effluents [1]. A pictorial representation of gas hydrate structure is given in Figure 1.1.

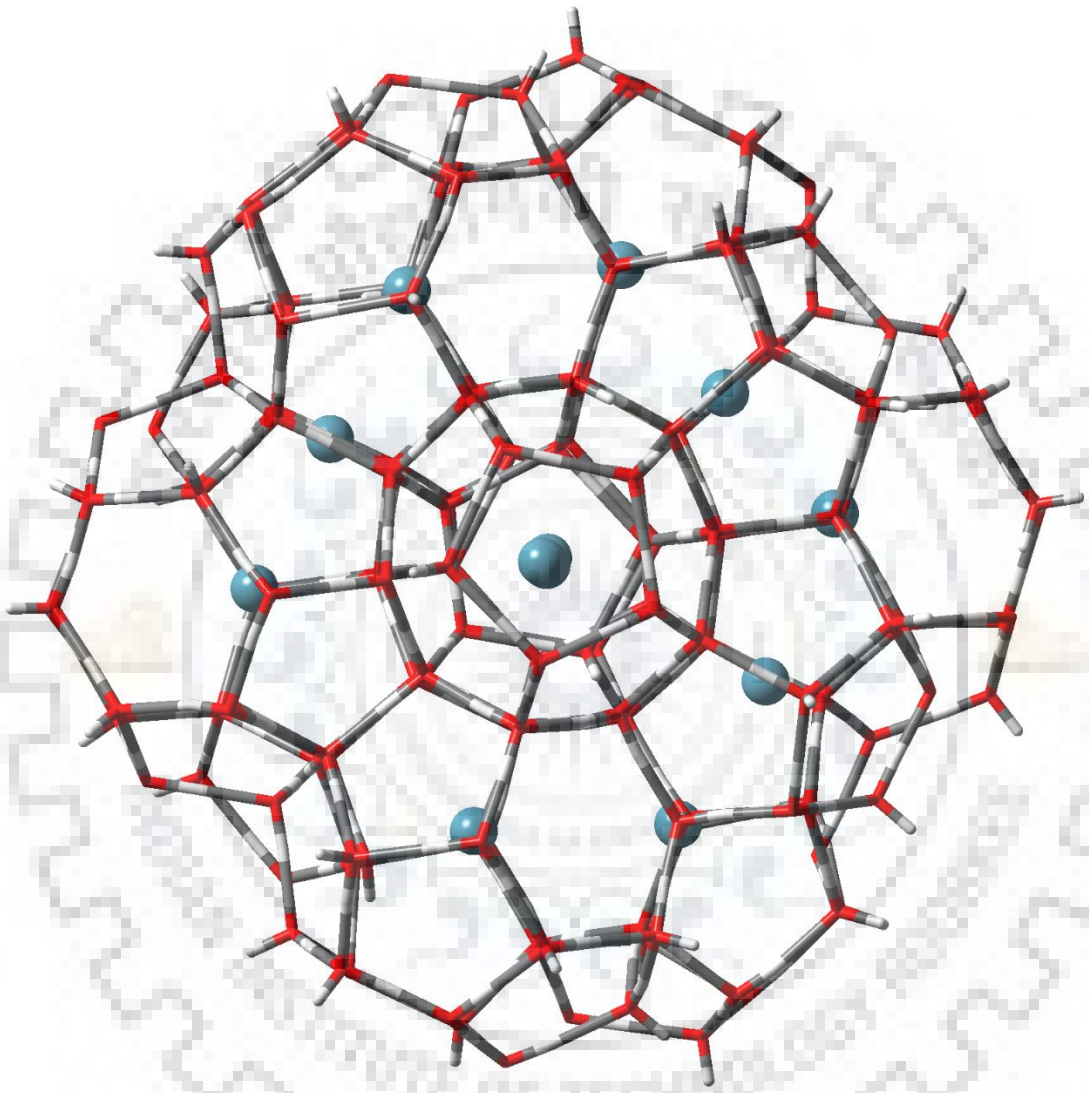

Figure 1.1 A pictorial representation of gas hydrate structure. The water molecules are shown by sticks and gas molecules by balls.

1.2 Classification of gas hydrates

Depending on the size and shape of water cages which in turn depends on the number of water molecules present, the hydrates are mainly classified into three: sI, sII and sH structures. The various types of water cages which constitute the above hydrate structures include (i) Dodecahedron (5^{12}), (ii) Irregular dodecahedron ($4^3 5^6 6^3$), (iii) Tetrakaidecahedron ($5^{12}6^2$), (iv) Hexakaidecahedron ($5^{12}6^4$) and (v) Icosahedron ($5^{12}6^8$). The notations given in the parentheses are known as Jeffery's notation [1, 2]. For example, a dodecahedral cage which is formed by the combination of twelve five-membered rings is represented by 5^{12}. An irregular-dodecahedral cage formed by the combination of three four-membered, six five-membered and three six-membered rings of water molecules is designated as $4^3 5^6 6^3$. Similarly, the tetrakaidecahedral, hexakaidecahedral, and icosahedral cages are represented as $5^{12}6^2$, $5^{12}6^4$ and $5^{12}6^8$, respectively, depending upon the number of five and six membered rings present in such cages. The formation of different types of gas hydrate structures from various water cages mentioned above is schematically illustrated in figure 1.2.

1.2.1 Structure I (sI) and structure II (sII) hydrates

The geometries of sI and sII gas hydrates [9, 10] were proposed by W. F. Claussen in 1951. The unit cells of these hydrate structures are cubic in nature. Both sI and sII hydrates differ from each other in terms of the number of water molecules of the host cages in their respective unit cells as illustrated in Figure 1.2. The unit cell of sI type hydrates contains 46 water molecules and is made up of two dodecahedral (5^{12}) and six tetrakaidecahedral ($5^{12}6^2$) host cages. The cubic sI hydrates are mainly available in the Earth's crust and consist guests of smaller size (0.4-0.55 nm). For example, pure methane, ethane, carbon dioxide and hydrogen sulfide form sI hydrates.

The unit cell of sII type of gas hydrates are made up of sixteen dodecahedral (5^{12}) and eight hexakaidecahedral ($5^{12}6^4$) cages by 136 water molecules. Guests of molecular size 0.6-0.7 nm form sII hydrates. Thus, argon (Ar), nitrogen (N_2) and oxygen (O_2) hydrates belong to sII type.

1.2.2 Structure H (sH) hydrates

Structure H was discovered in the laboratory for the first time by Ripmeester *et al.* in 1987 [11]. The unit cell of sH clathrate hydrates consists of three dodecahedral (5^{12}), two irregular-dodecahedral ($4^3 5^6 6^3$) and one icosahedral ($5^{12}6^8$) water cages. It is hexagonal in nature and has 34 water molecules. A mixture of small and large gas molecules forms sH hydrates.

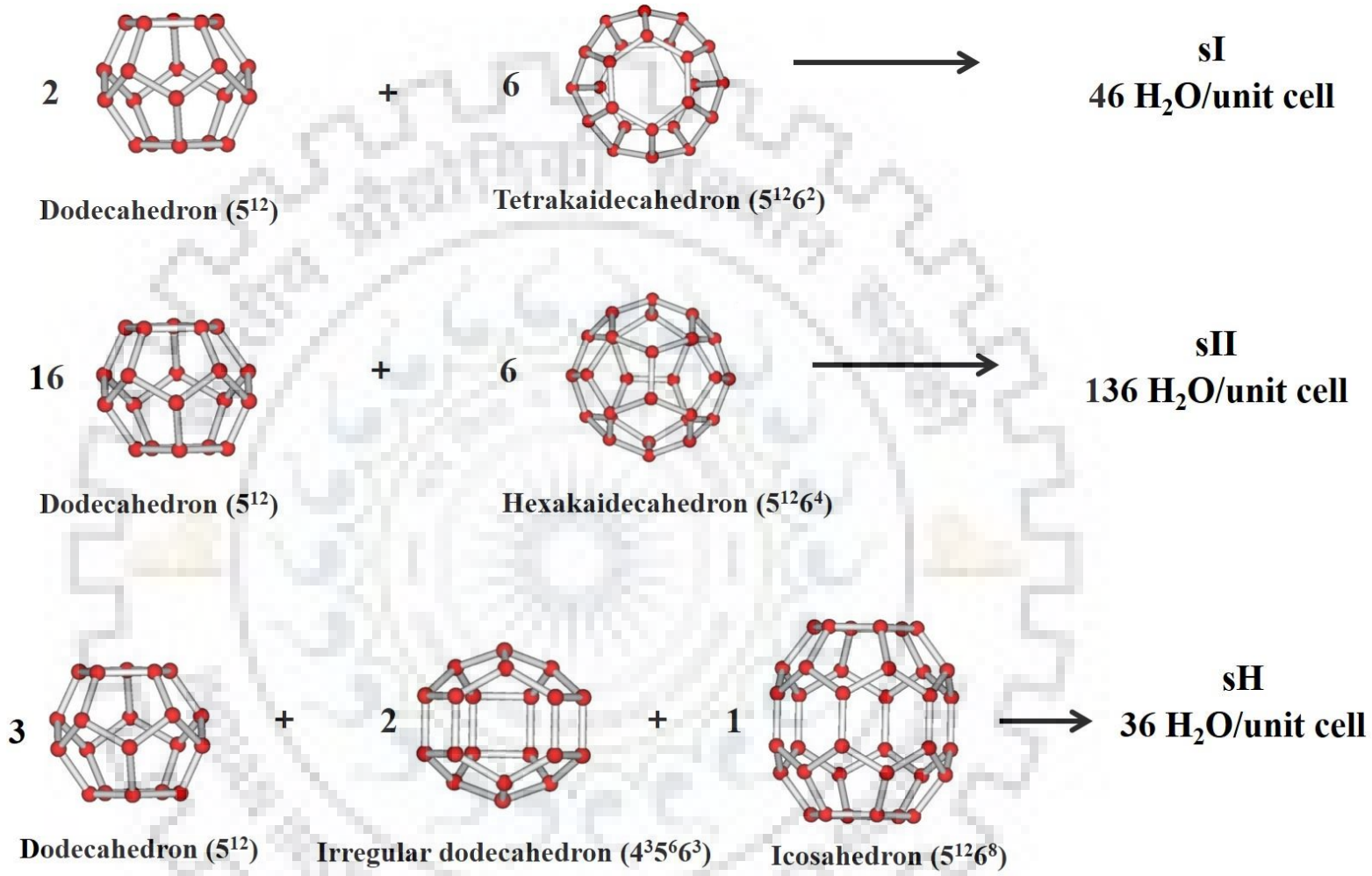

Figure 1.2 Illustration of the formation of host cages of different gas hydrate structures from water cages of different size and shape.

1.3 Gas composition in hydrate structures

The gas hydrates are non-stoichiometric in nature due to the absence of guest species in some of the constituting cages. Gas molecules of different size form different hydrate structures which are stable at various thermodynamic conditions. In 1998, Sloan reported that the stability of hydrate structures can be explained in terms of guest to cavity size ratio [12]. Due to the difference in the size of guests, methane forms hydrates of sI structure, propane results in the formation of sII hydrates [12] and larger molecules such as methyl-cyclohexane forms sH hydrates. The structure of gas hydrates of a given species was found to be dependent on the concentration of the guest molecules as well as the thermodynamic conditions.

Von Stackelberg in his studies reported that guest molecules which form sI hydrates can form sII hydrates in the presence of other gas molecules [13]. For example, the natural gas hydrates which are rich in methane are of sI type, whereas hydrates found in oil and gas pipelines are of sII type because of the presence of traces of larger hydrocarbons such as propane, isobutene, *etc.* along with methane.

1.4 Gas hydrate reservoirs

It has been reported that the gas hydrate reservoirs are present in continental margin settings and in onshore or offshore permafrost settings. It is also expected that 99% of the total natural gas hydrates exist in marine sediments [2, 14]. There are estimations that the energy stored in the form of gas hydrate deposits in United States (US) is approximately 300 times greater than the energy present in the other recoverable reservoirs. The reservoirs of natural gases, the latter in the form of sI type hydrates were located in the Gulf of Mexico and South China Sea [15]. Gas hydrate deposits of sII and sH structures were found in Caspian Sea and Northern Cascadia Margin [16]. The deposits of hydrates also exist in the permafrost regions of Alaska North Slope [17]. Gas hydrate deposits have also been reported in Indian on shores and off shores. The exploration of natural hydrates as well as the energy production efforts have been initiated in India with the help of international partnerships. For example, a multinational team led by the Directorate General of Hydrocarbons, India and the U.S. Department of Energy [18] was organized to exploit the core hydrate deposits along the coasts of India and the nearby Andaman islands. There are evidences of the occurrence of huge thickness of gas hydrate deposits in Krishna-Godavari basin in India. The laboratory level experiments are in progress for their exploitations [19]. Gas hydrates have been recovered from

deposits under the Lake Baikal in Russia, which is the earth's largest freshwater lake [14]. During the Mallik field of Mackenzie Delta in Canada, an extensive amount of gas was obtained from the hydrate reservoirs. Depressurization technique was used to extract methane from their sediments in the Nankai Trough off the central Japan. Thus, it can be seen that the interest in gas hydrates grows worldwide [14].

1.5 Hydrates as energy storage materials

As mentioned above, gas hydrates can be used as energy storage materials because of their high gas density under mild conditions [20]. Therefore, clathrate hydrates are of research interest [21] to explore them as energy storage and transport materials. It has been estimated that one unit volume of hydrate can release up to 160 unit volumes of natural gas.

1.5.1 Methane hydrates

The possibility of transportation of methane gas as its hydrates at temperature below the melting point of ice under atmospheric pressure was first reported by Gudmundsson and his co-workers in 1996 [22]. It was found that methane can be preserved in the form of hydrates for several days or weeks [23-25]. Pure methane hydrates belong to structure I hydrates in which methane molecules reside in both small and large cages. Besides that methane hydrates also exist in the form of sII and sH structures at higher pressure [26]. The stability of the synthesized hydrates at moderate temperature is crucial for the economical use of methane hydrates. Several studies have been done in this direction and some of them are discussed in the later part of this chapter.

1.5.2 Hydrogen hydrates

Hydrogen is a clean and efficient fuel which can be considered as a future energy resource. One of the major challenges in creating the hydrogen economy is storage and transportation of hydrogen. Various methods have been proposed in the past for hydrogen storage [27-30]. These include molecular hydrogen adsorption on surfaces of large surface area, bonded hydrogen on hydrogen-hydrides and in the form of clathrate hydrates [31-33]. Among these methods, the clathrate hydrates have taken much attention as they are compact and light weighted. Earlier, it was believed that size of hydrogen is too small to stabilize the hydrate structure. However, in 1999, Dyadin *et al.* demonstrated the possibility of hydrogen storage in the form of clathrate hydrates at high pressure (1.5 GPa) [34].There are several advantages on storing of hydrogen in the form of its hydrates. As the storage material is made of pure water, the by-product after the extraction of hydrogen is only

water, which is not toxic and can be reused. Secondly, H_2 is stored in molecular form in clathrate cages and hence, it can be recovered without any chemical reaction. However, the formation of stable hydrogen hydrates requires high pressure (~220 MPa) and hence, its application is limited.

1.5.3 Experimental studies of methane and hydrogen hydrates

Natural gas hydrates which are mainly composed of methane gas can be stored for long period of time even at ambient pressure and temperature slightly below the freezing point of water. This property of methane hydrates is known as self-preservation effect [23, 24]. Due to the stability of methane hydrates at ambient pressure, gas hydrates have been considered as methane storage materials. Experimental studies have been performed by several research groups to exploit hydrates as methane storage materials [35-39]. Stern *et al.* investigated the effect of temperature on the rate of dissociation of methane hydrates [23]. They reported that the dissociation is significantly reduced due to the self-preservation at atmospheric pressure when the temperature ranges between 240 and 270 K. Takeya *et al.* claimed that the interactions between guests and water molecules of host cages play an important role in the self-preservation phenomenon [39].

The use of hydrates as hydrogen storage materials was proposed by Mao *et al.* [40, 41]. They reported that pure hydrogen hydrates are stabilized with double and quadruple occupancy of hydrogen in small and large cavities of sII hydrates. Lokashin *et al.* performed neutron diffraction studies on deuterium hydrates and reported the single occupancy of deuterium in dodecahedral cages of sII hydrates, whereas the occupancy in large cages varied from two to four depending on the temperature and the pressure [42].

Spectroscopic techniques [43-45] are found to be useful for the identification of types of crystalline phases, cage occupancies and structural transformations of methane and hydrogen hydrates. Two main spectroscopic techniques used in the hydrate studies are

i) Raman spectroscopy
ii) Nuclear magnetic resonance spectroscopy (NMR).

Although the principle behind these spectroscopic techniques are different, they can be complementary to each other to elucidate information about gas hydrates. Both these techniques are sensitive probes to investigate the surrounding environment of the guest molecules.

Sum *et al.* used Raman spectroscopic technique to investigate the properties of methane hydrates at a pressure of 33.6 bar [45]. They recorded and analysed the Raman spectra of methane

in all the three hydrate phases and observed the shifting of the signature peaks of methane towards lower frequency (red shift) in three different types of hydrates compared to those in gas phase. With the help of Raman spectroscopic technique, Subramanian *et al.* [46] investigated the structural transition from sI to sII for the mixtures of methane and ethane. Red shifts of 4 cm^{-1} in the C-H and 8 cm^{-1} in the C-C stretching frequencies for ethane were observed when sI hydrates transform into sII.

It is very important to determine water to guest ratio in hydrate structures for using methane hydrates as an energy storage materials as methane hydrates are formed only at certain compositions. Uchida *et al.* reported the utilization of Raman spectroscopy in the investigation of hydration number (water to methane gas ratio) of methane in its synthesized hydrates [47]. They determined the hydration number of methane hydrates synthesized at a range of temperatures and pressures. Their analysis indicated that the hydration number is independent of the hydrate formation conditions.

Vibrational Raman spectroscopic technique is also an effective tool to determine the relative occupancy of H_2 molecules in the cavities of sII hydrates. Strobel *et al.* [48] observed an increase in stretching frequency of H_2 (blue shift) for the quadruple occupancy of large cages, whereas singly occupied small cavities showed a decrease in their stretching frequency (red shift). The studies also reported a red shift in the stretching frequencies of confined hydrogen molecules compared to that in the gas phase. Vibrational spectra of H_2 in its hydrates have been recorded for a range of compositions at different temperature and pressure. The studies revealed variation of the vibrational frequencies of confined hydrogen molecules on changing the temperature and pressure [49].

Like Raman spectroscopic method, nuclear magnetic resonance spectroscopic technique has also been used to determine the cage occupancies in hydrates [50-53]. For example, ^{13}C NMR spectroscopic technique was used for the first time by Ripmeester *et al.* to study the cage occupancies of sI and sII methane hydrates [50]. Further, in 2006, Dec *et al.* recorded ^{13}C magic angle spinning (MAS) NMR spectra of solid methane hydrates at 243 K and 1.4 MPa [38]. They observed two lines corresponding to the chemical shifts -3.6 and -5.9 ppm due to the carbon nuclei of methane molecules in dodecahedral and tetrakaidecahedral cages, respectively. NMR studies have also been performed for the mixed hydrates of methane with ethane or propane [46, 54-56]. Kida *et al.* [52] recorded solid state ^{13}C NMR spectra of methane, ethane, propane and adamantane in their clathrates at different temperature. They observed a decrease in the shielding of the carbon nuclei of guest molecules in large cages on increasing the temperature, whereas shielding increased in small host cages with an

increase in temperature. This variation in chemical shift arises due to the change in van der waals interaction between host and guest molecules with temperature.

1.5.4 Computational studies of methane and hydrogen hydrates

A prior knowledge on host-guest interactions and thermodynamics of hydrate formation is important for considering hydrates as energy storage materials. Several theoretical studies have been performed by different research groups on the stability of water clusters and the role of hydrogen bond interactions of their stability [57-66]. Khan [58-60] studied a series of water cage structures at MP2/6-31G* level, and validated that dodecahedral cage is the most suitable for hosting methane. Hexakaidecahedral and icosahedral cages are large compared to the size of methane. Thus, it is natural to speculate whether more than one methane molecules can reside in these cages [61]. Based on the results obtained, Khan suggested that the hexakaidecahedral cage can store up to two CH_4 molecules, although the doubly occupied clathrate structure is less stable than the singly occupied one [60]. Román-Pérez calculated the adsorption energies of CH_4 molecules in methane hydrates with the help of density functional theoretical calculations [67]. They observed that the adsorption energy is dominated by the van der Waals interactions between methane and water molecules. Further, they reported that the hexakaidecahedral and icosahedral cages can encapsulate a maximum of one and five methane molecules, respectively.

In order to understand the mechanism of hydrate formation at molecular level, stability of methane encapsulated dodecahedral and tetrakaidecahedral cages were studied by Ramya *et al.* using quantum mechanical methods [68]. They calculated the interaction energy and change in Gibbs free energy of the complexes formed by the encapsulating guest molecules in dodecahedral and tetrakaidecahedral cages. On the basis of interaction energy and change in Gibbs free energy, they found that the encapsulation of methane in dodecahedral cage is more favorable than in a tetrakaidecahedral cage using *ab initio* molecular dynamics methods. Liu *et al.* investigated the structure and stability of methane hydrates formed by the encapsulation of more than one CH_4 molecule [69]. Their results indicated that dodecahedral, tetrakaidecahedral and irregular-dodecahedral cages can encapsulate one molecule of CH_4, whereas hexakaidecahedral and icosahedral cages can encapsulate two and five molecules, respectively.

Papadimitriou *et al.* performed grand canonical Monte Carlo simulations to determine the amount of methane gas that can be stored in small as well as large cavities of sI hydrates over a range

of temperature (200-300 K) and pressure (0.1-220 MPa) [70]. Their studies revealed that each cavity can encapsulate only one molecule. They have also developed simple equations to correlate the occupancy in each cavity of sI hydrate as a function of temperature and pressure. These equations can be used to determine the amount of methane present in the hydrate synthesized. Further, they extended their studies to determine the amount of methane that can be stored in sII and sH hydrates at different temperature and pressure [71]. Their simulations showed that average occupancy of methane in icosahedral cage increases with an increase of pressure.

Ripmeester and his co-workers studied the stability of structure H methane hydrates at 300 K and 2 GPa using molecular dynamics simulations [72]. In their studies, the optimum occupancy of methane in the large cages of sH hydrates was found to be five. They also reported an expansion of the unit cell of the hydrate with an increase in occupancy.

Using ab initio MP2 and DFT calculations, Patchkovskii *et al.* investigated the stability of sII type hydrogen hydrates [73] and reported that the hydrogen molecules form stable hydrate structures due to the dispersive interactions between H_2 and water molecules.

Theoretical studies have also been carried out by many research groups to infer about the maximum storage capacity of hydrogen in small and large cages of sII hydrates [73-75]. Both experimental and theoretical results gave a consistent picture on the occupancy of up to four H_2 molecules in the large cavities of pure H_2 hydrates [39-41, 76, 77]. However, conflicting results exist about the maximum storage capacity of hydrogen in the small cavities.

Tachikawa *et al.* performed MP2 and DFT calculations to determine the maximum storage capacity of dodecahedral, tetrakaidecahedral and hexakaidecahedral water cages. They reported that at most three, six and eight hydrogen molecules can be encapsulated in dodecahedral, tetrakaidecahedral and hexakaidecahedral cages, respectively [76].

In order to investigate the occupancy of H_2 molecules in small cages of sII hydrates, Inerbaev *et al.* studied the thermodynamic properties of hydrogen hydrates as a function of cage occupancy [77]. Their lattice dynamic calculations studies showed that small cages occupied by two hydrogen molecules are dynamically more stable than the cages occupied by one molecule. Alavi and co-workers performed molecular dynamics simulations for a range of pressure and temperature to study the effect of multiple hydrogen occupancy on the stability of sII clathrates [74]. The simulations showed that the unit cell of the most stable sII hydrogen hydrate has one and four hydrogen

molecules in its small and large cages, respectively. The spatial distribution of H_2 molecules inside these cages was determined from host-guest and guest-guest radial distribution functions. Based on this, they concluded that the double occupancy of small cavities of sII hydrates by H_2 is not favored energetically leading to a tetragonal distortion of the hydrate lattice.

Papadimitriou *et al.* performed the grand canonical Monte Carlo simulations to test the hydrogen storage capacity of sH hydrates at a wide range of temperatures and pressures. They reported the possibility of storage of 3.6 wt% of hydrogen in the form of sH hydrate at a pressure of 500 MPa. In their hypothetical pure hydrogen sH hydrate, icosahedral cage accommodated eight hydrogen molecules, whereas the dodecahedral and irregular dodecahedral cages were singly occupied [78]. Furthermore, they examined the effect of the size of cavity on the storage of hydrogen [79]. They studies also revealed that storage of hydrogen molecules in the large cages can be improved by changing the lattice constant of sII hydrates, whereas no such change was observed for small cages.

As already mentioned, theoretical methods can also be used to investigate the spectroscopic properties of gas hydrates. Ramya *et al.* adopted density functional theoretical calculations to study the vibrational modes of guest methane molecule and water molecules of the host cages dodecahedral, tetrakaidecahedral and hexakaidecahedral using dispersion corrected B97D functional [68, 80]. They found that the vibrational modes of methane inside the cavities are red shifted compared to those in the free state. Furthermore, they also reported that the encapsulated methane molecule behaves like a free gaseous molecule with an increase in the size of the cavity.

Greenhouse and his co-workers studied the vibrational spectra of pure methane hydrates by molecular dynamics simulations [81]. The symmetric stretch of methane in the dodecahedral cage was observed to occur at 14 cm^{-1} higher frequency than that observed in the tetrakaidecahedral cavity. However, the C-H stretching frequency of methane in the large cavity occurred at the same frequency as that of methane in the gas phase, showing the free rigid rotor behaviour of methane in large cages. Their studies also showed the expansion of the unit cell on increasing the temperature from 60 to 300 K.

In 2000, Tse *et al.* used the *ab initio* molecular dynamic calculations to elucidate the stretching frequencies of methane in sI hydrates [82]. Their results were in qualitative agreement with the experimental results which indicate that methane molecule behaves as a free rotor inside the

tetrakaidecahedral cage due to its larger cavity size. In their studies, the calculated C-H stretching frequencies were found to be lower than the gas phase. They did not find the dependency of the vibrational frequencies of the guest molecules on the interactions between host and guest molecules as suggested by the loose cage-tight cage Charles Pimentel model [83].

The vibrational Raman spectra of hydrogen molecules encapsulated in various water cages have also been reported by quantum mechanical methods and molecular dynamics simulations [49, 84]. Wang *et al.* performed calculations at B3LYP/6-31++G (2d, 2p) level to study the shifts in the Raman stretching frequencies of encapsulated hydrogen molecules [84]. Their results showed that the vibrational Raman stretching frequency of hydrogen molecules in singly occupied small cage and that in large cages with one to form hydrogen molecules are red shifted with respect to the stretching frequency in free state. On the other hand, the vibrational frequency was found to be blue shifted when two such molecules are encapsulated in small cages.

The change in NMR chemical shift values of guest species have also been used to understand the nature of host-guest interactions [85, 86]. Siuda *et al.* calculated the nuclear shielding and spin-spin coupling constants of methane molecules encapsulated in dodecahedral and tetrakaidecahedral water cages at B3LYP/huzIII-su3 level of theory [85]. The chemical shift values obtained for carbon nuclei in dodecahedral and tetrakaidecahedral cages were 6.7 and 4.4 ppm, respectively, indicating that the deshielding is reduced with an increase in the size of the cage.

Liu *et al.* calculated ^{13}C NMR chemical shifts of methane and ethane by performing quantum mechanical calculations for the solid phases of natural gas hydrates. They reported a decrease in the chemical shift values of carbon of methane molecule with an increase in the size of host cage [87]. Further, for multiple occupancy, they observed an increase in the value of ^{13}C chemical shift.

The proton NMR shielding constants and chemical shifts for hydrogen molecules which encapsulated in small and large cages of sII hydrates were calculated using B3LYP functional in conjunction with 6-311++G (d, p) basis set by Alavi *et al.* [88]. They reported that single and multiple occupancy of different cages cannot be distinguished by ^{1}H NMR chemical shift values.

1.6 Inhibitors in gas hydrates

There are variety of methods available for the extraction of natural gas from hydrate sediments [89-92]. In one such methods known as chemical inhibitor injection, the dissociation of hydrates is carried out by the injection of some chemicals. The commonly used inhibitors are glycol,

methanol and calcium chloride [93-96]. The chemical inhibitor injection method is advantageous over dissociation [89, 90, 97] and thermal stimulation [98, 99] methods as the former enhances the rate of gas production within a short time. The effect of chemical inhibitors on the thermodynamic conditions of gas hydrate dissociation have been studied by many research groups [93-96]. Chemical inhibitors are broadly classified into three categories as discussed below:

1.6.1 Thermodynamic inhibitors

Thermodynamic inhibitors disturb the gas hydrate equilibrium and helps to push the hydrate out of its stable phase. The injection of thermodynamic inhibitors into hydrate deposits causes instability of the hydrate structures [100, 101]. The chemical inhibitors form hydrogen bonds with water molecules and prevent the formation of water cages. The addition of inhibitors is economically not viable and environmentally hazardous.

1.6.2 Kinetic inhibitors

Kinetic inhibitors slow down the hydrate nucleation process for long time by bonding to the hydrate surface. Kinetic inhibitors are preferred over thermodynamic inhibitors as the former requires in lower concentrations compared to latter for the extraction of gases from natural gas hydrates. Poly (N-Vinylcaprolactum), Poly (N-Vinylpyrrolidone) and several surfactants are commonly used as kinetic inhibitors [102, 103].

1.6.3 Antiagglomerates

Antiagglomerates inhibit the accumulation of gas hydrate particles avoiding the formation of bigger particles, without completely stopping the hydrate nucleation process. These inhibitors keep the hydrates into the dispersed phase thereby preventing the blockage of pipelines due to hydrate formation. The mechanism by which antiagglomerates control the hydrate nucleation is not clear till date. Mixtures of kinetic inhibitors as well as antiagglomerates are also generally used as inhibitors at large scale [104, 105].

1.7 Promoters in gas hydrates

The storage of methane and hydrogen as their hydrates at moderate pressure can be achieved by stabilizing the host water cages using another guest species called promoters. The promoter facilitates the formation of hydrates at moderate conditions. It also helps to achieve stability for the hydrates at moderate temperature and pressure. Tetrahydrofuran (THF) is one of the commonly used

hydrate promoters. The type of gas hydrate structure formed by a gas molecule may be different in presence of a promoter. For example, pure methane forms sI hydrates, however, in presence of THF it forms sII hydrates.

In 1996, Udachin *et al.* performed high pressure studies of H_2 and THF mixed hydrates [106]. The mixed hydrates of structure II hydrates in which H_2 molecules were trapped in small cages, whereas THF molecules were confined in the large cages. They also demonstrated that an increase of pressure from 350 to 700 MPa increases the hydrogen occupancy of small cages indicating that more than one hydrogen molecule can be trapped in dodecahedral cages at high pressure. However, breakthrough in the studies of hydrogen storage materials came when Flouresse *et al.* [107] demonstrated that the minimum pressure required for the formation of hydrogen hydrates can be reduced in presence of THF.

Using Raman and nuclear magnetic resonance spectroscopic techniques, Mao *et al.* [40, 41] showed that small water cages of hydrogen hydrates are occupied by two hydrogen molecules, whereas large cages are occupied by one THF molecule. Their study deduced that stable H_2-THF binary hydrates can be obtained by the encapsulation of THF in the large cavities of sII hydrates at the expense of reduced hydrogen storage efficiency. Therefore, major limitation of this approach is that the storage of hydrogen in the clathrate hydrates is reduced due to the non-availability of large cages for H_2.

In 2005, Lee *et al.* proposed a way to avoid this problem. They suggested the possibility of increasing hydrogen storage capacity by tuning the concentrations of H_2 and THF [108]. Using Raman and NMR spectroscopic studies, they reported that hydrogen storage capacity in H_2-THF binary hydrates can be enhanced from 2.1 wt% to ~4 wt% by decreasing the amount of THF from 5.6 wt% to 0.15 wt%. The observed increase arises because some of the large cages are partially occupied by hydrogen molecules. Sugahara *et al.* [109] recorded Raman spectra of H_2 molecules in H_2-THF mixed hydrates by varying the concentration of THF at ~76 K. They reported the additional bands in the range 4130-4155 cm^{-1} along with the bands in the range 4140-4180 cm^{-1} due to the occupancy of H_2 molecules in large cages when the concentration of THF is reduced below their eutectic composition (x_{THF}=0.0106).

Unlike in the above cases, there are some studies which disprove such claims [110, 111]. In 2006, Strobel *et al.* [111] determined the hydrogen storage capacity of mixed H_2-THF sII hydrates

as a function of pressure, composition of THF, and time. They observed that the hydrogen storage capacity followed Langmuir adsorption isotherm and showed asymptotic behavior at higher pressures corresponding to the formation of binary hydrate with one hydrogen molecule per small cavity. Furthermore, they did not observe any significant change in hydrogen storage capacity by decreasing the THF concentration from 5.56 to 0.5 mol%.

Anderson *et al.* analyzed the phase equilibrium for THF-H_2-H_2O system as a function of THF concentration at 290 K and 45 MPa. The measured data suggested the encapsulation of one hydrogen molecule per small cage independent of THF concentration [112]. Hashimoto *et al.* performed Raman spectroscopic studies on H_2-THF mixed hydrates for various THF concentrations in aqueous solutions [113]. The recorded Raman spectra did not show any change in the vibrational frequencies of hydrogen molecules for different THF concentration suggesting that the tuning effect is not observed in the hydrate structures up to a pressure of 110 MPa.

Ulivi *et al.* [114] performed inelastic neutron diffraction and gas release measurements of THF-H_2 hydrates. Their measured data showed single occupancy of small cavities. Ogata *et al.* performed pressure-volume-temperature (p-V-T) measurements to determine the hydrogen occupancy in binary H_2-THF hydrates as a function of formation pressure. They reported that hydrogen occupancy in the small cages of binary H_2-THF hydrates is not greater than unity [115].

Apart from experimental studies, molecular dynamics [110, 116-122] and quantum mechanical studies [123-126] have also been performed in the past to infer about the energy storage capacity of hydrates in presence of THF. Yedlapalli *et al.* performed quantum chemical calculations to determine the feasibility of multiple H_2 occupancy in the small cavities of H_2-THF sII hydrates [123]. They calculated the binding energy at the MP2 level using various basis sets for the fused dodeca-hexakaidecahedral complexes with up to two H_2 molecules in the small cage while THF occupies in the large cage. Based on the results they reported that single occupancy of H_2 is preferred over its double occupancy inside the dodecahedral cage.

With the help of molecular dynamics simulations, Alavi *et al.* studied the hydrogen storage capacity by tuning the concentrations of THF in H_2-THF hydrates [116]. They performed simulations at various temperature and pressure and showed that the volume of the unit cell of sII hydrate increases with an increase in the number of guest molecules at all temperatures studied. A large increase in the unit cell volume was observed with the encapsulation of two H_2 molecules in the

dodecahedral cages of sII hydrates. Based on these studies, they concluded that the hydrogen storage capacity depends on the concentration of promoter.

Recently, Liu *et al.* investigated the hydrogen storage capacity of H_2-THF mixed hydrates using *ab initio* molecular dynamics simulations and showed that small cages are singly occupied by hydrogen, whereas large cages can be simultaneously occupied by hydrogen and THF [127]. The studies also showed that THF not only acts as a thermodynamic promoter by reducing the hydrate formation pressure, but also acts as a kinetic promoter by increasing the rate of uptake of H_2 molecules in small cages.

The kinetic promoters, such as sodium dodecyl sulfate (SDS) and sodium dodecyl benzyl sulfate (SDBS) enhance the hydrate formation by reducing the surface tension at the liquid interface thereby promoting the dissolution of gas into liquid [128-131]. Surfactants which are amphiphilic in nature are notable kinetic promoters. Mechanism by which surfactants affect the formation rate of hydrates is still not clear. Many research groups suggested that the water soluble surfactants form supramolecular structures such as spherical and rod-like micelles and multilayers which reduce the interfacial tension. However, the micelle formation mechanism claims that the surfactant micelles are not present at the hydrate formation conditions suggesting the need for further studies on the formation of hydrates in the presence of promoters.

1.8 Extraction of methane gas from natural gas hydrates using CO_2

The replacement of CH_4 in natural gas hydrates with CO_2 is considered as an attractive way for CH_4 recovery along with CO_2 sequestration. The CO_2 hydrates were found to be more stable compared to CH_4 hydrates suggesting that replacement of CH_4 by the injection of CO_2 is a promising approach towards the long-term storage of CO_2 in hydrate regime.

The possibility of sequestration of CO_2 along with the extraction of methane by the injection of CO_2 into methane hydrates was proposed by Ohgaki *et al.* in 1996 [132]. Both pure as well as mixture of CH_4 and CO_2 forms sI hydrates. In CH_4-CO_2 hydrates, CH_4 occupies both in small and large cavities, whereas CO_2 prefers to occupy in the large cavities of sI hydrates.

Thermodynamic feasibility of CH_4-CO_2 replacement in natural gas hydrates has been investigated by many research groups both experimentally and theoretically. Uchida and his coworkers considered the formation and decomposition of CH_4 and CO_2 hydrates using gas chromatography and Raman spectroscopic techniques [133]. They observed that the equilibrium

pressure of methane hydrates is higher compared to that of carbon dioxide hydrates at a particular temperature. Similar results were also obtained by Anderson *et al.* in their studies [134]. Hirohama *et al.* studied the extraction of CH_4 from the bulk phase with liquid CO_2 and observed the consumption of water in CO_2 soaking step [135]. To study the formation and dissociation of methane hydrates during CO_2 sequestration, many research groups used analytical and spectroscopic techniques, such as X-Ray diffraction (XRD), neutron diffraction, Raman, nuclear magnetic resonance (NMR) [136-140], etc. *In situ* Raman spectroscopic technique has also been used to study the CH_4-CO_2 replacement process. During the swapping of CO_2 with CH_4, a decrement in the occupancy of CH_4 was reported. NMR spectroscopic technique has also been widely used to examine the variation in the occupancy of CH_4 and CO_2 in small as well as large cages of sI hydrates by varying the composition of CH_4 and CO_2. However, the mechanism of replacement of CH_4 with CO_2 is not very clear till date. To know whether the dissociation of methane hydrate occurs first followed by the formation of CO_2 hydrates or CO_2 molecules directly enter the hydrate cavities and replace methane molecules, further studies are required.

The kinetic feasibility of the replacement has also been investigated by several research groups. The fugacity difference between hydrate and gas phase can act as a driving force during the CH_4-CO_2 replacement process. The fugacity difference between both phases has been calculated by Ota *et al.* by using van der Waals-Platteeuw theory and the Soave-Redlich-Kwong equation of state (SRK-EOS) [141]. The activation energy for CO_2 hydrate formation as well as decomposition of CH_4 hydrate have been studied experimentally by many research groups [142, 143] and it was concluded that the formation of CO_2 hydrate is an exothermic process and the energy released by this process is utilized in the decomposition of methane hydrate.

Apart from experimental studies, molecular dynamic simulations [144, 145] have also been performed to get insight on the exchange reaction between CH_4 and CO_2. For example, Geng *et al.* studied the stability of pure as well as CH_4 and CO_2 mixed hydrates at a range of temperature and pressure [144]. The higher stability of CH_4 and CO_2 mixed hydrate with respect to pure CH_4 and CO_2 hydrates indicated the thermodynamic feasibility of the sequestration of CO_2 hydrates. Their results on Gibbs free energy also indicated that the transformation of CH_4 hydrates into CO_2 hydrates is a thermodynamically feasible process.

Although guest replacement method has attained wide attention, it is not accepted much for the production of gas at industrial level due to the poor efficiency of extraction. Raman spectroscopic

studies showed that 100% extraction of methane is not possible by this method as methane has a tendency to go back and occupy small cages of sI hydrates. Experimental studies reported that only 60-64% methane can be recovered by this method. Thus, the efficiency of methane recovery needs to be improved from economic point of view.

1.9 Replacement of methane from natural gas hydrates using a mixture of CO_2 and N_2

To enhance the percentage recovery of methane from natural gas hydrate deposits, some of the research groups investigated on the use of a mixture of N_2 and CO_2 instead of pure CO_2. Park *et al.* used Fourier transform-Raman and solid-state NMR spectroscopic techniques and showed that ~85% of methane can be recovered by injecting a mixture of N_2 and CO_2 gases. This is ~20% higher than that could be recovered by injection of pure CO_2 into methane hydrates [146]. The recovery of CH_4 that resides in small cages by the injection of N_2 leads to an increase in the recovery of methane although it affects the rate of recovery. It was also found that the rate of recovery of CH_4 depends on the pressure at which the CH_4 replacement by CO_2 and N_2 gases is carried out.

Lee *et al.* applied ^{13}C NMR spectroscopy and differential scanning calorimetry (DSC) methods to study the percentage recovery of CH_4 from methane hydrate by the injection of a mixture of N_2 and CO_2 gases and estimated that 74% of methane can be recovered through this process [147, 148]. Koh *et al.* [149] studied the direct extraction of CH_4 from methane hydrates, using either CO_2 or a mixture of N_2 and CO_2 gases (80 mol% of N_2 and 20 mol% of CO_2) for methane replacement in complex marine systems. The effect of replacement of CH_4 by a mixture of N_2 and CO_2 gases on the structural properties of gas hydrates has also been studied in the past. On the basis of crystallographic analysis, Shin *et al.* [150] reported 92% of methane recovery from sH hydrates during a swapping process between CH_4 and CO_2-N_2 mixtures followed by a structural transition from sH to sI hydrate.

Seo *et al.* [151] used several analytical techniques to examine the replacement reaction of sII (C_3H_8 + CH_4) hydrate by externally injecting a mixture of CO_2 and N_2 (50:50). The results of these studies did not show any structural transition during the replacement process.

Lee *et al.* examined the change in thermodynamic and structural properties associated with the replacement process in the hydrate sediments using differential scanning calorimetric (μ-DSC) technique [148]. Any significant change in the heat flow during the replacement process was not reported indicating that the exchange of methane with a mixture of CO_2 and N_2 occurs without noticeable dissociation of methane hydrate.

The mechanism of replacement of CH_4 by a mixture of CO_2 and N_2 gases has also been investigated by spectroscopic techniques. Zhou *et al.* [152] studied the effect of N_2 on the replacement of CH_4 by CO_2 and by a mixture of CO_2 and N_2 gases using Raman spectroscopic techniques. From the spectroscopic analysis it was found that the rate of CH_4 recovery is unaffected by the pressure when CO_2 is in gaseous state. However, the rate was found to be dependent on the pressure when N_2 is added to the gaseous CO_2. Spectroscopic analysis revealed that N_2 molecules assist the replacement of CH_4 molecules from small cages of sI hydrates thereby increasing the CH_4 production.

Apart from laboratory studies, field tests of CH_4 recovery using CO_2 and N_2 gas mixture were also performed in Alaska North Slope, which successfully demonstrated the commercial viability of replacement method [16].

In addition to the laboratory and field works, few theoretical works have also been reported on the replacement of CH_4 by a mixture of CO_2 and N_2 gases from methane hydrates [153, 154]. With the aid of molecular dynamics simulations Dornan *et al.* [153] studied the change in Gibb's free energy during the exchange process to understand the pathway of substitution of methane from both small and large cages of sI hydrates by CO_2 and N_2 gases. They suggested that the substitution of methane by a mixture of N_2 and CO_2 followed a complex mechanism in which replacement of methane by nitrogen occurrs simultaneous to the substitution by carbon dioxide.

Recently, Liu *et al.* investigated the thermodynamic and kinetic feasibility of replacement of CH_4 from methane hydrates by a mixture of N_2 and CO_2 with the help of *ab initio* molecular dynamics simulations. Their investigations revealed that the substitution of CH_4 by CO_2 in large cages is followed by the substitution of CH_4 by N_2 in small cages and is thermodynamically favored [154]. Furthermore, it was also found that the replacement of CH_4 by N_2 is kinetically more favored over that by CO_2 as N_2 has higher rotational and translational diffusivity inside the hydrate cavity.

1.10 Outline of the thesis

This thesis is divided into seven chapters. In the first chapter, we introduced different types of natural gas hydrates, and their applications. This brief discussion on gas hydrates was followed by a literature review focused on the gas hydrates of various molecules, their stability, and various spectroscopic properties.

In the second chapter, we discussed the computational methodology used in our work. We discussed about the quantum chemical methods, which include a brief discussion on Hartree-Fock, post Hartree-Fock and density functional theoretical methods. A brief discussion on the classical molecular dynamics method with details on various types of interaction potentials *i.e.* bonding and non-bonding interaction potentials and force fields used in simulations are given. This chapter also covers the discussion on basis sets and their classifications.

In the earlier reported studies, the role of guest molecules on the host-guest interactions and the stability of the hydrate structure were studied by considering single water cages as a host model system. In real hydrate structures, the host water cages are connected to the neighboring water cages which may also play a role in the stabilization of these hydrate structures. Thus, it is very important to consider the effect of neighboring cages as well as the guest species in those cages. Further, the stability of hydrate structures may also depend on the size and shape of the guest residing in the host cavities. The noble gas atoms can be considered as prototypes to study the effect of size of guest species on the stability of hydrates. Keeping this in mind, we studied the stability of the complexes formed by the encapsulation of noble gas atoms in the cavities of dodecahedral, fused dodecahedral and triple-fused dodecahedral water cages and the results are discussed in chapter 3. The thermodynamic feasibility associated with the encapsulation of guest species of different size in the above mentioned host cages is calculated in terms of change in enthalpy and change in Gibbs free energy at a range of temperature and pressure comparable to experimental conditions. In the actual hydrate structures, a dodecahedral cage is surrounded by neighboring cages in all the directions. Therefore, to make our study more realistic, we also considered a segment of sII hydrate in which central dodecahedral cage is surrounded by six dodecahedral and hexakaidecahedral water cages. The effect of size of guest atom on host-guest interaction energy as well as change in enthalpy and change in Gibbs free energy associated with the encapsulation are calculated at B97D/cc-pVTZ level of theory.

A slight interaction between krypton atoms residing in the neighboring host cages was observed in our studies, whereas such interactions were not observed in the case of helium, neon and argon atoms. It emphasizes the need to unravel the effect of size and shape of guest species on the guest-guest interactions in hydrate structures, which in turn affect the stability of these clathrates.

Therefore, in fourth chapter, diatomic (H_2), triatomic (CO_2) and polyatomic (CH_4) molecules are considered as guest species. Fused-dodecahedral, fused-dodecahedral-irregular-dodecahedral

and fused-irregular-dodecahedral water cages were used as host cages which were modeled by the combinations of dodecahedral and irregular dodecahedral water cages. In this chapter, we also computed the vibrational Raman stretching frequencies of the guest molecules as well as nuclear magnetic resonance (NMR) chemical shifts for ^{1}H and ^{13}C nuclei of the guest molecules in their free and encapsulated states to understand the effect of confinement on the spectral features of these molecules.

It is known that hydrates can be used as hydrogen storage materials. Multiple encapsulation of hydrogen molecules in the cavities of water cages those constitute various hydrate structures were claimed by many research groups in the past. However, the optimum occupancy of hydrogen remained disputed.

In the fifth chapter, using density functional theoretical calculations at B97D/cc-pVTZ level, we investigated the change in host-guest interaction energy due to the successive addition of H_2 molecules in dodecahedral and hexakaidecahedral water cages. In this chapter, we also studied the possibility of simultaneous encapsulation of both H_2 and THF in the large cavities of fused-dodeca-hexakaidecahedral water cages. The ^{1}H and ^{13}C chemical shifts values of H_2 and THF molecules were computed to infer about the host cages in which the guest species are confined. The effect of neighboring water cages on the above parameters are also discussed.

It is predicted that the replacement of methane from its hydrate by gas swapping method is a two-step mechanism. In the first step, injection of a mixture of CO_2 and N_2 gases leads to the dissociation of hydrate sediment. This dissociation of methane hydrate results in the formation of aqueous mixture of CH_4, CO_2, and N_2 gases and is followed by the formation of new hydrate structure. The study of the evolution of dissolved gases is very important to understand the mechanism of hydrate formation of the entering gas.

In the sixth chapter, by applying classical molecular dynamics simulations, we studied the evolution of dissolved gas molecules from a mixture of CH_4, CO_2, N_2 and H_2O. The distribution of different gases in the nano bubble is studied by varying the concentration of CO_2 and N_2. The role of dissolved gas evolution on subsequent processes such as hydrate regeneration in the mixture is also discussed.

The seventh chapter provides the conclusion and future scope of the thesis.

Chapter-2
Theoretical background

2.1 Quantum chemical methods

Computational methods are used to study the chemical systems based on theoretical principles. Two main approaches *viz.* classical and quantum mechanics are used to describe the chemical systems on the basis of various interactions involved in the system. The relevant methods used for the calculations are discussed in this chapter.

2.1.1 The Schrödinger equation

According to quantum mechanics, the wave function (ψ) contains all the information regarding the chemical system [155-159]. Quantum mechanical methods can describe a chemical system by solving the many-body Schrödinger wave equation either in the time-dependent form

$$\hat{H}\psi(x,t) = i\hbar\frac{\partial\psi(x,t)}{\partial t} \tag{2.1}$$

or in the time-independent form

$$\hat{H}\psi = E\psi \tag{2.2}$$

where $\hat{H}$ is the Hamiltonian operator corresponding to the total energy of the system E and ψ is the wave function of the system. The Hamiltonian operator represents the sum of kinetic and potential energy operators for both the nuclei and electrons, which can be expressed as,

$$\hat{H} = \hat{T}_n + \hat{T}_e + \hat{V}_{ee} + \hat{V}_{nn} + \hat{V}_{ne} \tag{2.3}$$

where $\hat{T}_n$ and $\hat{V}_{nn}$ are the kinetic and potential energy operators for nuclei, $\hat{T}_e$ and $\hat{V}_{ee}$ are equivalent operators for electrons and $\hat{V}_{ne}$ is the potential energy operator that describes the nucleus and electron interactions .

The Schrödinger equation can be solved accurately only for one electron bodies. To solve it for many electron systems, a series of approximations are implemented one of the most important approximations is Born-Oppenheimer approximation [160], which separates the electronic and nuclear motions on the fact that the electrons are lighter and faster than the nuclei and hence, the above two motions can be separated. This allows the nuclei to be described as fixed point masses of different charges.

Based on this, electronic Hamiltonian for a system containing M nuclei and N electrons is given by:

$$\hat{H} = -\sum_{i=1}^{N} \frac{1}{2} \nabla_i^2 - \sum_{i=1}^{N} \sum_{A=1}^{M} \frac{Z_A}{r_{iA}} + \sum_{i=1}^{N} \sum_{j>i}^{N} \frac{1}{r_{ij}} \quad (2.4)$$

where the first operator corresponds to the kinetic energy of electrons, second term is the operator for electrostatic interactions between nuclei and electrons and third term corresponds to the operator for electron-electron repulsive interactions.

2.1.2 Hartree-Fock theory

Hartree-Fock theory is one of the simplest theories in which each electron is assumed to move under the average field of all the remaining electrons. The wave function can be written as:

$$\psi(r_1, r_2, \ldots, r_N) = \Phi_1(r_1)\Phi_1(r_2) \ldots \Phi_1(r_N) \quad (2.5)$$

which is known as a Hartree product.

The major shortcoming of the above form of wave function is that it does not satisfy the antisymmetry principle. However, for the electrons, which are fermions, the requirement of antisymmetric wave function must be fulfilled with respect to the exchange of space-spin coordinates.

For a system of N electrons, the required antisymmetric wave function can be obtained by writing the wave function in the form of a Slater determinant. Thus, the total wave function can be represented as

$$\Psi = \frac{1}{\sqrt{N!}} \begin{vmatrix} \chi_1(X_1) & \chi_2(X_1) & \cdots & \chi_N(X_1) \\ \chi_1(X_2) & \chi_2(X_2) & \cdots & \chi_N(X_2) \\ \vdots & \vdots & \ddots & \vdots \\ \chi_1(X_N) & \chi_2(X_N) & \cdots & \chi_N(X_N) \end{vmatrix} \quad (2.6)$$

where $\frac{1}{\sqrt{N!}}$ is the normalization factor. The above Slater determinant defines the occupancy of N spin orbitals by N electrons, without specifying which spin orbital is exactly occupied by which electron.

It is assumed that an electron is moving independently and experiences coulomb repulsions due to the averaged positions of all the other electrons. Therefore, it is also known as independent or mean field theory.

An exact solution in a single determinant approximation can be attained by complete expansion. However, to make it useful in computational problems, the truncation of this equation and the use of approximate functions known as basis functions are used in computational problems.

The variational flexibility in the wave function lies in the choice of spin orbitals. Thus, the best wave function of any system is the one that provides the lowest energy by minimization of energy with respect to the spin orbitals. An equation that satisfies the above conditions is known as Hartree-Fock equation. This equation further helps to determine the spin orbitals.

The Hartree-Fock equation is an eigenvalue equation and is written as

$$\hat{f}(x_1)\chi_i(x_1) = \epsilon_i\chi_i(x_1) \tag{2.7}$$

where $\hat{f}(x_1)$ is an effective one electron operator, also known as Fock operator.

The Hartree-Fock equation is non-linear in nature and can be solved iteratively. The procedure of solving this equation is known as self-consistent-field (SCF) method.

The basic idea of the SCF method is that with an initial guess of spin orbitals, one can calculate the average field experienced by each electron which further helps to calculate the Eigen value from equation 2.7 for a new set of orbitals. With the obtained spin orbitals, averaged fields can be obtained. The above procedure is repeated until the self-consistency is achieved.

Furthermore, Hartree-Fock equation does not consider the pair-wise interactions between electrons. Therefore, the calculated ground state energy always comes out to be higher than the true energy value. As a result, the correlation energy is described as a difference between the exact energy and the Hartree-Fock energy.

2.1.3 Post Hartree-Fock methods

As mentioned above, the Hartree-Fock procedure assumes the movement of an electron under the influence of an averaged field of all the other electrons. Therefore, it cannot recover the correlation energy [155]. The correlation energy can be recovered by replacing the single determinant wave function by a multi-determinant wave function. The total number of determinants depend on the size of the basis set *i.e.* larger the size of basis set, the large number of determinants can be obtained. An infinitely large basis set can help to recover all the correlation energy, although it is not possible for large systems.

The methods that gives correlation energy are discussed below.

2.1.3.1 Configuration Interaction (CI)

The expansion of wave function in the multiple excited determinant configurations can be expressed as

$$|\psi_{CI}\rangle = a_0|\theta_{CI}\rangle + \sum_S a_S\,|\theta_S\rangle + \sum_D a_D\,|\theta_D\rangle + \sum_T a_T\,|\theta_T\rangle + \ldots. \quad (2.8)$$

where S, D, T represents singly (S), doubly (D), and triply (T) excited determinant configurations, respectively. This expression is known as configuration interaction (CI) expansion. Its application is limited to small molecules because large number of determinant configurations are involved.

2.1.3.2 Many-Body Perturbation Theory (MBPT)

The many-body perturbation theory (MBPT) is considered as a powerful alternative to CI approach. In many-body perturbation theory, corrections are added to the solutions that are obtained from an independent particle approximation.

The Schrödinger wave equation can be written as

$$\widehat{H} = \widehat{H_0} + \lambda H' \quad (2.9)$$

$$\widehat{H_0}\Phi_i = E_i\Phi_i \quad (2.10)$$

An unperturbed Hamiltonian operator gives a complete set. The parameter λ, is a variable that decides the strength of perturbation.

The solution of perturbed Schrodinger wave equation is given as

$$\widehat{H}\Psi = E\Psi \quad (2.11)$$

The perturbation increases from zero to a finite value, which in turn imposes a continuous change in the energy as well as wave function.

For $\lambda = 0$, $\Psi_0 = \Phi_0$ and $E = E_0$, which represents an unperturbed wave function or energy. This is also known as zeroth order wave function and energy. The zeroth order perturbation equation represents a simple Schrödinger wave equation. Further, Ψ_1, Ψ_2,….are the first order, second order wave functions *etc*. The solutions to unperturbed wave functions are incorporated by Rayleigh-Schrodinger perturbation theory which describes the interactions between the pair of electrons qualitatively.

In order to calculate the correlation energy, the selection of unperturbed Hamiltonian is very important. The most common method is to choose sum of Fock operators which counts the electronic repulsions. Incorporation of second order corrections describes the most widely used method, known as second order Møller-Plesset perturbation theory. In MP2 method, the Fock operator counts the pair-wise electronic repulsions twice. In MP(n) techniques, all types of corrections, such as S, D, Q,…, *etc*. are summed up to a limited order (2, 3, 4, *etc*.). These are also size extensive methods and their use is limited depending on the size of the system.

2.1.3.3 Coupled Cluster (CC)

The other most reliable post Hartree-Fock method is Coupled Cluster (CC). The main criteria of this method is to incorporate all the possible corrections of a given type to infinite order. The coupled cluster methods are based on exponential expansion of wave function rather than a linear expansion.

It is a size-extensive method and depending on the truncation of terms of different orders results in different levels of coupled-cluster methods. These methods are computationally very expensive for large molecular systems and hence is not used in the present study.

2.4. Density functional theory

Over the past few years, density functional theory (DFT) has become very popular in the field of computational chemistry to describe the properties of chemical systems [161, 162]. In DFT, a many-body interacting system is described in terms of its particle density. The main advantage of this technique is that it reduces the 3N degrees of freedom of the N-body system to three spatial coordinates which lead to accurate outcomes at low computational cost.

2.4.1. Thomas-Fermi-Dirac approximation

The density functional theory is based on the Thomas-Fermi model that is proposed independently by Thomas [163] and Fermi [164] in 1927. In this method, instead of wave function, the electron density $\rho(r)$ is used as a basic variable. Thus, in this model, the total energy of a system in the presence of an external potential $V_{ext}(r)$ is expressed as a function $\rho(r)$

$$E_{TF}[\rho(r)] = A_1 \int \rho(r)^{5/3}\, dr + \int \rho(r)\, V_{ext}(r) dr + \frac{1}{2} \iint \frac{\rho(r)\rho(r)'}{|r-r'|}\, dr dr' \qquad (2.12)$$

where the first term is the kinetic energy of the non-interacting electrons in the uniform electron gas model. The second term is the classical electrostatic energy of the nucleus-electron Coulomb

interaction. The third term is the classical Coulomb repulsion between electrons. Although, the Thomas-Fermi model is a first step towards the mapping of energy onto density, its importance is limited because the exchange and correlation interactions between electrons are totally ignored. Therefore, in 1930, Dirac [165] incorporated a local exchange term A_2 to equation 2.12 yielding

$$E_{TFD}[\rho(r)] = A_1 \int \rho(r)^{5/3} dr + \int \rho(r)\, V_{ext}(r) dr + \frac{1}{2} \iint \frac{\rho(r)\rho(r)'}{|r-r'|}\, dr dr' + A_2 \int \rho(r)^{\frac{4}{3}} dr \qquad (2.13)$$

The equation 2.13 is known as Thomas-Fermi-Dirac equation. The solution to this equation can be obtained in the stationary condition by using Lagrange multipliers:

$$\delta\{E_{TDF}[\rho(r)] - \mu(\int \rho(r) dr - N)\} = 0 \qquad (2.14)$$

where μ is known as a Lagrange multiplier, which is the chemical potential or Fermi energy at T=0 K and leads to the Thomas-Fermi-Dirac equation,

$$\frac{5}{3} A_1 \rho(r)^{2/3} + V_{ext}(r) + \frac{1}{2} \int \frac{\rho(r')}{|r-r'|}\, dr' + \frac{4}{3} A_2 \rho(r)^{1/3} - \mu = 0 \qquad (2.15)$$

from which ground state density can be obtained. The limitation of this theory is that it neglects the bonding between atoms and hence is not appropriate for chemical systems.

2.4.2 The Hohenberg-Kohn (HK) theorems

In 1964, Hohenberg and Kohn proved that DFT is an appropriate theory for many body systems [166]. It is applicable to condensed-matter systems of electrons with fixed nuclei and the systems of interacting particles. The present form of density functional theory is based on two fundamental theorems:

Theorem I

The ground state particle density $\rho_0(r)$ of a system of interacting particles in an external potential $V_{ext}(r)$ uniquely determines the external potential $V_{ext}(r)$.

This states that there is a one-to-one mapping between the ground-state wave function and the ground-state electron density. Thus, the properties of the system can be determined from ground state particle density. The total energy of the system is the functional of density and given as

$$E[\rho] = F[\rho] + \int \rho(r)\, \mathrm{v}^{ext}(r) dr \qquad (2.16)$$

where the functional $F[\rho] = T[\rho] + V_{ee}[\rho]$ represents the kinetic and electron-electron interaction energy functional.

Theorem II

The electron density that minimizes the energy of the overall functional is the true electron density corresponding to the solution of the Schrödinger equation.

The HK theorem II constitutes the variational principle. It states that by minimizing the total energy of the system with respect to the density$\rho(r)$, it is possible to find out the approximation to the electron density. If the given density is ρ' and the ground state density is ρ_0, then for a fixed external potential, the energy functional follows the equality

$$E[\rho'] \geq E[\rho_0] \tag{2.17}$$

Although, the Hohenberg and Kohn proposed very powerful theorems, they do not offer any way to compute the ground state density of any system in practice. To overcome this difficulty, Kohn and Sham proposed the well-known Kohn-Sham approach in 1965 [167].

2.4.3 The Kohn-Sham equations

The Hohenberg-Kohn theorems came into practical use with the help of Kohn-Sham (KS) approach [167]. This approach turned into the most popular tool for electronic structure calculations. In this approach, real many-body system is considered as a non-interacting particle system and assumes that both the real as well as non-interacting systems possess exactly the same ground state density. In the non-interacting particle system, electrons are moving under the influence of an effective Kohn-Sham single-particle potential $\hat{V}_{KS}(r)$ and the Hamiltonian is written as

$$\hat{H}_{KS} = -\frac{1}{2}\nabla^2 + \hat{V}_{KS}(r) \tag{2.18}$$

For a system consists of N electrons, the ground state is obtained by solving the N one-electron Schrödinger equations,

$$(-\frac{1}{2}\nabla^2 + V_{KS}(r))\psi_i(r) = \epsilon_i\psi_i(r) \tag{2.19}$$

where ϵ_i is the lowest eigenvalues for each of the N orbitals. For the non-interacting systems, kinetic energy $T_S[\rho(r)]$ is given by,

$$T_S[\rho(r)] = -\frac{1}{2}\sum_{i=1}^{N}\int \psi_i^*(r)\nabla^2\psi_i(r)dr \tag{2.20}$$

As non-interacting kinetic energy is different from that of true kinetic energy of the interacting system, Kohn and Sham introduced universal functional $E[\rho(r)]$:

$$\mathrm{E}[\rho(r)] = T_S[\rho(r)] + \mathrm{J}[n(r)] + E_{XC}[\rho(r)] + E_{ne}[\rho(r)] \quad (2.21)$$

$$= T_S[\rho(r)] + \frac{1}{2}\iint \frac{\rho(r_1)\rho(r_2)}{r_1 r_2} dr_1 dr_2 + E_{XC}[\rho(r)] + \int V_{Ne}\rho(r)dr \quad (2.22)$$

$$= -\frac{1}{2}\sum_i^N \langle\varphi_i|\nabla^2|\varphi_i\rangle + \frac{1}{2}\sum_i^N \sum_j^N \iint |\varphi_i(r_1)|^2 dr_1 dr_2 + E_{XC}[\rho(r)] - \sum_i^N \int \sum_A^M \frac{Z_A}{r_{1A}} |\varphi_i(r_1)|^2 dr_1 \quad (2.23)$$

Although, Kohn-Sham approach is exact in principle, it is inexact in practice as XC energy functional $E_{XC}[n(r)]$ is unknown. An accurate description of XC energy functional $E_{XC}[n(r)]$ or potential $V_{XC}[n(r)]$ is very essential to deal with the chemical systems precisely.

2.4.4 Approximations of the exchange-correlation functional

As stated above, the exact XC energy functional $E_{XC}[\rho(r)]$ is very complex and therefore, simple approximations have been made to it. These approximations not only predict numerous properties of chemical systems reasonably well but also significantly reduce the computational cost.

2.4.4.1 Local density approximation (LDA)

The local density approximation is the simplest approximation to calculate the exchange-correlation energy in density functional theory. In this, the XC energy is considered to be exclusively dependent on the local electron gas. The total exchange-correlation functional $E_{XC}[\rho(r)]$ can be written as,

$$E_{XC}^{LDA}[\rho(r)] = \int \rho(r)\epsilon_{XC}^{hom}\big(\rho(r)\big)dr \quad (2.24)$$

$$= \int \rho(r)\left[\epsilon_X^{hom}\big(\rho(r)\big) + \epsilon_C^{hom}\big(\rho(r)\big)\right]dr \quad (2.25)$$

where ϵ_X^{hom} and ϵ_C^{hom} represent the exchange and correlation energies for the homogenous electron gas of density $\rho(r)$.

The major limitation of this approximation is that the results are not adequate enough for a quantitative discussion of the chemical systems. However, the LDA approximations were helpful in the building of more refined approximations such as the generalized gradient approximation (GGA) and meta-GGA.

2.4.4.2 Generalized gradient approximation (GGA)

This approximation includes gradient corrections. Unlike LDA approximation, in generalized gradient approximation, the exchange-correlation energy depends not only on the

electron at the particular point but also on the gradient of the electron density ($\nabla\rho$(r)), as per the equation

$$E_X^{GGA}[\rho] = \int \rho(r)\, \epsilon_{XC}^{GGA}[\rho(r)]dr + \int F_{XC}\,[\rho(r), \nabla\rho(r)]dr \qquad (2.26)$$

where F_{XC} is a correction term selected to fulfil the limits of E_{XC}. In these approximations, the choice of F_{XC} does not rely on a specific method and therefore, different functionals have been proposed. For example, Perdew, Burke and Ernzerhof proposed a GGA functional known as PBE functional [168].

2.4.4.3 Hybrid-GGA functional

The next improvement in the exchange-correlation functionals was carried out by incorporating the Hartree-Fock exact exchange term for the determination of E_{XC}. The most extensively used hybrid functional B3LYP (Becke, three-parameter, Lee-Yang-Parr) [169] is written as:

$$E_{XC}^{B3LYP} = E_{XC}^{LDA} + a_0(E_{XC}^{HF} - E_{XC}^{LDA}) + a_x(E_X^{GGA} - E_X^{LDA}) + a_c(E_C^{GGA} - E_C^{LDA}) \qquad (2.27)$$

where a_0=0.20, a_X=0.72 and a_C=0.81. The $E_{XC}^{LDA}$is the VWN (Vosko-Wilk-Nusair) exchange correlation, E_X^{GGA} is the Becke88 exchange and the E_C^{GGA} the LYP (Lee-Yang-Parr) correlation. Other than this, PBE0 [170] and HSE [171] are also the commonly used hybrid functionals.

2.4.4.4 Meta GGA functional

In order to study the properties such as charge-transfer, kinetics, and thermo-chemical properties, a new class of functional known as meta-hybrids was also developed [172-173]. These functional include the terms which are parametrized on high-quality benchmark databases. Minnesota functionals, developed by group of Donald Truhlar belongs to the family of meta-hybrid functional. It also includes the class of functionals such as Minnesota 05 [174], Minnesota 06 [172], Minnesota 08 [175], Minnesota 11 [176, 177], and Minnesota 12 [178] which differ from each other on the basis of amount of exact exchange functional. For example, in the functional M05, the contribution of Hartree-Fock exchange functional is 28%, whereas in M05-2X, the contribution is 56% [174-179].

2.4.4.5 Long range corrected functional

The functional discussed above underestimate the nonlocal contributions. The most substantial non local contribution neglected in GGA functional is the long-range electron correlation interactions which are accountable for the van der Waals forces (vdW, dispersive) [180, 181]. The vdW interactions between atoms and molecules play an important role in the studies of many chemical systems such as host–guest systems, the structures of proteins and DNA, and the alignment of molecules on surfaces. Therefore, to use density functional theory for such systems, new long range corrected density functional are introduced. The empirical-long range C_6R^{-6} corrections are incorporated by Stefan Grimme and his group to GGA functionals to include long range interactions [182]. In the dispersion corrected density functional, total energy of the system is expressed as

$$E_{DFT-D} = E_{KS-DFT} + E_{disp} \tag{2.28}$$

where E_{KS-DFT} is the self-consistent Kohn–Sham energy attained from the selected density functional and E_{disp} represents an empirical dispersion correction

$$E_{disp} = -s_6 \sum_{i=1}^{N_{at}-1} \sum_{j=j+1}^{N_{at}} \frac{C_6^{ij}}{R_{ij}^6} f_{dmp}(R_{ij}) \tag{2.29}$$

where N_{at} represents the total number of atoms present in the system, C_6^{ij} denotes the dispersion coefficient for atom pair *ij*, s_6 is a global scaling factor which depends on the density functional used, and R_{ij} is an interatomic distance. The f_{dmp} is a damping function used in order to avoid near-singularities for small R. The f_{dmp} is given by

$$f_{dmp}(R_{ij}) = \frac{1}{1+e^{-d\left(\frac{R_{ij}}{R_r}-1\right)}} \tag{2.30}$$

where R_r is the sum of atomic vdW radii.

In 2006, Grimme introduced the B97-D functional which includes the dispersion correction terms in its GGA precursor [183]. The functionals, B97-D3 [184], ωB97-XD [185, 186], *etc*. also fall into the category of long range correlated GGA functional. This functional is widely used for weakly interacting systems and is also chosen for the present study.

2.5 Basis sets

In computational chemistry, quantum calculations are performed with the help of finite basis sets. The basis sets are defined as a linear combination of mathematical functions mimicking the

atomic orbitals of various atoms. Initially, the atomic orbitals were expressed as Slater orbitals which decayed exponentially with distance from the nuclei [187]. Later, to speed up molecular integral evaluation, Gaussian type orbitals (GTOs) were proposed by Boys in 1950 [188]. The GTOs can be written in terms of polar or Cartesian coordinates as

$$\chi_{nlm}^{\zeta}(r,\theta,\phi) = \mathrm{N} r^{2n-2-l} e^{\zeta r^2} Y_l^m(\theta,\phi) \quad (2.31)$$

$$\chi_{nlm}^{\zeta}(r,\theta,\phi) = N x^{l_x} y^{l_y} z^{l_z} e^{\zeta r^2} \quad (2.32)$$

where N is the normalization constant and the summation of the Cartesian coordinates, $l = l_x + l_y + l_z$ represents the type of orbital. For example, l =1 describes a p type orbital. In GTOs, the variable *r* in the exponential function is squared which distinguishes Gaussian type orbitals from slater type orbitals. The Gaussian primitives are further contracted as contracted Gaussian type orbitals (CGTOs) which can be written as

$$\chi_v = \sum_{v=1}^{M} d_{\mu v}\, g_v(\alpha_v) \quad (2.33)$$

where $g_v's$ are primitive Gaussians functions, and $d_{\mu v}$ is contraction coefficient. A CGTO is a linear combination of Gaussian primitives.

2.5.1 Classification of basis sets

2.5.1.1 Minimal basis sets

The basis set in which smallest number of functions are used to define all the electrons in a neutral atom is known as minimal basis set. For example, two s-functions (1*s*, 2*s*) and one set of p-functions ($2p_x$, $2p_y$, $2p_z$) are required to define the first row elements of the periodic table. Whereas, three *s*-functions (1*s*, 2*s* and 3*s*) and two *p*-functions (2*p* and 3*p*) are employed for the second row elements.

2.5.1.2 Split-valence basis sets

The next improved class of basis set is known as *Double zeta* (DZ) type basis. The DZ basis set results in the doubling of all the basis functions. Calculations using DZ for every orbital is computationally expensive. Thus, it is common to do simpler calculation using DZ only for the valence orbitals. This method is known as a *split-valence basis set*. Further, *Triple Zeta* (TZ), *Quadruple Zeta* (QZ), and *Quintuple Zeta* (5Z) basis sets contain three, four and five times more basis functions as compared to respective minimal basis sets.

2.5.1.3 Pople basis sets

The group of John Pople represented the split valance basis set by the notation $n-ij$G or $n-ijk$G, where n denotes the number of primitives used to describe the inner shells and ij or ijk is the number of primitives for contractions in the valence shell. For example, in 6-31G basis [189], the core shell orbitals are described by six GTOs, the valence orbitals are described by two different types of GTOs, the one with a contraction of three GTOs and the other by one GTO.

In order to consider the polarization of orbitals, functions of higher angular momentum are usually added. Incorporation of one set of polarization functions (*p*-functions on hydrogens and *d*-functions on heavy atoms) to the double zeta basis sets forms a new class of basis known as *Double Zeta plus Polarization* (DZP) type basis. A triple zeta plus polarization (TZ2P) is formed by employing two sets of polarization functions to a triple zeta type basis. For example, in 6-31G** basis, the first asterisk indicates the addition of *d* functions on the non-hydrogen atoms (except helium) and the second asterisk is for the addition of *p* function on hydrogen or helium atom. Further, to describe the electron density far from the nucleus, another class of functions *i.e.* diffuse functions is introduced. The notation "+" is used to introduce diffuse functions. For example, in the 6-31++G basis set, the "++" indicates the addition of diffuse functions to all atoms including H and He.

2.5.1.4 Correlation-consistent basis sets

The correlation consistent basis sets are very well suited to study weakly interacting systems. The most widely used basis sets of this category were developed by Dunning and coworkers [190]. This class of basis sets is denoted as cc-pVXZ where, the "cc" denotes that this is a correlation-consistent basis, "*p*" denotes that polarization functions are included on all atoms. The "VXZ" stands for valence and the cardinal number X = D, T, Q indicates double-, triple- or quadruple-zeta, respectively. The presence of diffuse functions, which can improve the description of the outer valence region, leads to the evolution of augmented correlation-consistent basis set family, aug-cc-pVXZ.

2.6 Molecular dynamics simulations

Molecular dynamic simulations (MD) are used in this thesis to study macroscopic properties of gas hydrates from time averages over the molecular trajectories. Molecular dynamics methods are classified into two categories *viz.* classical and *ab initio* [191, 192]. The classical molecular dynamics treats the atoms and molecules as point masses, whereas *ab initio* works on the principles of quantum

chemistry to study the movement of atoms and molecules. Although, *ab initio* molecular simulations are more accurate than that of classical simulations, high computational cost limits their use for the systems possessing lesser number of atoms. Thus, the classical molecular dynamics which are faster as compared to *ab initio* simulations, are widely used to investigate the properties of the complex systems at molecular levels. As in this thesis, work is based on large number of molecules constituting the gas hydrate systems, classical molecular dynamics simulation method is used. Some of the key features of this method are discussed below.

2.6.1 Classical molecular dynamics

In classical molecular simulations, the classical equations of motion (Newton's equations) are solved for the trajectories of *N* particles, mass *m*, interacting with a given potential. The choice of proper molecular potential or force fields is very important to describe the system adequately in terms of inter and intramolecular interactions.

2.6.2 Interaction potentials

The force acting on every particle in the system is derived from the potential energy function

$$\mu(_{r_N}) = \mu_{bonded} + \mu_{non-bonded} \tag{2.34}$$

The bonded energy contains the contributions of covalent bonds bending, stretching and torsional movements, whereas the non-bonded interactions consists of long range (Coulomb interactions) and the short range forces (Van der Waals interactions). A brief discussion related to these potentials is given below.

2.6.3 Bonding interaction potential

Bonded interaction potential considers the intramolecular interactions present in a molecule. It is expressed as harmonic potential which depends on the force constant and the first power of the deviation of the angle or the bond distance from the respective equilibrium values. In order to describe the harmonicity in bond stretching and bending potentials, Morse potential is also used.

2.6.4 Non-bonding interaction potential

2.6.4.1 Lennard-Jones interactions

The simplest and the best known potential to consider the non-bonding interactions is the Lennard-Jones potential [193]. The summation of attractive and repulsive interaction components gives Lennard-Jones potential which is expressed as

$$V_{LJ} = 4\epsilon \left[\left(\frac{\sigma}{r}\right)^{12} - \left(\frac{\sigma}{r}\right)^{6} \right] \tag{2.35}$$

The ϵ represent the well depth of the potential and σ represents inter atomic distance where inter-particle potential is zero. The first term in the equation corresponds to the repulsive interaction component which occurs due to the overlap of electronic clouds of two atoms when they approach very close to each other. The second term in the equation represents the attractive interactions between the atoms. The repulsive term rules at very small values of *r*, whereas the attractive potential term dominates at intermediate and large values of *r*.

2.6.4.2 Coulomb potential interactions

The contribution of coulombic interactions to the total potential energy is dominant when the system consists of ions or molecules with partial charges [194]. All partially charged species in molecular system interact through coulomb potential which is given below

$$V_c = \left(\frac{1}{4\pi\epsilon_0}\right) . \left(\frac{q_i q_j}{\epsilon_r r_{ij}}\right) \tag{2.36}$$

where q_i and q_j represent the partial charges on the atoms i and j, respectively, ϵ_0 represents vacuum permeability, ϵ_r is the relative permeability of the system and r_{ij} is the inter-atomic distance.

Coulomb interactions decay slowly as compared to van der Waals interactions due to which computation of these forces is the most time taking part of the force computing process in molecular dynamics. A variety of methods have been developed to reduce the computational time required for the computation of long range interactions in molecular dynamics. A widely used method is the implementation of a cut off distance which means that the forces are computing up to a fixed distance beyond which the columbic interaction is neglected.

2.6.5 Force field

The potential energy function that describes the interactions between atoms is known as force field in molecular dynamics. A force field is established by fitting the parameters to experimentally or computationally derived properties. Each force field is usually well suited to reproduce the results of a particular class of molecular system. Hence, the choice of proper force field for the description of desired molecular system is one of the crucial steps in molecular dynamics simulations. A brief description of the force fields which are used in the thesis is provided in chapter 6.

2.7 Strategies used for the modelling of various water cages

As mentioned earlier, molecular level studies reported on gas hydrates in this thesis were performed with the help of quantum chemical calculations. For this, the initial geometries of host water cages with minimum energy were generated using two models *viz*. Strong-weak hydrogen bond (SWB) and strong weak effective hydrogen bond model (SWEB). These models were originally proposed by Kirov *et al.* [195, 196]. A brief discussion of these models is given below.

2.7.1 Strong-weak hydrogen bond model (SWB)

In this model, a hydrogen bond is considered to be strong, if the dihedral angle between the molecular plane of one the water molecule and the plane involving the hydrogen bond and the bisector of ∠HOH of the neighboring water molecule is 180˚. Whereas, the bond is considered to be weak if the dihedral angle is 0˚.

2.7.2 Strong weak effective hydrogen bond model (SWEB)

To consider the effect of next-nearest neighbors, strong weak effective hydrogen bond model (SWEB) was proposed by Kirov *et al.*. In this model, hydrogen bonds present in host water cages are classified into five different categories as listed below.

i) *t1d* hydrogen bond

This is a trans hydrogen bond in which dangling O-H bond is associated with the donor water molecule.

ii) *t1a* hydrogen bond

It also represents a trans hydrogen bond. However, in this type of hydrogen bonds one dangling O-H bond is associated with the acceptor water molecule.

iii) *c0* hydrogen bond

A cis hydrogen bond having no dangling O-H bond on donor and acceptor water molecule is denoted as *c0*.

iv) *c1a* hydrogen bond

In this category of cis hydrogen bond one dangling O-H bond is on the acceptor water molecule.

v) *c2* hydrogen bond

This is a cis hydrogen bond having dangling O-H bonds on the acceptor as well as donor water molecules.

A pictorial illustration of the above different types of hydrogen bonds in a dodecahedral water cage on the basis of SWEB model is given in Figure 2.1.

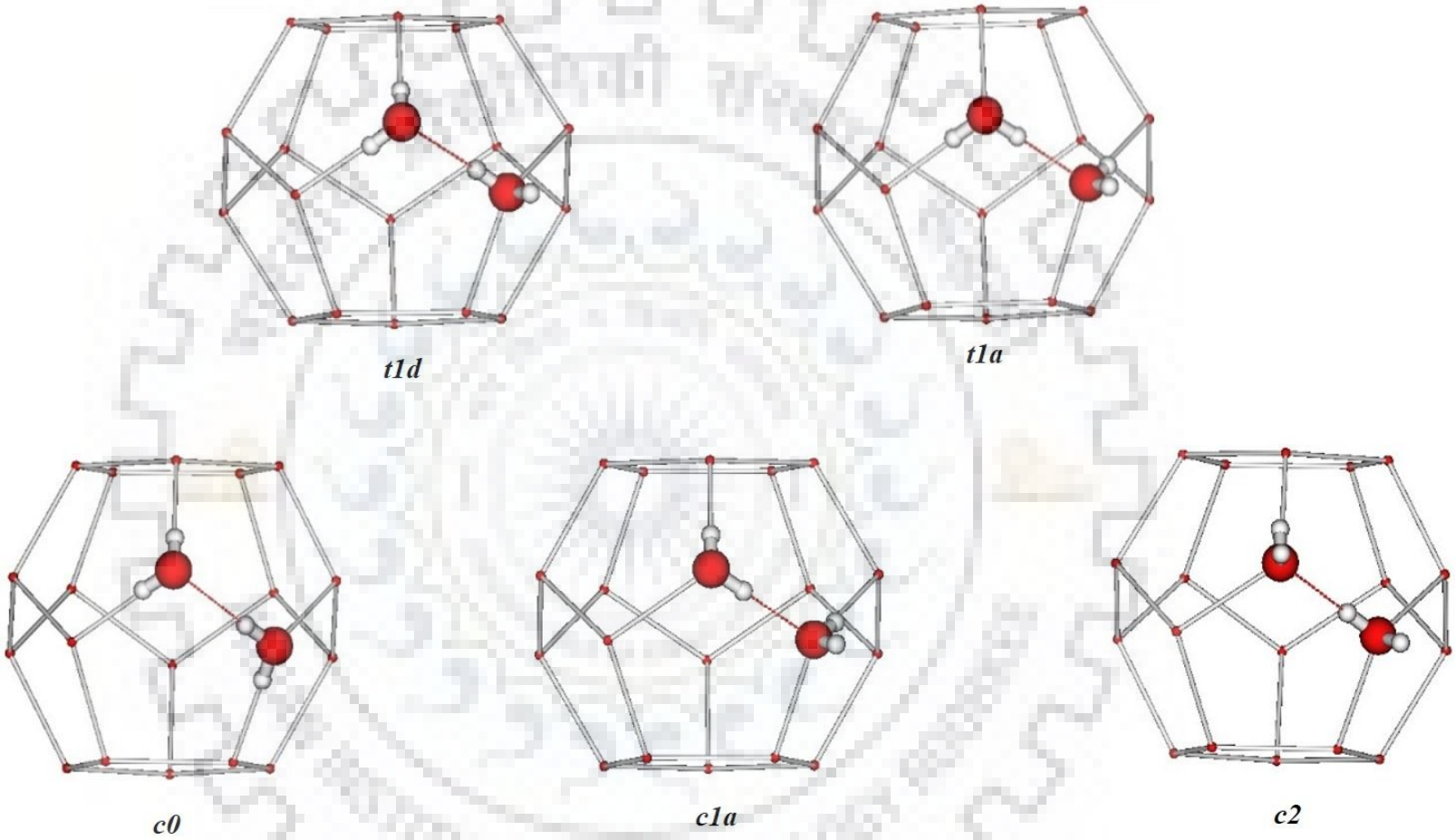

Figure 2.1 A pictorial representation of various types of hydrogen bonds in a dodecahedral water cage [197].

2.8 Modelling of single and fused host water cages

In the thesis, dodecahedral, irregular-dodecahedral, tetrakaidecahedral and hexakaidecahedral water cages are used as single host water cages for the molecular level studies on gas hydrates. The host water cages were modelled by using the concept of strong weak effective hydrogen bond model (SWEB) which is discussed above. The optimized minimum energy geometry of the above mentioned cages having maximum number of strong t*1d* hydrogen bonds is considered as host cages. The optimized minimum energy geometries of dodecahedral and irregular-dodecahedral, tetrakaidecahedral and hexakaidecahedral water cages are represented by the notation DD, IDD, TD and HD for further discussion in the thesis.

Furthermore, the concept of SWEB model is also extended for the modelling of fused water cages. The minimum energy single cage was considered as the initial geometry in the modelling of fused cages. For example, to model a fused-dodecahedral water cage with maximum number of t*1d* hydrogen bonds, two DD cages were fused through a five membered ring [197, 198]. For the modelling of fused-dodeca-irregular-dodecahedral water cages, fusion of DD and IDD cages was carried out by combination of a five membered ring. Same strategy was used in the modelling of fused-irregular-dodecahedral water cages. The optimized minimum energy fused cage geometries with maximum number of strong t*1d* hydrogen bonds are considered as host cages in the thesis. For further discussions, minimum energy geometries of fused-dodecahedral, fused-dodeca-irregular-dodecahedral and fused-irregular-dodecahedral are denoted as FDD, FDI and FII, respectively. Similarly, the minimum energy fused-dodeca-hexakaidecahedral cage (DD-HD) was modelled based on the SWEB model.

This concept is also used in the modelling of a triple-fused-dodecahedral water cage with a maximum number of 17 t*1d* hydrogen bonds. The optimized minimum energy geometry of triple-fused-dodecahedral water cage is represented as TFDD in the thesis.

Chapter-3
Binary hydrates of selected noble gas atoms

3.1 Introduction

Gas hydrates occur in different forms depending on the size and shape of guest molecules and achieve stability by hydrogen bond [199, 200] interactions between water molecules as well as van der Waals interactions between guest and host species. Studies have been done by many research groups about the stability of hydrates of various guest species [45, 201-207]. As the guests differ in their size, shape and polarity, the role of each of the above properties on the stability of gas hydrates is not well understood in the past [61, 67, 68, 208-210]. In this regard, the hydrates of noble gas atoms can serve as prototypes in the studies on the variation of interaction energy as a function of the size of guest species.

The research activities on noble gas hydrates got the attention for the first time after the discovery of argon hydrates by Villard *et al* in 1896 [211]. Later on, Londono *et al* showed that hydrates of helium in ice-II structure can be obtained by applying a pressure of 0.28-0.48 GPa on helium gas in water [212]. With the aid of differential thermal analysis, Dyadin *et al* investigated the formation of ice II clathrate hydrates of helium (He), neon (Ne), argon (Ar) and krypton (Kr) from the respective aqueous solutions [213]. Abbondondola *et al* [214] studied the rate of absorption of hydrogen, argon, and xenon into sII propane hydrate and found that hydrogen due to its smaller size diffuses more in the hydrates. In another study, the same research group reported that a mixture of xenon (Xe) and propane forms sII hydrate [215]. They also observed that the presence of Xe accelerates the formation of propane hydrate. Using the three phase coexisting curves for Kr and Xe hydrates, Sugahara *et al* investigated the thermodynamic stability boundaries of these hydrates up to a pressure of 445 MPa [216]. They observed that Kr hydrates undergo a structural transition from sII to sH around 414 MPa, in contrast to Xe hydrates (sI), for which any phase transition was not observed. Falently *et al* [217] studied the role of host-guest interaction on the stability of the hydrates and the limit of meta-stability of ice XVI structure by emptying Ne atoms from sII clathrate hydrates. Due to the presence of host-guest interactions in the hydrates, they observed a reduction in the volume of dodecahedral cages by 0.5% compared to that of a vacant cage. They reported that vacant structures possess negative thermal expansion due to the absence of host-guest interactions.

To study the influence of size of a guest atom on the stability of sI and sII hydrate structures of noble gas hydrates (He, Ne, Ar, Kr, and Xe), lattice dynamics simulations have also been performed [218]. These studies showed that the dodecahedral cage stabilizes the crystal structure with the inclusion of Ar or Kr atoms. With the help of molecular dynamic simulations, Alavi *et al* investigated the lattice parameters and the expansivities of rare gas sH clathrates at 760 MPa and 150 K [219]. Kumar *et al* [209] studied the host-guest interactions in the complexes formed between noble gas atoms and dodecahedral cage at MP2/6-31G* level of theory and found that, except Xe, all other rare gas atoms form stable complexes with dodecahedral cage. Mondal *et al* quantum mechanically studied the optimal occupancy of He, Ne, Ar and Kr inside dodecahedral and hexakaidecahedral cavities as well as in their respective HF doped analogues [220]. Their studies concluded that HF doping facilitates the encapsulation of noble gas atoms.

Although several studies have been carried out in the past to examine the role of host-guest interactions on the stability of noble gas hydrates, the interaction between noble gas atoms trapped in adjacent cages is not well discussed. In this regard, the study of hydrates of various noble gas species trapped in adjacent cages is of utmost important. Therefore, the encapsulation of a series of noble gas atoms inside dodecahedral (DD), fused-dodecahedral (FDD) and triple-fused-dodecahedral (TFDD) water cages is investigated in this chapter. The change in enthalpy (ΔH) and Gibbs free energy (ΔG) for the encapsulation of noble gas atoms in dodecahedral, fused-dodecahedral and triple-fused-dodecahedral cages are also studied at different temperature and pressure.

In gas hydrates, a dodecahedral cage is surrounded by the neighboring cages [1, 2, 11]. Thus, to make the study more realistic, the effect of adjacent cages is also considered. As noble gas hydrates form sII clathrates [218], a segment of sII unit cell in which central dodecahedral (DD) cage surrounded by six dodeca- and six hexakai- decahedral water cages is taken for this purpose. The effect of the size of a guest atom on the stability of hydrates as mentioned above is manifested in terms of host-guest interaction energy (E_{int}) as well as the interaction energy per guest species ($E_{int/guest}$).

3.2 Computational details

Geometry optimizations of all the systems were carried out using the Gaussian 09 program [221]. The dispersion corrected density functional B97-D along with cc-pVTZ basis set were used

for the calculations. The choice of the B97-D functional is justified based on its capability to account for the long range dispersion interactions present in the noble gas atoms with the host water cages [80]. The method and basis set used in the present work are well validated in earlier studies on similar complexes [61, 68, 80].

The maximum occupancy of two guest atoms were considered inside the dodecahedral cage, except for Ar and Kr, for which the cage disintegrated on encapsulating two such atoms. The optimized geometries of the complexes are depicted in figures 3.1-3.4. The notations G@DD and 2G@DD (G=He, Ne, Ar and Kr) are used for the complexes with one and two guest species encapsulated in dodecahedral cages, respectively. Similarly, the notations G@FDD and G@TFDD are used to represent the complexes of fused and triple-fused dodecahedral cages, respectively. Further, the complexes of fused cages with filled and empty cavities are denoted by the subscripts 1 and 0, respectively. For example, $G_{1\text{-}0}$@FDD indicates that the guest atom is encapsulated in one of the dodecahedral cages, when the other cage is empty. A similar notation is used for the complexes of triple fused dodecahedral cage. The complexes of mixed noble gas hydrates which are formed by encapsulating different noble gas atoms (G and G') in the neighboring cages are also examined in this chapter. The notation $(G)_{DD}(G')_{DD}$@FDD is used to represent such complexes.

To model the host water cages in which the central dodecahedral cage is surrounded by other cages, initial positions of the oxygen atoms were taken from the X-ray diffraction results reported by McMullan *et al*. [222]. In this structure, the dodecahedral cage present at the center has six dodecahedral and six hexakaidecahedral cages in its neighborhood. The orientation of hydrogen atoms of the central dodecahedral cage was kept similar to the most stable dodecahedral cage mentioned above for the comparison of the results. The hydrogen atoms were added to the surrounding water cages by following the Burner-Fowler rule [223]. The optimized geometry of this structure, in which the central cage possesses seven strong hydrogen bonds, is designated hereafter as $DD_{surrounded}$. The optimized geometries of these structures are given in figure 3.4. The notation G@DD-surrounded is used to represent the presence of a guest inside the central dodecahedral cage.

The stabilization energy due to encapsulation (E_{stab}) of guest molecules (He, Ne, Ar and Kr) inside the cages is calculated using the expression

$$E_{stab} = E_{complex} - E_{cage} - m \times E_{guest} \quad (3.1)$$

where, $E_{complex}$, E_{H_2O} and E_{guest} are the energies of the complex, water molecule and the guest species, respectively. The stabilization energy of the complex (E_{stab}), which is the difference in energy between the complex and the sum of the energies of free components, is given in table 3.1.

The interaction energy (E_{int}) between the guests and the host cage is calculated using the expressions

$$E_{int} = E_{complex} - E_{cage\ as\ in\ complex} - m \times E_{guest\ as\ in\ complex} \quad (3.2)$$

where $E_{complex}$ is the energy of the complex, $E_{cage\ as\ in\ complex}$ and $E_{guest\ as\ in\ complex}$ are energies of the cage and the guest species using the respective geometries in the optimized complex. The interaction energies are further corrected for basis set superposition error (BSSE) using the counterpoise method proposed by Boys and Bernardi [224]. As the present study involves the complexes with more than one guest atoms, the interaction energy per guest ($E_{int/guest}$) is also calculated and is given in table 3.2. The frequency calculations were performed for the optimized geometries of the cages and the complexes of dodecahedral, fused-dodecahedral and triple-fused-dodecahedral cages to confirm that the optimized geometries correspond to minima in the respective potential energy surface.

3.3 Results and discussion

3.3.1 Stabilization energy (E_{stab})

The water molecules of the host cages are hydrogen bonded, whereas the cage and the guest species are held together by van der Waals interactions leading to the stabilization of the complex. From table 3.1, it can be seen that the stabilization energy is higher for the encapsulation of large guest species. The values of E_{stab} obtained in the present study for G@DD and 2G@DD complexes are also compared with the values reported earlier [209, 220]. The results are in qualitative agreement with the results reported independently by Chattaraj *et al* [220] and Kumar *et al* [209], suggesting an increase in the stabilization energy with an increase in the size of the guest atom.

Considering the encapsulation of guest atoms in the neighboring cavities, the interaction between the guest molecules present in the adjacent cavities are analyzed in terms of interaction energy and interaction energy per guest molecule rather than the stabilization energy and are discussed below.

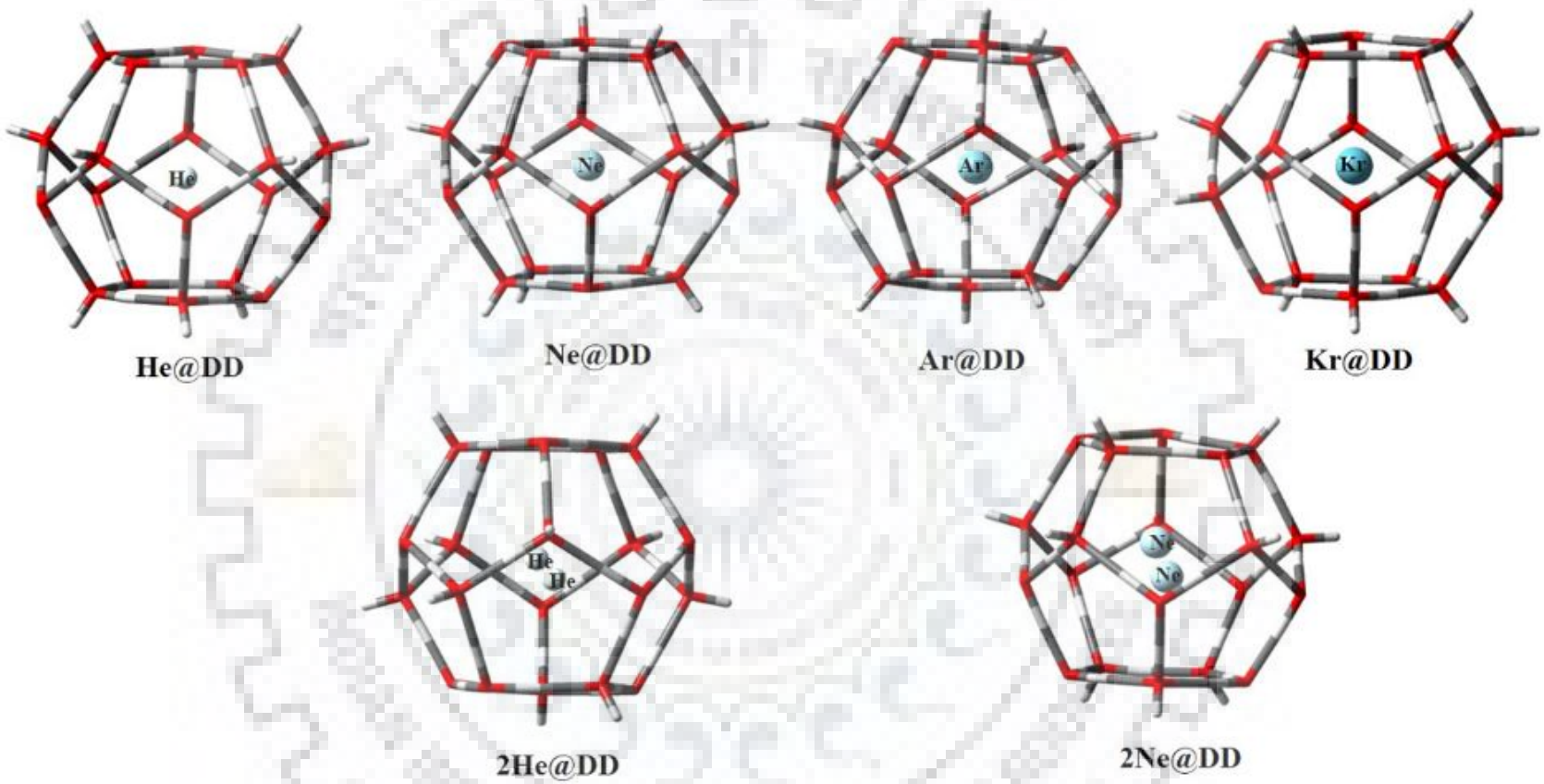

Figure 3.1. Optimized geometries of the complexes G@DD and 2G@DD for various noble gas species obtained at B97-D/cc-pVTZ level. The water cage and the guests are shown using wire-frame and ball-stick models, respectively.

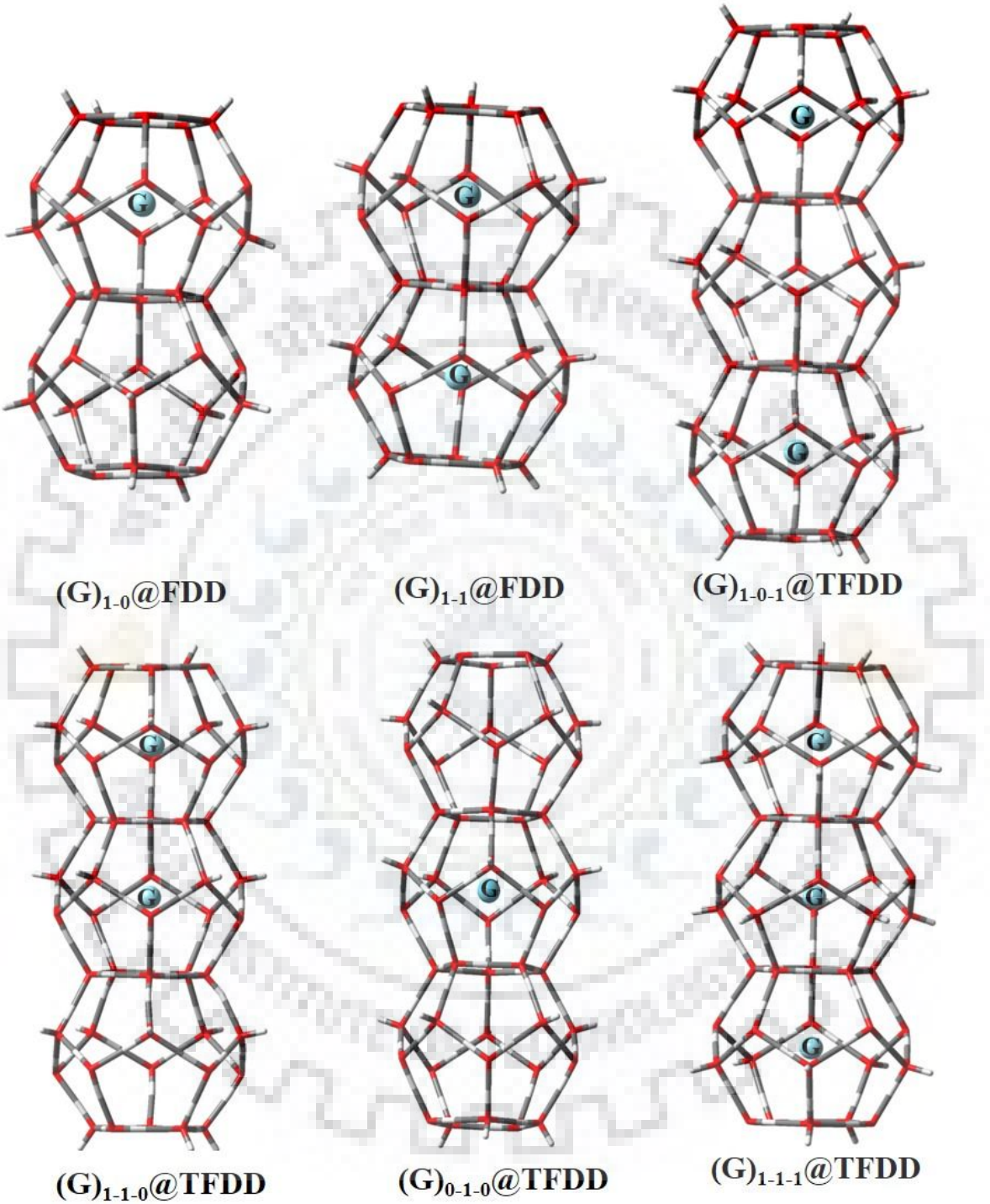

Figure 3.2. The pictorial representations of the optimized geometries of the complexes $G_{1\text{-}0}$@FDD, $G_{1\text{-}1}$@FDD, $G_{1\text{-}0\text{-}1}$@TFDD, $G_{1\text{-}1\text{-}0}$@TFDD, $G_{0\text{-}1\text{-}0}$@TFDD and $G_{1\text{-}1\text{-}1}$@TFDD (where G=He, Ne, Ar or Kr) for various guests obtained at B97-D/cc-pVTZ level.

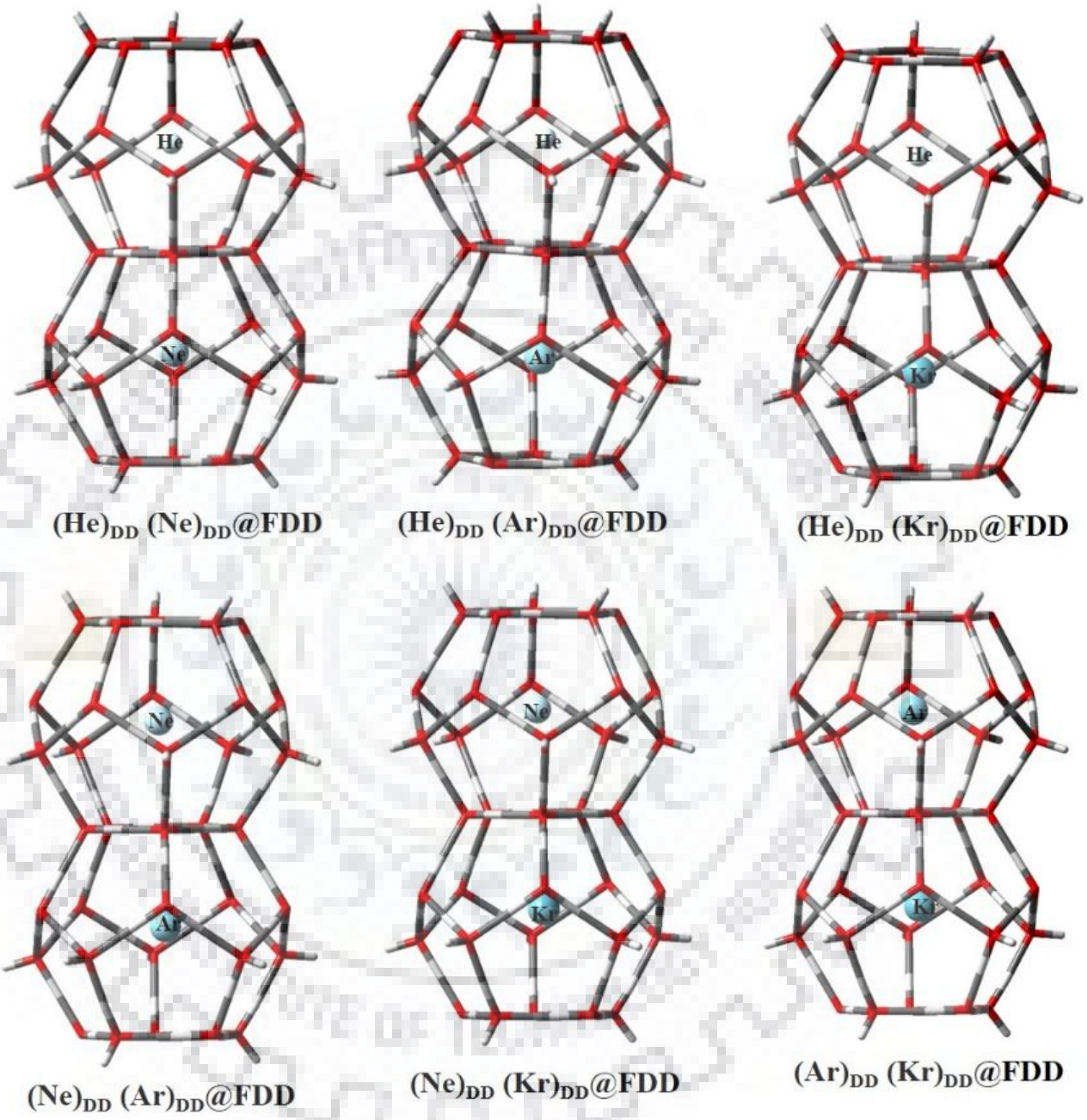

Figure 3.3 Optimized geometries of the complexes $(G)_{DD}(G')_{DD}$@FDD for various noble gas species obtained at B97-D/cc-pVTZ level.

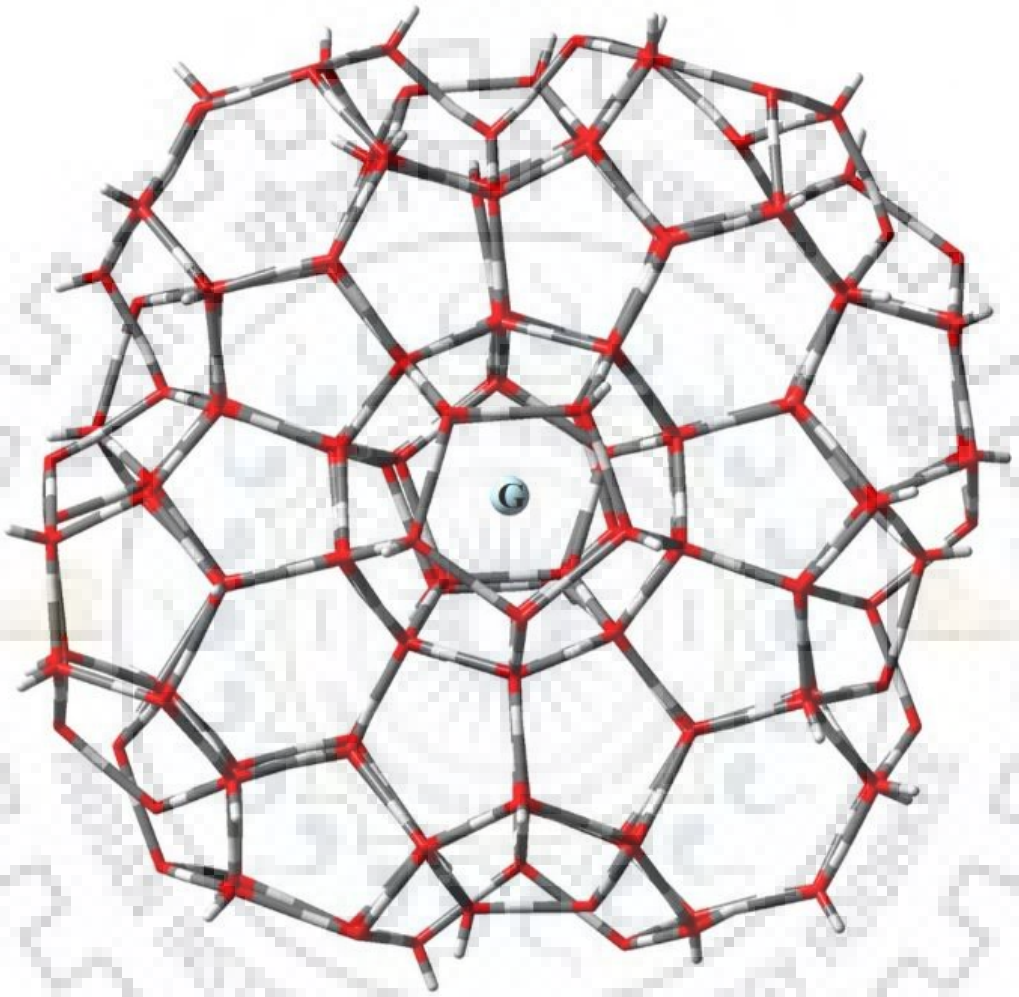

Figure 3.4. The pictorial representation of the optimized geometries of the complexes of G@DD-surrounded (where G=He, Ne, Ar or Kr) obtained at B97-D/cc-pVTZ level.

3.3.2 Host-guest interaction energy (E_{int})

As mentioned earlier, in order to assess the stability of the complexes, interaction energy between the guest and the host species (E_{int}) was calculated and are analyzed.

3.3.2.1 Effect of the size of guest

The host-guest interaction energies (E_{int}) for the complexes G@DD with and without BSSE corrections are listed in table 3.2. For the complex He@DD, the value of E_{int} is -0.75 kcal/mol. It can be seen from the table that the value of E_{int} for He@DD is the lowest which is due to the small size of helium that causes less interaction between the guest and the water molecules of the host cage. The host-guest interaction energy increases while moving from Ne to Ar to Kr. The highest value of E_{int} is obtained for the complex Kr@DD. The value of interaction energy for the complex Kr@DD is -4.03 kcal/mol, which is 1.42 kcal/mol higher than that of Ar@DD.

Thus, it can be concluded from the table that the values of E_{int} follow the order: He@DD < Ne@DD < Ar@DD < Kr@DD indicating that the interaction between host and guest molecules increases with an increase in the size of guest atom. This observation is in agreement with the previously reported quantum mechanical [220] and lattice dynamic simulation studies [218]. The above order in interaction energy can be explained based on the van der Waals radii of the noble gas atoms trapped inside the dodecahedral cavity. For this purpose, the interaction energy is plotted as a function of van der Waals radii of the guest species and is shown in figure 3.5. From the figure, it is clear that the interaction energy is increased with an increase in the size of guest atom as the latter enhances the attractive interactions between the host and the guest.

To get insight about the effect of multiple occupancy on the host-guest interaction energy, the $E_{int/guest}$ for the complexes 2G@DD is also calculated and is listed in table 3.2. It can be seen that the BSSE corrected $E_{int/guest}$ values for the complexes 2He@DD and 2Ne@DD are 0.17 and 5.74 kcal/mol, respectively, suggesting that the encapsulation of a second atom inside a DD cage is not energetically favorable. The study also showed a high repulsion between the guests when two Ar or Kr atoms are encapsulated inside a DD cage leading to the disintegration of the host cage.

3.3.2.2 Effect of an adjacent cage and the presence of a guest in the neighboring cavity

To study the interactions of a guest atom with the neighboring cavity and its interactions with the guest species residing in the neighboring cage, the interaction energy per guest molecule ($E_{int/guest}$) was calculated for various complexes and are listed in table 3.2. It can be seen from the table that the value of $E_{int/guest}$ for He@DD and $(He)_{1-0}$@FDD is -0.75 kcal/mol. This indicates that the presence of a neighboring cavity has no effect on the interaction between encapsulated He and its host cage. The lack of significant interaction in the above case is understandable, due to the small size of He atom which is far from water molecules of the cage. The interaction energy per guest for Ne@DD and Ar@DD is increased slightly in their respective fused cages, although the difference is not significant. The values of $E_{int/guest}$ for the complexes Kr@DD, and $(Kr)_{1-0}$@FDD are -4.03 and -4.11 kcal/mol, respectively. Although the change in interaction energy is nominal, there is a steady increase in the interaction energy with the size of guest species.

To know more about the interactions between the guest species of neighboring cavity, $E_{int/guest}$ is calculated for the complexes G@DD, $(G)_{1-1}$@FDD and $(G)_{1-1-1}$@TFDD and is listed in table 3.2. From the values of $E_{int/guest}$, it is clear that the interaction between the guest species is not significant for small species, as expected. Thus, the interaction between two helium, neon or argon atoms encapsulated in the adjacent cavities is very unlikely to occur, however, possible between two Kr atoms trapped in adjacent cages. The values of $E_{int/guest}$ for Kr@DD and $(Kr)_{1-1}$@FDD are -4.03 and -4.15 kcal/mol, respectively, suggesting that the presence of Kr atom in the neighboring dodecahedral cavities further stabilizes the complex. For $(Kr)_{1-1-1}$@TFDD, the $E_{int/guest}$ is increased to -4.31 kcal/mol. From the above discussion, it can be concluded that the size of guest atom plays an important role in the stabilization of the complex. The values of $E_{int/guest}$ for the complexes $(G)_{1-0-1}$@TFDD and $(G)_{1-1-0}$@TFDD listed in the table, unequivocally confirm that the interaction between the guest species of two adjacent cages and the interactions of guest species with water molecules of neighboring cages are appreciable only for large noble gas atoms.

To know more about the host-guest interactions, the interaction energy for the complexes of DD cage surrounded by other water cages is also calculated. The values of $E_{int/guest}$ for these complexes are also listed in table 3.2. From the table, one can see that in most of the cases, presence of neighboring cages has little effect on the interactions between the guests as well as that between the guest and the host cage. The change is noticeable only when the size of the guest is considerable.

For example, the values of E_{int} for Ar@DD, $(Ar)_{0\text{-}1\text{-}0}$@TFDD and Ar@DD-surrounded are -2.61, -2.68 and -3.04 kcal/mol, respectively.

The slight increase in the interaction energy for the complexes $(Ar)_{0\text{-}1\text{-}0}$@TFDD and Ar@DD-surrounded compared to Ar@DD can be attributed to two factors, *viz.*, the decrease in the diameter of the central cage in presence of other cages and also to the interaction of the guest species with water molecules beyond the first solvation shell. The slight contraction of the dodecahedral cavity in presence of neighboring cages may lead to more attraction between the guest and the host cage.

To assess the role of water molecules connected to the host dodecahedral cage (*i.e.* role of water molecules beyond the first solvation shell of the guest) in the interaction energy, the interaction energy is calculated for the complexes having more solvation shells. For this purpose, two different types of complexes are formed from the optimized geometry of G@DD-surrounded. This was done by retaining the second and third solvation shells without further optimization of the complexes. The above complexes are illustrated in figure 3.6 and the interaction energy obtained for these complexes are listed in table 3.3. From the values of interaction energy, it can be concluded that the interaction between guest species and water molecules beyond the first solvation shell is considerable only for large guest species. For example, in the case of complexes formed by the encapsulation of krypton inside DD cage, the value of E_{int} is increased up to 0.6 kcal/mol for the complexes with second and third solvation shell.

To know about the stability of mixed noble gas hydrates, complexes of the type $(G)_{DD}(G')_{DD}$@FDD are studied. The E_{int} for various mixed noble gas hydrates obtained is given in table 3.4. The interaction energy of $(G)_{DD}(G')_{DD}$@FDD is compared with that of $(G)_{1\text{-}1}$@FDD complexes. The BSSE corrected value of interaction energy for the complex $(Kr)_{1\text{-}1}$@FDD is -8.29 kcal/mol and is found be the highest value among all the studied complexes. However, for the complex $(Ar)_{DD}(Kr)_{DD}$@FDD, where Ar and Kr are encapsulated in adjacent cages, the interaction energy is reduced by ~1.5 kcal/mol compared to that for the complex $(Kr)_{1\text{-}1}$@FDD. Further reduction of 0.34 kcal/mol is observed in the value of interaction energy for the complex $(Ne)_{DD}(Kr)_{DD}$@FDD. Thus, it can be concluded from the above discussion that krypton atom residing in one of the cavities of a fused cage complex prefers to have a guest atom of larger size in its neighboring cavity. Similar results are also observed for other noble gas complexes.

Table 3.1 The values of stabilization energy (E_{stab}) for various complexes obtained at B97-D/cc-pVTZ level. The BSSE corrected energies are given in bold letters. All energies are in kcal/mol.

Energies	Guest	G@ DD	$G_{1\text{-}0}$@ FDD	$G_{1\text{-}1}$@ FDD	$G_{1\text{-}0\text{-}1}$@ TFDD	$G_{1\text{-}1\text{-}0}$@ TFDD	$G_{1\text{-}1\text{-}1}$@ TFDD	2G@ DD	G@ DD-surrounded
E_{stab}	He	-1.17 **-0.74** **-0.62**[a] **-0.01**[b]	-1.16 **-0.75**	-2.36 **-1.50**	-2.37 **-1.52**	-2.39 **-1.55**	-3.55 **-2.30**	-0.54 **0.63** **0.52**[a]	-1.17 **-0.75**
	Ne	-4.29 **-2.37** **-2.63**[a] **-1.52**[b]	-4.39 **-2.42**	-8.80 **-4.84**	-8.82 **-4.87**	-8.94 **-4.91**	-13.30 **-7.33**	-4.72 **1.04** **1.23**[a]	-4.73 **-2.57**
	Ar	-4.89 **-2.63** **-2.59**[a] **-3.03**[b]	-4.75 **-2.58**	-9.54 **-5.23**	-9.54 **-5.27**	-9.36 **-5.33**	-14.10 **-7.93**	---	-4.92 **-3.04**
	Kr	-6.92 **-4.02** **-9.59**[b]	-6.87 **-4.09**	-13.70 **-8.29**	-13.60 **-8.28**	-13.40 **-8.45**	-20.30 **-12.90**	---	-6.99 **-4.53**

Ref [a][220], [b][209].

Table 3.2 The values of interaction energy (E_{int}) and interaction energy per guest ($E_{int/guest}$) for various complexes obtained at B97-D/cc-pVTZ level. The BSSE corrected energies are given in bold. All energies are in kcal/mol.

	Guest	G@ DD	$(G)_{1\text{-}0}$@ FDD	$(G)_{1\text{-}1}$@ FDD	$(G)_{0\text{-}1\text{-}0}$@ TFDD	$(G)_{1\text{-}0\text{-}1}$@ TFDD	$(G)_{1\text{-}1\text{-}0}$@ TFDD	$(G)_{1\text{-}1\text{-}1}$@ TFDD	2G@ DD	G@ DD-surrounded
E_{int}	He	-1.18	-1.17	-2.37	-1.17	-2.37	-2.37	-3.54	-1.00	-1.21
		-0.75	**-0.75**	**-1.52**	**-0.76**	**-1.52**	**-1.53**	**-2.28**	**0.17**	**-0.79**
	Ne	-4.32	-4.42	-8.86	-4.51	-8.85	-8.95	-13.40	-0.01	-4.70
		-2.40	**-2.45**	**-4.90**	**-2.47**	**-4.90**	**-4.92**	**-7.37**	**5.74**	**-2.57**
	Ar	-4.86	-4.81	-9.62	-4.29	-9.60	-9.42	-14.20	----	-4.90
		-2.61	**-2.64**	**-5.30**	**-2.68**	**-5.32**	**-5.34**	**-8.03**		**-3.04**
	Kr	-6.93	-6.89	-13.7	-6.67	-13.70	-13.50	-20.3	----	-6.71
		-4.03	**-4.11**	**-8.29**	**-4.35**	**-8.36**	**-8.54**	**-12.93**		**-4.84**
$E_{int/guest}$	He	**-0.75**	**-0.75**	**-0.76**	**-0.76**	**-0.76**	**-0.76**	**-0.76**	**0.09**	**-0.79**
	Ne	**-2.40**	**-2.45**	**-2.45**	**-2.47**	**-2.45**	**-2.46**	**-2.46**	**2.87**	**-2.57**
	Ar	**-2.61**	**-2.64**	**-2.65**	**-2.68**	**-2.66**	**-2.67**	**-2.68**	**----**	**-3.04**
	Kr	**-4.03**	**-4.11**	**-4.15**	**-4.35**	**-4.18**	**-4.27**	**-4.31**	**----**	**-4.84**

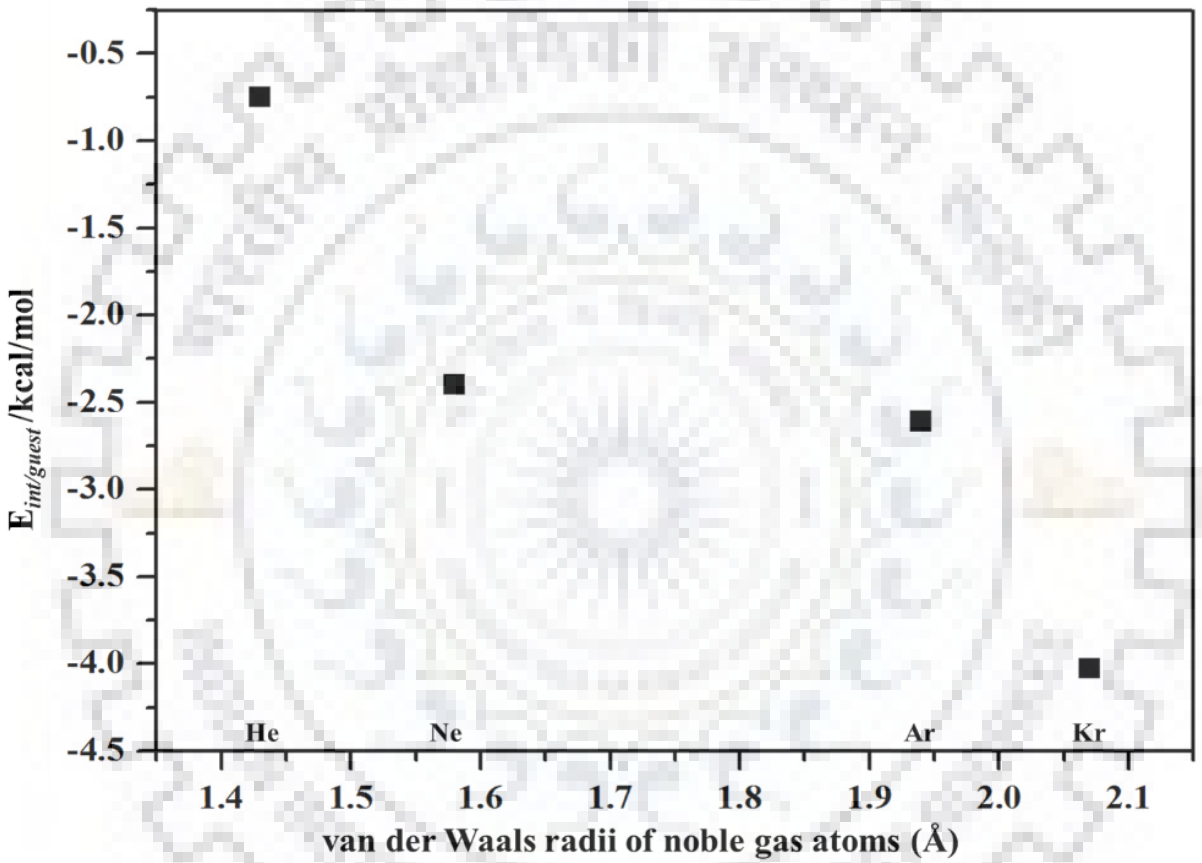

Figure 3.5. Interaction energy per guest molecule ($E_{int/guest}$) as a function of van der Waals radii of the guest atoms for the complexes G@DD. The van der Waals radii of noble gas atoms are taken from reference [225].

Table 3.3 The values of interaction energy (E_{int}) obtained at B97-D/cc-pVTZ level for various complexes in the absence and presence of water molecules attached to the dodecahedral cage. The BSSE corrected energies are given in bold. All energies are in kcal/mol.

Guest	G@DD$_{\text{without solvation shell}}$	G@DD$_{\text{with first solvation shell}}$	G@DD$_{\text{with second solvation shell}}$
He	-1.18	-1.18	-1.18
	-0.74	**-0.75**	**-0.77**
Ne	-4.31	-4.44	-4.65
	-2.40	**-2.47**	**-2.51**
Ar	-4.85	-4.63	-4.68
	-2.61	**-2.68**	**-2.85**
Kr	-6.93	-6.34	-6.48
	-4.03	**-4.35**	**-4.59**

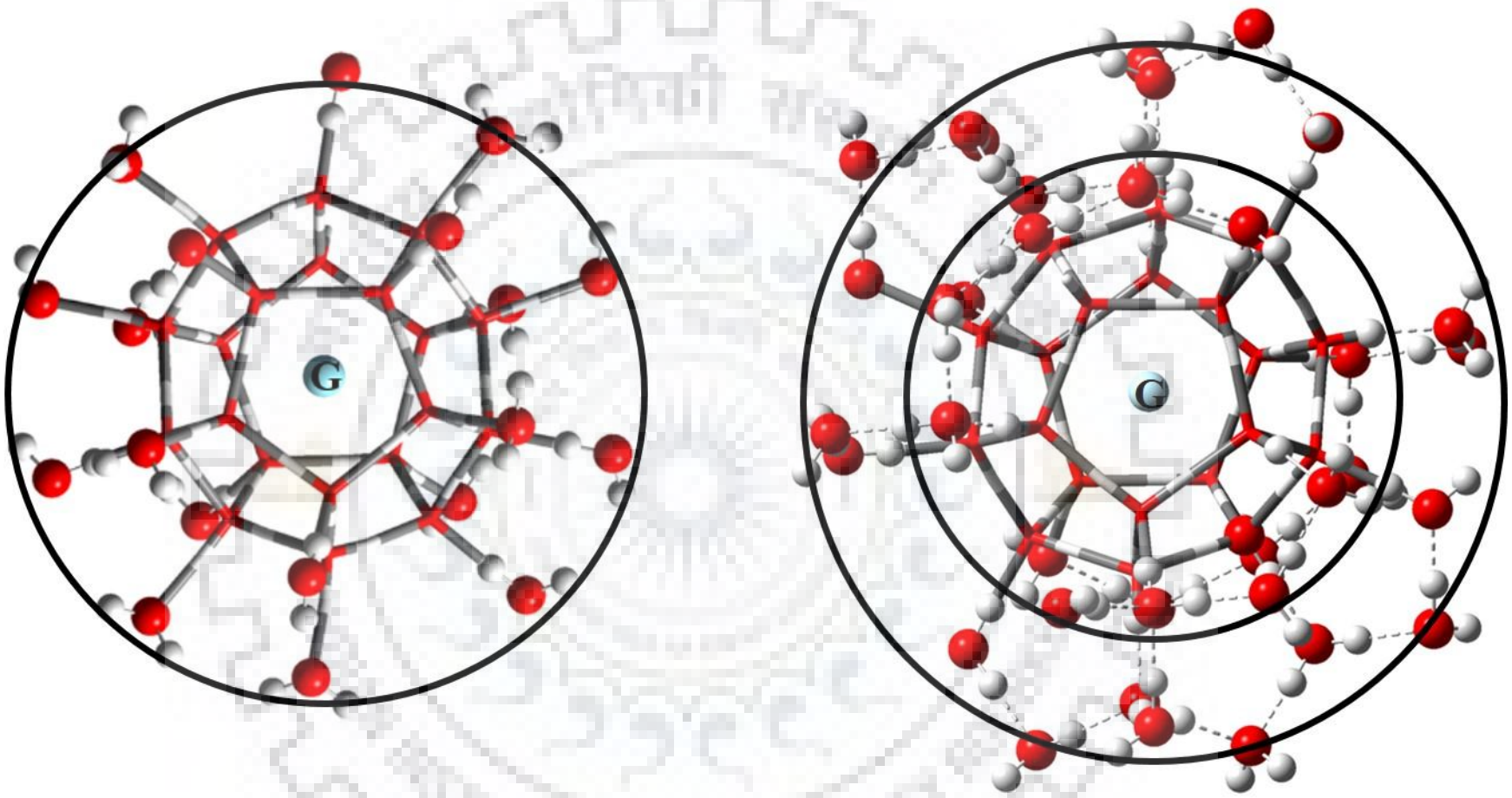

Figure 3.6 The pictorial representation of the geometries of the G@DD complexes (G=He, Ne, Ar or Kr) with (a) water molecules of the first and (b) second solvation shells around the cage. The water molecules belonging to the solvation shells are shown in ball and stick models and the water molecules of the central cage are shown in stick model.

Table 3.4 The values of interaction energy (E_{int}) for various mixed noble gas hydrates obtained at B97-D/cc-pVTZ level. The BSSE corrected energies are given in bold. All energies are in kcal/mol.

	Guest (G)	Guest' (G')	$(G)_{DD}(G')_{DD}$@FDD
E_{int}	He	Ne	-5.61 **(-3.20)**
		Ar	-5.99 **(-3.40)**
		Kr	-8.00 **(-4.91)**
	Ne	Ar	-9.24 **(-5.08)**
		Kr	-11.30 **(-6.56)**
	Ar	Kr	-11.70 **(-6.83)**

Comparison of the interaction energy of $(G)_{DD}(G')_{DD}$@FDD with that of the complexes $(G)_{1\text{-}1}$@FDD showed that the interaction energy follows the order: $(Kr)_{1\text{-}1}$@FDD > $(Ar)_{DD}(Kr)_{DD}$@FDD> $(Ne)_{DD}(Kr)_{DD}$@FDD > $(Ar)_{1\text{-}1}$@FDD> $(Ne)_{DD}(Ar)_{DD}$@FDD > $(He)_{DD}(Kr)_{DD}$@FDD > $(Ne)_{1\text{-}1}$@FDD > $(He)_{DD}(Ar)_{DD}$@FDD > $(He)_{DD}(Ne)_{DD}$@FDD > $(He)_{1\text{-}1}$@FDD. Thus, it is evident that the presence of a guest atom in one of the cavities prefers another noble gas atom of larger size in the neighboring cavity.

3.3.3 Thermodynamics of encapsulation

To infer about the feasibility of encapsulation of noble gas atoms inside the cages, changes in enthalpy (ΔH) and Gibb's free energy (ΔG) of encapsulation are calculated for single and fused cage complexes at a wide range of temperatures and pressures [226] comparable to the experimental conditions [216, 227, 228]. The values of ΔH (ΔG) are calculated as the difference in the enthalpy (Gibbs free energy) of the complex and the sum of the enthalpy (Gibbs free energy) of the components in their free states. The change in Gibbs free energy of the complex at different pressure is determined using the Gibbs Helmholtz expression

$$\Delta G' = G(P_2) - G(P_1) = RTln(P_2/P_1) \quad (3.3)$$

where $G(P_2)$ and $G(P_1)$ are the values of Gibbs free energy at pressure P_1 and P_2 for a given temperature T.

3.3.3.1 Effect of size of the guest

The enthalpy change associated with the encapsulation of various noble gas atoms in the dodecahedral cavity is calculated for different temperatures and is listed in table 3.5. It can be seen from the table that the change in enthalpy is negative for all complexes, suggesting that the encapsulation of noble gas atoms inside a dodecahedral cage is an exothermic process. This is in agreement with the results reported by Mondal *et al* [220]. It can be also seen that the value of ΔH is more negative for a large atom. For example, at T=180 K, the change in enthalpy of various complexes follows the order: He@DD < Ne@DD < Ar@DD < Kr@DD. The above trend remains the same at higher temperatures (T=298, 260, 240, 220 and 200 K) as well. It is also evident from the table that, for a given noble gas atom, the magnitude of ΔH decreases insignificantly with an increase in temperature. For example, for the complex Kr@DD, the value of ΔH showed a decrease of only ~0.08 kcal/mol when the temperature is increased from 180 to 298 K. This difference is negligible for the atoms of size smaller than Kr when they are confined in the cavity of a DD cage.

Table 3.5 The change in enthalpy due to encapsulation (ΔH) for various complexes obtained at B97-D/cc-pVTZ level at different temperatures. The values are in kcal/mol.

Complexes	180K	200K	220K	240K	260K	298K
He@DD	-0.97	-0.96	-0.93	-0.91	-0.89	-0.86
Ne@DD	-4.03	-4.02	-4.01	-4.01	-3.98	-3.97
Ar@DD	-4.33	-4.32	-4.31	-4.30	-4.29	-4.27
Kr@DD	-6.53	-6.52	-6.51	-6.49	-6.48	-6.45

3.3.3.2 Effect of temperature and pressure

In order to study the feasibility of formation of these complexes, the change in Gibbs free energy (ΔG) is calculated for different temperature and pressure and is listed in table 3.6. The effect of temperature and pressure on Gibbs free energy associated with the encapsulation of noble gas atoms is also depicted in the form of graphs. The effect of temperature on ΔG for the complexes G@DD for a range of pressures is shown in figure 3.7. As expected, the value of ΔG becomes more negative on decreasing the temperature as reflected from the values given in the table. For example, the value of ΔG for Kr@DD shows an increase from -1.00 to -3.20 kcal/mol as the temperature decreases from 298 K to 180 K for 1 atm pressure. An analysis of the values of ΔG indicates that the formation of the complex He@DD is thermodynamically not feasible even at 180 K, although the formations of complexes Ne@DD and Ar@DD are feasible at 180 K and 1 atmospheric pressure.

Further, to infer about the effect of pressure on the feasibility of encapsulation, the value of ΔG is also determined for a range of pressure. From the values of ΔG listed in table 3.6, it can be seen that ΔG for the complex He@DD is positive even at a pressure of 150 atm at 180 K suggesting that the encapsulation of He inside a dodecahedral cage is not thermodynamically feasible. On the other hand, Ne, Ar and Kr form stable complexes with the dodecahedral water cages on applying a pressure of ~100 atm at ambient temperatures (260-298 K).

3.3.3.3 Effect of an adjacent cage and guest species in a neighboring cavity

In order to know how the presence of a neighboring cage and the guest in that affects the thermochemical parameters of encapsulation of noble gas atoms, the values of ΔH and ΔG for the complexes $(G)_{1\text{-}0}$@FDD and $(G)_{1\text{-}1}$@FDD at a temperature of 180 K and a pressure of 1 atm are calculated. From table 3.7, it can be seen that the enthalpy of encapsulation does not change considerably due to the presence of an adjacent cavity. It also holds true for the free energy change associated with the encapsulation. Thus, it is clear that neither a neighboring cage nor the guest atom in that affects the thermochemical parameters associated with the encapsulation of noble gas atom in a dodecahedral water cage.

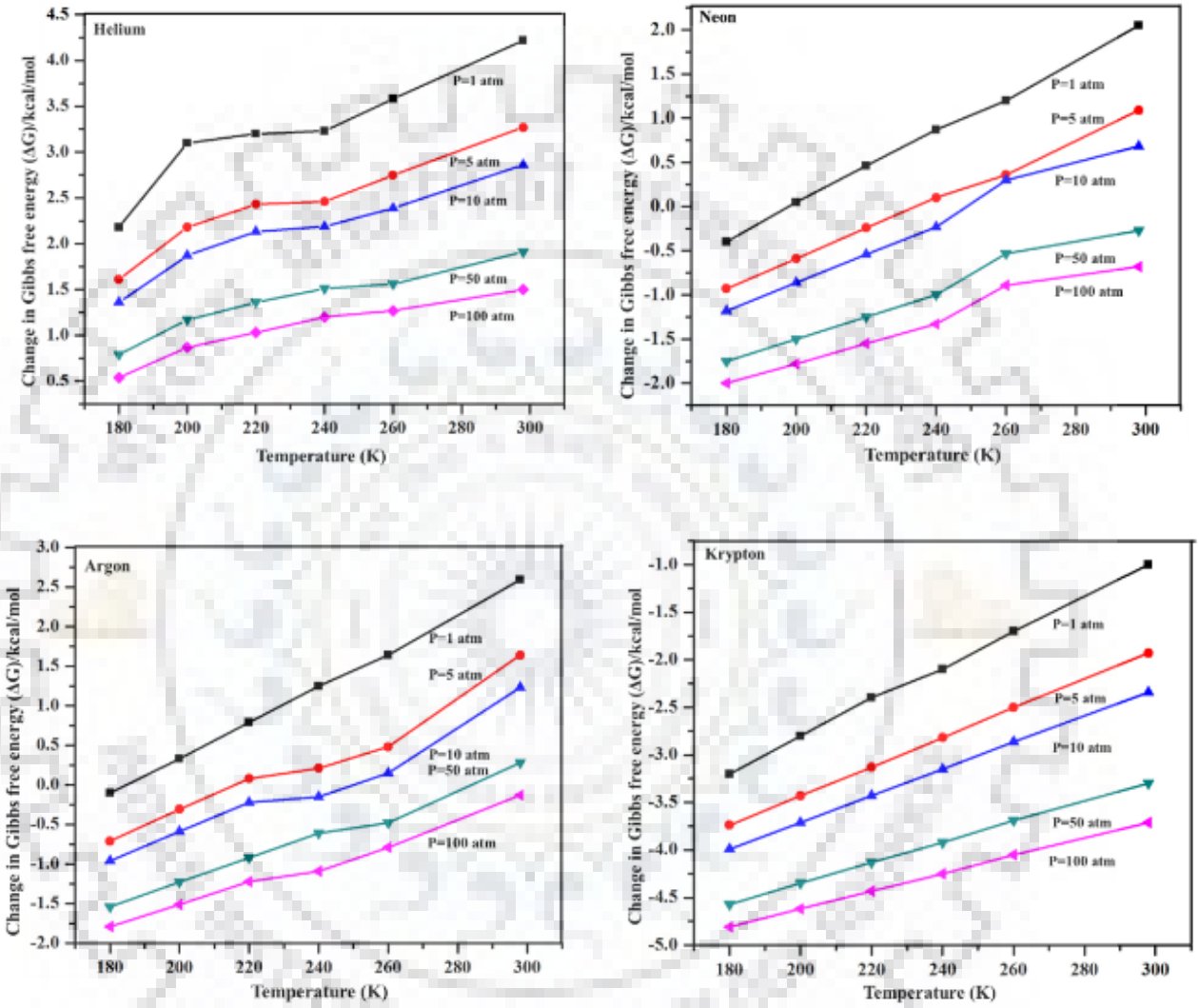

Figure 3.7 The change in the values of Gibbs free energy associated with the encapsulation of noble gas atoms for the complexes G@DD obtained at different temperature and pressure.

Table 3.6. The values of change in Gibbs free energy due to encapsulation (ΔG) in kcal/mol at different temperature (T) and pressure (P) for various complexes obtained at B97-D/cc-pVTZ level. The values are in kcal/mol.

Complexes	Pressure	T=180K	T=200K	T=220K	T=240K	T=260K	T=298K
He@DD	P=1	2.18	3.10	3.20	3.23	3.58	4.22
Ne@DD		-0.40	0.05	0.46	0.87	1.20	2.05
Ar@DD		-0.10	0.33	0.79	1.25	1.64	2.59
Kr@DD		-3.20	-2.80	-2.40	-2.10	-1.70	-1.00
He@DD	P=5	1.61	2.18	2.43	2.46	2.75	3.27
Ne@DD		-0.93	-0.59	-0.24	0.10	0.36	1.09
Ar@DD		-0.71	-0.31	0.08	0.21	0.48	1.64
Kr@DD		-3.74	-3.43	-3.13	-2.82	-2.50	-1.93
He@DD	P=10	1.36	1.87	2.13	2.19	2.39	2.86
Ne@DD		-1.18	-0.86	-0.54	-0.23	0.30	0.68
Ar@DD		-0.96	-0.59	-0.22	-0.15	0.15	1.23
Kr@DD		-3.99	-3.71	-3.43	-3.15	-2.86	-2.34
He@DD	P=50	0.79	1.17	1.36	1.51	1.56	1.91
Ne@DD		-1.75	-1.50	-1.25	-1.00	-0.53	-0.27
Ar@DD		-1.54	-1.23	-0.92	-0.61	-0.48	0.28
Kr@DD		-4.57	-4.35	-4.13	-3.92	-3.69	-3.30
He@DD	P=100	0.54	0.87	1.03	1.20	1.27	1.50
Ne@DD		-2.00	-1.78	-1.55	-1.33	-0.89	-0.68
Ar@DD		-1.79	-1.51	-1.22	-1.09	-0.79	-0.13
Kr@DD		-4.81	-4.62	-4.43	-4.25	-4.05	-3.71

Table 3.7 The values of change in enthalpy (ΔH) and Gibbs free energy (ΔG) due to encapsulation for various complexes at 180 K and 1 atm obtained at B97-D/cc-pVTZ level. The values are in kcal/mol.

Thermodynamic Parameter	Complexes	G@DD	$(G)_{1\text{-}0}$@FDD	$(G)_{1\text{-}1}$@FDD	$(G)_{0\text{-}1\text{-}0}$@TFDD
ΔH (kcal/mol)	He@DD	-0.97	-0.95	-0.96	-0.97
	Ne@DD	-4.03	-4.04	-4.03	-4.04
	Ar@DD	-4.33	-4.31	-4.34	-4.32
	Kr@DD	-6.53	-6.54	-6.53	-6.53
ΔG (kcal/mol)	He@DD	2.18	2.16	2.18	2.19
	Ne@DD	-0.40	-0.39	-0.41	-0.42
	Ar@DD	-0.10	-0.17	-0.17	-0.16
	Kr@DD	-3.20	-3.19	-3.19	-3.20

To confirm the above, thermodynamic parameters for the complexes of triple-fused-dodecahedral water cages of the type $(G)_{0\text{-}1\text{-}0}$@TFDD are also calculated. It was found that the ΔH and ΔG values obtained for $(G)_{0\text{-}1\text{-}0}$@TFDD are comparable to those obtained for the complexes G@DD and $(G)_{1\text{-}0}$@FDD. For example, the ΔH values for Kr@DD, $(Kr)_{1\text{-}0}$@DD and

$(Kr)_{0\text{-}1\text{-}0}$@TFDD are -6.53, -6.54 and -6.53 kcal/mol, respectively. Similarly, the ΔG values obtained for Kr@DD, $(Kr)_{1\text{-}0}$@DD and $(Kr)_{0\text{-}1\text{-}0}$@TFDD are -3.20, -3.19 and -3.20 kcal/mol, respectively, suggesting that the neighboring cages do not significantly affect the encapsulation of guest species in a cavity.

3.4 Conclusion

The interactions of encapsulated noble gas atoms with their single and fused dodecahedral host water cages were investigated employing the dispersion corrected B97-D functional with cc-pVTZ basis set. The study showed that the size of guest species plays an important role in the host-guest interaction. Thus, among the guest species He, Ne, Ar and Kr, interaction energy was found to vary in the order: He@DD < Ne@DD < Ar@DD < Kr@DD. The encapsulation of all types of noble gas atoms except helium inside the dodecahedral cages was found to be thermodynamically favorable. The minimum temperature and pressure required for the encapsulation of different guest species showed size dependency. Thus, the encapsulation of He inside a dodecahedral cage is very unlikely to occur at a temperature of 180 K and a pressure of 150 atmosphere, whereas, the encapsulation of Kr inside the dodecahedral cage is thermodynamically feasible at ambient conditions.

The studies on the interaction of guest species trapped in a cage surrounded by other water cages did not reveal any significant effect on the interaction between the guest and the surrounding water molecules, especially when the size of the guest is not very large. However, a consistent increase in interaction energy per guest species was observed with the successive addition of guest atoms in the cavities of a neighboring cage. This gradation in interaction energy was more prominent for the encapsulation of Kr. The values of interaction energy obtained for the mixed noble gas hydrates showed that the presence of a guest in one of the cavities favors a guest atom of larger size in the neighboring cavity. It was also revealed that the changes in enthalpy and Gibbs free energy associated with the encapsulation of noble gas atoms are independent of the presence of a neighboring cage or the guest atom present in that.

It should be mentioned that the temperature and pressure considered in the present study is far from the pressure at which the natural gas hydrates exist. However, there are several reports on the synthesis of gas hydrates including the noble gas hydrates in the laboratory at moderate temperature and pressure. It is believed that the present results about the feasibility of formation of the complexes of noble gas atoms with host water cages at moderate conditions will lead more experimental studies in the near future. Although the study is limited to dodecahedral water cages, the conclusions deduced here are not expected to change for other hydrate structures as well.

Chapter-4
Binary hydrates of H_2, CO_2 and CH_4

4.1 Introduction

The importance of quantum chemical studies to understand the host-guest interactions in the stability of hydrate structures was well discussed in the previous chapters. With the aid of quantum mechanical calculations, the encapsulation of mono-, di- and poly-atomic species in all types of water cages which constitute the structural motifs of gas hydrates has been investigated [61, 67, 68, 208, 209, 229]. It is known experimentally and theoretically that methane can be accommodated in small dodecahedral (5^{12}) as well as large tetrakaidecahedral cages ($5^{12}6^2$) [38, 68, 230]. On the other hand, the encapsulation of CO_2 preferably occurs in large cavities due to its substantial size [202, 206]. Multiple occupancies of small guest species in single water cages have been also reported [231].

The interactions between the host cage and the guest species govern the stability of their complexes. In most of the cases, van der Waals interactions stabilize the complex, albeit they are weak. Using MP2/6-31G** level of calculations, Kumar *et al* investigated the interactions of dodecahedral cage with a variety of guest species encapsulated and reported that the interaction energy between the guest species and the host cage depends on the size of the molecule trapped [209]. Using *ab initio* calculations taking Ne, N_2, CH_4 and C_2H_6 as guest species Arshad Khan reported that the stability of a tetrakaidecahedral cage depends on the size of the guest molecules [60].

The perturbation methods account for the dispersion interaction between a gas molecule and a host cage, however, they are computationally expensive and are not affordable for large systems such as gas hydrates. Density functional theoretical methods have been used by several research groups to study the structure and the stability of gas hydrates. For example, the stability of the complexes of CH_4 and CO_2 in dodecahedral water cage has been studied by Geng *et al* using the functional B3LYP in conjunction with 3-21G basis-set [119]. Using B3LYP/6-31G(d) level of calculations, Chattaraj *et al* studied the stability and reactivity of various water cages with and without the encapsulation of hydrogen molecules [231]. In the above studies, oxygen atoms of water molecules were fixed during optimization to avoid the deformation of the cages [119, 231]. To

consider the long range interactions present in natural gas hydrates, Liu *et al* used the dispersion corrected density functional method B97-D [69, 207].

Apart from the structure and the stability of gas hydrates, the spectroscopic properties of gas hydrates have been also investigated [61, 69 59, 62, 232-234]. The vibrational Raman spectroscopy has been suggested as a powerful tool to study the host-guest interactions present in gas hydrates. The vibrational Raman spectral properties of hydrogen in pure and tetrahydrofuran doped water cages using B97-D functional has been examined by Ramya *et al* [126, 235]. They observed that the vibrational frequencies of water molecules in mixed hydrates of H_2 and tetrahydrofuran (THF) in dodecahedral cage are shifted towards lower frequencies compared to those in pure hydrates of H_2. Ramya *et al* [80] examined the vibrational modes of small and large cavities of sI hydrates encapsulating methane molecules. They observed a red shift for the O-H stretching modes of water for the dodecahedral and hexakaidecahedral cages. Like the host cages, the spectral features of guest species have been also reported to be altered due to encapsulation. They observed a blue shift in the vibrational stretching frequencies of the hydrogen molecules with their multiple encapsulation in a single cavity. Using Raman spectroscopic techniques, Liu *et al* demonstrated that C-C stretching frequencies of hydrocarbons trapped inside the cavities of water cages shift to lower frequencies as the size of the cage increases [69].

The nuclear magnetic resonance (NMR) technique has been also reported to be a useful tool to investigate the structural properties of gas hydrates [232-234]. The ^{13}C NMR spectroscopic technique was used for the first time by Ripmeester *et al* to study the guest occupancies in gas hydrates [50]. Theoretical studies have been reported to predict the shielding constants for ^{1}H, ^{13}C and ^{17}O for CH_4 @DD and CH_4@TD at B3LYP/aug-cc-pVDZ level [234].

As mentioned earlier, several studies have been done in the past about the encapsulation of molecules inside various types of single cages, the encapsulation of guest molecules in fused water cages is not much available in literature [86]. It was shown in the previous chapter that the interactions between guest species residing in adjacent cavities depend on the size of the guest. For example, the interaction between two krypton atoms residing in adjacent cages cannot be neglected, and play a significant role in the stabilization of the hydrate structures. On the other hand, no such interaction was observed in the case of helium atoms. Guest molecules of different shape, size and polarizability result in the formation of different hydrate structures. This emphasizes the need for the further investigation to unravel the effect of both size as well as shape of the guest species in host-

guest and guest-guest interactions. Therefore, in this chapter, the encapsulation of different types of guest species inside the cavities of fused water cages is studied. For this purpose, molecules which differ in size and shape including diatomic (H_2), triatomic (CO_2) and polyatomic (CH_4) molecules are selected as guest species. The combinations of various types of fused cages *viz.* the fused dodecahedral (FDD), fused dodecahedral-irregular dodecahedral (FDI) and fused irregular dodecahedral-irregular dodecahedral (FII) water cages are considered as host cages in the present work.

In this chapter, the interactions between the guest molecules and the host water cages are analyzed in terms of host-guest interaction energy (E_{int}) and interaction energy per guest molecule ($E_{int/guest}$). The vibrational Raman spectra of the complexes of single and fused dodecahedral cages are simulated to study the effect of host-guest and guest-guest interactions on the vibrational frequencies of guest species. The nuclear magnetic resonance (NMR) chemical shifts for ^{1}H and ^{13}C nuclei of the guest molecules are computed in their free and encapsulated states to get more insight about the effect of confinement on the spectral features of these molecules.

4.2 Computational details

All the calculations were performed at B97-D/cc-pVTZ level of theory using the electronic structure program Gaussian 09 [221]. Selection of the functional B97-D was already justified in chapter 3. The encapsulation of up to two guest molecules is considered for all the single cages (DD, IDD, TD and HD). However, in the case of CO_2, the DD and IDD cages disintegrated upon the encapsulation of two molecules. The optimized geometries of water cages encapsulating the guest species are depicted as in figures 4.1-4.4. In the figures and in the subsequent sections of the manuscript, the notation H_2@DD is used to represent the complex formed by the encapsulation of one molecule of hydrogen inside the cage DD. Similarly, the notation $2H_2$@DD indicates the complex formed by the encapsulation of two hydrogen molecules inside a DD cage. The same strategy is used to denote the complexes of CO_2 and CH_4. Accordingly, the complexes formed by the encapsulation of one and two guest species inside the irregular dodecahedral (IDD) cage are represented by G@IDD and 2G@IDD, respectively, for various guest species considered (G = H_2, CO_2 and CH_4). The complexes formed by the encapsulation of one guest molecule in the cages TD and HD are denoted as G@TD and G@HD, respectively. For example, the complexe formed by the encapsulation of one hydrogen molecule inside a TD cage is denoted as H_2@TD. The notation $2H_2$@TD represents the complex formed by the encapsulation of two hydrogen molecules in the

cavity of a TD cage. Same strategy is used to represent the complexes formed by the single and double occupancy of CO_2 and CH_4 in the cavity of TD cage. Similarly, the complexes formed by the single and double occupancy of HD are denoted as G@HD and 2G@HD, respectively.

The fused cages can accommodate guest species in both cages. Although, the constituting cages are of similar type in FDD or FII, they are different in FDI. Thus, to represent the complexes of fused cages with one guest species, the type of cage in which the guest species located is given as a subscript. The notations $(H_2)_{DD}$@FDI and $(H_2)_{IDD}$@FDI represent the complexes of FDI in which one molecule of H_2 is located in DD and IDD cages, respectively. For consistency, a similar strategy is followed to represent the complexes of FDD and FII with one guest molecule. Therefore, $(H_2)_{DD}$@FDD and $(H_2)_{IDD}$@FII represent the complexes of FDD and FII, respectively, encapsulating one molecule of H_2 in one of the constituent cages. Similar notations are also used for the complexes formed by the encapsulation of single CO_2 and CH_4 molecule in one of the cavities of FDD, FDI and FII cages.

The present chapter also discusses the complexes formed by the encapsulation of guest species in both cages of the fused system to study the effect of neighboring cage on the stability as well as spectroscopic properties of guest molecules trapped in a cage. Such complexes are represented by the notations as described below.

The fused dodecahedral cage in which one molecule of H_2 located in both the cavities are denoted by $(H_2)_{1\text{-}1}$@FDD. Similarly, the fused irregular dodecahedral cage in which one molecule of H_2 located in both of the cavities are denoted by $(H_2)_{1\text{-}1}$@FII. The endohedral complex of fused dodecahedral-irregular dodecahedral cage in which each of the cavities occupied by one hydrogen molecule is represented by $(H_2)_{1\text{-}1}$@FDI. For the complexes of other guest species such as CO_2 and CH_4, H_2 is replaced by the respective guest molecules.

To know the effect of different guests in the same or adjacent cavities on the stability of hydrate structures, studies are also extended to mixed hydrates. For this purpose, different guest species are encapsulated in the cavities of single as well as fused cages. The optimized geometries of these complexes are given in figures 4.5 and 4.6. To represent the fused cage complexes of mixed hydrates, the type of cage in which guest is located is given as subscript. For example, a complex of FDI cage, in which H_2 molecule is present in the dodecahedral cavity and CH_4 in the irregular-dodecahedral cavity is denoted by $(H_2)_{DD}(CH_4)_{IDD}$@FDI. Whereas, $(CH_4)_{DD}(H_2)_{IDD}$@FDI represents

the presence of CH_4 in the dodecahedral cavity and H_2 in the irregular-dodecahedral cavity. Similar strategy is used to represent the complexes of FDD and FII cages having two different guests in the adjacent cavities.

The interaction energy ($\boldsymbol{E_{int}}$) associated with the encapsulation of guest molecules (H_2, CO_2 and CH_4) inside the cages of different size and shapes was calculated using equation 3.1 and further corrected for basis set superposition error (BSSE) using the counterpoise method [224]. Considering the encapsulation of different number of guest molecules, interaction energy per guest species ($E_{int/guest}$) is also calculated.

Frequency calculations of the optimized geometries were carried out at the same level of theory to ensure that the reported geometries belong to minima of the potential energy surface. The Raman active vibrational modes of guest molecules in their free and confined states are analyzed. The nuclear magnetic resonance (NMR) calculations were performed using the gauge-independent atomic orbital (GIAO) method [236]. The change in chemical shift for ^{1}H and ^{13}C nuclei of the guest species due to their encapsulation in various cages is also studied.

4.3 Results and Discussion

4.3.1 Interaction energy

The interaction energy of different guest species with various types of single and fused cages in which they are encapsulated is calculated and the results are analyzed as below. For the sake of clarity, the discussion is divided into two parts. In the first part, the interaction energy of the guest species trapped in a single cage is discussed. The effects of an adjacent cage and the guest species present in that on the interaction energy are discussed in the second part. The difference in interaction energy due to the encapsulation of two guest species in the same cage is also examined.

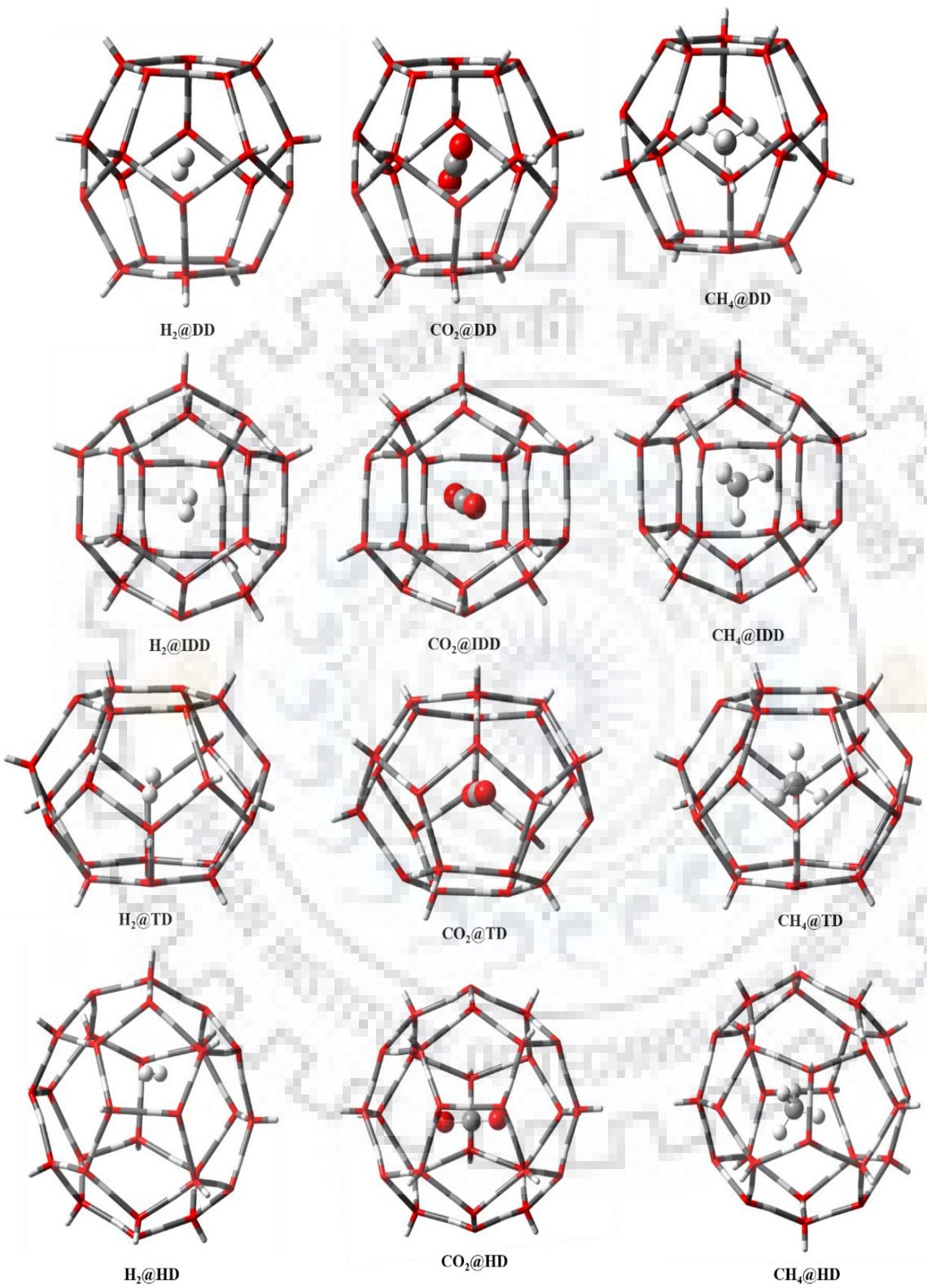

Figure 4.1 Optimized geometries of the complexes with single occupancies for various guest species obtained at B97-D/cc-pVTZ level.

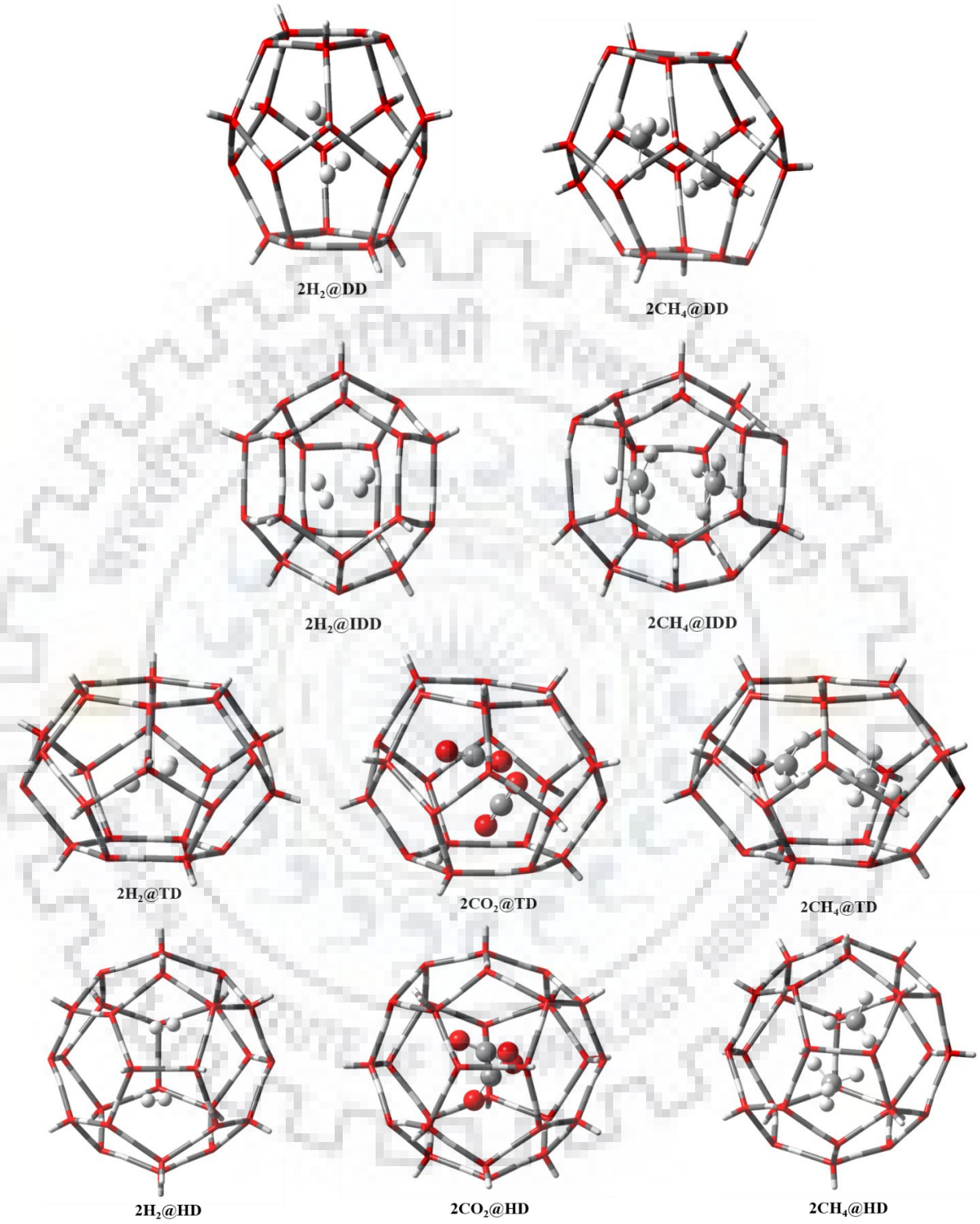

Figure 4.2 Optimized geometries of the complexes with double occupancies for various guest species obtained at B97-D/cc-pVTZ level.

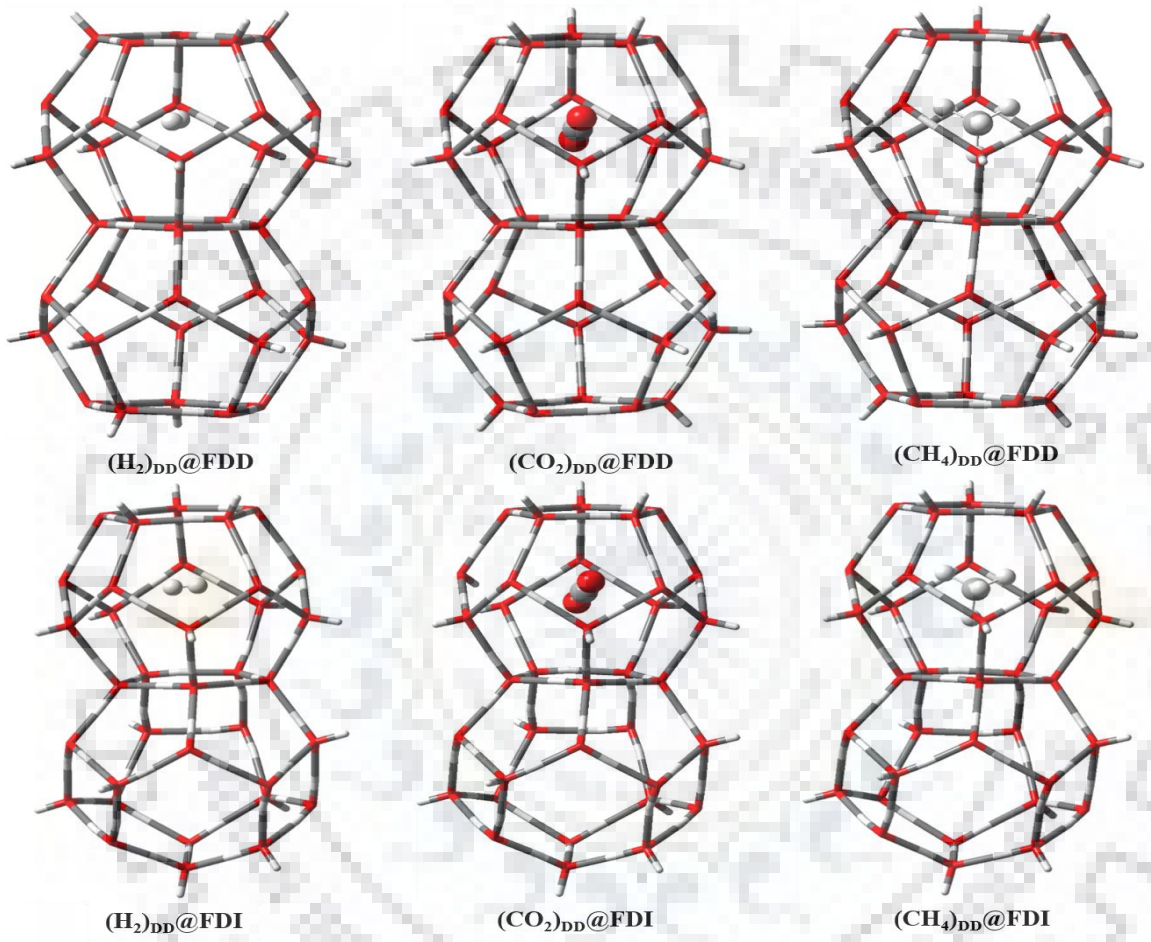

Figure 4.3 Optimized geometries of G_{DD}@FDD, G_{DD}@FDI, G_{IDD}@FDI and G_{IDD}@FII for various guest species obtained at B97-D/cc-pVTZ level.

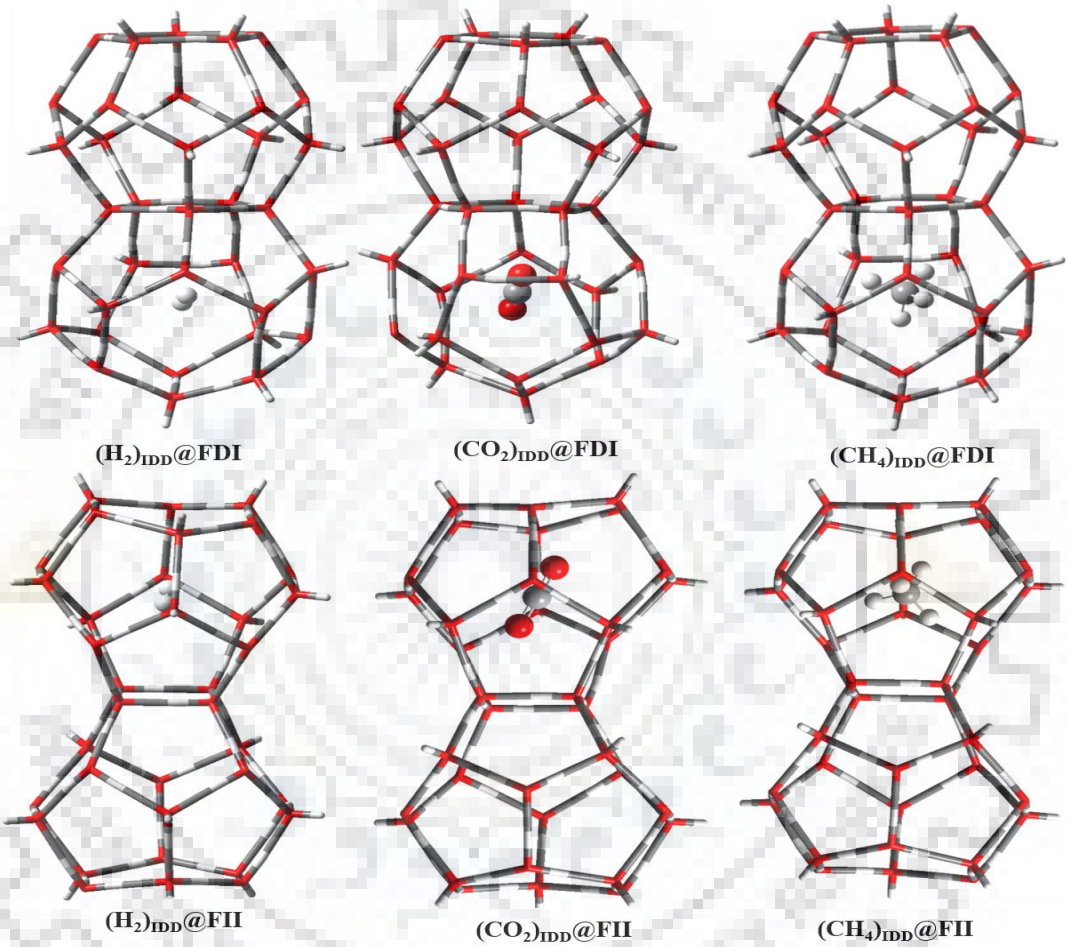

Figure 4.3 continued.

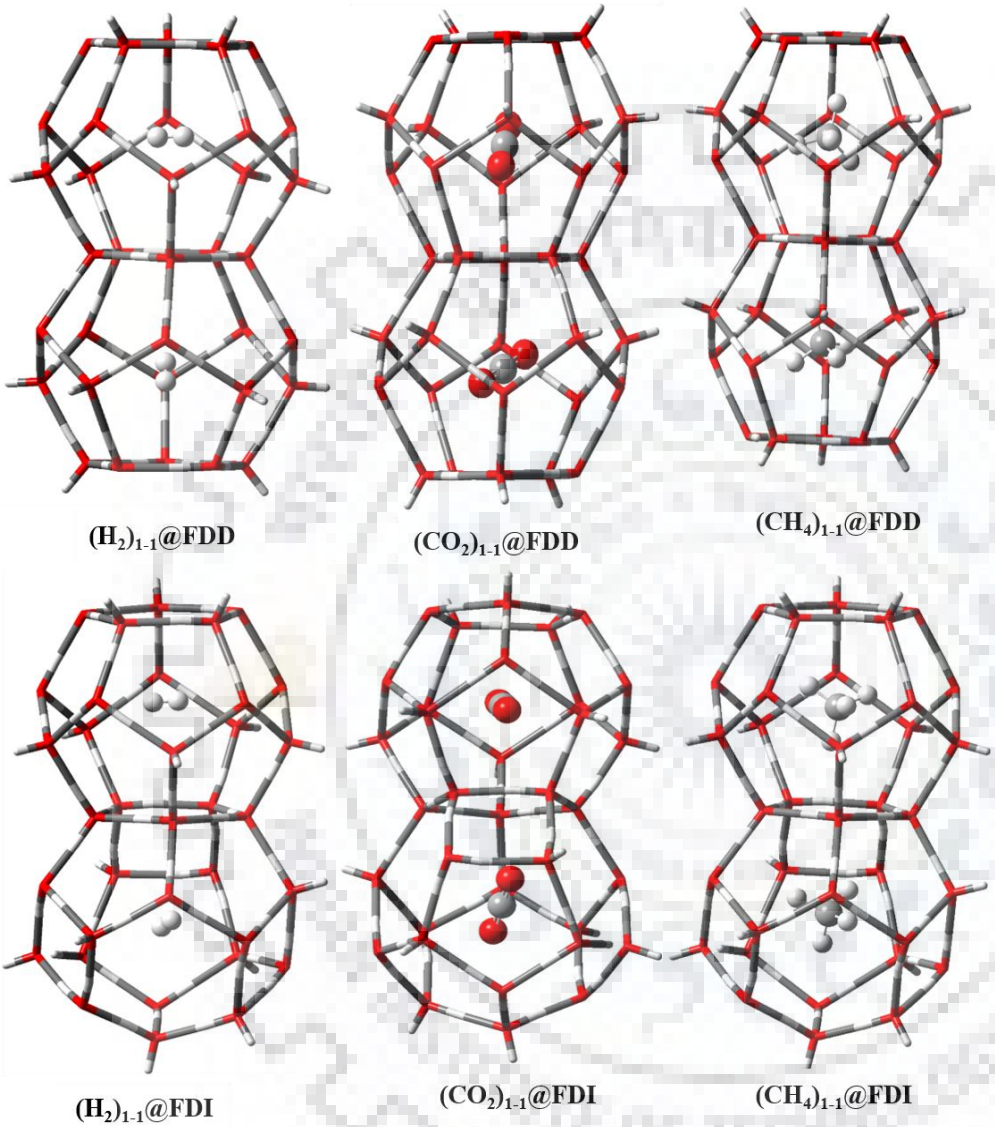

Figure 4.4 Optimized geometries of $G_{1\text{-}1}$@FDD, $G_{1\text{-}1}$@FDI and $G_{1\text{-}1}$@FII for various guest species obtained at B97-D/cc-pVTZ level.

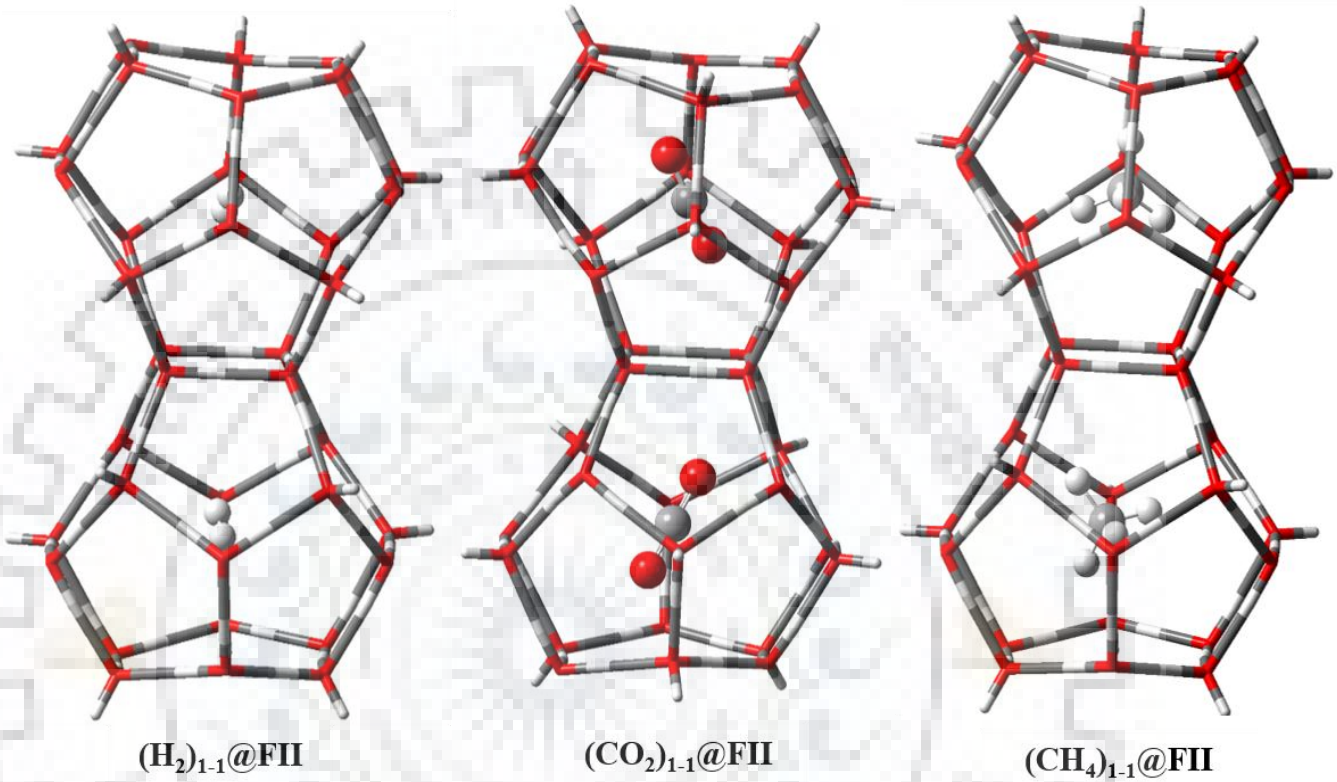

Figure 4.4 continued.

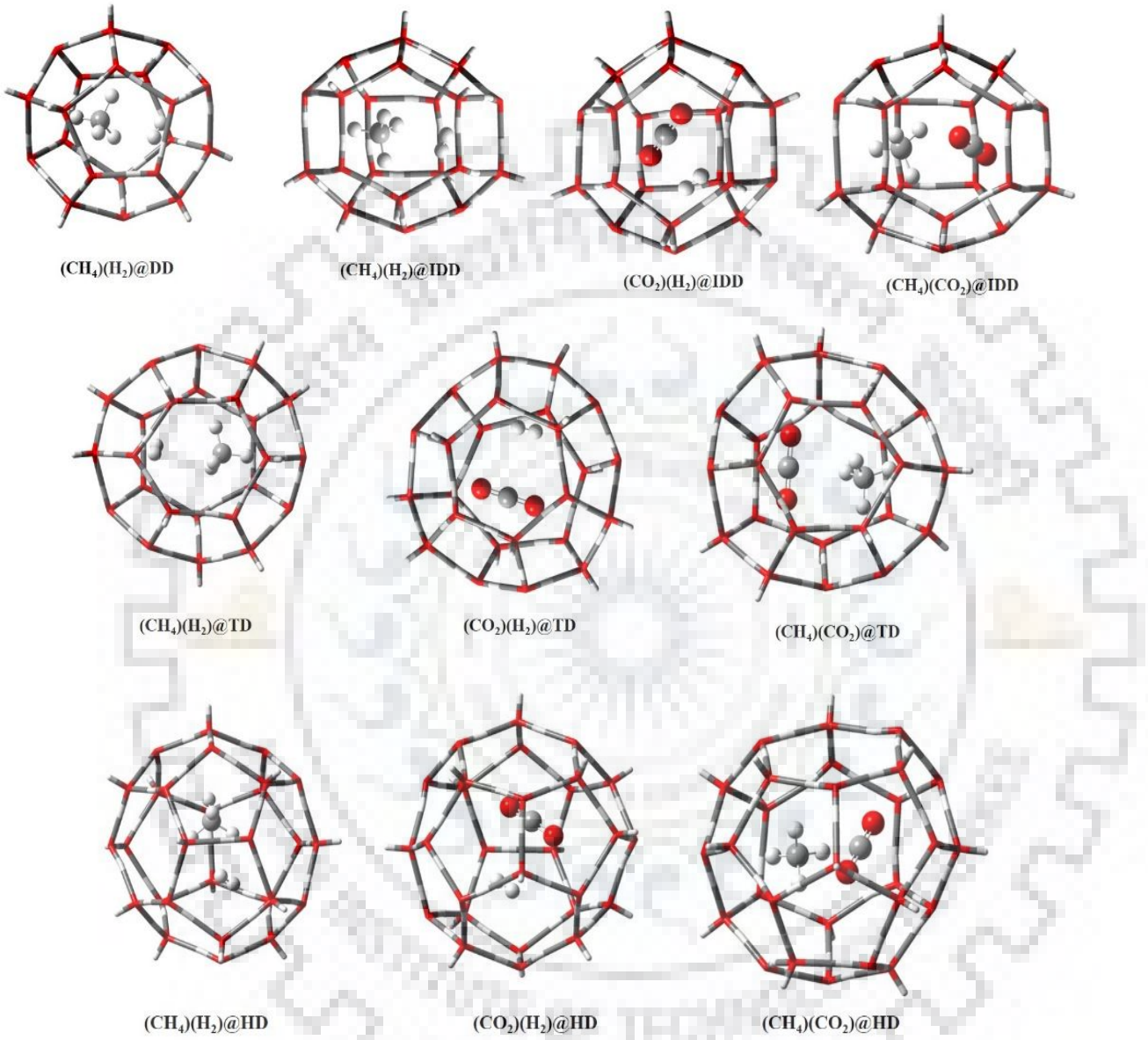

Figure 4.5 Optimized geometries of various mixed single hydrates obtained at B-97D/cc-pVTZ level.

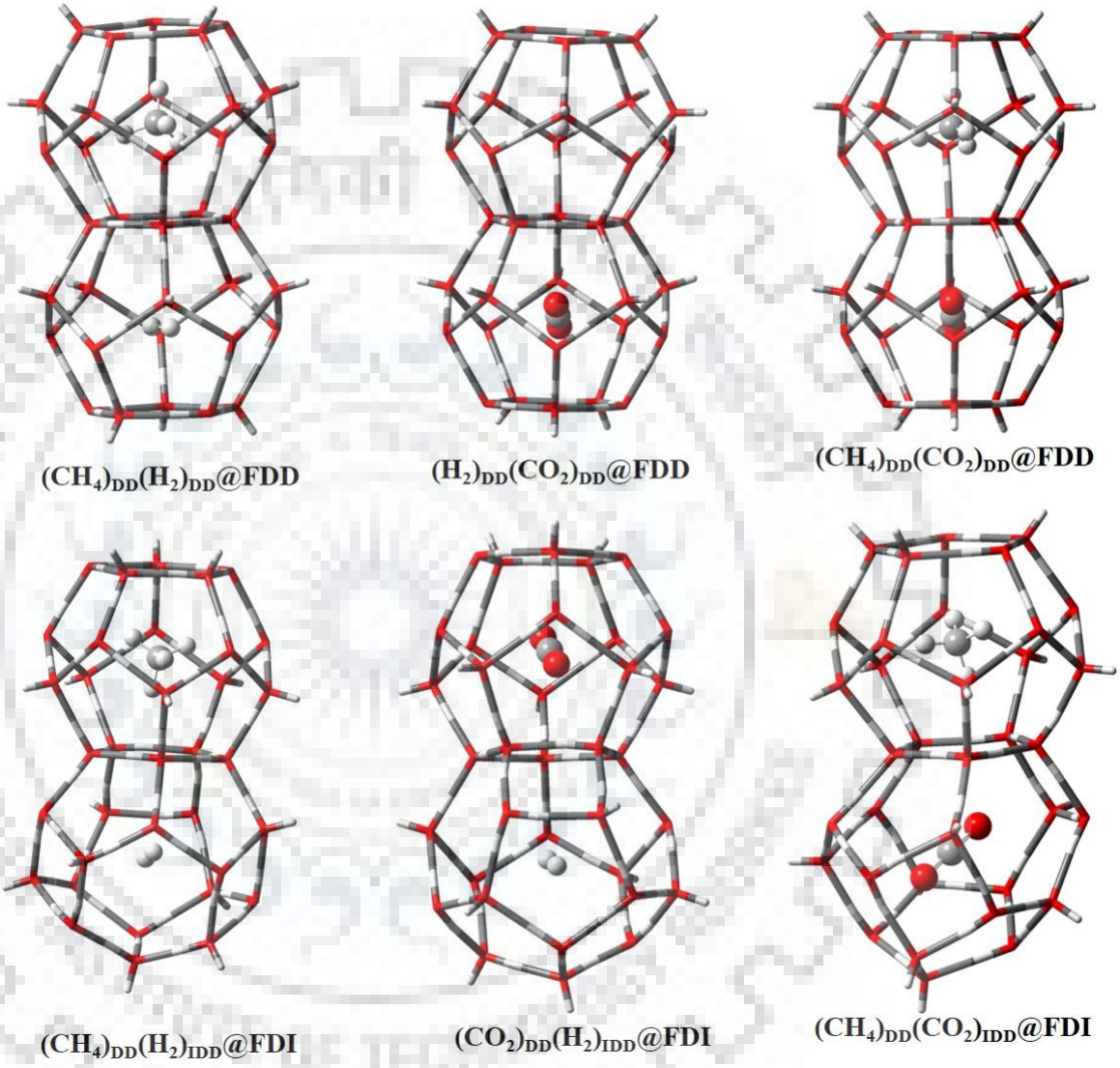

Figure 4.6 Optimized geometries of fused mixed hydrates obtained at B97D/cc-pVTZ level of theory.

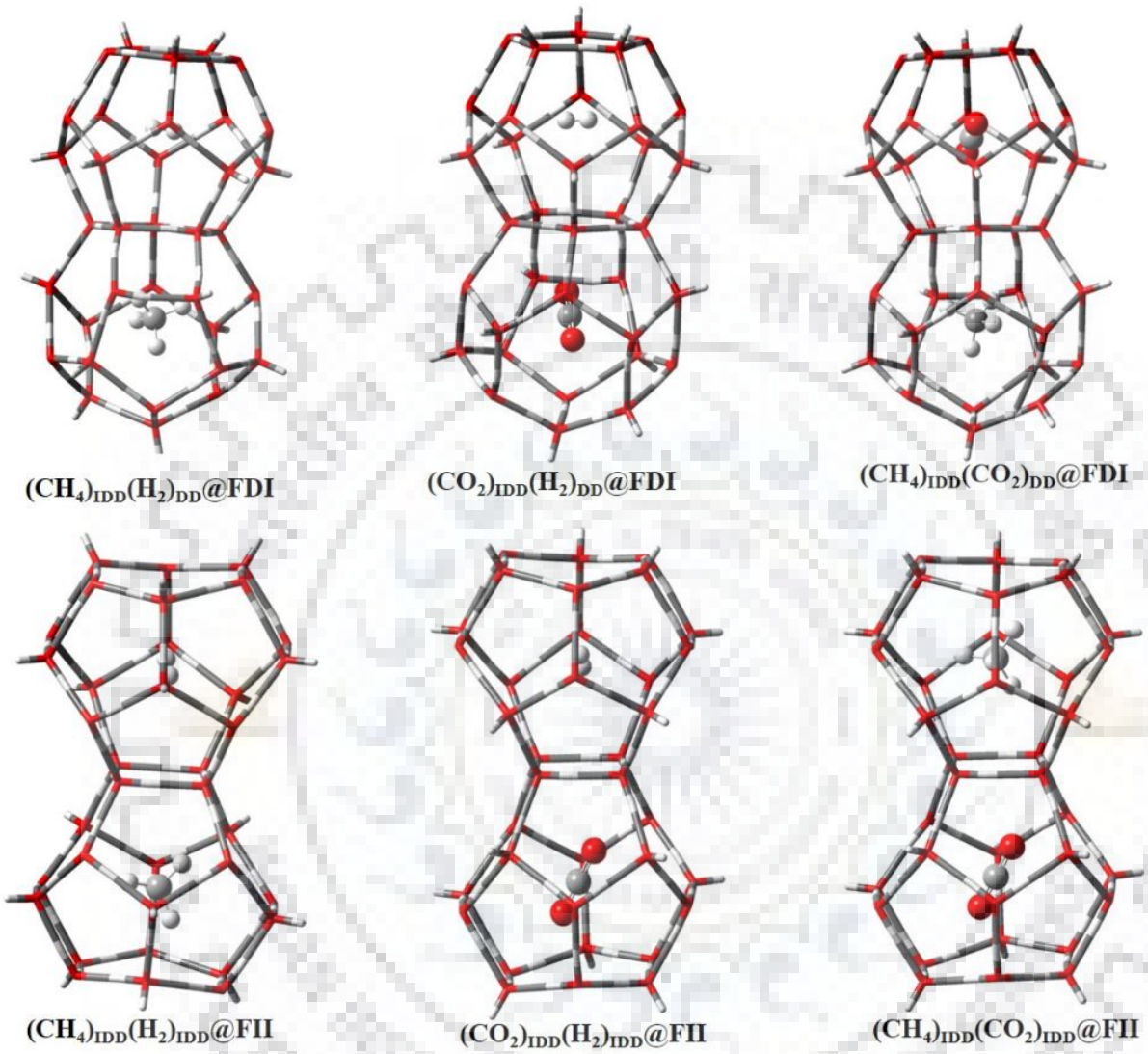

Figure 4.6 continued.

4.3.1.1 Encapsulation in single cages

From table 4.1, it can be seen that the interaction energy of encapsulated H_2 with DD cage is -1.60 kcal/mol. The values of interaction energy for H_2 with IDD, TD and HD are -1.57, -1.55 and -1.17 kcal/mol, respectively, indicating that the interaction energy of H_2 decreases with increase in the size of the cage. However, an opposite trend is observed for the encapsulation of CO_2 in various single cages. The values of E_{int} for CO_2 with DD, IDD, TD and HD cages are -3.11, -3.26, -4.37 and -4.93 kcal/mol, respectively, as listed in table 4.1. The interaction energy of encapsulated CO_2 is increased with an increase in the size of the host single cage. Thus, among DD, IDD, TD and HD cages, the interaction of CO_2 with HD is more attractive. Furthermore, from the table, it can be seen that the interaction energy of CH_4 with different cages follows a similar trend as for CO_2 except that the interaction energy in HD is slightly less than that in TD (< 0.1 kcal/mol). The above observations show that the interaction energy of an encapsulated molecule depends on the size of both the guest molecule and the cavity. It is worth to mention that in the studies of endohedral fullerenes of small guest molecules, Williams *et al* have emphasized that the interaction between the guest and the host largely depends on the extend of overlap between their van der Waals radii [237]. Their studies showed that a small degree of overlap between van der Waals radii of the cage and the molecule is attractive, while larger overlap leads to repulsive interaction between the two. Thus, due to small size and the lack of significant van der Waals overlap with the water cages, the interaction energy of H_2 with different cages is negligible and decreases with increase in the size of the cage. Contrary to this, the interaction energy of CO_2 increases with the size of the cage due to less repulsion between two units, suggesting large cages as ideal hosts for CO_2 in agreement with the experimental studies [45, 238]. In addition to this, it has been also reported experimentally and computationally that the dipolar interaction between CO_2 and the host cage results to strong host-guest interaction in CO_2 complexes [217, 239, 240]. Due to the relatively small size of CH_4 than CO_2, the overlap between the former and the cage is optimum in TD and decreases thereafter in HD as reflected from the respective interaction energy. The relatively high value of interaction energy for CH_4 than that for CO_2 in DD, IDD and TD can be attributed to the nearly spherical shape of CH_4 leading to more attractive interaction with maximum number of water molecules around.

In order to verify the above observation, the double occupancy of the cage is also studied. The encapsulation of two molecules of H_2 inside DD leads to the formation of the complex $2H_2$@DD. The interaction energy of two molecules of hydrogen with the host cage is -0.71 kcal/mol,

which is less than that in H_2@DD. This difference in interaction energy arises due to the repulsion between the guest species as well as that between the guests and the host cage. For the same reason, the interaction energy is also reduced in $2H_2$@IDD compared to H_2@IDD. For $2H_2$@TD, the calculated interaction energy of -1.93 kcal/mol is less than twice the value of interaction energy obtained for H_2@TD, suggesting that repulsion exists even in a cage of appreciable size. However, inside a sufficiently large cage HD, the interaction energy for double encapsulation of H_2 is nearly twice as that for its single occupancy. The repulsion between the guest species and that between the guest and the host cage in DD, IDD, TD and HD are not sufficient to break any of these cages. On the other hand, the encapsulation of two molecules of CO_2 inside DD and IDD leads to high repulsion between the component species resulting in the disintegration of the cage. The cage TD remained intact even after encapsulating two molecules of CO_2 despite the repulsions. Two molecules of CO_2 can occupy in HD cage with a total interaction energy of -6 kcal/mol compared to ~-5kcal/mol for its single occupancy. In the case of CH_4, the interaction is repulsive in DD for its double occupancy, although the cage is intact. The repulsion is reduced with an increase in the size of the cage. However, the interaction energy is still less than twice as that of the corresponding single occupancy. A careful examination of the interaction energies for the complexes of CO_2 and CH_4 with all types of cages with double occupancy reveals that the repulsion is more in the complexes of CO_2.

The values of E_{int} for mixed hydrates are also calculated in this chapter which are listed in table 4.2. For the mixed hydrates, it is observed that the values of E_{int} are reduced compared to the values of the respective encapsulated complexes of individual guest species. For example, for the complex, $(H_2)(CH_4)$@DD, the value of E_{int} is -0.95 kcal/mol, which is significantly less than that of the complexes CH_4@DD and H_2@DD. This decrease in the interaction energy is mainly due to the guest-guest repulsion. Similar results are also observed for the mixed complexes formed by the encapsulation of two different gas molecules in the cavities of IDD, TD and HD cages.

Furthermore, the interaction energy of the complexes with double occupancy of different guests in the single cages is also compared with the complexes formed by the double occupancy by guests of same type. The value of E_{int} for $(H_2)(CH_4)$@DD is -0.95 kcal/mol which is found to be 0.71 and 1.42 kcal/mol higher than that of $2H_2$@DD and $2CH_4$@DD, respectively, indicating that the encapsulation of H_2 and CH_4 inside dodecahedral cage is energetically more favored over the double occupancy of same guest (H_2 or CH_4) in the cage DD.

Table 4.1 The values of interaction energy (E_{int}) and interaction energy per guest ($E_{int/guest}$) for various complexes obtained at B97-D/cc-pVTZ level. The BSSE corrected energies are given in bold letters. All energies are in kcal/mol.

Energy	Guest	G@DD	G@IDD	G@TD	G@HD	2GDD	2G@IDD	2G@TD	2GHD
E_{int}	H_2	-3.45 **-1.60**	-3.44 **-1.57**	-2.81 **-1.55**	-2.73 **-1.17**	-4.41 **-0.71**	-4.52 **-1.10**	-5.06 **-1.93**	-4.75 **-2.21**
	CO_2	-8.51 **-3.11**	-8.50 **-3.26**	-8.97 **-4.37**	-8.47 **-4.93**	-	-	-11.10 **-2.02**	-14.50 **-6.00**
	CH_4	-9.22 **-4.27**	-9.09 **-4.31**	-9.01 **-4.54**	-8.24 **-4.43**	-6.04 **1.42**	-7.67 **-0.39**	-11.50 **-3.75**	-13.10 **-5.94**
$E_{int/guest}$	H_2	**-1.60**	**-1.57**	**-1.55**	**-1.17**	**-0.36**	**-0.55**	**-0.97**	**-1.11**
	CO_2	**-3.11**	**-3.26**	**-4.37**	**-4.93**	-	-	**-1.01**	**-3.00**
	CH_4	**-4.27**	**-4.31**	**-4.54**	**-4.43**	**0.71**	**-0.20**	**-1.88**	**-2.97**

Table 4.2 The values of interaction energy (E_{int}) and interaction energy per guest ($E_{int/guest}$) for various complexes obtained at B97-D/cc-pVTZ level. The BSSE corrected energies are given in bold letters. All energies are in kcal/mol.

	Guest		GG'@DD	GG'@IDD	GG'@TD	GG'@HD
	G	G'				
E_{int}	H_2	CH_4	-6.73 **-0.95**	-7.64 **-1.82**	-9.91 **-4.03**	-9.67 **-4.43**
	H_2	CO_2	---	-5.42 **0.83**	-9.96 **-3.71**	-10.20 **-4.85**
	CO_2	CH_4	---	-6.59 **1.57**	-11.20 **-2.90**	-14.20 **-6.18**

Similarly, the values of interaction energy for $(H_2)(CH_4)$@IDD and $(H_2)(CH_4)$@TD are higher than those for the complexes formed by the double occupancy of same guest (H_2 or CH_4) molecules. However, the value of E_{int} for $(H_2)(CH_4)$@HD is ~1.51 kcal/mol lower than that for $2CH_4$@HD indicating that the feasibility of double occupancy of same or different guest species depends on the size and shape of both the host cage and the guest molecules. The value of E_{int} for $(H_2)(CO_2)$@IDD is 0.83 kcal/mol, indicating the repulsive interactions between host and guest molecules. However, due to the larger size of the cages TD and HD, the interactions between host and guest molecules are attractive for the complexes $(H_2)(CO_2)$@TD and $(H_2)(CO_2)$@HD. The value of E_{int} for the complex $(CH_4)(CO_2)$@TD is ~0.44 kcal/mol higher than $2CO_2$@TD, indicating less feasibility for the formation of the later due to the dipolar interactions between two CO_2 molecules. Similarly, the formation of mixed complex $(CH_4)(CO_2)$@HD is energetically favored over $2CH_4$@HD and $2CO_2$@HD.

4.3.2.1 Encapsulation in fused cages

In order to know the effect of an adjacent cage and the guest species in an adjacent cage on the stability, the encapsulation of different types of guest species inside the cavities of fused water cages are studied. The values of E_{int} and $E_{int/guest}$ for fused cage complexes are also provided in table 4.3 and 4.4. The interaction energy for the complex in which one molecule of H_2 occupies in one of the cavities of the fused cage FDD is -1.50 kcal/mol. This is almost the same as that for H_2@DD. For the complexes, $(H_2)_{DD}$@FDI, $(H_2)_{IDD}$@FDI and $(H_2)_{IDD}$@FII, the values of E_{int} are -1.51, -1.59 and -1.61 kcal/mol, respectively, which is close to E_{int} obtained for a single DD cage. Thus, it is clear that the adjacent cage has no effect on the interaction of H_2 with its host cage. This is expected due to the small size of H_2.

Similarly, the interaction energy of CH_4 with the host cage in presence of an attached adjacent empty cage is almost the same as obtained for its complex with DD or IDD cage. For example, the values of E_{int} for the complexes $(CH_4)_{DD}$@FDI and $(CH_4)_{IDD}$@FDI are -4.43 and -4.51 kcal/mol, respectively. From the table 4.1, it can be seen that these values are very close to that obtained for the interaction of encapsulated CH_4 molecule in a single dodecahedral or irregular-dodecahedral water cage. This indicates that the interaction between the guest methane molecule and the host cage is independent of the type of the cage in which CH_4 is trapped and the type of the cage adjacent to that. Thus, it can be inferred from the above observation that the interaction of CH_4 is not extended beyond a cage.

Table 4.3 The values of interaction energy (E_{int}) and interaction energy per guest ($E_{int/guest}$) for various complexes obtained at B97-D/cc-pVTZ level. The BSSE corrected energies are given in bold letters. All energies are in kcal/mol.

Energy	Guest	G_{DD}@FDD	G_{DD}@FDI	G_{IDD}@FDI	G_{IDD}@FII	$G_{1\text{-}1}$@FDD	$G_{1\text{-}1}$@FDI	$G_{1\text{-}1}$@FII
E_{int}	H_2	-3.34	-3.34	-3.30	-3.35	-6.63	-6.63	-6.67
		-1.50	**-1.51**	**-1.59**	**-1.61**	**-3.08**	**-3.08**	**-3.22**
	CO_2	-7.76	-7.81	-8.32	-9.30	-15.40	-16.1	-16.90
		-2.80	**-2.83**	**-3.76**	**-4.11**	**-5.42**	**-6.26**	**-6.77**
	CH_4	-8.80	-8.78	-8.92	-8.70	-17.5	-17.6	-17.38
		-4.44	**-4.43**	**-4.51**	**-4.31**	**-8.88**	**-8.89**	**-8.63**
$E_{int/guest}$	H_2	**-1.50**	**-1.51**	**-1.59**	**-1.61**	**-1.54**	**-1.54**	**-1.61**
	CO_2	**-2.80**	**-2.83**	**-3.76**	**-4.11**	**-2.71**	**-3.13**	**-3.39**
	CH_4	**-4.44**	**-4.43**	**-4.51**	**-4.31**	**-4.44**	**-4.45**	**-4.32**

Table 4.4 The values of interaction energy (E_{int}) and interaction energy per guest ($E_{int/guest}$) for various complexes obtained at B97-D/cc-pVTZ level. The BSSE corrected energies are given in bold letters. All energies are in kcal/mol.

	Guest					
			$(G)_{DD}(G')_{DD}$@FDD	**$(G)_{DD}(G')_{IDD}$@FDI**	**$(G)_{IDD}(G')_{DD}$@FDI**	**$(G)_{IDD}(G')_{IDD}$@FII**
	G	G'				
E_{int}	H_2	CH_4	-12.10 **-5.87**	-12.26 **-5.99**	-12.06 **-5.98**	-12.04 **-5.92**
	H_2	CO_2	-11.04 **-4.37**	-11.60 **-4.97**	-11.08 **-4.38**	-11.95 **-5.17**
	CO_2	CH_4	-16.44 **-7.11**	-16.71 **-7.31**	-16.99 **-7.84**	-17.39 **-7.91**

On the other hand, for the complexes in which one molecule of CO_2 occupies in one of the cavities of a fused cage leaving the other cavity vacant, it can be seen that the interaction energy follows the order $(CO_2)_{IDD}$@FII > $(CO_2)_{IDD}$@FDI > $(CO_2)_{DD}$@FDI ≈ $(CO_2)_{DD}$@FDD. This suggests that the interaction of CO_2 extends beyond a cage, probably due to its large size. An analysis of the above optimized geometries revealed that the IDD cages are distorted relative to DD and is elongated in one direction. When CO_2 is encapsulated inside an irregular or a fused irregular dodecahedral cage, it aligns in the elongated direction of the cage, giving stability to the complex.

A comparison of the interaction energy of a given guest species (G) in complexes of the type G@DD or G@IDD with that in fused cages $G_{1\text{-}1}$@FDD, $G_{1\text{-}1}$@FDI and $G_{1\text{-}1}$@FII shows that the interaction energy of guest species with the fused cage is nearly equal to the sum of the interaction energies of the guest species with the individual cages. For example, the value of E_{int} for $(CH_4)_{1\text{-}1}$@FII is -8.63 kcal/mol, which is twice as that obtained for the complex CH_4@IDD. Similar results are also observed for the other fused cage complexes. The maximum difference obtained is 0.8 kcal/mol for CO_2 in $(CO_2)_{1\text{-}1}$@FDD, for which the interaction energy is found to be -5.42 kcal/mol compared to -6.22 kcal/mol expected for two units of CO_2@DD. The difference could be due to the repulsion between the guest species of two different cages and/or due to the reduced attraction of each CO_2 with the cage in which they are encapsulated. The latter can arise due to the presence of a pentagonal ring made of water molecules common to both the cages. In such cases, the decrease in attraction is expected to be independent of the guest species. However, it was found that it is not true for the corresponding complexes of CH_4. This shows the possibility of interaction between the guests is limited to those species of appreciable size and polarity when they are confined in different cages.

Table 4.3 lists the interaction energy per guest molecule for the complexes with guests trapped in different cages. It is evident from the table that the molecules H_2, CO_2 and CH_4 prefer to be distributed in two cages rather than occupying in the same cage. This is understandable, because of the high repulsion between the molecules when they are confined within the same cage.

The interaction energies for the mixed hydrates are given in table 4.4. From the table it can be seen that E_{int} follows the order: $(CO_2)_{IDD}(CH_4)_{IDD}$@FII > $(CO_2)_{IDD}(CH_4)_{DD}$@FDI > $(CO_2)_{DD}(CH_4)_{DD}$@FDD. The results also show that E_{int} for $(CO_2)_{DD}(CH_4)_{DD}$@FDD complex is -7.11 kcal/mol which is almost equal to the sum of $E_{int/guest}$ for $(CO_2)_{DD}$@FDD and $(CH_4)_{DD}$@FDD complexes suggesting that the presence of guest in one cavity is not affecting the host-guest interaction in a neighboring cage. Similar results are also observed for $(H_2)_{DD}(CH_4)_{DD}$@FDD and

$(H_2)_{DD}(CO_2)_{DD}$@FDD complexes. A similar observation is found to be valid for the complexes of FDI and FII with different guests in their cavities.

4.4 Vibrational Raman Spectra

The vibrational Raman spectrum is an effective tool to identify guest molecules and is widely used in the studies of gas hydrates as mentioned before. In the present work, the vibrational Raman spectra of H_2, CO_2 and CH_4 molecules trapped in cavities of various types of cages are simulated. The values of Raman frequencies for symmetric stretching of the guest species in their free and encapsulated states are listed in table 4.5 to 4.8. For comparison, the values available in literature are also given in the tables [45, 80, 126, 202, 235, 241-243].

From table 4.5, it can be seen that the stretching frequency of H_2 in its free state occurs at 4376 cm^{-1} which is blue shifted due to encapsulation in various types of cages considered. In DD and IDD cages, a blue shift of 8cm^{-1} is observed which is decreased with an increase in the size of the cage showing a blue shift of 5cm^{-1} in TD. Due to large size of the cavity and small size of H_2, the blue shift in HD is negligible. For free CO_2, the symmetric stretch is observed at a frequency of 1322cm^{-1}. On confining inside DD, this mode undergoes a blue shift of 13cm^{-1}. However, the blue shift is reduced to 10 cm^{-1} and 5cm^{-1} inside IDD and TD, respectively. Inside the large cavity of HD cage, CO_2 vibrates with a stretching frequency of 1324 cm^{-1}, close to its free state. Like in H_2 and CO_2, the symmetric stretching frequency of CH_4 also undergoes blue shift on confining inside DD, IDD and TD cages. The values of blue shift inside these cages are 14 cm^{-1}, 12 cm^{-1} and 10 cm^{-1}, respectively. Thus, the extent of blue shift is decreased with an increase in the size of the cavity and is in agreement with the earlier reports [80, 202, 242, 244, 245].

The blue shifts in stretching frequencies of the guest species due to their confinement inside the water cages are significantly increased when a cage is doubly occupied. For example, the encapsulation of an additional molecule of H_2 to H_2@DD leads to an enhancement in blue shift from 8cm^{-1} to 36-38cm^{-1}. A large shift in stretching frequency is also observed for H_2 in other cages for their double occupancy compared to the respective single occupancy.

Table 4.5 The symmetric stretching vibrational Raman frequencies (in cm^{-1}) for different guest species in their free and various encapsulated states.

Guest	Free	G@DD	G@IDD	G@TD	G@HD	2G@DD	2G@IDD	2G@TD	2G@HD
H_2	4376	4384 4372[a]	4384	4381	4377 4372[a] 4366[h]	4412 4414 4405[a]	4399 4399	4386 4388	4386 4390 4380[a]
CO_2	1322	1335 1366[c] 1325[d]	1332 1325[d]	1327 1321[d] 1364[c]	1324 1312[d]	----	----	1333 1333	1328 1329
CH_4	2934 2917[b] 2911[c]	2948 2957[d] 2939[e] 2915[f] 2920[c]	2946 2949[d]	2944 2942[d] 2918[e] 2905[g] 2901[c]	2933 2929[d] 2904[g]	2984 2986	2983 2988	2971 2975	2953 2957

Experimental [b] Ref [241] [f]Ref [243] [g]Ref [45]
Calculated [a] Ref [126] [c] Ref [242] [d]Ref [202] [e]Ref [80] [h]Ref [235]

Table 4.6 The symmetric stretching vibrational Raman frequencies (in cm^{-1}) for different guest species in their various encapsulated states for mixed hydrates.

Guest		**GG'@DD**		**GG'@IDD**		**GG'@TD**		**GG'@HD**	
G	G'	G	G'	G	G'	G	G'	G	G'
H_2	CH_4	4465	2968	4440	2963	4415	2945	4406	2943
H_2	CO_2	----	----	4432	1337	4404	1330	4391	1325
CO_2	CH_4	----	----	1337	2976	1335	2972	1327	2952

From the values of blue shift, it can be also inferred that the extent of blue shift due to double occupancy decreases with increase in size of the cage. It is also evident from the table that with the size of the guest molecule, blue shifts are further enhanced. Thus, the blue shift observed for the symmetric stretching frequency of CH_4 in CH_4@DD is increased from 14 cm^{-1} to 51cm^{-1} in $2CH_4$@DD. However, the blue shift is decreased with increase in the size of the cage due to less repulsion inside large cages. From the above discussion it can be inferred that the extent of blue shift can be used as a measure of cage occupancies in gas hydrates. This is in agreement with the observation reported earlier based on the experimental studies on the hydrates of hydrogen [81, 246].

A comparison of the vibrational Raman frequencies of the symmetric stretching modes of various guest molecules in their encapsulated state obtained in the present study with those reported in earlier studies listed in table 4.5 clearly indicates that the conclusions deduced based on these results are qualitatively in agreement with the earlier observations. A quantitative agreement between the results is very unlikely, because the calculations were performed at different levels of theory. In addition, the host cages used in these studies are also different. It has been reported that depending upon the hydrogen topology of water molecules constituting the cage, the guest molecules interact differently with the host cage leading to slight changes in their properties [126]. Based on the qualitative agreement of the present results with most of the earlier reports, the studies were extended for fused cages to infer about the role of nearby cages and guest species on the vibrational properties of encapsulated molecules.

Prior to this, the effect of encapsulation of two different guest species on the vibrational stretching frequencies in the single cages is examined by encapsulating them in single cages. The stretching frequencies obtained for different guest species encapsulated in single cages are listed in table 4.6. Significantly large blue shifts in the stretching frequencies of the guest species are observed when a cage is doubly occupied with two different gas molecules. For example, the symmetric stretching frequencies of H_2 and CH_4 in $(H_2)(CH_4)$@DD showed blue shifts of 89 and 34 cm^{-1}, respectively, compared to the stretching frequencies of these guest species in their free state. As observed for the double occupancy by similar guest molecules in single cages, the extent of blue shift is also decreased with an increase in the size of the cavity for their mixed hydrate analogues.

The vibrational stretching frequencies of the guests residing in the fused cages are listed in table 4.7 and 4.8. The analysis of the vibrational frequencies of guest molecules in fused water

Table 4.7 The symmetric stretching vibrational Raman frequencies (in cm^{-1}) for different guest species in their various encapsulated states.

Guest	G_{DD}@FDD	G_{DD}@FDI	G_{IDD}@FDI	G_{IDD}@FII	$G_{1\text{-}1}$@FDD	$G_{1\text{-}1}$@FDI	$G_{1\text{-}1}$@FII
H_2	4386	4388	4380	4381	4386 4387	4386 4387	4382 4382
CO_2	1335	1337	1333	1332	1335 1335	1332 1336	1333 1333
CH_4	2950	2948	2945	2948	2949 2951	2944 2949	2948 2949

Table 4.8 The symmetric stretching vibrational Raman frequencies (in cm^{-1}) for different guest species in their various encapsulated states.

Guest		**$(G)_{DD}(G')_{DD}$@FDD**		**$(G)_{DD}(G')_{IDD}$@FDI**		**$(G)_{IDD}(G')_{DD}$@FDI**		**$(G)_{IDD}(G')_{IDD}$@FII**	
G	G'	G	G'	G	G'	G	G'	G	G'
H_2	CH_4	4387	2951	4385	2945	4385	2950	4382	2949
H_2	CO_2	4385	1335	4388	1333	4385	1337	4383	1332
CO_2	CH_4	1336	2951	1337	2946	1333	2949	1332	2948

cages with those in single cages indicated that the blue shift observed for the symmetric stretching frequencies of various guest species is almost the same as that observed in the respective single cages. For example, the blue shifts observed for the stretching frequency of H_2 in H_2@DD and $(H_2)_{DD}$@FDD are 8 cm^{-1} and 10 cm^{-1}, respectively as listed in table 4.5 and 4.7. A significant change in the stretching frequency is also not observed for H_2 in $(H_2)_{IDD}$@FDI and $(H_2)_{IDD}$@FII compared to that in H_2@IDD. This also holds true for the respective complexes of CO_2 and CH_4.

In order to know how the presence of similar guest species in an adjacent cage affects the stretching frequencies of a trapped molecule, the vibrational frequencies obtained for the complexes $G_{1\text{-}1}$@FDD, $G_{1\text{-}1}$@FII and $G_{1\text{-}1}$@FDI for various guest species are analyzed. From table 4.7, it can be seen that there is no notable change in the stretching frequency of the trapped guest molecule due to the presence of a molecule in the neighboring cage. For example, the stretching of H_2 occurs at 4384 cm^{-1} in H_2@DD, whereas the stretching of two H_2 molecules of $(H_2)_{1\text{-}1}$@FDD occurs at 4386 and 4387 cm^{-1}. This also holds true for other guest species and in the fused cages FDI and FII.

The presence of different guest species in adjacent cage on the stretching frequencies of a trapped molecule is also examined in the present work. It can be seen from table 4.8 that a noticeable change is not observed in the stretching frequency of a guest molecule in the presence of another type of guest molecule in the adjacent cage. For example, the stretching frequencies of CO_2 and CH_4 occur at 1335 and 2948 cm^{-1}, respectively, in CO_2@DD and CH_4@DD. The stretching frequencies of CO_2 and CH_4 in $(CO_2)_{DD}(CH_4)_{DD}$@FDD occur at 1336 and 2951 cm^{-1}, respectively. Similar results are also observed for other mixed complexes. A noticeable change in the stretching frequency of guest species is not expected because of the large distance between the guest molecules.

4.5 Chemical shifts

The chemical shift in NMR spectroscopy is a sensitive tool to probe the influence of the surrounding environment on the electronic structure of a molecule. In the present work, the chemical shift values of hydrogen and carbon nuclei of different guest species in their free and various encapsulated states are calculated using tetra methyl silane (TMS) as reference. To consider the influence of standard references in the NMR chemical shifts, the values of chemical shifts for the guest species are also calculated using multi standard references benzene and methanol [247-250].

4.5.1 Chemical shifts of the encapsulated molecules in single cages

From table 4.9, it can be seen that the calculated ^{1}H-chemical shift for H_2 in free state is 4.72 ppm in close agreement with its experimental value (4.73 ppm) [251]. The encapsulation of H_2 in the cavities of various single cages results in the deshielding of hydrogen nuclei by 0.01-0.1ppm. Such a small difference in the chemical shift values for H_2 inside various types of cages is not sufficient to distinguish the host cage experimentally. Unlike in H_2, the protons of CH_4 are deshielded more (0.04-0.4 ppm) and can be correlated to the relatively large size of CH_4, where the hydrogen nuclei are perturbed more by the host water cage due to their close proximity to the cage atoms. It is also noted that the chemical shift values of all protons are not identical inside the cages. It can be also inferred from the table that with an increase in the size of the cage, the chemical shift values of hydrogen nuclei of encapsulated CH_4 tend to that in the gas phase, in general.

The calculated value of ^{13}C chemical shift of CH_4 in free state is -6.16 ppm and is close to the experimentally reported value of -7.00 [50, 251, 252] and -10.30 ppm [38] as listed in table 4.10. Like hydrogen nuclei, ^{13}C nuclei are also deshielded in various cages, however, at different amounts. Among the cages DD, IDD, TD and HD, ^{13}C NMR chemical shift of CH_4 in HD is close to that of free CH_4 in agreement with the experimental observations reported earlier [37, 52].

The ^{13}C chemical shift of CO_2 remains the same inside the cages without any perturbation by the cage and the calculated value of ^{13}C-NMR chemical shift of CO_2 in the present study (~122 ppm) is very close to that of the experimentally reported value of 125 ppm [238, 253].

To get more insight on the effect of guest-guest interactions on the chemical shift values, the ^{1}H and ^{13}C NMR parameters for the double occupancy of various cages are calculated and are listed in table 4.9 and 4.10, respectively. The averaged ^{1}H chemical shift value for $2H_2$@DD is 5.13 ppm and is in agreement with the experimental result [251].

In the case of $2H_2$@DD and $2H_2$@IDD, the protons are deshielded by 0.2-0.6 ppm with respect to its free state. The change in chemical shift for single occupancy of these cages is in the range 0.01-0.03 ppm. The chemical shift values of H_2 in large cages tend towards its free state value both for single and double occupancies. A similar conclusion can be drawn from the ^{1}H and ^{13}C chemical shift values of CH_4. It can also be seen from the tables that the values obtained by using multi standard references are in qualitative agreement with the chemical shift values obtained using TMS as the reference.

Further, the ^{1}H and ^{13}C chemical shift values of mixed hydrates in single cage are also calculated and analyzed in the present study. The values of ^{1}H and ^{13}C chemical shift values of guest molecules in mixed complexes are reported in table 4.11 and 4.12, respectively. The averaged ^{1}H chemical shift values of H_2 and CH_4 in $(H_2)(CH_4)$@DD are 5.23 and 0.52 ppm, respectively, which are deshielded by 0.51 and 0.37 ppm with respect to the free H_2 and CH_4 molecules. Further, the ^{13}C chemical shift for CH_4 in $(H_2)(CH_4)$@DD shows a significant deshielding of ~15 ppm compared to its free state. This deshielding in the ^{1}H and ^{13}C chemical shift values occurs mainly due to the repulsive interactions between guest molecules. The deshielding in the chemical shifts values are also observed for the guest molecules trapped in other single cages such as IDD, TD and HD. However, the deshielding is decreased with an increase in the size of the cage. For example, the averaged ^{1}H chemical shift values of H_2 and CH_4 in $(H_2)(CH_4)$@HD are 4.79 and 0.39 ppm, respectively, which are deshielded only by 0.07 and 0.24 ppm with respect to the free H_2 and CH_4 molecules.

Further, the ^{13}C chemical shift for CH_4 in $(H_2)(CH_4)$@DD shows a deshielding of ~7 ppm with respect to its free state. A close agreement of the ^{1}H chemical shift values for the guest species in various types of water cages obtained at B97-D/cc-pVTZ level of theory in the present study with the previously reported experimental and computational results listed in table 4.9 justifies the methodology adopted in the present work.

Table 4.9 The values of ^{1}H chemical shifts (in ppm) for different guest species in their free and various encapsulated states.

NMR nuclei	Reference standard	Guest	Free	G@DD	G@IDD	G@TD	G@HD	2G@DD	2G@IDD	2G@TD	2G@HD
^{1}H	TMS	H_2	4.72 4.73[a]	4.72 4.94[a]	4.72	4.70 4.84[a]	4.76	5.12, 5.14 5.10[a]	4.89, 5.31	4.93, 4.96 5.04[a]	4.78, 4.79
	TMS	CH_4	0.15 0.23[a]	0.33 0.54 0.60 0.19	0.32 0.19 0.46 0.58	0.30 0.27 0.29 0.28	0.08 0.64 0.13 0.04	0.59 0.59 0.72 0.79 0.68 0.72 0.59 0.57	0.54 0.81 0.41 0.94 0.30 0.65 0.86 0.70	0.27 0.31 0.45 0.75 0.57 0.49 0.35 0.53	0.38 0.53 0.06 0.22 0.44 0.30 0.47
	Methanol	CH_4	0.02	0.05 0.19 0.40 0.46	0.05 0.19 0.32 0.44	0.13 0.14 0.15 0.16	-0.10 -0.10 0.05 0.51	0.45 0.45 0.59 0.65 0.59 0.59 0.46 0.43	0.40 0.68 0.27 0.81 0.17 0.51 0.72 0.56	0.44 0.36 0.22 0.39 0.13 0.17 0.31 0.62	0.09 0.30 0.16 0.34 0.25 0.39 0.21 0.46

Experimental [a]Ref [251]

Table 4.10 The values of ^{13}C chemical shifts (in ppm) for different guest species in their free and various encapsulated states.

NMR nuclei	Reference standard	Guest	Free	G@DD	G@IDD	G@TD	G@HD	2G@DD	2G@IDD	2G@TD	2G@HD
^{13}C	TMS	CH_4	-6.16 -7.00[a] -10.31[b] -11.41[c]	-0.58 -2.84 [a] -3.60 [b] -4.00[d] -6.02[e] -6.84[c]	-1.24	-2.40 -4.75[e] -5.71 [a] -5.90 [b] -6.10[d] -8.45[c]	-4.39 -3.26[e]	12.33 13.49	10.80 8.98	5.51 7.42	3.49 2.54
	Methanol	CH_4	-10.63	-5.14	-5.80	-6.96	-9.95	7.77 8.93	6.24 4.43	2.87 0.96	-2.02 -1.06
	TMS	CO_2	122.60 124.20[f] 125.00[g] 125.72[c]	122.10 125.30[c]	122.43	122.60 125.74[c]	122.64	-	-	122.85 122.91	123.03 123.18
	Benzene	CO_2	123.95	123.44	123.77	123.93	123.97	-	-	124.25 124.19	124.37 124.52

Experimental: [a]Ref [50] [b]Ref [38] [d]Ref [46] [f]Ref [253] [g]Ref [238]
Calculated: [c]Ref [232] [e]Ref [85]

Table 4.11 The values of ^{1}H chemical shifts (in ppm) for different guest species in their various types of mixed gas hydrates.

NMR	Guest		Reference Standard	GG'@DD		GG'@IDD		GG'@TD		GG'@HD	
	G	G'		G	G'	G	G'	G	G'	G	G'
^{1}H	H_2	CH_4	TMS	5.26 5.21	0.59 0.36 0.76 0.37	5.05 5.33	0.39 0.55 0.49 0.63	4.94 4.97	0.25 0.24 0.36 0.66	4.82 4.77	0.34 0.34 0.40 0.50
			Methanol	-	0.45 0.22 0.62 0.23	-	0.25 0.41 0.35 0.50	-	0.12 0.11 0.22 0.53	-	0.21 0.20 0.10 0.36
^{1}H	H_2	CO_2	TMS	-	-	5.28 5.47	-	5.03 5.21	-	4.86 5.07	-
^{1}H	CO_2	CH_4	TMS	-	-	-	1.05 0.70 0.78 0.56	-	0.40 0.85 0.52 0.75	-	0.19 0.56 0.58 0.69
			Methanol	-	-	-	0.91 0.56 0.64 0.61	-	0.26 0.72 0.38 0.61	-	0.05 0.42 0.44 0.56

Table 4.12 The values of ^{13}C chemical shifts (in ppm) for different guest species in their various types of mixed gas hydrates.

NMR	Guest		Reference Standard	GG'@DD		GG'@IDD		GG'@TD		GG'@HD	
	G	G'		G	G'	G	G'	G	G'	G	G'
^{13}C	H_2	CH_4	TMS	-	8.76	-	7.81	-	2.61	-	0.44
			Methanol	-	4.20	-	3.25	-	-1.95	-	-4.12
^{13}C	H_2	CO_2	TMS	-	-	-	122.55	-	122.66	-	122.57
			Benzene	-	-	-	123.90	-	124.0	-	123.90
^{13}C	CO_2	CH_4	TMS	-	-	122.98	9.84	122.68	5.15	122.87	0.76
			Methanol	-	-	-	5.28	-	0.59	-	-3.80

Table 4.13 The values of ^{1}H chemical shifts (in ppm) for different guest species in their free and various encapsulated states.

NMR nuclei	Reference standard	Guest	G_{DD}@FDD	G_{DD}@FDI	G_{IDD}@FDI	G_{IDD}@FII	$G_{1\text{-}1}$@FDD	$G_{1\text{-}1}$@FDI	$G_{1\text{-}1}$@FII
^{1}H	TMS	H_2	4.78	4.78	4.74	4.73	4.76, 4.74	4.77 4.73,	4.74 4.74
	TMS	CH_4	0.65 0.18 0.68 0.30	0.21 0.69 0.66 0.27	0.41 0.12 0.41 0.58	0.36 0.29 0.36 0.62	0.61 0.30 0.36 0.43 0.67 0.68 0.32 0.18	0.25 0.67 0.67 0.27 0.41 0.15 0.43 0.58	0.36 0.29 0.35 0.62 0.63 0.24 0.40 0.40
	Methanol	CH_4	0.51 0.04 0.54 0.16	0.08 0.55 0.53 0.13	0.27 0.27 0.28 0.44	0.22 0.16 0.22 0.49	0.47 0.16 0.22 0.30 0.54 0.54 0.18 0.05	0.11 0.53 0.53 0.13 0.28 0.02 0.29 0.44	0.22 0.15 0.21 0.49 0.49 0.10 0.26 0.26

Table 4.14 The values of ^{13}C chemical shifts (in ppm) for different guest species in their free and various encapsulated states.

NMR nuclei	Reference standard	Guest	G_{DD}@FDD	G_{DD}@FDI	G_{IDD}FDI	G_{IDD}@FII	$G_{1\text{-}1}$@FDD	$G_{1\text{-}1}$@FDI	$G_{1\text{-}1}$@FII
^{13}C	TMS	CH_4	-0.60	-0.57	-1.21	-1.00	-0.46 -0.42	-0.44 -1.15	-1.00 -1.12
	Methanol	CH_4	-5.20	-5.13	-5.77	-5.58	-4.98	-5.0 -5.71	-5.59 -5.68
	TMS	CO_2	122.29	122.33	122.44	122.55	122.25 122.30	122.34 122.48	122.42 122.43
	Benzene	CO_2	123.63	123.67	123.78	123.89	123.64 123.59	123.68 123.81	123.76 123.77

Table 4.15 The values of ^{1}H chemical shifts (in ppm) for different guest species in their various types of mixed gas hydrates.

NMR	Guest		Reference Standard	$G_{DD}G'_{IDD}$@FDD		$G_{DD}G'_{IDD}$@FDI		$G_{IDD}G'_{DD}$@FDI		$G_{IDD}G'_{IDD}$@FII	
	G	G'		G	G'	G	G'	G	G'	G	G'
^{1}H	H_2	CH_4	TMS	4.76 4.79	0.57 0.25 0.41 0.41	4.74 4.73	0.21 0.67 0.68 0.26	4.74 4.74	0.21 0.67 0.68 0.26	4.81 4.66	0.36 0.29 0.34 0.62
			Methanol	-	0.43 0.12 0.27 0.28	-	0.07 0.53 0.54 0.12	-	0.07 0.53 0.54 0.12	-	0.22 0.16 0.21 0.48
^{1}H	H_2	CO_2	TMS	4.84 4.64	-	4.79 4.76	-	4.75 4.72	-	4.77 4.69	-
^{1}H	CO_2	CH_4	TMS	-	0.54 0.31 0.42 0.43	-	0.39 0.16 0.45 0.56	-	0.22 0.67 0.67 0.29	-	0.61 0.35 0.41 0.21
			Methanol	-	0.40 0.18 0.28 0.29	-	0.25 0.02 0.31 0.42	-	0.09 0.54 0.53 0.16	-	0.48 0.22 0.28 0.07

Table 4.16 The values of ^{13}C chemical shifts (in ppm) for different guest species in their various types of mixed gas hydrates.

NMR	Guest		Reference Standard	$G_{DD}G'_{IDD}$@FDD		$G_{DD}G'_{IDD}$@FDI		$G_{IDD}G'_{DD}$@FDI		$G_{IDD}G'_{IDD}$@FII	
	G	**G'**		**G**	**G'**	**G**	**G'**	**G**	**G'**	**G**	**G'**
			TMS	-	-0.30	-	-0.41	-	-0.40	-	-1.00
^{13}C	H_2	CH_4	Methanol	-	-4.85	-	-4.95	-	-4.96	-	-5.59
^{13}C	H_2	CO_2	TMS	-	122.30	-	122.44	-	122.29	-	122.47
			Benzene	-	123.60	-	123.63	-	123.62	-	123.80
			TMS	122.30	-0.30	122.30	-1.20	122.44	-0.60	122.47	-1.20
^{13}C	CO_2	CH_4	Methanol	-	-4.82	-	-5.76	-	-5.14	-	-5.73

4.5.2 Chemical Shifts of the encapsulated molecules in fused cages

To analyze whether the neighboring cage and the guest species in it affect the chemical shift value of an encapsulated molecule in a cage, the ^{1}H and ^{13}C NMR parameters of the guest species trapped in fused cages are calculated. These results are provided in table 4.13-4.16.

From the table 4.13, it can be seen that the ^{1}H chemical shift value for H_2 in $(H_2)_{DD}$@FDD and $(H_2)_{1\text{-}1}$@FDD are nearly the same as that in H_2@DD. It holds true for the complexes $(H_2)_{IDD}$@FDI and $(H_2)_{1\text{-}1}$@FII. This indicates that the neighboring cage or the guest species in that has little effect on the NMR properties of the tiny H_2 molecule residing in a water cage. Similarly, the chemical shift values of the protons of CH_4 in $(CH_4)_{DD}$@FDD and $(CH_4)_{1\text{-}1}$@FDD are also not differ from that of CH_4@DD. A noticeable change in ^{1}H or ^{13}C chemical shifts is also not observed in other fused cages FDI and FII compared to those of CH_4 in their component cages, irrespective of the type and vacancy of the adjacent cage.

The ^{1}H and ^{13}C chemical shifts values for the mixed hydrates are listed in table 4.15 and 4.16. A significant change in chemical shift for a given guest species is not observed in presence of a different type of guest molecule in the neighboring cavity. The averaged ^{1}H chemical shift value of H_2 in $(H_2)_{DD}(CH_4)_{DD}$@FDD is 4.78 which is indistinguishable from that obtained for $(H_2)_{DD}$@FDD. The averaged ^{1}H chemical shift value of CH_4 in $(H_2)_{DD}(CH_4)_{DD}$@FDD is 0.41 ppm which is also not significantly different from that of $(CH_4)_{DD}$@FDD. A similar conclusion can also be drawn from the ^{1}H and ^{13}C chemical shift values of guests in FDI and FII cages.

4.6 Conclusion

The interaction energies of the guest species H_2, CH_4 and CO_2 with different types of host cages were calculated and the results are correlated to the size of the guest molecule and the host cages. Being the smallest species, the interaction energy of H_2 with the host cage was found to be the least among other guest species and it is decreased further with an increase in the size of the cage. On the other hand, the interaction of CO_2 is more attractive in large cages due to the favorable van der Waals overlap between them. Multiple occupancy of dodecahedral or irregular dodecahedral cage causes repulsion between the guest species. Such repulsion leads to the disintegration of DD and IDD cages when two molecules of CO_2 occupy in these cages. A comparison of the interaction energy obtained for a molecule trapped in a single cage with that obtained for fused cages suggests that the interaction of small guest species does not extend beyond a cage. However, the interaction

of large guest species is not limited to the cage where it is located; rather it extends to the neighboring cage thereby interacting with the guest species in those cages.

The study showed that the vibrational Raman frequencies of the molecules undergo blue shift when they are encapsulated inside water cages. It was also revealed that the blue shift depends on the size of the molecule such that a large molecule shows maximum blue shift in its stretching frequency. However, the blue shift observed for a guest molecule due to its confinement is decreased with an increase in the size of the cage. This is in accordance with the earlier reported experimental and theoretical observations. In the case of double occupancy, the blue shift is found to be enhanced further independent of the nature of guest species suggesting that the extent of blue shift can be used as a measure of cage occupancies in gas hydrates. The comparison of the stretching frequencies of a particular guest species in a DD or IDD cage with those obtained in a fused cage (FDD, FDI and FII) did not show any significant change indicating that the stretching frequencies of a trapped molecule are not influenced by the surrounding cages. This was also found to be true in presence of guest species in an adjacent cage.

The calculations of NMR chemical shifts for the nuclei ^{1}H and ^{13}C of the guest species trapped in various cages revealed that these nuclei are deshielded due to their confinement inside the water cages. The calculations showed that the change in the chemical shift is insignificant for H_2 in various types of cages due to its small size. The protons of CH_4 are down shielded more showing a change in their chemical shift values by 0.04-0.4 ppm with encapsulation in various cages. Apparently, the chemical shifts of guest molecules tend to their free state values with an increase in the size of the cage. Further, the deshielding was found to be more pronounced for the double occupancy. Like ^{1}H, ^{13}C chemical shifts of methane also showed a similar trend with respect to the size of the cage and the type of occupancy. A comparison of the respective chemical shift values of H_2 and CH_4 (for ^{1}H and ^{13}C) obtained for the complexes of single and fused cages revealed that neither the adjacent cage nor the guest species in that influences the NMR properties of an encapsulated molecule.

Chapter-5
Mixed hydrates of hydrogen and tetrahydrofuran

5.1 Introduction

The role of clathrate hydrates as hydrogen storage materials is well discussed in chapter 1. The formation of hydrogen hydrates at mild conditions in presence of promoter THF hydrates has been studied by several research groups [40-43, 107-109, 254, 255, 256]. The experimental [107, 109, 254], quantum mechanical [124-126] and molecular dynamic simulations [116, 123] studies have been performed in the past by several research groups to estimate the hydrogen storage efficiency of THF mixed sII hydrates. Although there are several reports about the multiple occupancy of H_2 in the cages of sII hydrates, the optimum number of H_2 molecules in hydrate cavities remains disputed. Therefore, in the present work, computational studies are carried out for the complexes formed by the successive addition of H_2 in isolated dodecahedral and hexakaidecahedral cages which are the building blocks of sII hydrates. The possibility of simultaneous occupancy of H_2 and THF in the large cages of sII hydrates is also investigated. The effect of a neighboring dodecahedral cage on the stability of complexes formed when THF or a mixture of THF and H_2 is confined in a hexakaidecahedral cage when both type of cages are fused together is investigated. The feasibility of subsequent addition of H_2 in the neighboring dodecahedral cavity is also examined.

The stability of single as well as fused cage complexes is analyzed in terms of host-guest interaction energy. The change in enthalpy (ΔH) and change in Gibbs free energy (ΔG) are calculated to assess the thermodynamic feasibility of the encapsulation of guest species. The contributions of different components of energies on the stability of fused cage complexes are analyzed based on the energy decomposition method. The ^{1}H and ^{13}C chemical shift values of H_2 and THF molecules for its free and encapsulated states are computed to infer about the number of guest molecules encapsulated in the same or adjacent water cages of the fused cage complexes.

5.2 Computational Details

Geometry optimizations of all the complexes were carried out using the software Gaussian 09 at the B97D/cc-pVTZ level of theory [126, 184, 221] as was done for other complexes studied in the previous chapters. The successive additions of H_2 in isolated dodecahedral and

hexakaidecahedral cages were examined. The encapsulation of up to five H_2 molecules in DD cage and eight in HD was considered. The optimized geometries of all the complexes are given in Figure 5.1 and 5.2. The complexes formed by the confinement of H_2 in DD and HD cages are represented by the notations $(\mathrm{DD})_{\mathrm{nH_2}}$and $(\mathrm{HD})_{\mathrm{nH_2}}$, respectively, where '*n*' denotes the number of H_2 molecules encapsulated.

To understand the role of neighboring cavity on the stabilization of the complexes, the complexes of THF with and without H_2 in an isolated HD cage as well as in a HD cage fused to an empty DD cage were examined. Further, the successive encapsulation of H_2 molecules in the small cage (DD) in presence of the neighboring HD cage, the latter occupied by THF was considered. In the following discussion, the above complexes of varying hydrogen molecules are represented by the notation $(DD)_{nH_2}(HD)_{THF}$, where '*n*' represents the number of H_2 molecules residing in the small cage. In a similar way, the complexes formed by the encapsulation of H_2 and THF in the large cage with H_2 molecules in an adjacent dodecahedral cage are represented by the notation $(DD)_{(\mathrm{n-1})\mathrm{H_2}}(HD)_{THF+H_2}$. The optimized geometries of such mixed hydrates are given in Figures 5.3 and 5.4.

The interaction energy (E_{int}) between the host cage and the guest molecule is calculated using the equation 3.1. The E_{int} is further corrected for basis set superposition error (BSSE) using the counterpoise method proposed by Boys and Bernardi [224].

In order to assess the contribution of different types of interactions in the stability of fused cage complexes, energy decomposition analysis by Symmetry Adaptive Perturbation Theory method (SAPT0) [257] at 6-31G** level using Psi4 program was performed [258]. In this method, the interaction energy of the complex is expressed as

$$E_{SAPT0} = E_{elst} + E_{exch} + E_{ind} + E_{disp} \quad (5.1)$$

where E_{elst}, E_{exch}, $E_{ind}$and E_{disp} represent the electrostatic, exchange repulsion, induction and dispersion energies, respectively.

The frequency calculations of all the optimized geometries were performed at the same level of theory. The absence of any imaginary frequency confirmed that the optimized geometries correspond to the minima in the potential energy surface. To assess the thermodynamic feasibility of encapsulation of guest molecules, the change in enthalpy (ΔH) and change in Gibbs free energy (ΔG)

associated with the encapsulation are also calculated at 298 K for a pressure of 1 bar [226].

Chemical shift values of the guest species in their free as well as encapsulated states are calculated [236] to infer about the occupancy of guest molecules in various cages.

5.3 Results and Discussion

5.3.1 Encapsulation of H_2 in dodecahedral (DD) and hexakaidecahedral (HD) cages

The values of interaction energy (E_{int}) and interaction energy per guest molecule ($E_{int/guest}$) for the complexes were calculated as mentioned before and are listed in table 5.1. It was observed that the DD cage remained intact up to the encapsulation of five H_2 molecules suggesting that the maximum occupancy of H_2 in DD cage is five. However, from table 5.1, it can be seen that the value of E_{int} for the complex becomes positive for n≥3. This indicates that the optimum occupancy of H_2 inside DD cage is two. This is in agreement with the experimental observations of Lee *et al* on the double occupancy in the small cages by H_2 in mixed hydrogen hydrates [108]. The above results are also in agreement with the results of other density functional studies reported earlier [231, 259]. From table 5.1, it can be seen that the interaction energy between the guest and the host cage for $(DD)_{1H_2}$ is -1.60 kcal/mol. The value of $E_{int/guest}$ for the complexes with the double occupancy of H_2 in DD cage is reduced by 1.26 kcal/mol compared to that of its single occupancy. With the encapsulation of three, four and five hydrogen molecules in the DD cage, the interaction becomes more repulsive.

From table 5.1, it can be inferred that for HD cage, the maximum occupancy is 8, whereas its optimum occupancy is 7. Chattaraj *et al* also studied the maximum occupancy of HD cage by H_2 molecules at B3LYP/6-31G level of theory [231]. They reported the disintegration of HD cage with inclusion of more than one H_2 molecule. However, the present study at B97D/cc-pVTZ level shows that the structure of HD cage remained intact till it encapsulates eight H_2 molecules. The available experimental result in this regard is the encapsulation of four H_2 molecules in H_2-THF mixed hydrates [108] and is expected to achieve more occupancy by tuning the concentrations of H_2 and THF molecules. It may also be achieved by altering temperature, pressure, etc.

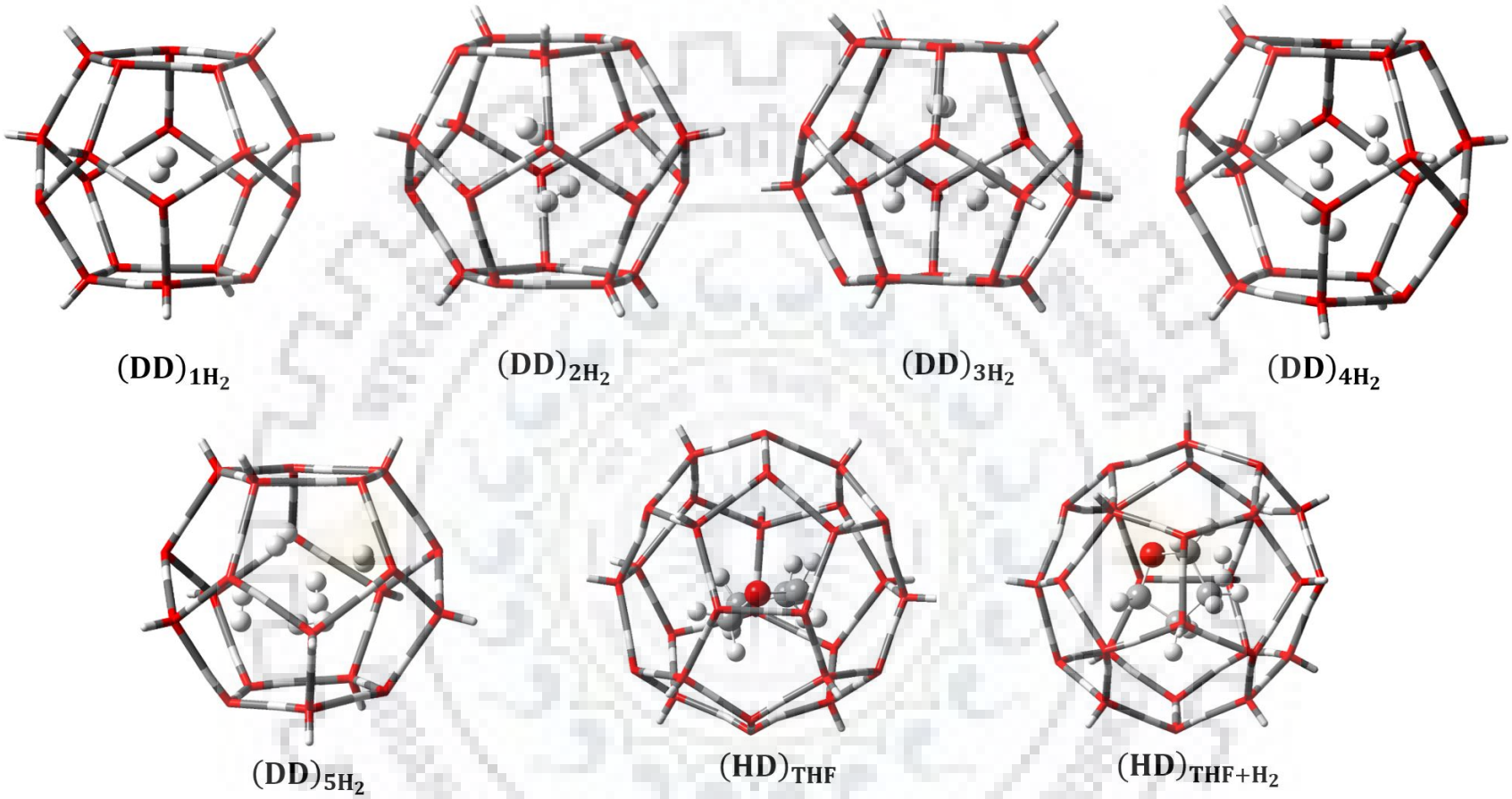

Figure 5.1 Optimized geometries of the complexes $(DD)_{nH_2}$, $(HD)_{THF}$ and $(HD)_{THF+H_2}$ at B97D/cc-pVTZ level.

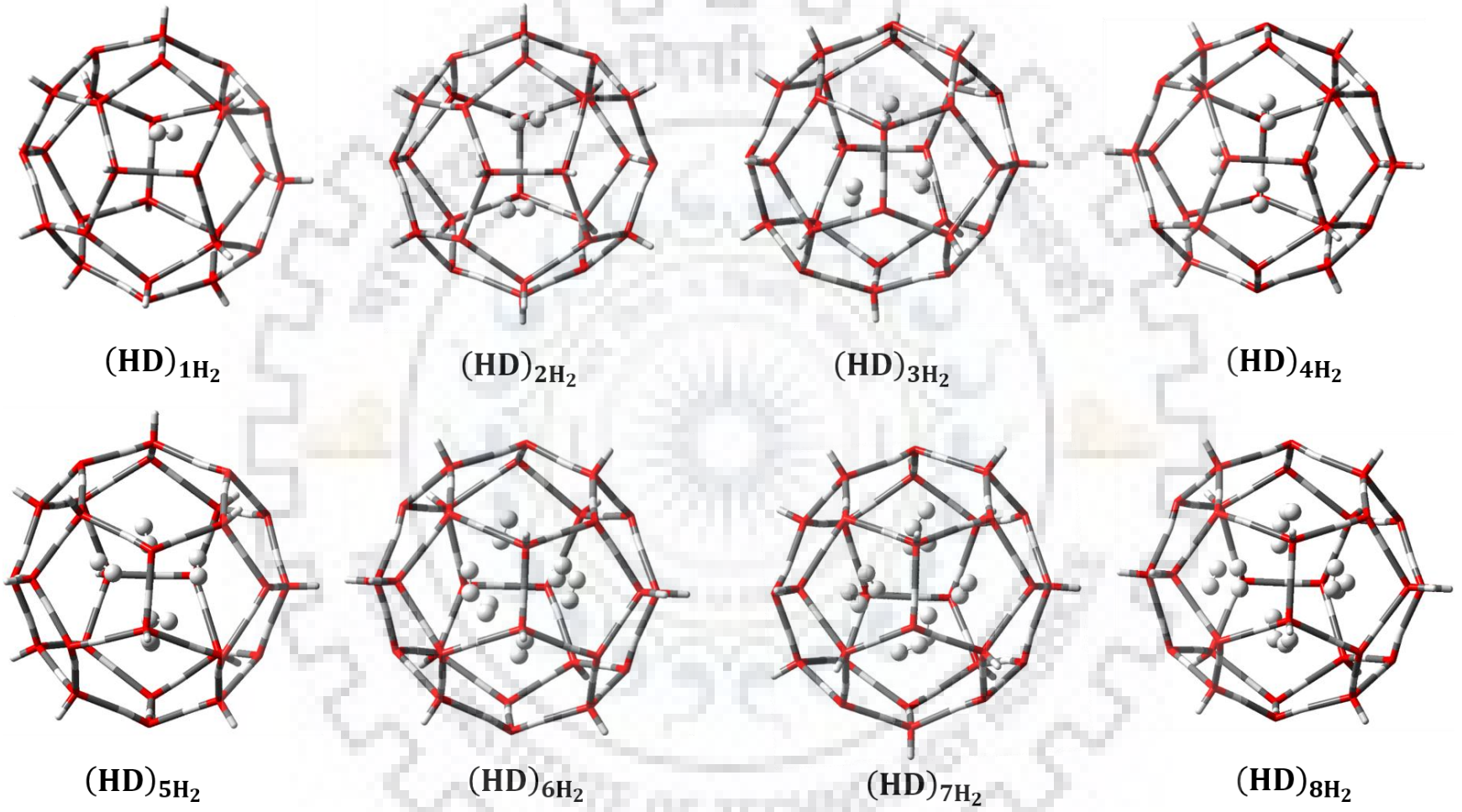

Figure 5.2 Optimized geometries of the complexes $(HD)_{nH_2}$ obtained at B97D/cc-pVTZ level.

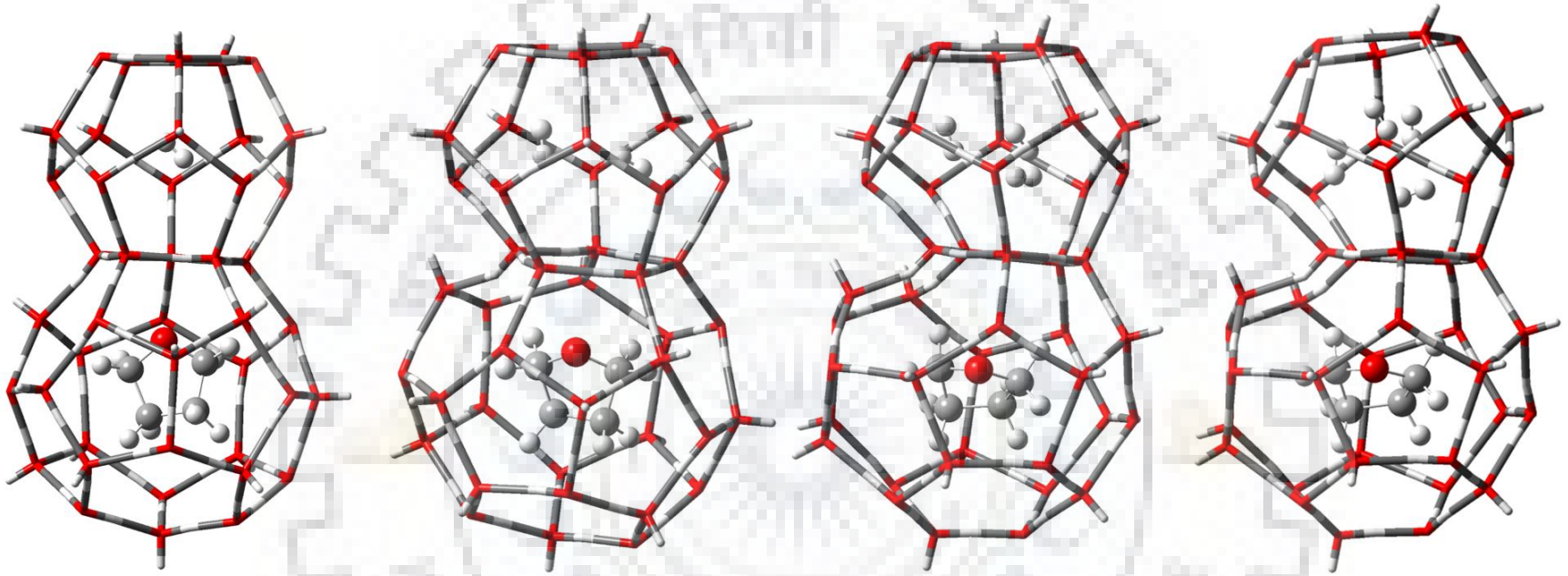

Figure 5.3 Optimized geometries of the complexes $(DD)_{nH_2}(HD)_{THF}$ obtained at B97D/cc-pVTZ level.

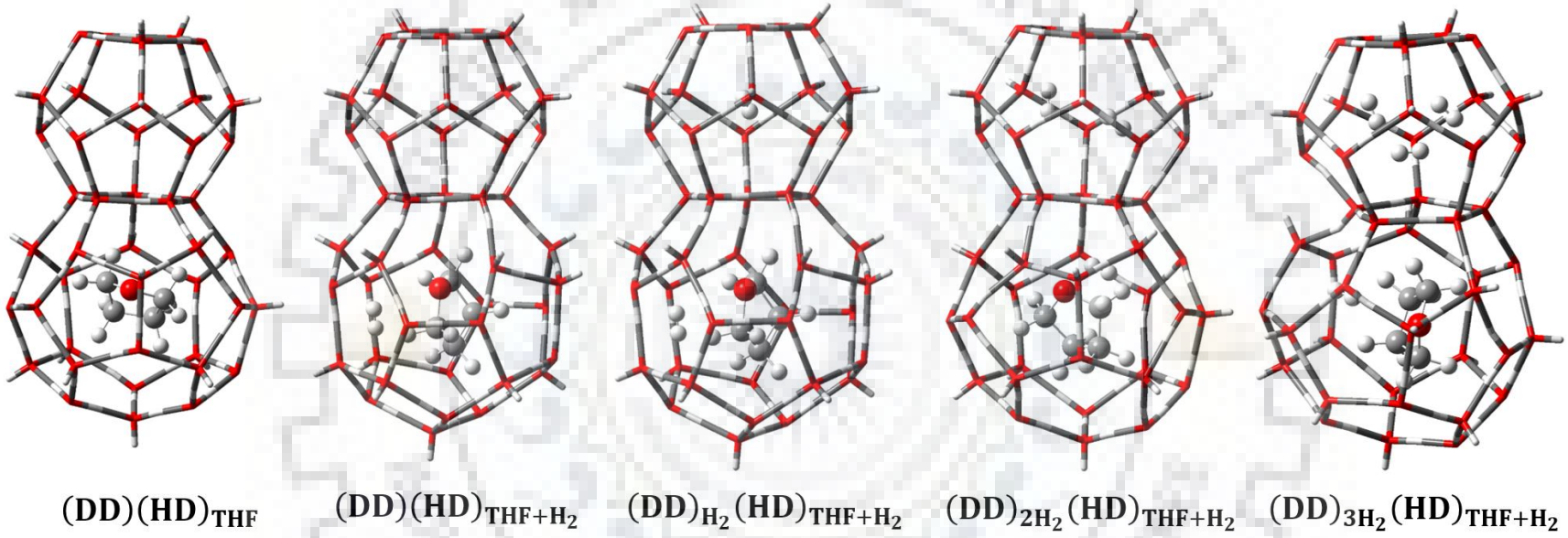

Figure 5.4 Optimized geometries of the complexes $(DD)_{(n-1)H_2}(HD)_{THF+H_2}$ obtained at B97D/cc-pVTZ level.

Table 5.1 The values of interaction energy (E_{int}) and interaction energy per guest molecule ($E_{int/guest}$) obtained for various complexes obtained at B97D/cc-pVTZ level of theory. The BSSE corrected values are given in bold. The energies are in kcal/mol.

Complex	E_{int} (kcal/mol)	$E_{int/guest}$ (kcal/mol)
$(DD)_{1H_2}$	-3.45	-3.45
	-1.60	**-1.60**
$(DD)_{2H_2}$	-4.45	-2.22
	-0.71	**-0.36**
$(DD)_{3H_2}$	-4.21	-1.40
	0.81	**0.27**
$(DD)_{4H_2}$	-3.20	-0.80
	2.85	**0.71**
$(DD)_{5H_2}$	-0.62	-0.12
	6.38	**1.28**
$(HD)_{1H_2}$	-2.73	-2.73
	-1.17	**-1.17**
$(HD)_{2H_2}$	-4.75	-2.37
	-2.21	**-1.11**
$(HD)_{3H_2}$	-7.17	-2.39
	-2.70	**-0.90**
$(HD)_{4H_2}$	-8.50	-2.12
	-2.90	**-0.75**
$(HD)_{5H_2}$	-8.99	-1.79
	-2.37	**-0.47**
$(HD)_{6H_2}$	-9.87	-1.64
	-2.07	**-0.34**
$(HD)_{7H_2}$	-8.97	-1.28
	-0.53	**-0.07**
$(HD)_{8H_2}$	-9.23	-1.15
	0.25	0.03
$(DD)_{H_2}(HD)$	-3.36	-3.36
	-1.58	**-1.58**
$(DD)(HD)_{THF}$	-23.51	-23.51
	-13.58	**-13.58**

5.3.2 Effect of an adjacent cage

In order to study the interaction of guest molecules with water molecules of the neighboring cages, the interaction energy of the complexes formed by encapsulating THF in a HD cage with or without H_2 molecules for the fused HD-DD cage is determined.

The values of interaction energies of the complexes mentioned above are provided in table 5.2. It can be seen from the table that the value of E_{int} is enhanced by 3.0 kcal/mol for the complex $(\mathrm{DD})(\mathrm{HD})_{\mathrm{THF}}$ as compared to $(\mathrm{HD})_{\mathrm{THF}}$. Similarly, the interaction energy of the complex $(\mathrm{DD})(\mathrm{HD})_{\mathrm{THF+H_2}}$ is more than that of $(\mathrm{HD})_{\mathrm{THF+H_2}}$.

The observed higher values of E_{int} for the fused complexes arise due to the interaction of THF with water molecules of the neighboring DD cage. Unlike THF, H_2 does not interact with the water molecules of the neighboring cage. For example, the BSSE corrected values of complexes $(\mathrm{DD})_{1\mathrm{H_2}}$ and $(\mathrm{DD})_{\mathrm{H_2}}(\mathrm{HD})$ are -1.60 and -1.58 kcal/mol, respectively. The above observation is also in agreement with the results of the previous chapter on the hydrates of H_2, CO_2 and CH_4.

The role of a neighboring DD cage on the thermodynamic parameters associated with the encapsulation of THF or a mixture of THF and H_2 (*i.e*. THF/H_2+THF) inside HD cavity of a fused dodeca-hexakaidecahedral cage is also investigated in terms of change in enthalpy and change in Gibbs free energy. The change in the values of Gibbs free energy associated with the encapsulation of THF/THF+H_2 inside the fused DD-HD cage is compared to that for the single cage complexes. The calculated values of ΔG of encapsulation for $(HD)_{THF}$ and $(DD)(HD)_{THF}$ are -5.00 and –6.73 kcal/mol, respectively. Similarly, the value of ΔG for the fused $(\mathrm{DD})(\mathrm{HD})_{\mathrm{THF+H_2}}$ complex is more negative compared to that of $(\mathrm{HD})_{\mathrm{THF+H_2}}$ suggesting that the presence of DD cage assists the encapsulation of THF/ THF+H_2 in HD cage.

Table 5.2 The values of interaction energy (E_{int}), interaction energy per guest molecule ($E_{int/guest}$), change in enthalpy (ΔH) and change in Gibbs free energy (ΔG) for various complexes obtained at B97D/cc-pVTZ level of theory. The BSSE corrected values are given in bold.

Complex	E_{int} (kcal/mol)	$E_{int/guest}$ (kcal/mol)	ΔH (kcal/mol)	ΔG (kcal/mol)
$(HD)_{THF}$	-21.25 **-10.72**	-21.25 **-10.72**	-18.45	-5.00
$(HD)_{THF+H_2}$	-19.97 **-8.95**	-9.98 **-4.48** **1.39**[a]	-48.18	-26.88
$(DD)_{H_2}(HD)$	-3.36 **-1.58**	-3.36 **-1.58**	-34.09	-28.4
$(DD)(HD)_{THF}$	-23.51 **-13.58**	-23.51 **-13.58**	-20.74	-6.73
$(DD)(HD)_{THF+H_2}$	-31.17 **-20.37**	-15.59 **-10.18**	-55.88	-32.90

[a]Ref [231]

5.3.3 Multiple guest occupancy of fused cages

It is observed that the neighboring dodecahedral cavity plays an important role in the stabilization of the complexes formed when THF/ THF+H_2 is encapsulated in the large cavities of fused cages. To examine the feasibility of multiple H_2 occupancy in the dodecahedral cages of the fused system in presence of THF, the stability of mixed hydrates of H_2 and THF in fused cages with varying number of H_2 is studied.

The effect of multiple occupancy of H_2 molecules in dodecahedral cage of the fused system is studied using the complexes, $(DD)_{nH_2}(HD)_{THF}$ and $(DD)_{(n-1)H_2}(HD)_{THF+H_2}$ by analyzing the respective interaction energy (E_{int}). The values of E_{int} for the complexes $(DD)_{nH_2}(HD)_{THF}$ with and without BSSE corrections are listed in table 5.3. In these complexes, H_2 molecules are added in the DD cage, keeping the neighboring HD cage occupied by THF/THF+H_2.

The negative values of E_{int} for $(DD)_{nH_2}(HD)_{THF}$ indicate that the formation of these complexes is energetically feasible. However, with the addition of multiple H_2 in the DD cage, the value of interaction energy per H_2 molecule of the complex is decreased compared to that of $(DD)_{H_2}(HD)_{THF}$. A similar decrease in the interaction energy with successive addition of H_2 in the DD cavity is also observed for the complexes $(DD)_{(n-1)H_2}(HD)_{THF+H_2}$. The decrease in the interaction energy per H_2 in the above two cases is evidently due to the repulsion between H_2 molecules occupying the same cavity.

Further, a comparison of the interaction energies of the complexes $(DD)_{nH_2}(HD)_{THF}$ and $(DD)_{(n-1)H_2}(HD)_{THF+H_2}$ given in table 5.3 and 5.4 revealed that the difference in the values of E_{int} for $(DD)_{H_2}(HD)_{THF}$ and $(DD)(HD)_{THF+H_2}$ is ~7 kcal/mol with the latter being more stable. Similarly, E_{int} for $(DD)_{H_2}(HD)_{THF+H_2}$ is higher than that of $(DD)_{2H_2}(HD)_{THF}$ by ~9 kcal/mol. Among the complexes $(DD)_{3H_2}(HD)_{THF}$ and $(DD)_{2H_2}(HD)_{THF+H_2}$, the difference in E_{int} is ~7 kcal/mol. This suggests that the accommodation of both H_2 and THF in the larger HD cage is energetically favored over the encapsulation of THF and H_2 molecules in different cages for n=1-4. However, the difference in E_{int} reduced to ~1 kcal/mol for the complexes with n=4. This indicates that the difference between the interaction energies of the complexes $(DD)_{nH_2}(HD)_{THF}$ and $(DD)_{(n-1)H_2}(HD)_{THF+H_2}$ diminishes with an increase in the value of n.

Table 5.3 The values of interaction energy (E_{int}), change in enthalpy (ΔH) and change in Gibbs free energy (ΔG) for various complexes obtained at B97D/cc-pVTZ level of theory. The BSSE corrected values are given in bold.

Complex	$(\mathbf{DD})_{\mathbf{H_2}}(\mathbf{HD})_{\mathbf{THF}}$	$(\mathbf{DD})_{\mathbf{2H_2}}(\mathbf{HD})_{\mathbf{THF}}$	$(\mathbf{DD})_{\mathbf{3H_2}}(\mathbf{HD})_{\mathbf{THF}}$	$(\mathbf{DD})_{\mathbf{4H_2}}(\mathbf{HD})_{\mathbf{THF}}$
E_{int} (kcal/mol)	-25.25 **-13.59**	-26.06 **-13.38**	-27.13 **-12.98**	-25.92 **-10.82**
ΔH (kcal/mol)	-53.13	-82.56	-112.2	-137.90
ΔG (kcal/mol)	-34.50	-56.0	-78.60	-95.99

Table 5.4 The values of interaction energy (E_{int}), change in enthalpy (ΔH) and change in Gibbs free energy (ΔG) for various complexes obtained at B97D/cc-pVTZ level of theory. The BSSE corrected values are given in bold.

Complex	$(\mathbf{DD})(\mathbf{HD})_{\mathbf{THF+H_2}}$	$(\mathbf{DD})_{\mathbf{1H_2}}(\mathbf{HD})_{\mathbf{THF+H_2}}$	$(\mathbf{DD})_{\mathbf{2H_2}}(\mathbf{HD})_{\mathbf{THF+H_2}}$	$(\mathbf{DD})_{\mathbf{3H_2}}(\mathbf{HD})_{\mathbf{THF+H_2}}$
E_{int} (kcal/mol)	-31.17 **-20.37**	-34.47 **-21.95**	-34.15 **-20.15**	-26.26 **-11.69**
ΔH (kcal/mol)	-55.88	-89.95	-119.0	-141.80
ΔG (kcal/mol)	-32.90	-61.50	-84.60	-99.0

As discussed earlier, the main factor that reduces the stabilization energy of the complexes with an increase in the number of guest species is the repulsion between guest molecules. Thus, in such complexes, the guest molecules orient in such a way to minimize the guest-guest repulsion. An analysis of the orientation of encapsulated guest molecules showed that two H_2 molecules are aligned perpendicular to each other when both of them are encapsulated in a DD cage. Similarly, three H_2 molecules aligned themselves in a triangular arrangement. The encapsulation of four H_2 molecules leads to a tetrahedral alignment with respect to each other. The shortest intermolecular distances between H_2 molecules residing in the DD host cage of the complexes $(DD)_{nH_2}(HD)_{THF}$ and $(DD)_{(n-1)H_2}(HD)_{THF+H_2}$ are given in table 5.5.

The multiple encapsulation of H_2 molecules in dodecahedral cage of the fused systems is expected to affect the geometry of the host cage. The change in the diameter of various host cages for the fused cage complexes considered in the present study was determined and is provided in table 5.6. It is observed that the diameter of small (DD) cavity is increased by 0.01-0.16Å as the number of H_2 molecules is increased from n=1 to 4. Similarly, the diameter of large (HD) cavity is also increased by 0.05 to 0.06 Å on encapsulating the guest species THF/THF+H_2 inside. It was also found that the bond length of H_2 in the multiply occupied dodecahedral cage (0.7380 Å) is shorter than that of a free H_2 molecule (0.7431 Å). However, the change in bond length of H_2 was not significant when H_2 was encapsulated in large cages along with THF.

It is known that in the sII type hydrate structure, each cage is surrounded by neighboring water cages which restrain the expansion or contraction of cage structure due to the encapsulation of guest molecule. Thus, it is important to test whether the energetic feasibility of multiple guest encapsulation observed in the present work is due to the expansion of the cages due to the presence of a guest. For this purpose, the optimization and frequency calculations were performed for the complexes $(DD)_{2H_2}(HD)_{THF}$ and $(DD)_{H_2}(HD)_{THF+H_2}$ by freezing the oxygen atoms of the host water molecules thereby preventing the expansion of the cage with guest encapsulation. The interaction energy of these complexes which show positive frequencies for all modes are listed in table 5.7. From the table, it is evident that the encapsulation of guest molecules in $(DD)_{H_2}(HD)_{THF+H_2}$ is energetically more feasible than that of $(DD)_{2H_2}(HD)_{THF}$ confirming that feasibility of encapsulation of H_2 and THF in the HD cavity is not merely due to the expansion of the cage but mainly due to the attractive interactions between the guest and the host.

Table 5.5 Shortest intermolecular distance between H_2 molecules encapsulated in the complexes $(DD)_{nH_2}(HD)_{THF}$ and $(DD)_{(n-1)H_2}(HD)_{THF+H_2}$.

Complex	$R_{H_2---H_2}$ (Å)
$(\mathbf{DD})_{\mathbf{2H_2}}(\mathbf{HD})_{\mathbf{THF}}$	2.345
	2.249
$(\mathbf{DD})_{\mathbf{3H_2}}(\mathbf{HD})_{\mathbf{THF}}$	2.319
	2.326
$(\mathbf{DD})_{\mathbf{4H_2}}(\mathbf{HD})_{\mathbf{THF}}$	2.161
	2.203
	2.450
	2.361
$(\mathbf{DD})_{\mathbf{2H_2}}(\mathbf{HD})_{\mathbf{THF+H_2}}$	2.195
$(\mathbf{DD})_{\mathbf{3H_2}}(\mathbf{HD})_{\mathbf{THF+H_2}}$	2.226
	2.355
	2.424

Table 5.6 The cage diameter of various fused cages.

Complex	Cage diameter (Å)	Complex	Cage diameter (Å)
(DD)(HD)	**7.64** *9.05*	$\mathbf{(DD)(HD)_{THF}}$	**7.64** *9.04*
$\mathbf{(DD)_{H_2}(HD)_{THF}}$	**7.64** *9.04*	$\mathbf{(DD)_{H_2}(HD)}$	**7.64** *9.05*
$\mathbf{(DD)_{2H_2}(HD)_{THF}}$	**7.65** *9.10*	$\mathbf{(DD)_{H_2}(HD)_{THF+H_2}}$	**7.64** *9.08*
$\mathbf{(DD)_{3H_2}(HD)_{THF}}$	**7.79** *9.11*	$\mathbf{(DD)_{2H_2}(HD)_{THF+H_2}}$	**7.68** *9.11*
$\mathbf{(DD)_{4H_2}(HD)_{THF}}$	**7.82** *9.11*	$\mathbf{(DD)_{3H_2}(HD)_{THF+H_2}}$	**7.80** *9.09*

Diameter of DD cage is in bold
Diameter of HD cage is in italics

Table 5.7 The values of interaction energy (E_{int}), change in enthalpy (ΔH) and change in Gibbs free energy (ΔG) for the complexes $(DD)_{2H_2}(HD)_{THF}$ and $(DD)_{H_2}(HD)_{THF+H_2}$ obtained at B3LYP/6-311+G** level of theory. The BSSE corrected values are in bold.

Complex	$\mathbf{(DD)_{2H_2}(HD)_{THF}}$	$\mathbf{(DD)_{H_2}(HD)_{THF+H_2}}$
$\mathbf{E_{int}}$	-7.32	-11.09
(kcal/mol)	**-4.29**	**-9.46**

5.4 Energy decomposition analysis

In order to know the contribution of different components of energy to the total interaction energy (E_{int}) and to the stability of the fused cage complexes, various components of interaction energy were determined using symmetry adapted perturbation theory (SAPT0). The percentage contributions of electrostatic, induction and dispersion interactions obtained for the complexes of fused cages are listed in table 5.8. It is observed that the electrostatic and dispersion interactions mainly contribute to the stability of the complexes. As expected, for the complexes $(DD)_{nH_2}(HD)_{THF}$, the contributions of electrostatic and dispersion interactions increase with an increase in the number of H_2 in the smaller (DD) cage. For singly and doubly occupied dodecahedral cage, the contribution of dispersion interaction is more as compared to that of electrostatic interaction. On the other hand, for triple and quadruple occupancy of H_2 (n=3 and 4) electrostatic interaction is predominant. For the mixed hydrates, $(DD)_{(n-1)H_2}(HD)_{THF+H_2}$, the contribution of electrostatic interaction is dominant for the single and double occupancy of H_2 inside the small cage. However, dispersion interaction is observed to have greater contribution to total interaction energy for $(DD)_{3H_2}(HD)_{THF+H_2}$.

5.5 Thermodynamics of encapsulation

To get more insight on the feasibility of encapsulation of different gas molecules in various water cages, the values of ΔH and ΔG associated with the encapsulation of guest molecules in the fused cages were calculated. The value of ΔH (or ΔG) is obtained as the difference of the enthalpy (or Gibbs free energy) of the complex and the total enthalpy (or total Gibbs free energy) of the cage and the guests as in their free states. The values of ΔH and ΔG for fused cage complexes are listed in table 5.3 and 5.4.

The negative values of ΔH for the complexes $(DD)_{nH_2}(HD)_{THF}$ and $(DD)_{(n-1)H_2}(HD)_{THF+H_2}$ indicates that the encapsulation of guests inside fused-dodeca-hexakaidecahedral cages is an exothermic process. The value of ΔG is also found to be negative for all the complexes considered suggesting the feasibility of such encapsulation. The value of ΔG per H_2 molecule is found to be decreased with an increase in the number of hydrogen molecules for both types of complexes $(DD)_{nH_2}(HD)_{THF}$ and $(DD)_{(n-1)H_2}(HD)_{THF+H_2}$.

Table 5.8 Decomposition of the total intermolecular interaction energy into its various components obtained at SAPT0/6-31G** level.

Complex	E_{ele}(%)	E_{ind}(%)	E_{disp}(%)
$(DD)_{H_2}(HD)$	27.90	5.42	66.66
$(DD)(HD)_{THF}$	35.34	7.79	56.85
$(DD)_{H_2}(HD)_{THF}$	32.31	8.06	59.61
$(DD)_{2H_2}(HD)_{THF}$	37.37	8.96	53.65
$(DD)_{3H_2}(HD)_{THF}$	46.99	11.15	41.84
$(DD)_{4H_2}(HD)_{THF}$	48.38	9.39	42.21
$(DD)(HD)_{THF+H_2}$	48.43	17.76	33.79
$(DD)_{H_2}(HD)_{THF+H_2}$	47.96	17.44	34.58
$(DD)_{2H_2}(HD)_{THF+H_2}$	49.01	17.41	33.57
$(DD)_{3H_2}(HD)_{THF+H_2}$	40.74	9.30	49.95

On comparing the thermodynamic parameters of the complexes $(DD)_{nH_2}(HD)_{THF}$ with $(DD)_{(n-1)H_2}(HD)_{THF+H_2}$, it is found that thermodynamically it is more feasible to encapsulate both H_2 and THF in the hexakaidecahedral cage. For example, the ΔG associated to $(DD)_{H_2}(HD)_{THF+H_2}$ is ~6.0 kcal/mol more than that of $(DD)_{2H_2}(HD)_{THF}$. A similar trend is also observed for the complexes with more H_2 molecules.

5.6 ^{1}H and ^{13}C NMR chemical shifts of encapsulated molecules

The number of guest molecules encapsulated in different types of host cages can be inferred by carefully analyzing the results of their NMR spectra. Considering this, the chemical shift values of the guests present in small as well as large cages of the fused systems were calculated. The ^{1}H chemical shift values of H_2 and THF in their free and encapsulated states are calculated with respect to the isotropic values of the respective nuclei of tetramethyl silane (TMS). The averaged values of ^{1}H and ^{13}C chemical shifts are listed in tables 5.9-5.11. For H_2 in its free state, the value of chemical shift is 4.72 ppm which is in excellent agreement with the experimental values reported earlier [251]. From the chemical shift values of ^{1}H given in the table 5.9, it can be seen that the ^{1}H undergoes a deshielding of ~0.05 ppm when it is encapsulated inside DD cage irrespective of the presence of THF in an adjacent HD cage. The averaged chemical shift for the guest H_2 in the doubly occupied small cage is 5.19 ppm and is ~0.5 ppm higher than that in the singly occupied DD cage. For the triple and quadruple encapsulation of H_2 molecules in the small cavities as in complexes $(DD)_{nH_2}(HD)_{THF}$, further deshielding of 0.67 and 0.73 ppm, respectively are observed. Thus, an increase in the number of H_2 molecules in small cavity when THF occupies the neighboring large cavity leads to deshielding of the ^{1}H NMR chemical shift values of H_2.

The calculated averaged values of ^{1}H chemical shifts of two types of protons of THF in its free state are 1.76 and 3.44 ppm. These are in close agreement with the experimental values of 1.85 and 3.76 ppm [260] as evident from the table 5.9. In $(DD)_{1H_2}(HD)_{THF}$, deshieldings of 0.24 and 0.56 ppm are observed for ^{1}H of THF compared to the free state as listed in table 5.9. A significant change in the ^{1}H NMR values of THF is not observed when the number of hydrogen molecules are increased in the neighboring DD cage in $(DD)_{nH_2}(HD)_{THF}$. Further, from the table 5.11, it can be seen that for the complexes $(DD)_{(n-1)H_2}(HD)_{THF+H_2}$, the ^{1}H chemical shift values of THF are deshielded by 0.40 and 0.75 ppm as compared to its free state. The above change in chemical shift

values is nearly similar to that observed for $(DD)_{nH_2}(HD)_{THF}$. Thus, the change in ^{1}H chemical shift values of THF is not sufficient to distinguish the occupancy of HD cage due to THF or THF+H_2.

The calculated ^{13}C chemical shifts of two different types of carbon nuclei of THF in its free state are 28.84 and 73.81 ppm as listed in table 5.10. The experimentally reported ^{13}C NMR values for THF are 25.62 and 67.97 ppm [260] indicating a reasonable agreement between the calculated and the experimental values. For $(DD)(HD)_{THF+H_2}$, the ^{13}C chemical shifts of THF are not changed significantly compared to those of free THF, listed in table 5.10. A similar observation can be noticed for the complexes $(DD)_{nH_2}(HD)_{THF}$ having single, double, triple, and quadruple occupancy of small cavities by H_2. This is expected as the presence of H_2 in a neighboring cage does not alter the electronic environment of THF.

On the other hand, from tables 5.10 and 5.11, it can be seen that for the mixed hydrates of the type $(DD)_{(n-1)H_2}(HD)_{THF+H_2}$, the ^{13}C chemical shift of THF is down shielded by ~4.0 ppm compared to free THF. The change in ^{13}C chemical shift of THF in the complexes $(DD)_{(n-1)H_2}(HD)_{THF+H_2}$ is only 2ppm compared to that in $(DD)_{nH_2}(HD)_{THF}$, which is not a significant change. Thus, one cannot distinguish the above two types of complexes using ^{13}C chemical shift values.

However, the splitting patterns of protons chemical shifts of hydrogen molecules can help to distinguish the complexes $(DD)_{nH_2}(HD)_{THF}$ and $(DD)_{(n-1)H_2}(HD)_{THF+H_2}$. For example, the chemical shift for H_2 in $(DD)_{1H_2}(HD)_{THF}$ is 4.73 ppm, whereas two peaks at 4.75 ppm (H_2 in DD) and 5.45 ppm (H_2 in HD) can be observed for $(DD)_{H_2}(HD)_{THF+H_2}$. A Similar observation holds true for the complexes $(DD)_{2H_2}(HD)_{THF+H_2}$, and $(DD)_{3H_2}(HD)_{THF+H_2}$.

The ^{1}H and ^{13}C chemical shifts of THF in free and encapsulated are also calculated using the multi standard reference benzene and are listed in tables 5.9-5.11. From the values, it can be seen that the chemical shifts of the complexes using the references TMS and benzene are in qualitative agreement.

Table 5.9 The values of ^{1}H NMR chemical shifts for H_2 and THF in free and various $(DD)_{nH_2}(HD)_{THF}$ complexes.

NMR	Guest	Reference Standard	H_2	THF	$(DD)_{H_2}$ (HD)	(DD) $(HD)_{THF}$	$(DD)_{H_2}$ $(HD)_{THF}$	$(DD)_{2H_2}$ $(HD)_{THF}$	$(DD)_{3H_2}$ $(HD)_{THF}$	$(DD)_{4H_2}$ $(HD)_{THF}$
^{1}H	H_2	TMS	4.72 4.73[a]	-	4.73	-	4.73	5.19	5.39	5.45
	THF	TMS	-	1.76 3.44 1.85[b] 3.76[b]	-	2.01 4.02	2.00 4.00	2.00 4.00	2.17 4.05	2.16 4.06
		Benzene	-	1.72 3.39	-	1.96 3.97	1.96 3.97	1.88 3.95	2.12 4.01	2.12 4.01

Experimental [a]Ref. [251], [b]Ref. [260]

Table 5.10 The values of ^{13}C NMR chemical shifts for THF in free and various $(DD)_{nH_2}(HD)_{THF}$ complexes.

NMR	Guest	Reference Standard	THF	(DD) $(HD)_{THF}$	$(DD)_{H_2}$ $(HD)_{THF}$	$(DD)_{2H_2}$ $(HD)_{THF}$	$(DD)_{3H_2}$ $(HD)_{THF}$	$(DD)_{4H_2}$ $(HD)_{THF}$
^{13}C	THF	TMS	28.84					
			73.81	29.50	30.84	30.47	30.85	30.91
			25.62[a]	74.46	73.99	74.07	74.99	74.13
			67.97[a]					
		Benzene	30.19	30.87	32.18	31.81	32.19	32.37
			75.15	75.80	75.33	75.41	75.44	75.47

Experimental [a]Ref. [260]

Table 5.11 The values of ^{1}H and ^{13}C NMR chemical shifts for H_2 and THF in various $(DD)_{(n-1)H_2}(HD)_{THF+H_2}$ complexes. The values in parentheses correspond to ^{1}H chemical shift of H_2 in HD.

NMR	Guest	Reference Standard	$(DD)(HD)_{THF+H_2}$	$(DD)_{H_2}(HD)_{THF+H_2}$	$(DD)_{2H_2}(HD)_{THF+H_2}$	$(DD)_{3H_2}(HD)_{THF+H_2}$
^{1}H	H_2	TMS	-	4.75	5.17	5.21
			(5.50)	(5.45)	(5.47)	(5.49)
	THF	TMS	2.16	2.16	2.18	2.28
			4.19	4.19	4.18	4.09
		Benzene	2.11	2.12	2.24	2.04
			4.15	4.15	4.13	4.01
^{13}C	THF	TMS	32.06	32.42	32.55	32.40
			74.47	73.81	74.47	75.33
		Benzene	33.41	33.46	33.89	31.29
			75.81	75.80	75.81	76.67

5.7 Conclusion

The host-guest interaction energies of the complexes formed by the successive addition of H_2 molecules inside the cavities of isolated dodecahedral (DD) and hexakaidecahedral (HD) cages were studied using dispersion corrected density functional theoretical methods. The study showed an optimum occupancy of isolated DD and HD cages as two and seven H_2 molecules, respectively. The interaction of a THF molecule residing inside the larger HD cage of the sII hydrate structure with the water molecules of the neighboring DD cage was also examined and found that such interactions enhance the stability of the complex, which is not observed for the complexes of small guest species.

The stability of the complexes, $(DD)_{nH_2}(HD)_{THF}$ and $(DD)_{(n-1)H_2}(HD)_{THF+H_2}$, formed by encapsulating both H_2 and THF inside the cavities of fused-dodeca-hexakaidecahedral cages was also studied. The comparison of the host-guest interaction energies of $(DD)_{nH_2}(HD)_{THF}$ and $(DD)_{(n-1)H_2}(HD)_{THF+H_2}$, having the same number of H_2 indicated the latter complexes as more stable. The energy decomposition analysis revealed that the stability of these complexes is mainly due to the electrostatic and dispersion interactions. The negative values of the change in free energy associated with the encapsulation of guests also confirmed the feasibility of the formation of the complexes $(DD)_{nH_2}(HD)_{THF}$ and $(DD)_{(n-1)H_2}(HD)_{THF+H_2}$ with the latter as more feasible.

In order to get more insight on the occupancy of different types of cages of the fused systems, ^{1}H and ^{13}C NMR chemical shift values were calculated and results are analyzed. It was observed that the chemical shift values of H_2 are deshielded on encapsulation and the presence of THF in a neighboring cage has little influence on that. For the complexes $(DD)_{(n-1)H_2}(HD)_{THF+H_2}$, the presence of two peaks corresponding to protons of H_2 molecule inside small and large cavities can be used as an aid to distinguish it from $(DD)_{nH_2}(HD)_{THF}$. The calculated ^{13}C chemical shift values of THF encapsulated complexes indicated that carbon nuclei are deshielded significantly when H_2 molecules occupy in the large cavities of the fused cage along with THF.

In summary, the present study unequivocally confirmed that H_2 molecules can be occupied in the hexakaidecahedral cages along with THF, in addition to their occupancy in small cages.

Chapter-6
Clustering of dissolved gas molecules in CH_4-N_2-CO_2-H_2O mixture

6.1 Introduction

As mentioned in chapter 1, gas hydrates can be explored as a future energy resource. Keeping this in mind, efforts have been devoted to develop efficient methods to extract natural gas from hydrate sediments. Different techniques have been used in the past for the extraction of natural gas from hydrate sediments [99, 100-102, 261]. The guest replacement method for natural gas extraction is preferred over the other methods, as the former involves the extraction of natural gas along with the sequestration of CO_2 which is a greenhouse gas. This advantage of the replacement method has stimulated research to improve the efficiency of methane recovery. Several studies on the mechanism as well as on the factors affecting the efficiency of natural gas replacement by CO_2 in gas hydrates have been reported [135, 141, 262]. Though the guest replacement method for natural gas extraction has gained wide attention, its large scale application has been limited due to less efficiency of extraction. Several experimental studies have reported that in the replacement of CH_4 by CO_2, the yield of methane recovery was limited to 60-64% [230, 263]. Thus, improvement in the replacement method is required to increase the recovery of methane.

One of the most important findings of the studies on replacement method is that, the use of a mixture of N_2 and CO_2 in place of pure CO_2 in the process can significantly enhance the percentage of CH_4 recovered from the hydrates [146-150]. As mentioned earlier, the replacement of CH_4 from its hydrates by gas molecules such as CO_2 and N_2 involves the decomposition of the hydrate phase leading to the formation of a liquid containing dissolved gas molecules [141, 262]. Thus, the replacement process can be considered to take place in two steps. In the first step, the parent CH_4 hydrates undergo dissociation to form a liquid phase in the presence of another guest molecule with which CH_4 is to be replaced from the hydrate. Following this, the new hydrate phase is formed from the liquid in which the incoming gas molecules occupy the water cages. In the case of the replacement of CH_4 by a mixture of CO_2 and N_2, the intermediate liquid phase formed contain CH_4, N_2 and CO_2 dissolved in it. The evolution of dissolved gas molecules in this liquid is expected to significantly influence the subsequent steps which involve the formation of a new hydrate phase. The formation of gas bubbles in the liquid phase has an important role in the mass transfer of gas molecules in the beginning of the replacement process when the CH_4 hydrates dissociates [264].

Recently, using tunneling microscopic techniques Uchida *et al* pointed out the importance of evolution of dissolved gas molecules during the dissociation of hydrates [265]. The study revealed the formation of nanobubbles during the dissociation and further reported that the bubbles remained stable even after the complete dissociation of hydrates. The presence of the gas bubbles in the hydrate melt for a long time can lead to the regeneration of hydrate structures [266].

Given the significance of dissolved gas evolution during the hydrate dissociation, it is important to study the properties of a CH_4-N_2-CO_2-H_2O liquid mixture. Earlier studies on the replacement of CH_4 from its hydrates by N_2-CO_2 mixture did not consider the properties of the CH_4-N_2-CO_2-H_2O liquid formed during the process [146-150, 153, 154]. In the present work, the evolution of gas molecules dissolved in the CH_4-N_2-CO_2-H_2O mixture is studied using classical molecular dynamics simulations. The role of dissolved gas evolution on subsequent processes such as hydrate regeneration in the mixture is also examined. The details of the computational methods and models used in the study are explained below.

6.2 Computational methods

Classical molecular dynamics simulations were employed to study the evolution of aqueous gas molecules in the CH_4-N_2-CO_2-H_2O liquid mixture. The simulations were performed using the program, GROMACS-4.6.5 [267]. The simulation system consists of a cubic box enclosing 3000 H_2O molecules. In the initial conformation, CH_4, N_2 and CO_2 molecules were randomly dispersed in water present in the simulation box. The liquid mixture considered here resembles the liquid phase formed as a result of hydrate dissociation during CH_4 replacement by N_2-CO_2 mixture. For the simulations, the number of CH_4 and N_2 respectively, were fixed at 50 and that of CO_2 was increased from 0 to 250 in steps of 50. The increase in the number of CO_2 intends to vary the CO_2:N_2 ratio which corresponds to that of the N_2-CO_2 gas mixture injected into the CH_4 hydrate sediment. The number of CH_4 in the two sets of simulations corresponds to a mole fraction of 0.016 in water. The number of CH_4 molecules in the simulation systems corresponds to highly supersaturated concentration because of the very low solubility of CH_4 reported for similar force fields at identical thermodynamic conditions [268]. However, the concentrations of CH_4 considered are less than the reported limit of supersaturation at these conditions [268].

The CH_4 and CO_2 molecules were modelled using the single point Lennard-Jones and EPM2 models, respectively [269, 270]. The water molecules are modeled by the TIP4P potential [271] and

the parameters for N_2 molecule were obtained from reference [272]. The cross-interaction Lennard-Jones parameters were obtained by applying the Lorentz–Berthelot combination rule. For the EPM2 model for CO_2, which is a rigid three-site model, the O–C–O angle deviates from 180° due to the known problems in the constraint algorithm in the case of a linear angle. This problem is solved when point masses are introduced on each side of the carbon atom in the original EPM2 model as discussed elsewhere [268, 273, 274]. The force fields used in the present work have been applied earlier in the molecular dynamics simulations study of CH_4 replacement from its hydrate [262].

The simulations were performed in the NPT ensemble at 270 K and 20 bar. For the given force fields, the thermodynamic conditions applied in the present study were reported to favour the replacement of CH_4 molecules in hydrates by CO_2 [262]. The simulation started with an energy minimization of the initial conformation. In the next step, the system was simulated in the NVT ensemble for 100 ps during which it reached an equilibrium state with a temperature of 270 K. Following this, an NPT simulation was carried out for 250 ps, after which the system attained an equilibrium pressure and temperature of 20 bar and 270 K, respectively. The equilibrated system was then subject to production simulation for 60 ns with a time step of 2 fs. The system was coupled to the Nose-Hoover thermostat [275, 276] and Parrinello-Rahman barostat [277]. The coupling time constants for barostat and thermostat are 1 ps and 0.5 ps, respectively. During the simulations, LINCS [278] algorithm was applied to constrain the molecular geometries and the water molecules were maintained stable by applying SETTLE algorithm [279]. The short range interactions were considered within a cut off distance of 1.2 nm and the particle-mesh Ewald summation (PME) method was applied to treat the long range electrostatic interactions. During the simulations, periodic boundary conditions were applied in all directions.

6.3 Results and discussion

6.3.1 Evolution of dissolved gas in the CH_4-N_2-CO_2-H_2O mixture

Simulations were performed on the CH_4-N_2-CO_2-H_2O system containing varying concentrations of CO_2. As the simulation systems considered in the present work contain dissolved gas molecules at super saturated concentrations, demixing may occur through the aggregation of aqueous molecules forming gas bubbles. To examine this, each gas molecule in the system is defined as either belonging to the aqueous phase or as a part of the bubble (gas phase). For each gas molecule, the number of solvent molecules present within its first hydration shell was determined. Based on this, a gas

molecule in the bubble is differentiated from the one which is dissolved in water. A molecule present in the bubble will have significantly less water molecules in its hydration shell. In the present work, a gas molecule is considered as belonging to the bubble if the number of water molecules in its first solvation shell is less than 10 which corresponds to half of the hydration number of an aqueous gas molecule. The time evolution of the number of gas molecules in the bubble was examined for the CH_4-N_2-CO_2-H_2O mixture containing different concentrations of CO_2. The number of N_2 and CH_4 molecules in the bubble (gas phase) as a function of time in the mixture containing 50 CH_4 molecules is given in figure 6.1. The details of CO_2 molecules associated with the bubbles formed in the systems are discussed later. From figure 6.1, it can be observed that in CH_4-N_2-CO_2-H_2O system containing 50 CH_4 molecules, bubble formation does not occur without CO_2 molecules. This indicates that the total dissolved gas concentration of this system is not sufficient to overcome the energy barrier for gas bubble nucleation. However, as the number of CO_2 molecules in the system increases, gas bubble starts to form. In the systems containing up to 50 CO_2 molecules, bubble nucleation is not observed within the simulation time of 60 ns (figure 6.1). When the number of CO_2 molecules is increased to 100, the bubble starts to nucleate at ~1.6 ns. Following the nucleation, the bubble grows in size by absorbing aqueous gas molecules from the CH_4-N_2-CO_2-H_2O mixture. The growth of the bubble is complete by ~6 ns and the bubble formed remained stable throughout the 60 ns simulation. The formation of gas bubbles in the CH_4-N_2-CO_2-H_2O mixture containing 100 CO_2 molecules is illustrated in figure 6.2. For CH_4-N_2-CO_2-H_2O systems with high concentrations of CO_2, bubble nucleation is observed immediately at the beginning of the simulation and the bubbles formed are found to be stable.

To confirm that the size of the simulation system did not affect the stability of nanobubbles formed, an independent simulation was performed for the CH_4-N_2-CO_2-H_2O system containing 200 CH_4, 200 N_2, 600 CO_2 and 12000 H_2O molecules. The concentrations of dissolved gas in this larger simulation system is equivalent to that of the system containing 50 CH_4, 50 N_2 and 150 CO_2 in 3000 H_2O molecules. The time evolution of CH_4 and N_2 molecules in the larger simulation system containing 12000 H_2O molecules is given in figure 6.3. The figure indicates the formation of a stable bubble in the larger simulation system indicating that the size of the simulation system considered in the present study is adequate for observing bubble formation.

In all the cases mentioned above, the number of CH_4 and N_2 molecules in the gas phase starts increasing simultaneously indicating that both these molecules are part of the same bubble. A more

detailed analysis of the composition of the bubbles is given in the following section. The preliminary analysis of bubble formation (figure 6.1) indicates that the bubbles formed contain a mixture of more than one type of gas molecules. The studies of the mixed nature of the bubbles formed is significant as it has been reported earlier that the bubbles formed during hydrate dissociation remains in the hydrate melt for a long period [265].

These bubbles can act as a reservoir of gas molecules and facilitate the regeneration of hydrate structures as reported earlier by Bagherzadeh *et al* [266]. As the bubbles formed in CH_4-N_2-CO_2-H_2O contain CH_4 molecules, they can lead to the regeneration of CH_4 hydrate, which is not desirable to CH_4 extraction by replacement using N_2-CO_2 mixture.

6.3.2 Role of CO_2 molecules in the nucleation of the bubble

As discussed above, gas bubbles are formed in the CH_4-N_2-CO_2-H_2O mixture containing 50 CH_4 when the number of CO_2 molecules is 100 or higher. In the absence or at lower concentrations of CO_2, the system is unable to overcome the energy barrier for bubble nucleation. This indicates that the presence of CO_2 molecules has a role in inducing bubble formation in the CH_4-N_2-CO_2-H_2O mixture having 50 CH_4 molecules.

To understand how CO_2 assists bubble nucleation, the distribution of gas molecules in the bubble formed in the mixture was examined in detail. The average number density of CH_4, N_2 and CO_2 molecules in various regions of the gas bubble formed in the CH_4-N_2-CO_2-H_2O mixture was determined over a time interval from 50 to 60 ns of the simulation, at a frequency of 1 ps. During the time interval chosen for this analysis, the CH_4-N_2-CO_2-H_2O mixture contains a stable gas bubble present in it.

The average number density of molecules in the CH_4-N_2-CO_2-H_2O containing 50 CH_4 with 50 N_2 and 100 CO_2 molecules is given in figure 6.4. From the number densities, it is clear that the bubbles formed in the system contain a mixture of CH_4, N_2 and CO_2 molecules in it. However, the distribution of CO_2 molecules in the bubble is significantly different from that of CH_4 and N_2. For all the systems which differ in the concentration of CO_2, the number density of CO_2 molecules is found to reach a maximum at the surface of the bubble where it meets the liquid phase (figure 6.4). This is true for the bubble formed in the larger simulation system containing 200 CH_4, 200 N_2, 600 CO_2 and 12000 H_2O molecules as shown in figure 6.5. Whereas, the density of CH_4 and N_2 decreases on moving towards the surface of the bubble from its interior. The aggregation of CO_2 molecules at

the surface of the bubble resembles with the results reported by Sujith *et al* [268] on the three component CH_4-CO_2-H_2O mixture. However, the concentration of CO_2 inside the bubble in the present study is slightly more than that reported in the three component mixture [268]. The mixed nature of the bubbles as indicated by the number density supports the findings from the above analysis of dissolved gas evolution based on the number of gas molecules in the bubble. The role of CO_2 molecules in inducing bubble formation in supersaturated solutions of hydrophobic gas has been studied earlier [273]. In the CH_4-N_2-CO_2-H_2O mixture, the presence of CO_2 molecules on the surface of the gas bubbles formed may be enhancing the stability of the bubble, thereby making bubble nucleation energetically more feasible.

A detailed analysis of this is performed with the help of the Young-Laplace equation given by,

$$P_g - P_l = \frac{2\gamma}{R} \tag{6.1}$$

where, P_g and P_l are the pressure inside and outside the gas bubble. R stands for the radius of the bubble and γ is the value of surface tension at the bubble-liquid interface. Thus, from the value of excess pressure inside the bubble and its radius, the surface tension at the bubble-liquid interface can be determined. The surface tension was computed for the CH_4-N_2-CO_2-H_2O system containing 50 CH_4 molecules in which bubble nucleation was observed. The value of the excess pressure ($P_g - P_l$) inside the bubbles formed was determined from the averaged number density of molecules inside the bubbles. The pressure (P_g) corresponding to a given density of gas molecules was determined by performing independent NVT simulations at a temperature of 270 K considered in the present study. The value of P_l is taken as 20 bar which is the pressure applied in the NPT simulations of the CH_4-N_2-CO_2-H_2O mixture. The radius of the bubble (R) is defined as the distance from the centre of the bubble at which the number density of N_2 reaches half of its value in the interior of the bubble. A similar approach for determining the radius of the gas bubble in water was reported earlier [266]. From the values of $P_g - P_l$ and R, the value of surface tension, γ was determined. The value γ obtained for the CH_4-N_2-CO_2-H_2O system containing 50 CH_4 molecules is given in table 6.1. From these results, it is clear that at the bubble-liquid interface, the value of surface tension is lowered due to the presence of CO_2 molecules. The resultant decrease in surface energy of the bubble makes the nucleation of bubbles energetically more feasible. Another observation from table 6.1 is that the pressure inside the gas bubbles are significantly larger than the external pressure. This is

expected considering that the bubble has a radius of only ~1 nm. The presence of large excess pressure inside nanobubbles has been experimentally reported recently by Uchida *et al* [265].

As shown above, the bubbles formed in CH_4-N_2-CO_2-H_2O mixture contains all three gas species in significant amount. The mixed nature of the bubble affects the replacement process as the N_2 and CO_2 molecules present in the bubbles are not available for the formation of CO_2-N_2 binary hydrate during the process.

Thus, the properties of bubbles formed in the CH_4-N_2-CO_2-H_2O mixture influences the subsequent steps in the replacement of CH_4 in the hydrate by N_2 and CO_2. To get insight about this, the dynamic nature of the nanobubbles formed in the mixture was studied in detail as explained below.

6.3.3 Dynamic properties of nanobubbles in CH_4-N_2-CO_2-H_2O mixture

The nanobubbles formed in CH_4-N_2-CO_2-H_2O mixture can influence the subsequent steps of the CH_4 replacement process in the following ways. The bubbles formed may grow in size by absorbing gas molecules from the surroundings. Bigger gas bubbles thus generated will rise faster than the smaller ones which stay in the liquid for longer periods. Thus, rise of larger bubbles from the mixture can lead to more efficient mass transfer of gas molecules from the hydrate melt. The growth of a bubble occurs through a phenomenon known as Ostwald ripening [280] which involves the transfer of gas molecules from smaller bubbles to the larger ones causing the latter to grow in size. Another way in which the bubbles can influence the replacement process is by acting as a reservoir of gas molecules facilitating the regeneration of the hydrate phase once the thermodynamic conditions become favorable for hydrate formation [266].

Thus, the effect of nanobubble formation in the CH_4-N_2-CO_2-H_2O system on the replacement process is related to the transfer of gas molecules from the bubble to the surrounding liquid. For this purpose, the dynamic character of the nanobubbles arising from the transfer of gas molecules from the bubble to the liquid phase and vice versa was examined in detail. The details of this analysis and our observations are given below.

For a quantitative estimate of the dynamic nature of the nanobubble, the transfer of gas molecules between the bubble and the liquid phase was examined. This was obtained by tracking the location of each gas molecule at every pico second for a period of 10 ns after the bubble was

formed in the mixture. When a molecule shifts from the bubble to the liquid phase during consecutive time steps, an exchange of the molecule is considered to have happened. The total number of such exchanges in the system was determined which when divided by the number of gas molecules and the total time gives the average number of exchanges ($N_{exchange}$) per molecule per unit time.

The value of $N_{exchange}$ obtained for the CH_4-N_2-CO_2-H_2O mixture containing 50 CH_4 molecules for different number of CO_2 molecules is listed in table 6.2. It is clear from the value of $N_{exchange}$ that the average number of times a gas molecule is transferred between the bubble and the liquid phase decreases with an increase in the number of CO_2 molecules in the system. The trend observed in the value of $N_{exchange}$ can be explained based on the distribution of CO_2 molecules in the gas bubbles. It was shown above that CO_2 molecules accumulate at the surface of the bubble where it meets the liquid phase (figure 6.4 and 6.5). A consequence of the presence of CO_2 at the bubble-liquid interface is a decrease in the excess pressure inside the gas bubble as observed in table 6.1. A decrease in the pressure inside the gas molecules means that the driving force for a gas molecule present inside the bubble to diffuse into the surrounding liquid phase is low. This explains the observed decrease in the value of $N_{exchange}$ in the mixture with an increase in the concentration of CO_2.

Thus, the above analysis indicates that the dynamic character of the bubble is influenced by the presence of CO_2 molecules at the bubble-liquid interface. An increase in the concentration of CO_2, decreases the frequency with which gas molecules are transferred between the mixed gas bubble and the liquid phase thereby causing the bubble to less dynamic. Thus, the liquid region around mixed gas bubbles formed in CH_4-N_2-CO_2-H_2O mixture is richer in dissolved gas molecules when the mixture contains a lower concentration of CO_2. In mixtures containing higher concentration of CO_2, the mixed gas bubbles formed are less dynamic leading to a lower concentration of dissolved gas molecules in the surrounding aqueous region. The effect of concentration of dissolved gas molecules around the bubble on the structural ordering of water molecules is discussed below.

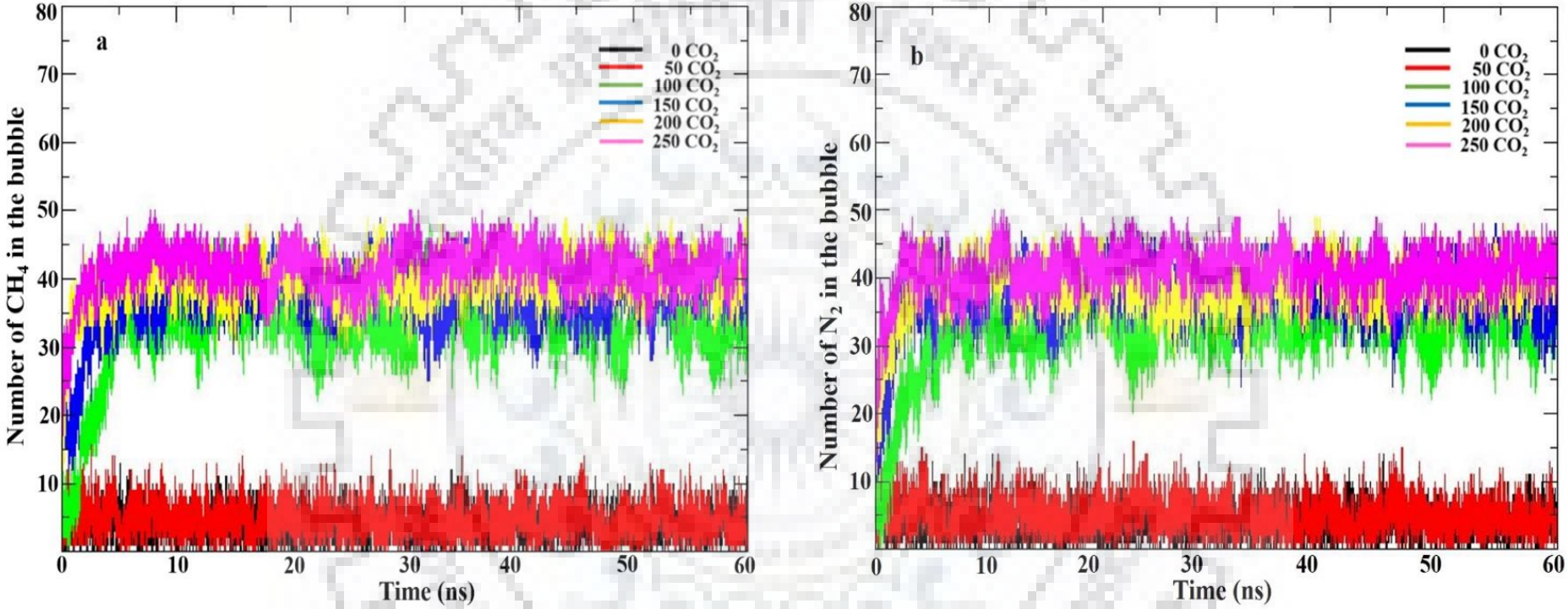

Figure 6.1 Time evolution of the number of N_2 (a) and CH_4 (b) in the nanobubbles formed in the CH_4-N_2-CO_2-H_2O mixture containing 50 CH_4, 50 N_2 and varying number of CO_2 molecules.

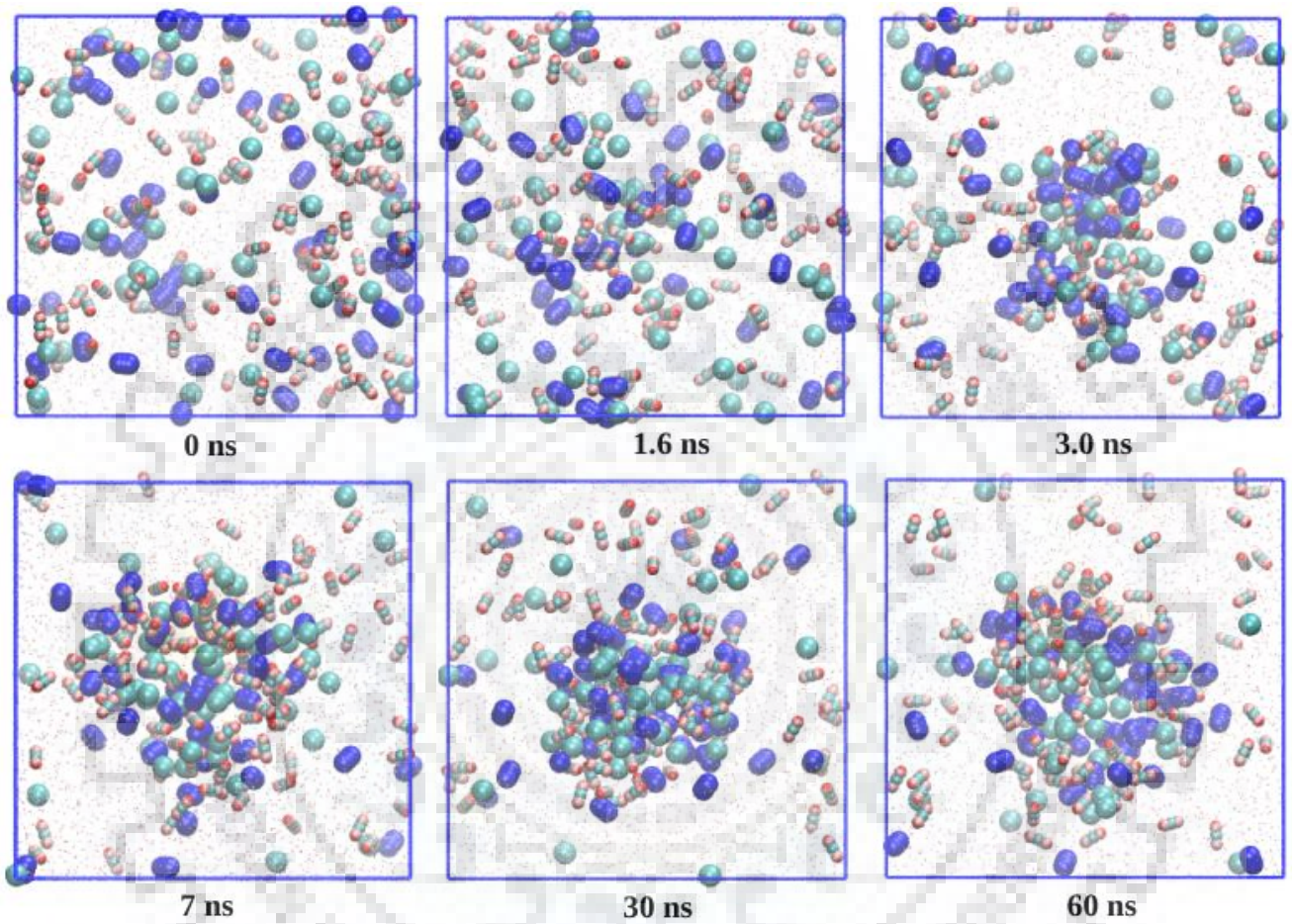

Figure 6.2 Formation of nanobubble in the CH_4-N_2-CO_2-H_2O mixture containing 50 CH_4 , 50 N_2 and 100 CO_2 molecules. CH_4 and N_2 molecules are represented by cyan and blue van der Waals spheres. CO_2 molecules are shown in the ball and stick model and H_2O molecules are indicated by points.

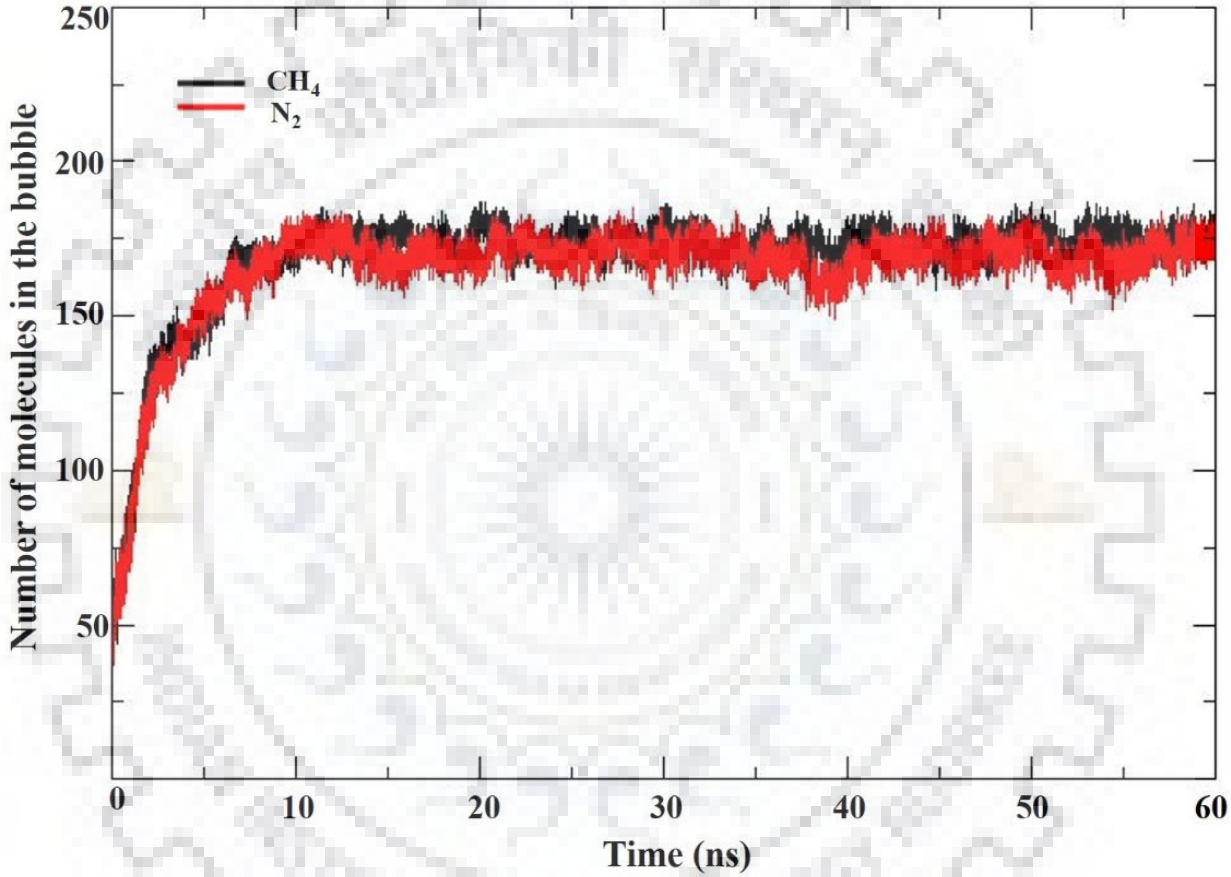

Figure 6.3 Time evolution of the number of CH_4 (black) and N_2 (red) in the nano bubbles formed in the CH_4-N_2-CO_2-H_2O mixture containing 200 CH_4, 200 N_2, 600 CO_2 and 12000 H_2O molecules.

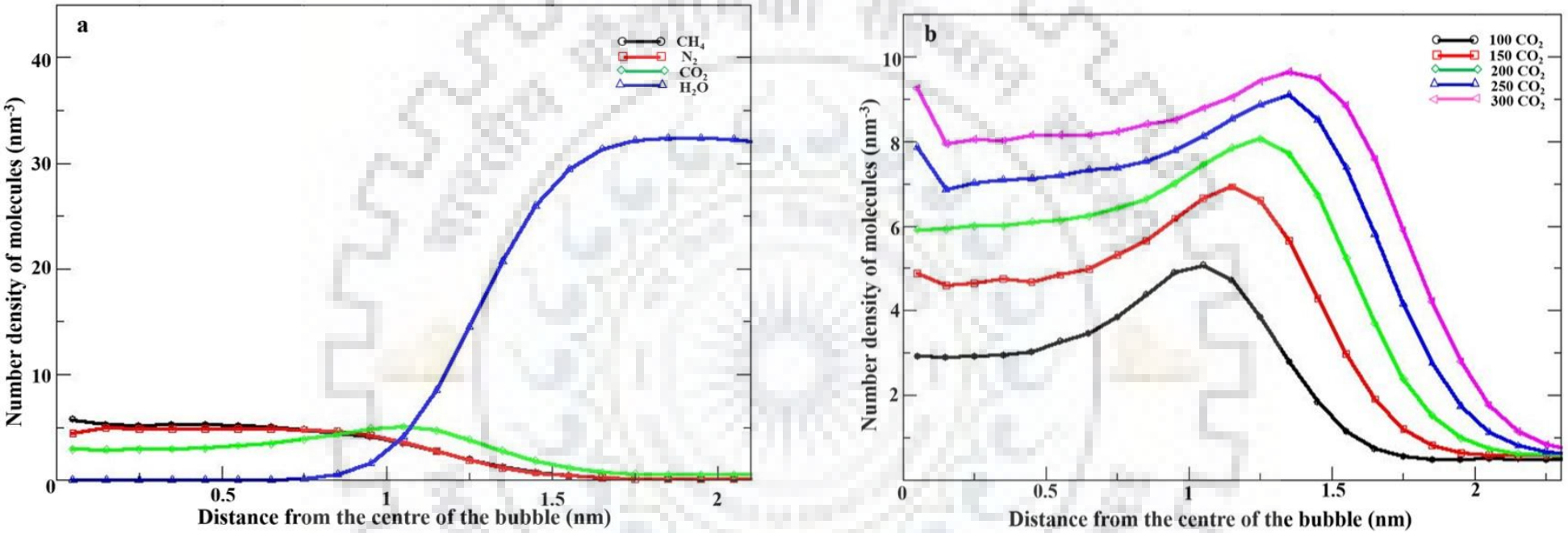

Figure 6.4 Average number density distribution of molecules in the CH_4-N_2-CO_2-H_2O mixture containing a) 50 CH_4, 50 N_2 with 100 CO_2 molecules b) Averaged number density distribution of CO_2 molecules in the mixtures as a function of distance from the center of the nano bubble.

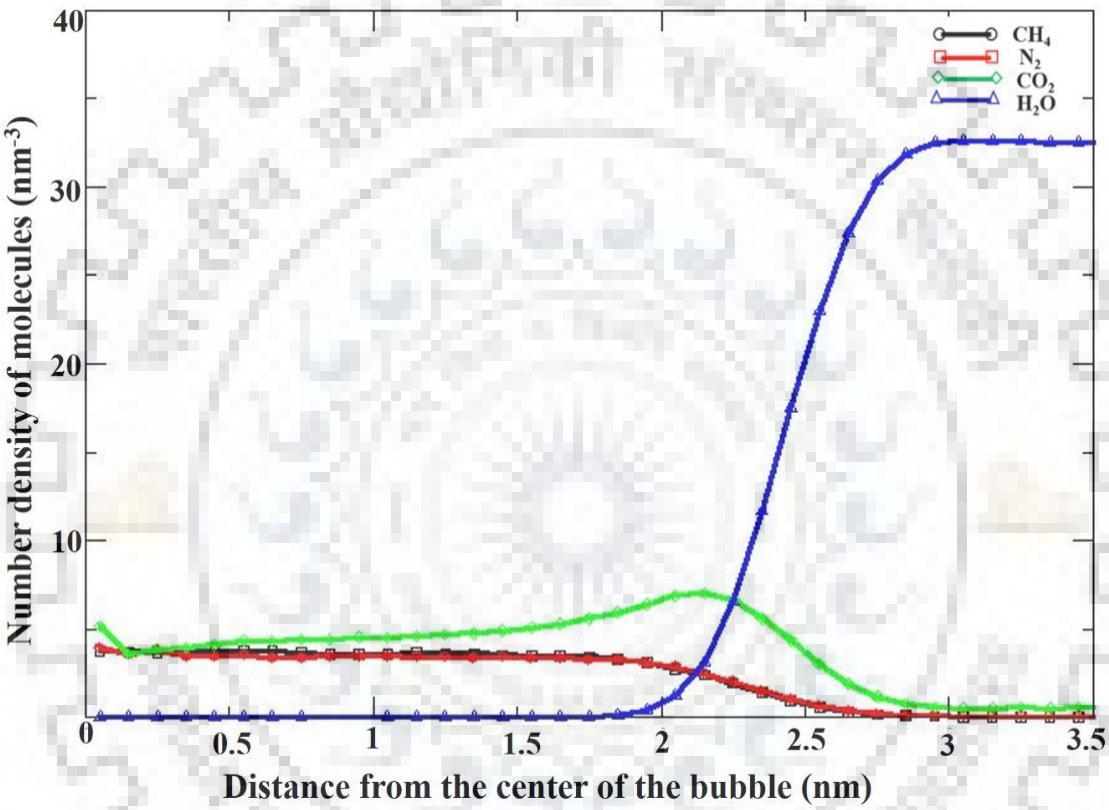

Figure 6.5 Average number density distribution of molecules in the CH_4-N_2-CO_2-H_2O mixture containing 200 CH_4, 200 N_2, 600 CO_2 and 12000 H_2O molecules as a function of distance from the centre of the nano bubble.

Table 6.1 Values of surface tension at the interface between the bubble and the surrounding liquid phase in the CH_4-N_2-CO_2-H_2O liquid containing 50 CH_4 molecules.

Number of CH_4	Number of N_2	Number of CO_2	Laplace pressure, $P_g - P_l$ (bar)	Radius of the bubble (nm)	Surface tension,γ (mN m^{-1})
50	50	0	ng	ng	ng
50	50	50	ng	ng	ng
50	50	100	688.08	1.03	35.43
50	50	150	602.16	1.15	34.62
50	50	200	533.64	1.25	33.35
50	50	250	472.03	1.33	31.38

*ng gas bubble formation is absent

6.3.4 Structural ordering of water molecules around the bubbles

The analysis of the formation of nanobubble in CH_4-N_2-CO_2-H_2O mixture and the dynamic character of the bubbles revealed that gas molecules in the bubble frequently enter the surrounding liquid region. Due to this, the aqueous region near the surface of the bubble has a higher concentration of dissolved gas molecules compared to the region away from the bubble. It was reported by earlier studies that there is a high probability for hydrate nucleation at the interface of the gas and liquid phases [281, 282].

In particular, studies have been reported on the role of nano and microbubbles in inducing hydrate nucleation [283, 284]. In CH_4-N_2-CO_2-H_2O mixtures considered in the present study, the nanobubbles formed were found to differ in their dynamic character depending on the composition of the system. To understand the role of nanobubbles in hydrate nucleation, the structural ordering of water molecules near the surface of the bubbles was examined.

To quantitatively analyse the role of nanobubbles in hydrate nucleation, the effect of the bubble on the formation of water rings in the aqueous region surrounding the bubble was probed. Water rings constitute the cage like architecture of gas hydrates and hence ring formation by water molecules is an important indicator of the probability of hydrate nucleation. The ring perception algorithm which was proposed by Matsumoto *et al* [285] was implemented to identify the four, five and six membered water rings formed in the CH_4-N_2-CO_2-H_2O mixture. These are the types of water rings found in the structure of most commonly observed gas hydrates. The number of water rings formed per unit volume in the various regions of the system containing the nanobubble was determined. For an accurate analysis, the distribution of the number density of water rings in the CH_4-N_2-CO_2-H_2O mixture containing the nanobubble was averaged over a total of 10000 steps during the time interval from 50 to 60 ns of the simulation. The average number density of water rings was thus determined at various distances from the centre of the bubble. The distribution of water rings around the nanobubble in the CH_4-N_2-CO_2-H_2O mixture containing 50 CH_4 molecules and varying number of CO_2 molecules is given in figure 6.6. From the figure it can be observed that the number density distribution curves shift to the right with an increase in the number of CO_2 molecules in the mixture.

Table 6.2 The average number of exchange of gas molecules ($N_{exchange}$) per nano second in the CH_4-N_2-CO_2-H_2O mixtures containing 50 CH_4 molecules.

Number of CH_4	Number of N_2	Number of CO_2	$N_{exchange}$(ns $^{-1}$)
50	50	50	ng
50	50	100	51.96
50	50	150	41.06
50	50	200	38.78
50	50	250	35.53

*ng gas bubble formation is absent

This is due to the fact that the bubble formed in the CH_4-N_2-CO_2-H_2O mixture containing higher number of CO_2 molecules has a slightly larger radii compared to those formed in the mixtures containing lesser number of CO_2 (table 6.1).

An important observation from figure 6.6 is that, in all the mixtures, there exists a maximum in the number density of water rings near the bubble-liquid interface. A similar trend was observed in the case of the larger system containing 200 CH_4, 200 N_2, 600 CO_2 and 12000 H_2O as shown in figure 6.7. However, on moving further away from the interface, the value of number density decreases. The number density is also found to be decreased on moving towards interior of the bubble from the interface. Walsh *et al* [286] studied the influence of curved water-methane interface on the structural ordering of water. They reported that the density of water reaches a maximum near the interface and that water is more disordered in this region. Whereas, the present results indicate an enhancement in the structural ordering of water near the bubble-water interface as indicated by an increase in the number of water rings per nm^{-3} at the interface. This may be due to the peculiar distribution of gas molecules in the mixed gas bubbles observed in the CH_4-N_2-CO_2-H_2O mixture. Unlike in the case of a pure methane bubble considered by Walsh *et al* [286] the mixed gas bubbles considered in the present work has a maxima in the number density of CO_2 at the interface. The CO_2 molecules accumulating at the interface facilitates the formation of water rings leading to an enhanced ordering of water molecules near the interface. Another factor which can affect the number density of water rings near the bubble-water interface is the dynamic character of the bubble. As mentioned earlier, gas molecules frequently leaves the bubble to enter the surrounding liquid phase leading to a high concentration of aqueous gas molecules near the bubble-water interface enhancing the formation of water rings. However, the gas molecules leaving the bubble does not diffuse farther from the bubble due to its low solubility in water. The hydrophobic nature of these gas molecules will cause them to re-enter the bubble phase and thus the concentration of aqueous gas molecules decreases on moving away from the bubble-water interface. This explains the decrease in the number density of water rings on moving away from the interface. Similarly, the value of number density is also found to be decreased and reach zero at shorter distances from the centre of the bubble. This decrease is due to the decrease in the number density of water molecules on moving towards the

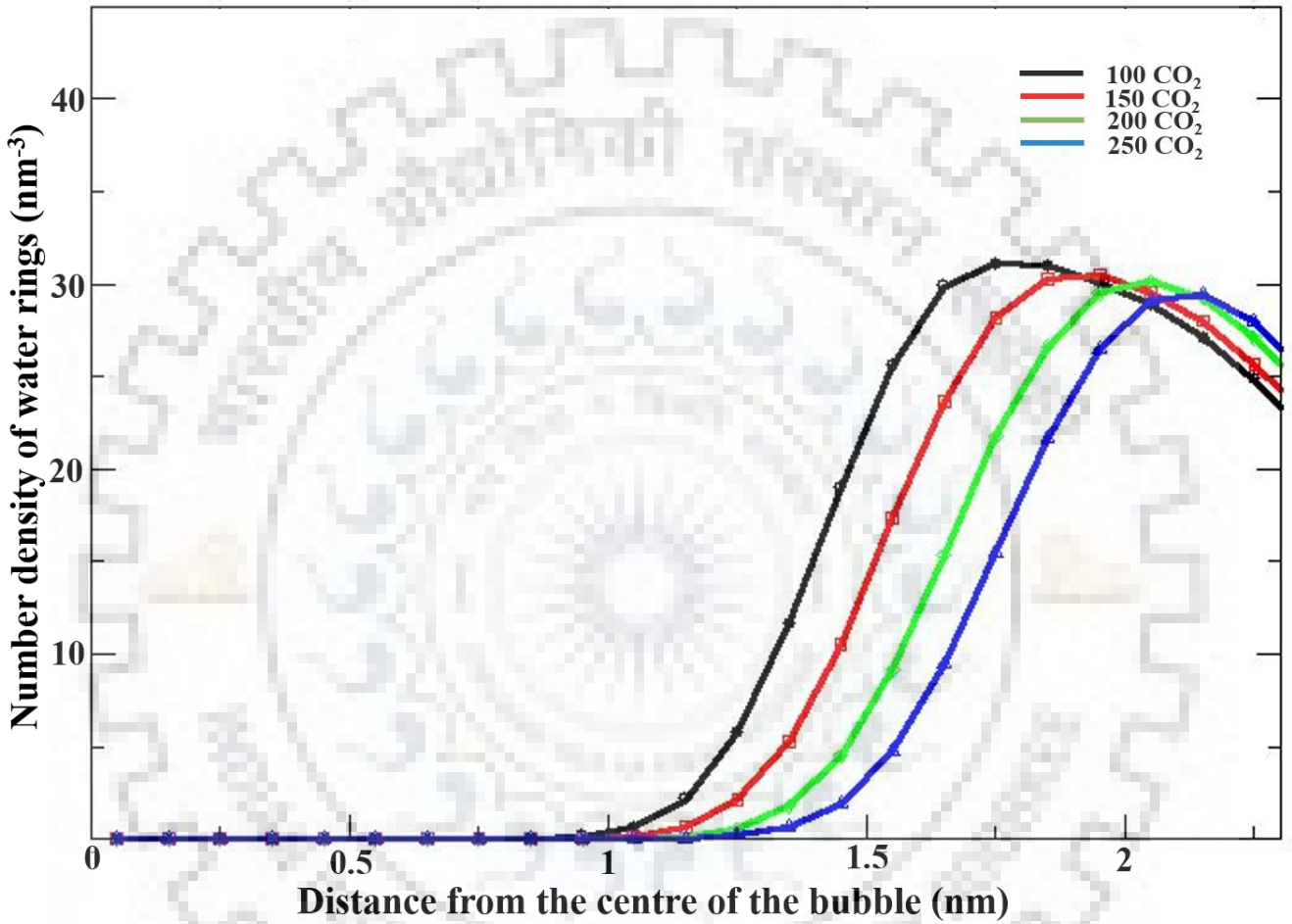

Figure 6.6 Average number density distribution of water rings in the CH_4-N_2-CO_2-H_2O mixture containing 50 CH_4, 50 N_2 and varying number of CO_2 molecules.

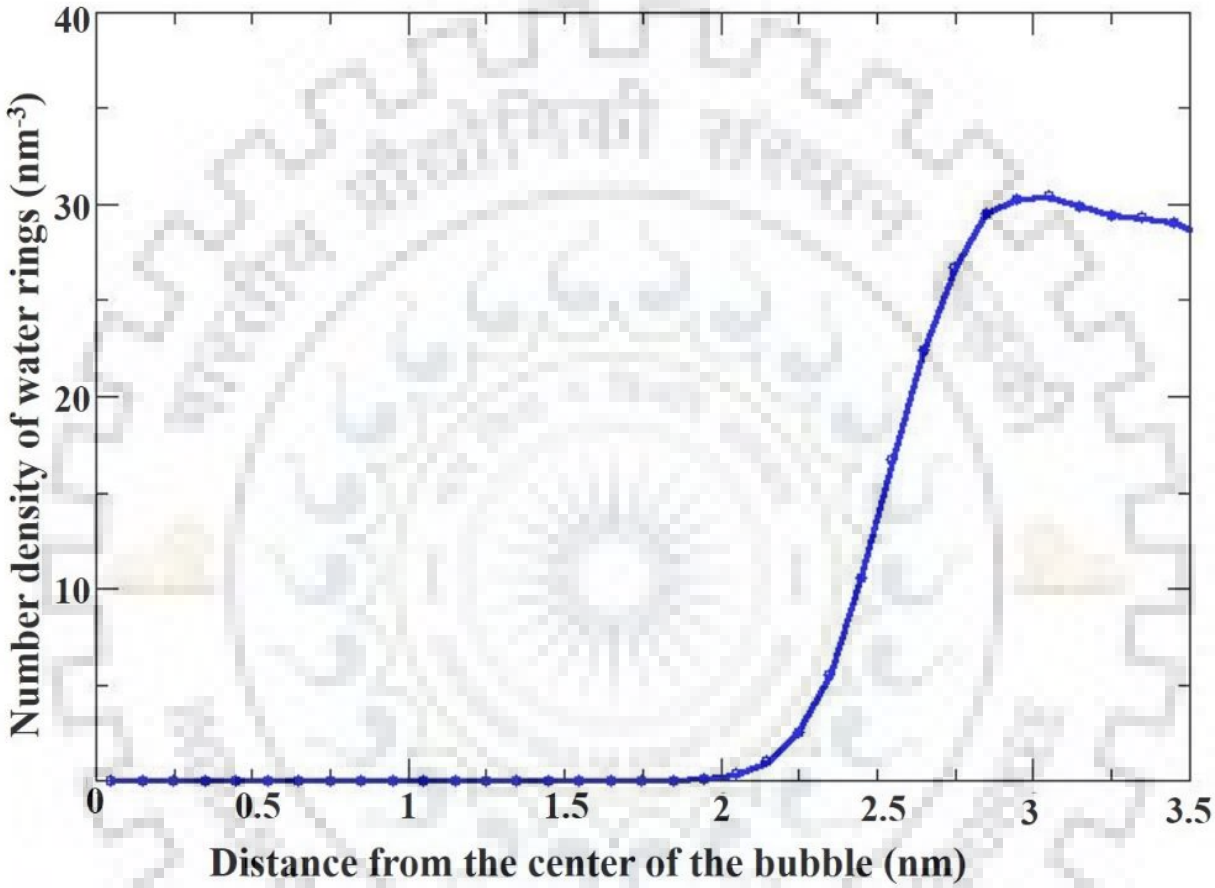

Figure 6.7 Average number density distribution of water rings in the CH_4-N_2-CO_2-H_2O mixture containing 200 CH_4, 200 N_2 and 600 CO_2 molecules.

interior of the bubble (figure 6.4 and 6.5). Another important observation from figure 6.6 is that the number density of water rings formed near the bubble-water interface in CH_4-N_2-CO_2-H_2O mixture decreases as the concentration of CO_2 in the mixture increases. This observation can be explained by examining the effect of CO_2 molecules on the dynamic character of the nanobubble as indicated by the values of $N_{exchange}$ given in table 6.2. It is clear from the table that with an increase in the concentration of CO_2, the frequency at which ($N_{exchange}$) gas molecules are transferred between the bubble and the liquid phase decreases thereby making the bubble less dynamic. This decrease in the exchange of gas lowers the concentration of gas molecules near the bubble-liquid interface thereby reducing the number of water rings formed near the interface.

6.4 Conclusion

Classical molecular dynamics simulations were applied to study the evolution of aqueous gas molecules in CH_4-N_2-CO_2-H_2O mixture formed during the replacement of methane in its hydrate by a mixture of N_2 and CO_2. The effect of concentration of CO_2 on the properties of the CH_4-N_2-CO_2-H_2O mixture was examined and its consequences to the subsequent steps in the replacement process were discussed.

The study revealed that an increase in the concentration of CO_2 assists the formation of nanobubbles in the CH_4-N_2-CO_2-H_2O mixture. The composition of the bubbles formed were analysed and it was revealed that the mixed gas bubbles contain CH_4, N_2 and CO_2 molecules. The entry of N_2 molecules into the bubble will influence the kinetics of the replacement process as these molecules in the bubble are not easily available for the replacing CH_4 molecules from the hydrate cages. To understand the role of CO_2 in assisting the formation of nanobubbles in the mixture, the distribution of gas molecules in the bubble was examined. It was observed that CO_2 molecules accumulate near the surface of the nanobubbles. The accumulation of CO_2 at the surface of the bubble was found to become more prominent with an increase in the concentration of CO_2 in the mixture. The CO_2 molecules at the surface of the bubble reduced the excess pressure inside the bubble as well the surface tension at the bubble-water interface. Thus, the energy barrier associated with bubble nucleation was lowered by the presence of CO_2, thereby enhancing the formation of gas bubbles in the mixture.

To understand how the properties of the nanobubbles in the CH_4-N_2-CO_2-H_2O mixture influence the subsequent steps of the replacement process, the dynamic nature of the nanobubble and its dependence on the concentration of CO_2 in the mixture was studied. The study showed that the nanobubbles formed are highly dynamic with gas molecules frequently leaving the bubble to enter the liquid phase. A quantitative analysis of the dynamic character of the bubble indicated that an increase in the concentration of CO_2 significantly reduces the gas exchange process thereby making the bubble less dynamic.

Finally, to understand the effect of nanobubbles on hydrate nucleation in the mixture, structural ordering of water molecules around the bubble was studied. The number of rings formed by hydrogen bonded water molecules in the CH_4-N_2-CO_2-H_2O mixture containing the bubble was analysed. It was observed that water rings are formed preferentially near the surface of the bubble. The number of water rings formed per unit volume near the bubble-liquid interface is correlated to the dynamic character of the bubbles. Due to the dynamic character of the bubbles, gas molecules frequently enter the surrounding water and therefore the aqueous region near the bubble-liquid interface is rich in dissolved gas molecules. Nanobubbles which are more dynamic have a larger number of water rings formed per unit volume near its surface compared to the less dynamic ones. Thus, the probability of gas hydrate nucleation near the nanobubbles formed in the CH_4-N_2-CO_2-H_2O mixture is found to be influenced by the dynamic character of the bubble.

Chapter-7
Conclusions and future scope

Gas hydrates are crystalline compounds in which water cages of various size and shape encapsulate different gas molecules. Depending upon the nature of guest species, gas hydrates occur in different forms. The hydrates achieve stability by the hydrogen bond interactions between water molecules and the van der Waals interactions between the guest and the host species.

In the present work, the stability of the hydrate complexes formed by the encapsulation of noble gas atoms inside the cavities of single as well as fused dodecahedral water cages was studied in terms of interaction energy at B97D/cc-pVTZ level of theory. The study showed that the size of the guest species plays an important role in the host-guest interactions. The thermodynamic feasibility associated with the encapsulation of guest species of different size in the above mentioned host cages was determined in terms of change in enthalpy and change in Gibbs free energy at a range of temperature and pressure. It was found that the values of ΔH and ΔG for the encapsulation do not depend on the presence of an adjacent cage or the guest species trapped in the neighboring cavity.

Density functional theoretical calculations were preformed to calculate the interaction energies of the guest species H_2, CH_4 and CO_2 with their different types of host cages. The interaction energy of H_2 was found to be the lowest among other guest species. The interaction of CO_2 was found to be more attractive in large cages due to favorable van der Waals overlap between CO_2 and the cage. A slight interaction between CO_2 and water molecules of the adjacent cage was also observed. The vibrational Raman spectrum of the complexes indicated that the symmetric stretching frequency of a molecule undergoes blue shift due to its confinement in a water cage which is decreased with an increase in the size of the cage. The vibrational stretching frequencies of the guest species were found to be independent of the presence of the surrounding cages. The ^{1}H and ^{13}C chemical shift values of guest species showed that the protons and carbon atoms of the confined molecules are deshielded. The deshielding was found to be more pronounced for the double occupancy of the cage. It was found that the chemical shift values of guest species were not influenced by the presence of the surrounding cages.

The interaction of a THF molecule encapsulated in HD cage of the sII hydrate structure with the water molecules of the neighboring DD cage was also examined and found that such interactions enhance the stability of the complex. The stability of the complexes,

$(DD)_{nH_2}(HD)_{THF}$ and $(DD)_{(n-1)H_2}(HD)_{THF+H_2}$, were also studied in terms of interaction energy. The negative values of the change in free energy associated with the encapsulation of guests showed the feasibility of the formation of the complexes $(DD)_{nH_2}(HD)_{THF}$ and $(DD)_{(n-1)H_2}(HD)_{THF+H_2}$ with the latter as more stable. The occupancy of guest species in different types of cages of the fused systems was examined by calculating the ^{1}H and ^{13}C NMR chemical shift values and it was revealed that for the complexes $(DD)_{(n-1)H_2}(HD)_{THF+H_2}$, the presence of two different types of peaks corresponding to protons of H_2 molecule inside small and large cavities can be used as an aid to distinguish these complexes from $(DD)_{nH_2}(HD)_{THF}$. The calculated ^{13}C chemical shift values of THF encapsulated complexes indicated that carbon nuclei are deshielded significantly when H_2 molecules occupy in the large cavities of the fused cage along with THF. The present study also showed that H_2 molecules can be occupied in the hexakaidecahedral cages along with THF, in addition to their occupancy in small cages.

The evolution of aqueous gas molecules in CH_4-N_2-CO_2-H_2O mixture formed during the replacement of methane in its hydrate by a mixture of N_2 and CO_2 was studied by performing classical molecular dynamics simulations. The study revealed the role of CO_2 in the formation of nanobubbles in the CH_4-N_2-CO_2-H_2O mixture. It was also observed that CO_2 molecules accumulate near the surface of the nanobubbles which increases with an increase in the concentration of CO_2. The presence of CO_2 molecules at the surface of the bubble was found to reduce the excess pressure inside the bubble as well the surface tension at the bubble-water interface. The effect of nanobubbles on hydrate nucleation in the mixture was investigated in terms of structural ordering of water molecules around the bubble. The water rings were formed preferentially near the surface of the bubble which was correlated to the dynamic nature of the bubble.

In summary, the results obtained in the present study show the importance of neighboring cages in the molecular level studies of gas hydrates, especially for the guest species of large size. The fused cages can be used for such studies at various levels to get insight on the structure, stability and properties of such complexes. The studies on the bubble formation may be extended to know the role of promoters and inhibitors in the early stages of gas hydrate dissociation.

References

[1] Sloan, E. D.; Koh, C. A. *Clathrate Hydrates of Natural Gases,* 3rd ed.; CRC Press, Boca Raton, FL, **2008**.

[2] Sloan, E. D. Jr. Fundamental principles and applications of natural gas hydrates. *Nature* **2003,** 426, 353-359.

[3] Hammerschmidt, E. G. Formation of gas hydrates in natural gas transmission lines. *Ind. Eng. Chem.* **1934**, 26, 851-855.

[4] Thomas, S.; Dawe, R. A. Review of ways to transport natural gas energy from countries which do not need the gas for domestic use. *Energy* **2003**, 28, 1461-1477.

[5] Shirota, H.; Hikida, K.; Nakajima, Y.; Ota, S.; Takaoki, T.; Iwasaki, T.; Ohgaki, K. Use of hydrate to natural gas transportation-introduction of research project. *Recent Adv. Mater. Sci. Technol.* 2002, 161-167.

[6] Rheinhardt, J. H.; Singh, P.; Tarakeshwar, P.; Buttry, D. A. Electrochemical capture and release of carbon dioxide. *ACS Energy Lett*. **2017**, 2, 454-461.

[7] Singh, P.; Rheinhardt, J. H.; Olson, J. Z.; Tarakeshwar, P.; Mujica, V.; Buttry, D. A. Electrochemical capture and release of carbon dioxide using a disulfide-thiocarbonate redox cycle. *J. Am. Chem. Soc.* **2017**, 139, 1033-1036.

[8] Kang, S.-P.; Lee, H., Recovery of CO_2 from flue gas using gas hydrate: thermodynamic verification through phase equilibrium measurements. *Environ. Sci. Technol*. **2000**, 34, 4397-4400.

[9] Claussen, W. F.; Suggested structures of water in inert gas hydrates. *J. Chem. Phys*. **1951**, 19, 259-260.

[10] Claussen, W. F.; A second structure for inert gas hydrates. *J. Chem. Phys*. **1951**, 19, 1425-1426.

[11] Ripmeester, J. A.; Tse, J. S.; Ratcliffe, C. I.; Powell, B. M. A new clathrate hydrate structure. *Nature* **1987,** 325, 135-136.

[12] Sloan, E. D.; Gas hydrates: Review of physical/chemical properties. *Energy & Fuels* **1998**, 12, 191-196.

[13] von Stackelberg, M.; Solid gas hydrates. *Naturwissenschaften* **1949**, 36, 359-362.

[14] Koh, C. A.; Sum, A. K.; Sloan. E. D.; Gas hydrates: unlocking the energy from icy cages. *J. Appl. Phys*. **2009**, 106, 061101.

[15] Milkov, A. V.; Sassen, R. Resource and economic potential of gas hydrates in the northwestern gulf of Mexico. Proc. *4th Int.Conf. Gas Hydrates*. **2002,** 111–114.

[16] Soloviev, V.; Ginsburg, G.; Telepnevm, E.; Mikhailyk, Y. Cryogeothermy and Natural Gas Hydrates of the Arctic Ocean Sediments (Ministry of Geology USSR, Leningrad, **1987**.

[17] Anderson, B. J.; Wilder, J.; Kurihara, M.; White, M.; Moridis, G.; Wilson, S.; Pooladi-Darvish, M.; Masuda, M.; Collett, T. S.; Hunter, R.; Narita, H.; Rose, K.; Boswell, R. *Proceedings of the Sixth International Conference on Gas Hydrates* Vancouver, Canada, **2008**.

[18] Collett, T. S.; Riedel, M.; Cochran, J. R.; Boswell, R.; Kumar, P.; Sathe, A.V. *Proceedings of the Sixth International Conference on Gas Hydrates* Vancouver, Canada, **2008**.

[19] Kumar, P; Collett, T. S.; Boswell, R.; Cochran, J. R.; Lall, M. (2014) NGHP Expedition 01 Scientific Party Geologic implications of gas hydrates in the offshore of India Krishna-Godavari Basin Mahanadi Basin Andaman Sea Kerala-Konkan Basin Marine and Petroleum. *Geology* **2014,** 58, 29-98.

[20] Mimachi, H.; Takahashi, M.; Takeya, S.; Gotoh, Y.; Yoneyama, A.; Hyodo, K.; Takeda, T.; Murayama, T. Effect of long-term storage and thermal history on the gas content of natural gas hydrate pellets under ambient pressure, *Energy Fuels* **2015**, 29, 4827−4834.

[21] Veluswamy, H. P.; Wong, A. J. H.; Babu, P.; Kumar, R.; Kulprathipanja, S.; Rangsunvigit, P.; Linga, P. Rapid methane hydrate formation to develop a cost effective large scale energy storage system. *Chem. Eng. J.* **2016**, 290, 161-173.

[22] Gudmundsson, J. S. Method for Production of Gas Hydrates for Transportation and Storage. U.S. Patent 5,536,893 A, July 16, **1996**.

[23] Stern, L. A.; Circone, S.; Kirby, S. Durham, W. B. Anomalous preservation of pure methane hydrate at 1 atm. *J. Phys. Chem. B* **2001**, 105, 1756-1762.

[24] Kanda, H. Economic Study on Natural Gas Transportation with Natural Gas Hydrate (Ngh) Pellets, Proceedings of 23rd world gas conference, Amsterdam, **2006**.

[25] Kida, M.; Jin, Y.; Watanbe, M.; Murayama, T.; Nagao, J. Improvement of gas hydrate preservation by increasing compression pressure to simple hydrates of methane, ethane, and propane. *Jpn. J. Appl. Phys*. **2017**, 56, 095601.

[26] Shu, J.; Chen, X.; Chou, I.-M.; Yang, W.; Hu, J.; Hemley, R. J.; Mao, H-K. Structural stability of methane hydrate at high pressures. *Geoscience Frontiers* **2011**, 2, 93-100.

[27] Zttel, A. Hydrogen storage methods. *Naturwissenschaften* **2004**, 91, 157-172.

[28] Fichtner, M. Nanotechnology aspects in materials for hydrogen storage. *Adv. Eng. Mater*. **2005**, 7, 443-455.

[29] Coontz, R.; Hanson, B. Not to simple. *Science* **2004**, 305, 957.

[30] Crabtree, G. W.; Dresselhaus, M. S.; Buchanan, M. V. The hydrogen economy. *Phys. Today*. **2004**, 57, 39-44.

[31] Gopalsamy, K.; Subramanian, V. Hydrogen storage capacity of alkali and alkaline earth metal ions doped carbon based materials: A DFT study. *Int. J. Hydrogen Energy*. **2014**, 39, 2549-2559.

[32] Samolia, M.; Kumar, T. J. D. A conceptual DFT study of the hydrogenated trapping efficiency in metal functionalized BN system. *RSC Adv*. **2014**, 4, 30758-30767.

[33] Weck, P. F.; Kumar, T. J. D. Computational study of hydrogen storage in organometallic compounds. *J. Chem. Phys.* **2007**, 126, 094703.

[34] Dyadin, Y. A.; Larionov, E. G.; Manakov, A. Y.; Zhurko, F. V.; Aladko, E. Y.; Mikina, T. V.; Komarov, V. Y. Clathrate hydrates of hydrogen and neon. *Mendel. Commun*. **1999**, 9, 209-210.

[35] Qin, J.; Kuhs, W. F. Quantitative Analysis of Gas Hydrates Using Raman Spectroscopy. *AlChE J.* **2013**, 59, 2155-2167.

[36] Lee, J-W.; Lu, H.; Moudrakovski, I. L.; Ratcliffe, C. I.; Ohmura, R.; Alavi, S.; Ripmeester, J. A. ^{13}C NMR Studies of Hydrocarbon Guests in Synthetic Structure H Gas Hydrates: Experiment and Computation. *J. Phys. Chem. A* **2011**, 115, 1650–1657.

[37] Jameson, A. K.; Jameson. C. J. Gas-phase ^{13}C chemical shifts in the zero-pressure limit: refinements to the absolute shielding scale for ^{13}C. *Chem. Phys .Lett*. **1987**, 134, 461-466.

[38] Dec, S. F.; Bowler, K. E.; Stadterman, L. L.; Koh, C. A.; Sloan, E. D. Direct measure of the hydration number of aqueous methane. *J. Am. Chem. Soc.* **2006**, 128, 414-415.

[39] Takeya, S.; Ripmeester, J. A. Anomalous preservation of CH_4 hydrate and its dependence on the morphology of hexagonal ice. *Chem Phys Chem*. **2010**, 11, 70-73.

[40] Mao, W. L.; Mao, H. -K.; Goncharov, A. F.; Struzhkin, V. V.; Guo, Q. Z.; Hu, J. Z.; Shu, J.; Hemley, R. J.; Somayazulu, M.; Zhao, Y.S. Hydrogen clusters in clathrate hydrate. *Science* **2002**, 297, 2247-2249.

[41] Mao, W. L.; Mao, H. -K. Hydorgen storage in molecular compounds. *Proc. Natl. Acad. Sci. U.S.A.* **2004**, 101, 708-710.

[42] Lokshin, K. A.; Zhao, Y.; He, D.; Mao, W. L.; Mao, H. –K.; Hemley, R. J.; Lobanov, M. V.; Greenblatt, M. Structure and dynamics of hydrogen molecules in the novel clathrate hydrate by high pressure neutron diffraction. *Phys. Rev. Lett.* **2004**, 93, 125503.

[43] Davidson, D. W.; Ripmeester, J. A.; Atwood, J. L., Davies, J. E. D., MacNichol, D. D., Eds. *In Inclusion Compounds* Academic Press: New York, **1984**; Vol. 3, Chapter 3.

[44] Ripmeester, J. A.; Ratcliffe, C. I. *Solid State NMR Studies of Inclusion Compounds* Report C1181-89S; National Research Council of Canada, **1989**.

[45] Sum, A. K.; Burruss, R. C.; Sloan, E. D. Measurements of clathrate hydrates via Raman spectroscopy. *J. Phys. Chem. B* **1997**, 101, 7371-7377.

[46] Subramanian, S.; Kini, R. A.; Sloan. E. D. Evidence of structure II hydrate formation from methane + ethane mixtures. *Chem. Eng. Sci.* **2000**, 55, 1981-1999.

[47] Uchida, T.; Hirano, T.; Ebinuma, T.; Narita, H.; Gohara, K.; Mae, S.; Matsumoto, R. Raman Spectroscopic Determination of Hydration Number of Methane Hydrates. *AlChE J*. **1996**, 45, 2641-2645.

[48] Strobel, T. A.; Koh, C. A.; Sloan, E. D. Hydrogen storage properties of clathrate hydrate materials. *Fluid Phase Equilib.* **2007,** 261, 382-389.

[49] Plattner, N.; Meuwly, M. The effect of classical and quantum dynamics on vibrational frequency shifts of H_2 in clathrate hydrates. *J. Chem. Phys*. **2014**, 140, 024311.

[50] Rimpeester, J. A.; Ratcliffe. C. I. Low-temperature cross-polarization/magic angle spinning ^{13}C NMR of solid methane hydrates: structure, cage occupancy, and hydration number. *J. Phys. Chem*. **1988**, 92, 337-339.

[51] Hansen, S. B.; Berg, R. W. Raman spectroscopic studies of methane gas hydrates. *App. Spec. Rev*. **2009**, 44, 168-179.

[52] Kida, M.; Sakagami, H.; Takahashi, N.; Nagao, J. Chemical Shift Changes and Line Narrowing in ^{13}C NMR Spectra of Hydrocarbon Clathrate Hydrates. *J. Phys. Chem. A* **2013**, 117, 4108−4114.

[53] Ripmeester, J. A.; Ratcliffe, C. I. Xe-129 NMR studies of clathrate hydrates: new guests for structure II and structure H. *J. Phys. Chem.* **1990**, 94, 8773-8776.

[54] Seo, Y.; Kang, S-P.; Jang, W. Structure and Composition Analysis of Natural Gas Hydrates: 13C NMR Spectroscopic and Gas Uptake Measurements of Mixed Gas Hydrates. *J. Phys. Chem. A* **2009**, 113, 9641-9649.

[55] Kumar, R.; Linga, P.; Moudrakovski, I. L.; Ripmeester, J. A.; Englezos, P. Structure and Kinetics of Gas Hydrates from Methane/Ethane/Propane Mixtures Relevant to the Design of Natural Gas Hydrate Storage and Transport Facilities. AIChE J. **2008**, 54, 2132-2144.

[56] Kida, M.; Sakagami, H.; Takahashi, N.; Hachikubo, A.; Shoji, H.; Kamata, Y.; Ebinuma, T.; Narita, H.; Takeya, S. Estimation of gas composition and cage occupancies in CH_4-C_2H_6 hydrates by CP-Mass ^{13}C NMR technique. *J. Jpn. Inst.* **2007**, 50, 132-138.

[57] Atilhan, M.; Pala, N.; Aparicio, S. A quantum chemistry study of natural gas hydrates. *J. Mol. Model*. **2014**, 20, 2182.

[58] Khan, A. Ab initio studies of $(H_2O)_{20}H^+$ and $(H_2O)_{21}H^+$ prismic, fused cubic and dodecahedral clusters: can H_3O^+ ion remain in cage cavity? *Chem. Phys. Lett*. **2000**, 319, 440-450.

[59] Khan, A. Examining the cubic, fused cubic, and cag structure of $(H_2O)_n$ for n=8, 9, 12, 16, 20, and 21: Do fused cubic structures form? *J. Phys. Chem*. **1995**, 99, 12450.

[60] Khan, A. Ab intio studies of $(H_2O)_{28}$ hexakaidecahedral cluster with Ne, N_2, CH_4, and C_2H_6 guest molecules in the cavity. *J. Chem. Phys*. **2002**, 116, 6628-6633.

[61] Ramya, K. R.; Venkatnathan, A. Characterization of interaction energy and vibrational Raman spectra of nitrogen clathrate hydrates. *Comp. Theor. Chem*. **2013**, 1023, 1-4.

[62] Kulkarni, A. D.; Gadre, S. R.; Nagase, S. Quantum chemical and electrostatic studies of anionic water clusters, $(H_2O)_n^-$. *J. Mol. Struct. : THEOCHEM* **2008**, 851, 213-219.

[63] Gadre, S. R.; Yeole, S. D.; Sahu, N. Quantum chemical investigations on molecular clusters. *Chem. Rev*. **2014**, 114, 12132-12173.

[64] Prakash, M.; Samy, K. G.; Subramanian, V. Benzene-water (BZWn (n=1-10)) clusters. *J. Phys. Chem. A* **2009**, 113, 13845-13852.

[65] Majumder, M.; Manogaran, S. Redundant internal coordinates, compliance constants and non-bonded interactions-some new insights. *J. Chem. Sci*. **2013**, 125, 9-15.

[66] Pandey, S. K.; Manogaran, D.; Manogaran, S.; Schaefer, H. F. Quantification of hydrogen bond strength based on interaction coordinates: A new approach. *J. Phys. Chem. A*. **2017**, 121, 6090-6103.

[67] Pérez, G. R.; Moaied, M.; Soler, J. M.; Yndurain, F. Stability, adsorption, diffusion of CH_4, CO_2, and H_2 in clathrate hydrates. *Phys. Rev. Lett*. **2010**, 105, 145901.

[68] Ramya, K. R.; Venkatnathan, A. Stability and reactivity of methane clathrate hydrates: Insights from density functional theory. *J. Phys. Chem. A*. **2012**, 116, 7742-7745.

[69] Liu, Y.; Ojamäe, L. C-C stretching Raman spectra and stabilities of hydrocarbon molecules in natural gas hydrates: A quantum chemical study. *J. Phys. Chem. A*. **2014**, 118, 11641-11651.

[70] Papadimitriou, N. I.; Tsimpanogiannis, I. N.; Economou, I. G.; Stubos, A. K. Storage of Methane in Clathrate Hydrates: Monte Carlo Simulations of sI Hydrates and Comparison with Experimental Measurements. *J. Chem. Eng. Data* **2016**, 61, 2886−2896.

[71] Papadimitriou, N. I.; Tsimpanogiannis, I. N.; Economou, I. G.; Stubos, A. K. Identification of conditions for increased methane storage capacity in sII and sH clathrate hydrates from Monte Carlo simulations. *J. Chem. Thermodyn.* **2018**, 117,128–137.

[72] Alavi, S.; Ripmeester, J. A.; Klug, D. D. Molecular dynamics study of the stability of methane structure H clathrate hydrates. *J. Chem. Phys.* **2007**, 126,124708.

[73] Patchkovskii, S.; Tse, J. S. Thermodynamic stability of hydrogen clathrates. *Proc. Natl. Acad. Sci. USA* **2003**, 100, 14645-14650.

[74] Alavi, S.; Ripmeester, J. A.; Klug, D. D. Molecular-dynamics study of structure II hydrogen clathrates. *J. Chem. Phys.* **2005**,123, 024507.

[75] Sebastianelli, F.; Xu, M.; Bačić, Z. Quantum dynamics of small H_2 and D_2 clusters in the large cage of structure II clathrate hydrate: Energetics, occupancy, and vibrationally averaged cluster structures. *J. Chem. Phys*. **2008**, 129, 244706–244709.

[76] Tachikawa, H. Maximum capacity of the hydrogen storage in water clusters. *Phys. Chem. Liq.* **2009**, 47, 103-109.

[77] Inerbaev, T. M. Dynamics and equation of state of hydrogen clathrate hydrate as a function of cage occupation. *Comput. Mat. Sci*. **2006**, 36, 229–233.

[78] Papadimitriou, N, I.; Tsimpanogiannis, N.; Economou, I. G.; Stubos, A. K. Storage of H_2 in clathrate hydrates: Evaluation of different force-fields used in Monte Carlo simulations. *Mol. Phys*. **2017**, 115, 1274-1285.

[79] Papadimitriou, N. I.; Tsimpanogiannis, I. N.; Papaioannou, A. Th., Stubos, A. K. Evaluation of the hydrogen-storage capacity of pure H_2 and binary H_2-THF hydrates with Monte Carlo simulations. *J. Phys. Chem. C*. **2008**, 112, 10294-10302.

[80] Ramya, K. R.; Kumar, G. V. P.; Venkatnathan, A. Raman spectra of vibrational and librational modes in methane clathrate hydrates using density functional theory. *J. Chem. Phys.* **2012**, 136, 174305.

[81] Greathouse, J. A.; Cygan. R. T. Vibrational Spectra of Methane Clathrate Hydrates from Molecular Dynamics Simulation. *J. Phys. Chem. B* **2006**, 110, 6428-6431.

[82] Tse, J. S. Vibrations of Methane in Structure I Clathrate Hydrate—an ab initio Density Functional Molecular Dynamics Study. *J. Supramol. Chem*. **2002**, 2, 429–433.

[83] Pimentel, G.C.; Charles, S. W. Infrared spectral perturbations in matrix experiments. *Pure Appl. Chem*. **1963**, 7, 111.

[84] Wang, J.; Lu, H.; Ripmeester, J. A. Raman Spectroscopy and Cage Occupancy of Hydrogen Clathrate Hydrate from First-Principle Calculations. *J. Am. Chem. Soc.* **2009**, 131, 14132–14133.

[85] Suida, P.; Sadlej, J. Calculations of NMR properties for sI and sII clathrate hydrates of methane, ethane and propane. *J. Mol. Model.* **2014**, 20, 2511.

[86] Terleczky, P.; Nyulszi, L. DFT study of possible lattice defects in methane-hydrate and their appearance in ^{13}C NMR spectra. *Chem. Phys. Lett.* **2010**, 488, 168–172.

[87] Liu, Y.; Ojamäe, L. ^{13}C chemical shifts in natural gas hydrates from first-principles solid-state NMR calculations. *J. Phys. Chem. C.* **2016**, 120, 1130-1136.

[88] Alavi, S.; Ripmeester, J. A.; Klug, D. D. NMR shielding constants for hydrogen guest molecules in structure II clathrates. *J. Chem. Phys.* **2005**, 123, 051107.

[89] Yousif, M. H.; Li, P. M.; Selim, M. S.; Sloan, E. D. Depressurization of natural gas hydrates in Berea sandstone cores. *J. Inclus. Phenom. Mol*. **1990**, 8, 71-88.

[90] Yousif, M. H.; Abass, H. H.; Selim, M. S.; Sloan, E. D. Experimental and theoretical investigation of methane-gas-hydrate dissociation in porous media. *Spe. Reserv. Eval. Eng*. **1991**, 6, 69-76.

[91] Davidson, D. W.; Garg, S. K.; Ratcliffe, C. I.; Tse, J. S.; Gough, S. R. Characterization of a clathrate hydrate of nitrogen trifluoride. *Can. J. Chem*. **1984**, 62, 1229-1235.

[92] Kamath, V. A.; Holder, G. D. Dissociation heat transfer characteristics of methane hydrates. *AlChE J.* **1987**, 33, 347-350.

[93] Tariq, M.; Rooney, D.; Othman, E.; Aparicio, S.; Atilhan, M.; Khraisheh, M. Gas hydrate inhibition: A review of the role of ionic liquids. *Ind. Eng. Chem. Res*. **2014**, 53, 17855-17868.

[94] Daraboina, N.; Malmos, C.; Solms, N. V. Synergistic kinetic inhibition of natural gas hydrate formation. *Fuel* **2013**, 108, 749-757.

[95] Lund, A.; Urdahl, O.; Kirkhorn, S. S. Inhibition of gas hydrate formation by means of chemical additives - II. An evaluation of the screening method. *Chem. Eng. Sci.* **1996**, 51, 3449-3458.

[96] Gryte, C.C. On the control of nucleation and growth by inhibition of gas hydrate formation. *Ann. Ny. Acad. Sci*. **1994**, 715, 323-329.

[97] Ji, C.; Ahmadi, G.; Smith, D. H. Natural gas production from hydrate decomposition by depressurization. *Chem. Eng. Sci*. **2001**, 56, 5801-5814.

[98] Pang, W. X.; Xu, W. Y.; Sun, C. Y.; Zhang, C. L.; Chen, G. J. Methane hydrate dissociation experiment in a middle-sized quiescent reactor using thermal method. *Fuel* **2009**, 88, 497-503.

[99] Tang, L. G.; Xiao, R.; Huang, C.; Feng, Z. P.; Fan, S. S. Experimental Investigation of Production Behavior of Gas Hydrate under Thermal Stimulation in Unconsolidated Sediment. *Energy Fuels* **2005**, 19, 2402-2407.

[100] Li, X. S.; Wan, L. H.; Li, G.; Li, Q. P.; Chen, Z. Y.; Yan, K. F. Experimental Investigation into the Production Behavior of Methane Hydrate in Porous Sediment with Hot Brine Stimulation. *Ind. Eng. Chem. Res*. **2008**, 47, 9696-9702.

[101] Ji, C.; Ahmadi, G.; Smith, D. G. Natural gas production from hydrate decomposition by depressurization. *Chem. Eng. Sci.* **2001**, 56, 5801-5814.

[102] Sharifi, H.; Ripmeester, J.; Walker, V. K.; Englezos, P. Kinetic inhibition of natural gas hydrates in saline solutions and heptane. *Fuel* **2014**, 117, 109-117.

[103] Lederhos, J. P.; Long, J. P.; Sum, A.; Christiansen, R. L.; Sloan, E. D. Effective kinetic inhibitors for natural gas hydrates, *Chem. Eng. Sci*. **1996**, 51, 1221-1229.

[104] Kelland, M. A. History of the development of low dosage hydrate inhibitors, *Energy Fuels* **2006**, 20, 825-847.

[105] Fu, B. The development of advanced kinetic hydrate inhibitors. *Spec. Publ-R. Soc. Ch*em. **2002**, 280, 264-276.

[106] Udachin, K.; Lipkowski, J.; Tkacz, M. Double clathrate hydrates with helium and hydrogen. *Supramol. Chem*. **1994**, 3, 181-183.

[107] Florusse, L. J.; Peters, C. J.; Schoonman, J.; Hester, K. C.; Koh, C. A.; Dec, S. F.; Marsh, K. N.; Sloan, E.D. Stable low-pressure hydrogen clusters stored in a binary clathrate hydrate. *Science* **2004,** 306, 469-471.

[108] Lee, H.; Lee, J. W.; Kim, D. Y.; Park, J.; Seo, Y. -T.; Zeng, H.; Moudrakovski, I. L.; Ratcliffe, C. I.; Ripmeester, J. A. Tuning clathrate hydrates for hydrogen storage. *Nature* **2005,** 434, 743-746.

[109] Sugahara, T.; Haag, J. C.; Warntjes, A. A.; Prasad, P. S. R.; Sloan, E. D.; Koh, C. A.; Sum, A. K. Large-cage occupancies of hydrogen in binary clathrate hydrates dependent on pressures and guest concentrations. *J. Phys. Chem. C.* **2010**, 114, 15218-15222.

[110] Hester, K.C.; Strobel, T. A.; Sloan, E. D.; Koh, C. A. Molecular Hydrogen Occupancy in Binary THF−H_2 Clathrate Hydrates by High Resolution Neutron Diffraction. *J. Phys. Chem. B* **2006**, 110, 14024-14027.

[111] Strobel, T. A.; Taylor, C. J.; Dec, S. F.; Koh, C. A.; Miller, K. T.; Sloan, E. D. Molecular Hydrogen Storage in Binary THF-H_2 Clathrate Hydrates. *J. Phys. Chem. B* **2006**, 110, 17121-17125.

[112] Anderson, R.; Chapoy, A.; Tohidi, B. Phase relations and binary clathrate hydrate formation in the system H_2-THF-H_2O. *Langmuir* **2007,** 23, 3440-3444.

[113] Hashimoto, S.; Murayama, S.; Sugahara, T.; Sato, H.; Ohgaki, K. Thermodynamic and Raman spectroscopic studies on H_2+tetrahydrofuran+water and H_2+tetra-n-butyl ammonium bromide+ water mixtures containing gas hydrates. *Chem. Eng. Sci.* **2006,** 61, 7884-7888.

[114] Ulivi, L.; Celli, M.; Giannasi, A.; Ramirez-Cuesta, A. J.; Bull, D. J.; Zoppi, M. Quantum rattling of molecular hydrogen in clathrate hydrate nanocavities. *Phys. Rev. B* **2007**, 76, 161401.

[115] Ogata, K.; Hashimoto, S.; Sugahara, T.; Moritoki, M.; Sato, H.; Ohgaki, K. Storage capacity of hydrogen in tetrahydrofuran hydrate. *Chem. Eng. Sci.* **2008**, 63, 5714-5718.

[116] Alavi, S.; Ripmeester, J. A.; Klug, D. D. Molecular-dynamics simulations of binary structure II hydrogen and tetrahydrofuran clathartes. *J. Chem. Phys.* **2006,** 124, 014704.

[117] Atamas, A. A.; Cuppen, H. M.; Koudriachova, M. V.; Leeuw, S. W. de. Monte Carlo calculations of the free energy of binary sII hydrogen clathrate hydrates for identifying efficient promoter molecules. *J. Phys. Chem. B.* **2013,** 117, 1155-1165.

[118] Iwai, Y.; Aokawa, R. Stability analysis for binary sII hydrogen-promoter hydrates by molecular dynamics simulation. *Mol. Simul*. **2015,** 41, 735-740.

[119] Geng, C. –Y.; Han, Q. Z.; Wen, H.; Dai, Z.-Y.; Song, C.-H. Molecular dynamics simulation on the decomposition of type sII hydrogen hydrate and the performance of tetrahydrofuran as a stabiliser. *Mol. Simul*. **2010,** 36, 474-483.

[120] Papadimitriou, N. I.; Tsimpanogiannis, I. N.; Papaioannou, A. Th.; Stubos, A. K. Evaluation of the hydrogen-storage capacity of pure H_2 and binary H_2-THF hydrates with Monte Carlo simulations. *J. Phys. Chem. C*. **2008,** 112, 10294-10302.

[121] Gorman, P. D.; English, N. J.; MacElroy, J. M. D. Dynamic and energetic properties of hydrogen and hydrogen-tetrahydrofuran clathrate hydrates. *Phys. Chem. Chem. Phys*. **2011,** 13, 19780-19787.

[122] Song, B.; Nguyen, A. H.; Molinero, V. Can guest occupancy in binary clathrate hydrates be tuned through control of the growth temperature? *J. Phys. Chem. C* **2014,** 118, 23022-23031.

[123] Yedlapalli, P.; Lee, S.; Lee, J. W. Stable occupancy of hydrogen molecules in H_2 clathrate hydrates and H_2+THF determined by Ab Initio calculations. *J. Thermodyn.* **2010,** 2010, 1-4.

[124] Cao, H.; English, N. J.; MacElroy, J. M. D. Diffusive hydrogen inter-cage migration in hydrogen and hydrogen-tetrahydrofuran clathrate hydrates. *J. Chem. Phys*. **2013,** 138, 094507.

[125] Patchkovskii, S.; Tse, J. S. Thermodynamic stability of hydrogen clathrates. *Proc. Natl. Acad. Sci. USA* **2003,** 100, 14645-14650.

[126] Ramya, K. R.; Kumar, R.; Venkatnathan, A. Energy and spectral characteristics of hydrogen occupies pure and tetrahydrofuran doped water cages. *Comp. Theor. Chem*. **2014,** 1039, 28-32.

[127] Liu, J.; Hou, J.; Liu, H.; Chen, G.; Zhang, J. Ab initio study of the molecular hydrogen occupancy in pure H_2 and binary H_2-THF clathrate hydrates. *Internat. J. Hyd. Ener*. **2017**, 42, 17136-17143.

[128] Zhang, J. S.; Lee, S.; Lee, J. W. Kinetics of methane hydrate formation form SDS solution. *Ind. Eng. Chem. Res*. **2007**, 46, 6353-6359.

[129] Zhong, Y.; Rogers, R. E. Surfactant effects on gas hydrate formation. *Chem. Eng. Sci*. **2000**, 55, 4175-4187.

[130] ZareNezhad, B.; Varaminian, F. A unified approach for description of gas hydrate formation kinetics in the presence of kinetic promoters in gas hydrate conversion. *Energ. Conver. manag*. **2013**, 73,144-149.

[131] Zhang, C. S.; Liang, D. Q.; Guo, K. H. Effect of additives on formation of natural gas hydrate. *Fuel* **2004**, 83, 2115-2121.

[132] Ohgaki, K.; Takano, K.; Sangawa, H.; Matsubara, T.; Nakano, S. Methane exploitation by carbon dioxide from gas hydrates-phase equilibria for CO_2-CH_4 mixed hydrate system. *J. Chem. Eng. J.* **1996**, 29, 478–83.

[133] Uchida, T.; Takeya, S.; Ebinuma, T.; Narita, H. Replacing methane with CO_2 in clathrate hydrate: Observations using Raman spectroscopy. In Williams. D.J., Durie, R. A., McMullan, P., Paulson, C. A. J., and Smith, A. Y. (eds.), *Proceedings of the 5th International Conference on Greenhouse Gas Control Technologies*. CSIRO Publishing, Collingwood, Greenhouse Gas Control Technologies, **2001**, 523-527.

[134] Anderson, R.; Llamedo, M.; Tohidi, B.; Burgass, R. W. Experimental measurement of methane and carbon dioxide clathrate hydrate equilibria in mesoporous silica. *J. Phys. Chem. B* **2003**, 107, 3507– 3514.

[135] Hirohama, S.; Shimoyama, Y.; Wakabayashi, A.; Tatsuta, S.; Nishida, N. Conversion of CH_4-hydrate to CO_2-hydrate in liquid CO_2. *J Chem. Eng. Jpn.* **1996**, 29, 1014-1020.

[136] Henning, R. W.; Schultz, A. J.; Thieu, V.; Halpern, Y. Neutron Diffraction Studies of CO_2 Clathrate Hydrate: Formation from Deuterated Ice. *J. Phys. Chem. A* **2000**, 104, 5066-5071.

[137] Komai, T.; Kawamura, T.; Kang, S.; Nagashima, K.; Yamamoto, Y. *In* situ observation of gas hydrate behaviour under high pressure by Raman spectroscopy. *J. Phys. Condens. Mat*. **2002**, 14, 11395-11400.

[138] Susilo, R.; Ripmeester, J. A.; Englezos, P. Characterization of gas hydrates with PXRD, DSC, NMR, and Raman spectroscopy. *Chem. Eng. Sci*. **2007**, 62, 3930-3939.

[139] Sloan, E. D. Clathrate hydrate measurements: microscopic, mesoscopic, and macroscopic

2003, 35, 41-53.

[140] Lee, H. H.; Ahn, S. H.; Nam, B. U.; Kim, B. S.; Lee, G. W.; Moon, D.; Shin, H. J.; Han, K. W.; Yoon, J. H. Thermodynamic Stability, Spectroscopic Identification, and Gas Storage Capacity of CO_2–CH_4–N_2 Mixture Gas Hydrates: Implications for Landfill Gas Hydrates. *Environ Sci Technol*. **2012**, 46, 4184-4190.

[141] Ota, M.; Morohashi, K.; Abe, Y.; Watanabe, M.; Smith, R. L.; Inomata, H. Replacement of CH_4 in the hydrate by use of liquid CO_2. *Energy Conver. Mange*. **2005**, 46, 1680-1691.

[142] Xu, C.-G.; Li, X.-S. Research progress on methane production from natural gas hydrates, *Rsc Adav*. **2015**, 6, 54672-54699.

[143] Zhou, X. T.; Fan, S. S.; Liang, D. Q.; Du, J. W. Determination of appropriate condition on replacing methane from hydrate with carbon dioxide. *Energ. Convers. Manag*. **2008**, 49, 2124–2129.

[144] Geng, C. Y.; Wen, H.; Zhou, H. Molecular simulation of the potential of methane reoccupation during the replacement of methane hydrate by CO_2. *J. Phys. Chem. A* **2009**, 113, 5463-5469.

[145] Yezdimer, E. M.; Cummings, P. T.; Chialvo, A. A. Determination of the Gibbs energy of gas replacement in sI clathrate hydrates by molecular simulation. *J. Phys. Chem. A* **2002**, 106, 7982-7987.

[146] Park, Y.; Kim, D-Y.; Lee, J-W.; Huh, D-G.; Park, K-P.; Lee, J.; Lee, H. Sequestering carbon dioxide into complex structures of naturally occurring gas hydrates. *Proc. Natl. Acad. Sci. U.S.A.* **2006**, 103, 12690-12694.

[147] Lee, Y.; Kim, Y.; Lee, J.; Lee, H.; Seo, Y. CH_4 recovery and CO_2 sequestration using flue gas in natural gas hydrates as revealed by a micro-differential scanning calorimeter. *App. Eng.* **2015**, 150, 120-127.

[148] Lee, Y.; Seo, Y-J.; Lee, J.; Lee, J. Y.; Kim, S-J.; Seo, Y. CH_4-Flue gas replacement occurring in sH hydrates and its significance for CH_4 recovery and CO_2 sequestration. *Chem. Eng. J.* **2017**, 308, 50-58.

[149] Koh, D. Y.; Kang, H.; Kim, D-O.; Park, J.; Cha, M.; Lee, H. Recovery of methane from gas hydrates intercalated within natural sediments using CO_2 and a CO_2/N_2 gas mixture. *ChemSusChem* **2012**, 5, 1443-1448.

[150] Shin, K.; Park, Y.; Cha, M.; Park, K-P.; Huh, D-G.; Lee, J.; Kim, S-J.; Lee, H. Swapping phenomena occurring in deep-sea gas hydrates. *Energy Fuels* **2008**, 22, 3160-3163.

[151] Seo, Y-J.; Park, S.; Kang, H.; Ahn, Y-H.; Lim, D.; Kim, S-J.; Lee, J.; Lee, J. Y.; Ahn. T.; Seo, Y.; Lee, H. Isostructural and cage-specific replacement occurring in sII hydrate with external CO_2/N_2 gas and its implications for natural gas production and CO_2 storage. *App. Eng.* **2016**, 178, 579.

[152] Zhou, X.; Liang, D.; Liang, S.; Yi, L.; Lin, F. Recovering CH_4 from natural gas hydrates with the injection of CO_2-N_2 gas mixture. *Energy Fuels* **2015**, 29, 1099-1106.

[153] Dornan, P.; Alavi, S. Woo, T. K. Free energies of carbon dioxide sequestration and methane recovery in clathrate hydrates. *J. Chem. Phys*. **2007**, 127, 124510.

[154] Liu, J.; Yan, Y.; Xu, J.; Li, S.; Chen, G.; Zhang, J. Replacement micro-mechanism of CH_4 hydrate by N_2/CO_2 mixture revealed by ab initio studies. *Comp. Mat. Sci*. **2016**, 123, 106-110.

[155] Szabo, A.; Ostlund, N. S. *Modern Quantum Chemistry: Introduction to Advanced Electronic Structure Theory*, Dover Publications Inc., Mineola, **1989**.

[156] Jensen, F. *Introduction to Computational Chemistry, John Wiley & Sons*, Chichester, **2013**.

[157] Atkins, P. W.; Friedman, R. S. *Molecular quantum mechanics*, Oxford University Press, Oxford, **2011**.

[158] Helgaker, T.; Jorgensen, P.; Olsen, J. *Molecular electronic-structure theory*, John Wiley & Sons, New York, **2014**.

[159] Griffiths, D. *Introduction to Quantum Mechanics. 2nd Edition*, Pearson, **2005**.

[160] Cramer, C. *Essentials of Computational Chemistry: Theories and Models*, Wiley, **2005**.

[161] Parr, R. G.; Yang, W. *Density Functional Theory of Atoms and Molecules*, Oxford University Press, Oxford, **1989**.

[162] Koch, W.; Holthausen, M. C. A Chemist's Guide to Density Functional Theory, Wiley-VCH, Weinheim, **2012**.

[163] Thomas, L. H. In Mathematical Proceedings of the Cambridge Philosophical Society, *Vol. 23*, Cambridge Univ Press, **1927**, 542.

[164] Fermi, E. Statistical method to determine some properties of atoms. *Rend. Accad. Naz. Lincei* **1927**, 6, 602.

[165] Dirac, P. A. M. On the annihilation of electrons and protons. Mathematical proceedings of the Cambridge philosophical society. *Proc. Cambridge Phil. Roy. Soc.* **1930,** 26, 361-365.

[166] Hohenberg, P.; Kohn, W. Inhomogeneous electron gas. *Phys. Rev. B* **1964**, 136, 864-871.

[167] Kohn, W.; Sham, L. J. Self-consistent equations including exchange and correlation effects. *Phys. Rev.* **1965**, 140, A1133-A1138.

[168] Perdew, J. P.; Burke, K.; Ernzerhof, M. Generalized gradient approximation made simple. *Phys. Rev. Lett.* **1996**, 77, 3865-3868.

[169] Becke, A. D. Density-functional thermochemistry. III. The role of exact exchange. *J. Chem. Phys*. **1993**, 98, 5648-5652.

[170] Adamo, C.; Barone, V. Toward reliable density functional methods without adjustable parameters: The PBE0 model. *J. Chem. Phys.* **1999**, 110, 6158-6170.

[171] Heyd, J.; Scuseria, G. E.; Ernzerhof, M. Hybrid functional based on a screened coulomb potential. *J. Chem. Phys*. **2003**, 118, 8207-8215.

[172] Zhao, Y.; Truhlar, D. G. The M06 suite of density functionals for main group thermochemistry, thermochemical kinetics, noncovalent interactions, excited states, and transition elements: two new functionals and systematic testing of four M06-class functionals and 12 other functionals. *Theor. Chem. Account* **2008**, *120*, 215-241.

[173] Zahariev, F.; Leang, S. S.; Gordon, M. S. Functional derivatives of meta-generalized approximation (meta-GGA) type exchange-correlation density functional. *J. Chem. Phys.* **2013**, 138, 244108.

[174] Zhao, Y.; Schultz, N. E.; Truhlar, D. G. Exchange-correlation functional with broad accuracy for metallic and nonmetallic compounds, kinetics, and noncovalent interactions *J. Chem. Phys*. **2005**, 123, 161103.

[175] Zhao, Y.; Truhlar, D. G. Exploring the limit of accuracy of the global hybrid meta density functional for main-group thermochemistry, kinetics, and noncovalent interactions. *J. Chem. Theor. Comput.* **2008**, 4, 1849-1868.

[176] Peverati, R.; Truhlar, D. G. M11-L: A local density functional that provides improved accuracy for electronic structure calculations in chemistry and physics. *J. Phys. Chem. Lett.* **2012**, 3, 117-124.

[177] Peverati, R.; Truhlar, D. G. Improving the accuracy of hybrid Meta-GGA density functionals by range separation. *J. Phys. Chem. Lett*., **2011**, 2, 2810-2817.

[178] Peverati, R.; Truhlar, D.G. Exchange–correlation functional with good accuracy for both structural and energetic properties while depending only on the density and its gradient. *J. Chem. Theor. Comput.* **2012**, 8, 2310-2319.

[179] Zhao, Y.; Schultz, N. E.; Truhlar, D. G. Design of density functionals by combining the method of constraint satisfaction with parametrization for thermochemistry, thermochemical kinetics, and noncovalent interactions. *J. Chem. Theor. Comput.* **2006**, *2*, 364-382.

[180] Hobza, P.; Šponer, J.; Reschel, T. Density functional theory and molecular clusters. *J. Comput. Chem.* **1995**, 16, 1315-1325.

[181] Allen, M.; Tozer, D. J. Helium dimer dispersion forces and correlation potentials in density functional theory. *J. Chem. Phys.* **2002**, 117, 11113-11120.

[182] Kristyán, S.; Pulay, P. Can (semi)local density functional theory account for the London dispersion forces? *Chem. Phys. Lett*. **1994**, 229, 175-180.

[183] Grimme, S. Semiempirical GGA-type density functional constructed with a long-range dispersion correction. *J. Comp. Chem*. **2006**, 27, 1787-1799.

[184] Grimme, S. Semiempirical GGA-type density functional constructed with a long-range dispersion correction. *J. Comp. Chem*. **2006**, 27, 1787-1799.

[185] Goerigk, L.; Grimme, S. Efficient and accurate double-hybrid-Meta-GGA density functionals-evaluation with the extended GMTKN30 database for general main group thermochemistry, kinetics, and noncovalent interactions. *J. Chem. Theor. Comput.* **2011**, *7*, 291-309.

[186] Chai, J.-D.; Gordon, M.-H. Long-range corrected hybrid density functionals with damped atom–atom dispersion corrections. *Phys. Chem. Chem. Phys*. **2008**, 10, 6615-6620.

[187] Slater, J. C. Atomic shielding constants. *Phys. Rev*. **1930,** 36, 57-64.

[188] Boys, S. F. Electronic wave functions - I. A general method of calculation for the stationary states of any molecular system. *Proc. R. Soc. London Ser. A*. **1950**, 200, 542.

[189] Ditchfield, R.; Hehre, W. J.; Pople, J. A. Self-consistent molecular-orbital methods. IX. An extended Gaussian-type basis for molecular-orbital studies of organic molecules *J. Chem. Phys*. **1971**, 54, 724-728.

[190] Dunning, T. H. Gaussian basis sets for use in correlated molecular calculations. I. The atoms boron through neon and hydrogen *J. Chem. Phys*. **1989**, 90, 1007-1023.

[191] Car, R.; Perrinello, M. Unified approach for molecular dynamics and density-functional theory. *Phys. Rev. Lett*. **1985**, 22, 2471-2474.

[192] Allen, M. P.; Tildesley, T. J. Computer Simulation of Liquids, Oxford University Press, **2002**.

[193] Jones, J. E.; Sc., D. On the determination of molecular fields. II. from the equation of state of a gas. *Proc. R. Soc. Lond. A* **1924**, 106, 463.

[194] Coulomb, C. *MEMOIRES DE COULOMB*, volume 1. LA SOCIETE FRANCAISE DE PHYSIQUE, **1884**.

[195] Kirov, M. V.; Fanourgakis, G. S.; Xantheas, S. S. Identifying the most stable networks in polyhedral water clusters. *Chem. Phys. Lett*. **2008**, 461, 180-188.

[196] Kirov, M. V. Energy optimization of water polyhedral. I. Predictive ability of discrete models for intermolecular interaction. *J. Struct. Chem*. **2006**, 47, 683-690.

[197] Shilpi, V.; Kaur, S. P.; Ramachandran, C.N. Revisiting the structural pattern and stability of $(H_2O)_{20}$ clusters using the dispersion corrected density functional method. *Chem. Phys. Lett*. **2015**, 626, 39-42.

[198] Shilpi, V.; Kaur, S.P.; Ramachandran, C.N. Density functional studies of fused dodecahedral and irregular-dodecahedral water cages. *RSC Adv.* **2015**, 5, 74270-74273.

[199] Grabowski, S. J. What is the covalency of hydrogen bonding? *Chem. Rev.* **2011**, 111, 2597-2625.

[200] Grabowski, S. J. Analysis of hydrogen bonds in crystals. *Crystals*. **2016**, 6, 59-63.

[201] Staykova, D. K.; Kuhs, W. F.; Salamatin, A. N.; Hansen, T. Formation of porous gas hydrates from ice powders: diffraction experiments and multistage model. *J. Phys. Chem. B* **2003,** 107, 10299-10311.

[202] Cao, X.; Su, Y.; Liu, Y.; Zhao, J.; Liu, C. Storage capacity and vibration frequencies of guest molecules in CH_4 and CO_2 hydrates by First-Principles calculations *J. Phys. Chem. A* **2014,** 118, 215-222.

[203] Deible, M. J.; Tuguldur, O.; Jordan, K. D. Theoretical Study of the Binding Energy of a Methane Molecule in a $(H_2O)_{20}$ Dodecahedral Cage. *J. Phys. Chem. B* **2014**, 118, 8257-8263.

[204] Khan, A. Theoretical studies of $CH_4(H_2O)_{20}$, $(H_2O)_{21}$, $(H_2O)_{20}$ and fused dodecahedral and tetrakaidecahedral structures: How do natural gas hydrates form? *J. Chem. Phys.* **1999**, 110, 11884-11889.

[205] Prasad, P. S. R.; Sowjanya, Y.; Prasad, K. S. Micro-Raman investigations of mixed gas hydrates. *Vib. Spectrosc.* **2009**, 50, 319-323.

[206] Srivastava, H. K.; Sastry, G. N. Viability of clathrate hydrates as CO_2 capturing agents: a theoretical study. *J. Phys. Chem. A* **2011**, 115, 7633-7637.

[207] Liu, Y.; Zhao, J.; Li, F.; Chen, Z. Appropriate description of intermolecular interactions in the methane hydrates: An assessment of DFT methods. **2013**, 34, 121-131.

[208] Khan, A. Stabilization of hydrate structure H by N_2 and CH_4 molecules in $4^3 5^6 6^3$ and 5^{12} cavities, and fused structure formation with $5^{12}6^8$ Cage: A theoretical study. *J. Phys. Chem. A* **2001**, 105, 7429-7434.

[209] Kumar, P.; Sathyamurthy, N. Theoretical Studies of Host–Guest Interaction in Gas Hydrates. *J. Phys. Chem. A* **2011**, 115, 14276-14281.

[210] Kumar, P.; Mishra, B. K.; Sathyamurthy, N. Density functional theoretic studies of host–guest interaction in gas hydrates. *Comput. Theor. Chem.* **2014**, 1029**,** 26-32.

[211] Villard, P. Combination of Argon with water. *C. R. Hebd. Seances Acad. Sci.* **1896**, *123,* 377.

[212] Londono, D.; Kuhs, W. F.; Finney, J. L. Enclathration of helium in ice II: the first helium hydrate. *Nature* **1988**, 332*,* 141-142.

[213] Dyadin, A. Y.; Larionov, E. G.; Aladko, E. Y.; Manakov, A. Y.; Zhurko, F. V.; Mikina, T. V.; Komarov, V. Y.; Grachev, E. V. Clathrate formation in water-noble gas (Hydrogen) systems at high pressures. *J. Struct. Chem*. **2000**, 40*,* 790-795.

[214] Abbondondola, J. A.; Fleischer, E. B.; Janda, K. C. Comparative study of hydrogen, argon, and xenon uptake into a propane hydrate. *AIChE J*. **2010**, 56*,* 2734-2741.

[215] Abbondondola, J. A.; Fleischer, E. B.; Janda, K. C. Propane Clathrate Hydrate Formation Accelerated by Xenon. *J. Phys. Chem. C* **2009,** 113**,** 4717-.

[216] Sugahara, K.; Sugahara, T.; Ohgaki, K. Thermodynamic and Raman Spectroscopic Studies of Xe and Kr Hydrates. *J. Chem. Eng. Data* **2005**, 50*,* 274-277.

[217] Falently, A.; Hansen, T. C..; Kuhs, W. F. Formation and properties of ice XVI obtained by emptying a type sII clathrate hydrate. *Nature* **2014**, 516*,* 231-232.

[218] Wang, L.; Dong, S. J. Interaction study of guest with host in clathrate hydrate. *Nat. Gas Chem*. **2007**, 16*,* 423-427.

[219] Alavi, S.; Ripmeester, J. A.; Kluq, D. D. Stability of rare gas structure H clathrate hydrates. *J. Chem. Phys.* **2006,** 125, 104501.

[220] Mondal, S.; Chattaraj, P.K. Noble gas encapsulation: clathrate hydrates and their HF doped analogues. *Phys. Chem. Chem. Phys*. **2014**, 16*,* 17943-17954.

[221] Frisch, M. J.; Trucks, G. W.; Schlegel, H. B.; Scuseria, G. E.; Robb, M. A.; Cheeseman, J. R.; Scalmani, G.; Barone, V.; Mennucci, B.; Petersson, G. A.; et al. Gaussian 09, Revision D.01; Gaussian, Inc.: Wallingford, CT, **2013.**

[222] McMullan, R. K.; Jeffery, G. A. Polyhedral Clathrate Hydrates. IX. Structure of Ethylene Oxide Hydrate. *J. Chem. Phys*. **1965***,* 42*,* 2725-2732.

[223] Bernal, J. D.; Fowler, R. H. A Theory of Water and Ionic Solution, with Particular Reference to Hydrogen and Hydroxyl Ions. *J. Chem. Phys*. **1933**, 7*,* 515-548.

[224] Boys, S. F.; Bernardi, R. The calculation of small molecular interactions by the differences of separate total energies. Some procedures with reduced errors. *Mol. Phys.* **1970**, 19*,* 553-566.

[225] Vogt, J.; Alvarez, S. van der Waals radii of noble gases. *Inorg. Chem.*, **2014**, 53, 9260-9266

[226] McQuarrie, D. A.; Simon, J. D. *Molecular Thermodynamics, 1st ed.; Viva Books*, **1997**.

[227] Murayama, K.; Takeya, S.; Ohmura, R. Phase equilibrium and crystallographic structure of clathrate hydrate formed in argon + 2, 2-dimethylbutane + water system. *Fluid phase Equilibria.* **2014**, 365*,* 64-67.

[228] Hallbruker, A.; Mayer, E. Unexpected stable nitrogen, oxygen, carbon monoxide and argon clathrate hydrates from vapour-deposited amorphous solid water: An X-ray and two-step differential scanning calorimetry study. *J. Chem. Soc. Faraday Trans*. **1990**, 86, 3785-3792.

[229] Lebsir, F.; Bouyacoub, A.; Bormann, D.; Krallafa, A. Theoretical investigations of CH_4, C_2H_6, CO_2 and N_2 guest molecules into a dodecahedral water cluster cavities, *J. Mol. Struct.: THEOCHEM* **2004**, 864, 42-47.

[230] Lee, H.; Seo, Y.; Seo, Y.-T.; Moudrakovski, I. L.; Ripmeester, J. A. Recovering methane from solid methane hydrate with carbon dioxide, *Angew. Chem. Int. Ed*. **2003**, *42*, 5048-5051.

[231] Chattaraj, P. K.; Bandaru, S.; Mondal, S. Hydrogen storage in clathrate hydrates, *J. Phys. Chem. A* **2011**, 115, 187-193.

[232] Ida, T.; Endo, K.; Matsumoto, D.; Kato, N.; Mizuno, M.; Suzuki Y.; Tadokaro, M. Dynamic and static behaviors of CH_4 and CO_2 in small and large cavities of hydrate, *J. Mol. Struct.* **2013**, 1032, 275-280.

[233] Ida, T.; Mizuno, M.; Endo, K. Electronic state of small and large cavities for methane hydrate, *J. Comp. Chem.* **2002**, 23, 1071-1075.

[234] Suida, P.; Sadlej, J. Nuclear magnetic resonance parameters for methane molecule trapped in clathrate hydrates, *J. Phys. Chem. A* **2011**, 115, 612-619.

[235] Ramya, K. R.; Venkatnathan, A. Vibrational raman spectra of hydrogen Clathrate hydrates from density functional theory. *J. Chem. Phys.,* **2013,** 138, 124305.

[236] London, F. Quantum theory of interatomic currents in aromatic compounds. *J. Phys. Rad.* **1937***,* 8, 397-409.

[237] Williams, C. I.; Whitehead, M. A.; Pang, L. Interaction and dynamics of endohedral gas molecules in fullerene C_{60} isomers and C_{70}, *J. Phys. Chem.* **1993**, 97, 11652-11656.

[238] Kumar, R.; Lang, S.; Englezos, P.; Ripmeester, J.; Application of the ATR-IR spectroscopy technique to the characterization of hydrates formed by CO_2, CO_2/H_2 and $CO_2/H_2/C_3H_8$, *J. Phys. Chem. A* **2009**, 113, 6308-6313.

[239] Ettinger, R.; Blume, P.; Patterson, A.; Lauterbur P. C. ^{13}C chemical shifts in CO and CO_2. *J. Chem. Phys.* **1960**, 33, 1597-1598.

[240] Wang, X.; Sang, D. K.; Chen, J.; Mi, J. Theoretical insights into nucleation of CO_2 and CH_4 hydrates for CO_2 capture and storage, *Phys. Chem. Chem. Phys.* **2014**, 16, 26929-26937.

[241] Lide, D.R. (Ed.), CRC Handbook of Chemistry and Physics. *A Ready-reference Book of Chemical and Physical Data*, 71st ed., CRC Press, Boca Raton, FL, 1990.

[242] Villa, R. M.; Marquez, M. F.; Mata, M. P.; Diaz, C. I.S. Crystal structure, stability and spectroscopic properties of methane and CO_2 hydrates. *J. Mol. Graph. and Mod.* 2013, **44,** 253-265.

[243] Strauch, B. T. ; Schicks, J. M. The driving forces of guest substitution in gas hydrates-A laser raman study on CH_4-CO_2 exchange in the presence of impurities. *Energies,* **2012**, 5**,** 420-437.

[244] Matsumoto, Y.; Grim, R. G.; Khan, N. M.; Sugahara, T.; Ohgaki, K.; Sloan, E. D.; Koh, C. A.; Sum, A. K. Investigation the thermodynamic stabilities of hydrogen and methane binary gas hydrates. *J. Phys. Chem. C*, **2014**, 118, 3783-3788.

[245] Strobel, T. A.; Sloan, E. D.; Koh, C. A. Raman spectroscopic studies of hydrogen clathrate hydrates. *J. Chem. Phys.,* **2009**, 130, 014506.

[246] Seitz, J. C.; Pasteris, J. D.; Wopenka, B. Characterization of CO_2+CH_4+H_2O fluid inclusion by microthermometry and laser raman microprobe spectroscopy: inferences for Clathrate and fluid equilibria. *Geochimica Cosmochimica Acta,* **1987**, 51, 1651-1664.

[247] Sarotti, A. M.; Pellegrinet, S. C.; A multi-standard approach for GIAO ^{13}C NMR calculations. *J. Org. Chem.* **2009,** 74, 7254-7260.

[248] Sarotti, A. M.; Pellegrinet, S. C. Application of the multi-standard methodology for calculating ^{1}H NMR chemical shifts, *J. Org. Chem.* **2012**, 77, 6059-6065.

[249] Watts, H. D.; Mohamed, M. N. A.; Kubicki, J. D. Comparison of multistandard and TMS-standard calculated NMR shifts for coniferyl alcohol and application of the multistandard method to lignin dimers, *J. Phys. Chem. B* **2011**, 115, 1958-1970.

[250] Yang, H.; Wang, T.; Oehme, D.; Petridis, L.; Hong, M.; Kubicki, J. D. Structural factors affecting ^{13}C NMR chemical shifts of cellulose: a computational study. *Cellulose.* **2018**, 25, 23-36.

[251] *Aldrich library of NMR Spectra, 2nd ed*., edited by Pouchert, C. J. (Aldrich Chemical Corp.), **1983**.

[252] Seo, Y. T.; Lee, H. ^{13}C NMR analysis and gas uptake measurements of pure and mixed gas hydrates: Development of natural gas transport and storage method using gas hydrate, *Korean J. Chem. Eng.* **2003,** 20, 1085-1091.

[253] Shin, W.; Park, S.; Lee, J. W.; Seo, Y.; Koh, D. Y.; Seol, J.; Lee, H. Structure transition from semi- to true clathrate hydrates induced by CH_4 enclathration. *J. Phys. Chem. C* **2012**, 116, 16352-16357.

[254] Kumar, R. M.; Sundar, J. V.; Subramanian, V. Improving the hydrogen storage capacity of metal organic framework by chemical functionalization. *Int. J. Hydrogen Energy.* **2012**, *37*, 16070-16077.

[255] Sugahara, T.; Haag, J.C.,; Prasad, P. S. R.; Warntjes, A. A.; Sloan, E. D.; Sum A. K.; Koh, C. A. Increasing hydrogen storage capacity using tetrahydrofuran. *J. Am. Chem. Soc.* **2009,** 131, 14616-14617.

[256] Martin, A.; Peters, C.J. Thermodynamics modelling of promoted structure II clathrate hydrates of hydrogen. *J. Phys. Chem. B.* **2009**, 113, 7548-7557.

[257] Jeziorski, B.; Moszynki, R.; Szalewicz, K. Perturbation theory approach to intermolecular potential energy surfaces of van der Waals complexes. *Chem. Rev.* **1994**, 94, 1887-1930.

[258] Turney, J. M.; Simmonett, A.C.; Parrish, R.M.; Hohenstein, E.G.; Evangelista, F.A.; Fermann, J. T. et al. Psi4: an open-source ab initio electronic structure program., WIREs *Comput. Mol. Sci.* **2012,** 2, 556-565.

[259] Sluiter, M.H.F.; Adachi, H.; Belosludov, R.V.; Belosludov, V.R.; Kawazoe, Y. Ab initio study of hydrogen storage in hydrogen hydrate clathrates. *Mater. Trans.* **2004,** 45, 1452-1454.

[260] Gottlieb, H. E.; Kotlyar, V.; Nudelman A. NMR chemical shifts of common laboratory solvents as trace impurities. *J. Org. Chem.* **1997,** 62, 7512-7515.

[261] Linga, P.; Haligva, C.; Nam, S. C.; Ripmeester, J. A.; Englezos, P. Recovery of methane from hydrate formed in a variable volume bed of silica sand particles. *Energy Fuels,* **2009,** 23, 5508−5516.

[262] Bai, D.; Zhang, X.; Chen, G.; Wang, W. Replacement mechanism of methane hydrate with carbon dioxide from microsecond molecular dynamics simulations. *Energy Environ. Sci.,* **2012,** 5, 7033–7041.

[263] Lee, S.; Lee, Y.; Lee, J.; Lee, H.; Seo, Y. Experimental verification of methane-carbon dioxide replacement in natural gas hydrates using a differential scanning calorimeter. *Environ. Sci. Technol*., **2013,** 47, 13184-13190.

[264] Yagasaki, T.; Matsumoto, M.; Andoh, Y.; Okazaki, S.; Tanaka, H. Effect of bubble formation on the dissociation of methane hydrate in water: A molecular dynamics study. *J. Phys. Chem. B*, **2014,** 118, 1900– 1906.

[265] Uchida, T.; Yamazaki, K.; Gohara, K. Generation of micro- and nano-bubbles in water by dissociation of gas hydrates. *Korean J. Chem. Eng*., **2016,** 33, 1749– 1755.

[266] Bagherzadeh, S. A.; Alavi, S.; Ripmeester, J.; Englezos, P. Formation of methane nano-bubbles during hydrate decomposition and their effect on hydrate growth. *J. Chem. Phys*., **2015**, 142, 214701.

[267] Hess, B.; Kutzner, C.; Spoel, D.; Lindal, E. GROMACS 4: Algorithms for highly efficient, load-balanced, and scalable molecular simulation. *J. Chem. Theory Comput.,* **2008,** 4, 435–447.

[268] Sujith, K. S.; Ramachandran, C. N. Natural gas evolution in a gas hydrate melt: effect of thermodynamic hydrate inhibitors. *J. Phys. Chem. B,* **2017,** 121, 153–163.

[269] Jorgensen, W. L.; Madura, J. D.; Swenson, C. J. Optimized intermolecular potential functions for liquid hydrocarbons. *J. Am. Chem. Soc.*, **1984,** 106, 6638– 6646.

[270] Harris, J. G.; Yung, K. H. Carbon dioxide's liquid-vapor coexistence curve and critical properties as predicted by a simple molecular model. *J. Phys. Chem.,* **1995,** 99, 12021–12024.

[271] Jorgensen, W. L.; Chandrasekhar, J.; Madura, J. D.; Impey, R. W.; Klein, M. L. Comparison of simple potential functions for simulating liquid water. *J. Chem. Phys.,* **1983,** 79, 926-935.

[272] Nohra, M.; Woo, T. K.; Alavi, S.; Ripmeester, J. A. Molecular dynamics Gibbs free energy calculations for CO2 capture and storage in structure I Clathrate hydrates in the presence of SO_2, CH_4, N_2, and H_2S impurities. *J. Chem. Thermodynamics,* **2012**, *44,* 5-12.

[273] Sujith, K. S.; Ramachandran, C. N. Carbon dioxide induced bubble formation in a CH_4- CO_2-H_2O ternary system: a molecular dynamics simulation study. *Phys. Chem. Chem. Phys*., **2016,** 18, 3746– 3754.

[274] Li, X.; Ross, D. A.; Trusler, J. P. M.; Maitland, G. C.; Boek, E. S. Molecular dynamics simulations of CO_2 and brine interfacial tension at high temperatures and pressures *J. Phys. Chem. B.,* **2013,** 117, 5647– 5652.

[275] Nosé, S. A unified formulation of the constant temperature molecular dynamics method. *J. Chem. Phys.,* **1984**, 81, 511-519.

[276] Hoover, W. G. Canonical dynamics: Equilibrium phase-space distributions. *Phys. Rev. A.* **1985,** 31, 1695– 1697.

[277] Parrinello, M.; Rahman, A. Polymorphic transitions in single crystals: A new molecular dynamics method. *J. Appl. Phys.* **1981,** 52, 7182.

[278] Hess, B.; Bekker, H.; Berendsen, H. J. C.; Fraaije, J. G. E. M. LINCS: A linear constraint solver for molecular simulations. *J. Comput. Chem*. **1997,** 18, 1463– 1472.

[279] Miyamoto, S.; Kollman, P. A. Settle: An analytical version of the SHAKE and RATTLE algorithm for rigid water models. *J. Comp. Chem.* **1992**, 13, 952– 962.

[280] Xu, Q.; Nakajima, M.; Ichikawa, S.; Nakamura, S.; Roy, P.; Okadome, H.; Shiina, T. Effect of surfactant and electrolyte concentrations on bubble formations and stabilizations. *J. Colloid Interface Sci.* **2009,** 332, 208–214.

[281] Ueno, H.; Akiba, H.; Akatsu, S; Ohmura, R. Crystal growth of clathrate hydrates formed with methane+carbon dioxide mixed gas at the gas/liquid interface and in liquid water. *New J. Chem.* **2015,** 39, 8254-8262.

[282] Moon, C.; Taylor, P. C.; Rodger, P. M. Molecular dynamics study of gas hydrate formation. *J. Am. Chem. Soc.* **2003,** 125, 4706– 4707.

[283] Takahashi, M.; Kawamura, T.; Yamamoto, Y.; Ohnari, H.; Himuro, S.; Shakutsui, H. Effect of Shrinking microbubble on gas hydrate formation. *J. Phys. Chem. B* **2003,** 107, 2171-2073.

[284] He, Z; Gupta, K. M.; Linga, P.; Jiang, J. Molecular insights into the nucleation and growth of CH_4 and CO_2 mixed hydrate from microseconds simulations. *J. Phys. Chem. C* **2016,** 120, 25225–25236.

[285] Matsumto, M.; Baba, A.; Ohmine, I. Topological building blocks of hydrogen bond network in water. *J. Chem. Phys.* **2007,** 127, 134504.

[286] Walsh, M. R.; Beckham, G. T.; Koh, C. A.; Sloan, E. D.; Wu, D. T.; Sum, A. K. Simulations: Effects of aqueous methane concentration, interfacial curvature, and system size. *J. Phys. Chem. C* **2011**, 115, 21241-21248.